UNIVERSITEIT VAN PRETORIA
UNIVERSITY OF PRETORIA
YUNIBESITHI YA PRETORIA

THE INFLUENCE OF SPECIMEN SIZE ON THE COMPRESSION STRESS BLOCK PARAMETERS OF REINFORCED CONCRETE

FRANCOIS VAN SCHALKWYK

2017

© University of Pretoria

THE INFLUENCE OF SPECIMEN SIZE ON THE COMPRESSION STRESS BLOCK PARAMETERS OF REINFORCED CONCRETE

FRANCOIS VAN SCHALKWYK

A project thesis submitted in partial fulfilment of the requirements for the degree of

MASTERS OF ENGINEERING (STRUCTURAL ENGINEERING)

In the

FACULTY OF ENGINEERING

UNIVERSITY OF PRETORIA

FEBRUARY 2017

© University of Pretoria

THESIS SUMMARY

THE INFLUENCE OF SPECIMEN SIZE ON THE COMPRESSION STRESS BLOCK PARAMETERS OF REINFORCED CONCRETE

FRANCOIS VAN SCHALKWYK

Supervisor: *Professor Elsabe Kearsley*

Department: *Civil Engineering*

University: *University of Pretoria*

Degree: *Masters of Engineering (Structural Engineering)*

The stress-strain distribution in flexural compression has been at the forefront of investigation ever since the 20th century. The original formulation of the flexural stress-strain distribution and the subsequent development of the stress block parameters, were based on specimens with a 127 x 203 mm (4 x 8 in.) cross section. The design of reinforced concrete flexural and flexural compression members at the Ultimate Limit State is based on the equilibrium of forces and moments obtained by using these stress block parameters. The calculation procedure entails the determination of the neutral axis depth, which varies depending on the magnitude of the applied action and the section dimensions. If the load action is small, the internal bending moment can be equilibrated with a reduced neutral axis depth, however, current design models do not consider the influence of a reduction in neutral axis depth (specimen size) on the stress block parameters, possibly resulting in an underestimation of the flexural compression capacity.

This study aimed to evaluate the influence of specimen size and compressive strength on the stress block parameters of concrete by testing twenty-seven plain concrete specimens in flexural compression. Nine specimens were tested for each specimen size (50 mm, 100 mm, and 200 mm), three for each of the cylinder target strengths of 40 MPa, 65 MPa, and 80 MPa. The stress block parameters, obtained from the stress-strain curves, were compared to the data obtained by previous researchers, and the influence of specimen size on the stress block parameters evaluated for the different concrete strengths. Along with the size effect in flexural compression, the size effect for cubes and cylinders were also evaluated, and the associated cylinder strength used to eliminate the size effect of the stress block parameters.

A comparison of the error between the predicted Moment-Axial force (M-N) interaction diagram, obtained by using the BS 8110-1 (1997), SANS 0100-1 (2000), ACI-318 (2014), and EN 1992-1-1 (2004) codes, and the actual M-N interaction diagram, obtained from the experimental points, were made, and conclusions regarding their applicability for the design of concrete containing South African materials drawn. Lastly, the flexural stress-strain behaviour was modelled, and a comparison made between the calculated and actual stress block parameters.

© University of Pretoria

DECLARATION

I, the undersigned hereby declare that:

- I understand what plagiarism is and I am aware of the University's policy in this regard;
- The work contained in this thesis is my own original work;
- I did not refer to work of current or previous students, lecture notes, handbooks or any other study material without proper referencing;
- Where other people's work has been used this has been properly acknowledged and referenced;
- I have not allowed anyone to copy any part of my thesis;
- I have not previously in its entirety or in part submitted this thesis at any university for a degree.

Signature of student: 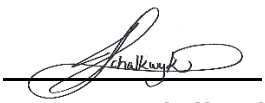

Name of student: Francois van Schalkwyk

Student number: 10036106

Date: 15/02/2017

© University of Pretoria

ACKNOWLEDGEMENT

I wish to express my appreciation to the following organisations and persons who made this thesis possible:

- The University of Pretoria Civil Engineering Department for the use of their facilities, materials, and testing equipment.
- Prof. E.P. Kearsley for her excellent advice and encouragement during the course of the study
- Mr. D. Mostert for his excellent advice and help during testing
- Mr. J. Scoltz for his excellent advice and help during testing
- Mr. J. Botha for his excellent advice and help in constructing the steel lever arms
- Ms. J. Callanan for the ordering of materials
- Ms. V. Doman for making personal appointments
- Mr. H. Jansen
- My parents, Bernadette van Schalkwyk and Francois van Schalkwyk for their continual love support and encouragement during the course of the year.

© University of Pretoria

TABLE OF CONTENTS

1 REPORT INTRODUCTION 1-1

1.1. Background 1-1

1.2. Objectives of the Study 1-2

1.3. Scope of the Study 1-2

1.4. Methodology 1-2

1.5. Report Organisation 1-3

2 LITERATURE REVIEW 2-1

2.1 Introduction 2-1

2.2 Concrete Composition and Factors Influencing its Behaviour 2-1

2.2.1 Water/Cement Ratio 2-2

2.2.2 Cement Type and Additions (Cement Extenders) 2-3

2.2.2.1 Ground Granulated Blast Furnace Slag and Fly Ash 2-3

2.2.2.2 Condensed Silica Fume 2-4

2.2.3 Admixtures 2-4

2.2.3.1 Entrained and Entrapped Air 2-4

2.2.3.2 Plasticisers or Water Reducers 2-4

2.2.4 Aggregate 2-5

2.2.4.1 Size 2-5

2.2.4.2 Grading 2-5

2.2.4.3 Texture 2-5

2.2.5 Curing Conditions 2-5

2.2.6 Specimen Parameters 2-6

2.2.7 Loading Conditions 2-6

2.3 Compressive Strength of Concrete 2-7

2.3.1 Nonlinearity of Stress-Strain Behaviour 2-8

2.3.2 Stress-Strain Models for the Compression Zone of Concrete 2-9

2.3.2.1 Jensen (1943) Model 2-9

2.3.2.2 Hognestad (1951) Model 2-9

2.3.2.3 Desayi & Krishnan (1964) Model 2-10

2.3.2.4 Sargin & Handa (1969) Model 2-10

2.3.2.5 Kent & Park (1971) Model 2-11

2.3.2.6 Popovics (1973) Model 2-11

2.3.2.7 Wang et al. (1978a) & Wang et al. (1978b) Model 2-11

2.3.2.8 Tomaszewicz (1984) Model 2-13

2.3.2.9 Carreira & Chu (1985) Model 2-13

2.3.2.10 Ahmad & Shah (1985) Model 2-14

2.3.2.11 Tsai (1988) Model 2-14

2.3.2.12 Hsu & Hsu (1994) Model 2-15

© University of Pretoria

Preference

2.3.2.13 Wee et al. (1996) Model 2-15
2.3.2.14 Attard & Setunge (1996) Model 2-16
2.3.2.15 Van Gysel & Taerwe (1996) Model 2-17
2.3.2.16 Oztekin et al. (2003) Model 2-18
2.4 Flexural Behaviour of Concrete 2-18
2.4.1 Stress Block Parameters 2-19
2.4.2 Eccentric Specimen Tests 2-20
2.4.2.1 Hognestad et al. (1955) Test Procedure 2-22
2.4.2.2 Nedderman (1973) Test Procedure 2-23
2.4.2.3 Kaar et al. (1978a) Test Procedure 2-23
2.4.2.4 Kaar et al. (1978b) Test Procedure 2-23
2.4.2.5 Swartz et al. (1985) Test Procedure 2-24
2.4.2.6 Pastor (1986) Test procedure 2-25
2.4.2.7 Ibrahim (1994) Test Procedure 2-25
2.4.2.8 Soliman & Yu (1967) Test Procedure 2-26
2.4.2.9 Sargin et al. (1971) Test Procedure 2-27
2.4.2.10 Schade (1992) Test Procedure 2-28
2.4.2.11 Tan & Nguyen (2005) Test Procedure 2-29
2.4.2.12 Mertol et al. (2008) Test Procedure 2-30
2.4.2.13 Khadiranaikar & Awati (2012) Test Procedure 2-31
2.4.3 Previous Test Results 2-32
2.4.4 History of Rectangular Stress Block Parameters 2-35
2.4.4.1 Whitney (1937) Model 2-35
2.4.4.2 Mattock et al. (1961) Model 2-35
2.4.4.3 Zia (1983) Model 2-35
2.4.4.4 Li (1993) Model and Regan (1999) Model 2-36
2.4.4.5 Ibrahim (1994) Model 2-36
2.4.4.6 Pendyala & Mendis (1998) Model 2-36
2.4.4.7 Attard & Stewart (1998) Model 2-36
2.4.4.8 Bae & Bayrak (2003) Model 2-36
2.4.4.9 Sun et al. (2003) Model 2-37
2.4.4.10 Oztekin et al. (2003) Model 2-37
2.4.4.11 Ozbakkaloglu & Saatcioglu (2004) Model 2-37
2.4.4.12 Tan & Nguyen (2005) Model 2-37
2.4.4.13 Mertol et al. (2008) Model 2-37
2.4.4.14 Khadiranaikar & Awati (2012) Model 2-37
2.4.5 Rectangular Stress Block Parameters: Design Codes 2-40
2.5 Poisson Ratio 2-42
2.6 Size Dependant Behaviour of Concrete 2-43
2.6.1 Basics of Scaling 2-43

© University of Pretoria

Preference

2.6.2 Uniaxial Compressive Strength 2-45
2.6.3 Flexural Compression Strength 2-45
2.7 Summary of Literature 2-49
3 EXPERIMENTAL PROGRAM 3-1
3.1 Introduction 3-1
3.2 Material Specification 3-1
3.2.1 Cement 3-1
3.2.2 Aggregate 3-1
3.3 Mix Proportions, Volumes, and Curing 3-2
3.4 Experimental Method and Equipment 3-3
3.4.1 Compressive Strength, Modulus of Elasticity, and Poisson Ratio 3-3
3.4.2 Flexural Compression 3-4
3.4.2.1 Selection of Flexural Compression Section 3-4
3.4.2.2 Test Specimens Reinforcing Layout and Preparation 3-5
3.4.2.3 Eccentric Specimen Lever Arms 3-8
3.4.2.4 Test Setup and Procedure 3-11
4 DISCUSSION AND ANALYSIS OF RESULTS 4-1
4.1 Introduction 4-1
4.2 Compressive Strength and Modulus of Elasticity 4-1
4.2.1 Cube Results 4-1
4.2.2 Cylinder Results 4-4
4.2.2.1 Cylinder Compressive Strength 4-4
4.2.2.2 Uniaxial Compressive Stress-Strain Curves 4-6
4.2.2.3 Modulus of Elasticity 4-8
4.2.2.4 Poisson Ratio (150 mm Cylinders) 4-8
4.2.3 Cube versus Cylinder Results 4-10
4.2.4 Cube and Cylinder Size Effect 4-11
4.3 Flexural Strength 4-13
4.3.1 General Observations 4-14
4.3.2 Surface Strain Measurements 4-16
4.3.3 Poisson Ratio (Flexural Compression) 4-17
4.3.4 Flexural Compression Stress-Strain Distribution 4-19
4.3.5 Stress Block Parameters 4-20
4.4 Influence of Specimen Size on the Flexural Compressive Behaviour 4-28
4.4.1 Size Effect for k_3 4-28
4.4.2 Size Effect for k_1k_3 4-29
4.4.3 Size Effect for α_1 4-31
4.4.4 Size Effect for ε_{cu} 4-32
4.5 Adequacy of Design Codes 4-33
4.6 Stress-Strain Behaviour 4-38

© University of Pretoria

Preference

4.6.1 Uniaxial Compression versus Flexural Compression Stress-Strain Curves 4-38
4.6.2 Proposed Flexural Compression Stress-Strain Relationship 4-39
4.7 Conclusions and Implications for Design 4-43
5 CONCLUSIONS AND RECOMMENDATIONS 5-1
5.1 Introduction 5-1
5.2 Conclusions 5-1
5.2.1 Cube and Cylinder Data 5-1
5.2.2 Flexural Compression Specimen Data 5-2
5.3 Recommendations 5-5
6 REFERENCES 6-1
A PREVIOUS RESEARCH RESULTS A-1
A.1 Eccentric Specimen Test Data A-1
A.2 Poisson Ratio Test Data A-4
A.3 Size Effect Specimen Data A-6

TABLE OF FIGURES

Figure 2.1 Factors Influencing Concrete Strength Adapted from Mehta (1986) 2-2
Figure 2.2 Influence of Water/Cement Ratio on Concrete Compressive Strength Adapted from Mehta (1986) 2-3
Figure 2.3 Uniaxial Compression Stress-Strain Curves Adapted from Ho et al. (2002) 2-7
Figure 2.4 Stress-Strain Curves of Cement Paste, Aggregate, and Concrete Adapted from Hsu et al. (1963) 2-8
Figure 2.5 Four Stages of Stress-Strain Distribution in a Reinforced Concrete Flexural Member 2-18
Figure 2.6 Strain, Three Parameter, and Two Parameter Equivalent Rectangular Stress Block 2-20
Figure 2.7 Hognestad et al. (1955) Test Specimen 2-22
Figure 2.8 Kaar et al. (1978b) Test Specimens 2-24
Figure 2.9 Swartz et al. (1985) Test Specimen 2-25
Figure 2.10 Ibrahim (1994) Test Specimens 2-26
Figure 2.11 Soliman & Yu (1967) Test Setup and Specimen Dimensions 2-27
Figure 2.12 Sargin et al. (1971) Test Setup and Specimen Dimensions 2-27
Figure 2.13 Schade (1992) Test Setup and Specimen Dimensions 2-28
Figure 2.14 Tan & Nguyen (2005) Test Setup and Specimen Dimensions 2-29
Figure 2.15 Mertol et al. (2008) Test Specimen 2-30
Figure 2.16 Mertol et al. (2008) Test Setup 2-31
Figure 2.17 Khadiranaikar & Awati (2012) Test Setup 2-32
Figure 2.18 k_1 Factor from Previous Research 2-32
Figure 2.19 k_2 Factor from Previous Research 2-33
Figure 2.20 k_3 Factor from Previous Research 2-33
Figure 2.21 k_1k_3 Factor from Previous Research 2-33
Figure 2.22 α_1 Factor from Previous Research 2-34
Figure 2.23 β_1 Factor from Previous Research 2-34
Figure 2.24 Ultimate Concrete Strain from Previous Research 2-34

© University of Pretoria

	Preference
Figure 2.25 α_1 Models from Previous Research	2-38
Figure 2.26 β_1 Models from Previous Research	2-38
Figure 2.27 α_1 Models from Design Codes	2-40
Figure 2.28 β_1 Models from Design Codes	2-40
Figure 2.29 Point Estimates of Poisson Ratio Obtained by Other Researchers	2-43
Figure 2.30 Plastic, LEFM, and Quasibrittle Size Effect	2-44
Figure 2.31 Size Effect for Cylinders Adapted from Yi et al. (2006)	2-46
Figure 2.32 Size Effect for Cubes Adapted from Yi et al (2006)	2-46
Figure 2.33 Specimen Sizes used by Kim et al. (2000)	2-47
Figure 2.34 Size Effect for Flexural Compressive Stress Adapted from Kim et al. (2000)	2-48
Figure 2.35 Size Effect for Ultimate Compressive Strain Adapted from Kim et al. (2000)	2-48
Figure 3.1 Aggregate Grading Curve	3-2
Figure 3.2 Configuration of Longitudinal and Shear Reinforcing in Flexural Compression Members	3-5
Figure 3.3 Reinforcing Layout and Fixing System for Scale 1:1 Specimens	3-6
Figure 3.4 Reinforcing Layout and Fixing System for Scale 1:2 (Left) and Scale 1:4 (Right) Specimens	3-6
Figure 3.5 Strain Gauge Layout for Scale 1:1 Flexural Compression Specimens	3-7
Figure 3.6 Strain Gauge Layout for Scale 1:2 Flexural Compression Specimens	3-7
Figure 3.7 Strain Gauge Layout for Scale 1:4 Flexural Compression Specimens	3-7
Figure 3.8 Scale 1:1 Detailed Lever Arm Drawing	3-8
Figure 3.9 Scale 1:1 Lever Arm, Back Plate, and Confinement Plate	3-9
Figure 3.10 Scale 1:2 Detailed Lever Arm Drawing	3-9
Figure 3.11 Scale 1:2 Lever Arm, Back Plate and Confinement Plate	3-10
Figure 3.12 Scale 1:4 Detailed Lever Arm Drawing	3-10
Figure 3.13 Isometric View Scale 1:4 Lever Arm, Back Plate and Confinement Plate	3-11
Figure 3.14 Scale 1:4, 1:2, and 1:1 Lever Arms	3-11
Figure 3.15 Detailed Layout of Scale 1:1 Test Setup	3-12
Figure 3.16 Scale 1:1 Specimen Layout Prior to Testing	3-13
Figure 3.17 Detailed Layout of Scale 1:2 Test Setup	3-13
Figure 3.18 Scale 1:2 Specimen Layout Prior to Testing	3-14
Figure 3.19 Detailed Layout of Scale 1:4 Test Setup	3-14
Figure 3.20 Scale 1:4 Specimen Layout Prior to Testing	3-15
Figure 4.1 Box-and-Whisker Plot of Cube Compressive Strengths	4-3
Figure 4.2 Box-and-Whisker Plot of Cylinder Compressive Strengths	4-5
Figure 4.3 50 mm Cylinder Stress-Strain Curves	4-6
Figure 4.4 100 mm Cylinder Stress-Strain Curves	4-7
Figure 4.5 150 mm Cylinder Stress-Strain Curves	4-7
Figure 4.6 200 mm Cylinder Stress-Strain Curves	4-7
Figure 4.7 Modulus of Elasticity versus Compressive Strength	4-8
Figure 4.8 Poisson Ratio versus Longitudinal Compressive Strain for 150 mm Cylinders	4-9
Figure 4.9 Poisson Ratio Point Estimates for 150 mm Cylinders	4-9

© University of Pretoria

Preference

Figure 4.10 Cylinder versus Cube Strength Results 4-10
Figure 4.11 Size Effect for Cubes 4-11
Figure 4.12 Size Effect for Cylinders 4-11
Figure 4.13 Comparison: Study Test Results and Results Obtained by Yi et al. (2006) for Cubes 4-13
Figure 4.14 Comparison: Study Test Results and Results Obtained by Yi et al. (2006) for Cylinders 4-13
Figure 4.15 Failure Mode of Scale 1:1 Specimen (Mix 1) 4-14
Figure 4.16 Failure Mode of Scale 1:1 Specimen (Mix 2) 4-15
Figure 4.17 Failure Mode of Scale 1:1 Specimen (Mix 3) 4-15
Figure 4.18 Strain Distribution through Depth of M3/50mm/S2 4-16
Figure 4.19 Strain Distribution through Depth of M3/100mm/S2 4-16
Figure 4.20 Strain Distribution through Depth of M3/200mm/S1 4-17
Figure 4.21 Poisson Ratio versus Longitudinal Compressive Strain for Flexural Compression Members 4-18
Figure 4.22 Point Estimates of the Poisson Ratios for Flexural Compression Specimens 4-18
Figure 4.23 Free Body Diagram of Scale 1:1 Eccentric Bracket Specimen 4-19
Figure 4.24 50 mm Specimens Flexural Stress-Strain Relationships 4-21
Figure 4.25 100 mm Specimens Flexural Stress-Strain Relationships 4-21
Figure 4.26 200 mm Specimens Flexural Stress-Strain Relationships 4-21
Figure 4.27 Effect of 150 mm Cylinder Compressive Strength on k_1 4-23
Figure 4.28 Effect of 150 mm Cylinder Compressive Strength on k_2 4-23
Figure 4.29 Effect of 150 mm Cylinder Compressive Strength on k_3 4-24
Figure 4.30 Effect of Associated Cylinder Compressive Strength on k_3 4-24
Figure 4.31 Effect of 150 mm Cylinder Compressive Strength on k_1k_3 4-25
Figure 4.32 Effect of Associated Cylinder Compressive Strength on k_1k_3 4-25
Figure 4.33 Effect of 150 mm Cylinder Compressive Strength on α_1 4-26
Figure 4.34 Effect of Associated Cylinder Compressive Strength on α_1 4-26
Figure 4.35 Effect of 150 mm Cylinder Compressive Strength on β_1 4-27
Figure 4.36 Effect of 150 mm Cylinder Compressive Strength on ε_{cu} 4-27
Figure 4.37 Effect of Specimen Size on $k_3/k_{3ave(20cm)}$ 4-28
Figure 4.38 Elimination of Size Effect for $k_3/k_{3ave(20cm)}$ 4-29
Figure 4.39 Effect of Specimen Size on $k_1k_3/ k_1k_{3ave(20cm)}$ 4-30
Figure 4.40 Elimination of Size Effect for $k_1k_3/k_1k_{3ave(20cm)}$ 4-31
Figure 4.41 Effect of Specimen Size on $\alpha_1/\alpha_{1ave(20cm)}$ 4-31
Figure 4.42 Elimination of Size Effect for $\alpha_1/\alpha_{1ave(20cm)}$ 4-32
Figure 4.43 Effect of Specimen Size on $\varepsilon_{cu}/\varepsilon_{cuave(20cm)}$ 4-33
Figure 4.44 Normalised M-N Interaction Diagram Obtained from Experimental Results 4-34
Figure 4.45 Percentage Error: BS 8110-1 (1997) & SANS 0100-1 (2000) and Experimental Results 4-36
Figure 4.46 Percentage Error: ACI-318 (2014) and Experimental Results 4-36
Figure 4.47 Percentage Error: EN 1992-1-1 (2004) and Experimental Results 4-36
Figure 4.48 Average Percentage Error versus Compressive Strength 4-37
Figure 4.49 100 mm Cylinder and 100 mm Flexural Compression Specimen Stress-Strain Curves 4-38

© University of Pretoria

Preference

Figure 4.50 150 mm Cylinder and 200 mm Flexural Compression Specimen Stress-Strain Curves 4-39
Figure 4.51 Instantaneous Elastic Modulus Estimate 4-40
Figure 4.52 Strain Associated with Peak Stress (ε_{c0}) Estimate 4-40
Figure 4.53 Ultimate Compressive Strain (ε_{cu}) Estimate 4-41
Figure 4.54 Actual and Carreira & Chu (1985) (Dotted Line) Model for 50 mm Specimens 4-41
Figure 4.55 Actual and Carreira & Chu (1985) (Dotted Line) Model for 100 mm Specimens 4-41
Figure 4.56 Actual and Carreira & Chu (1985) (Dotted Line) Model for 200 mm Specimens 4-42
Figure 4.57 Ratio between Calculated and Actual values of k_1 4-42
Figure 4.58 Ratio between Calculated and Actual values of k_2 4-42

LIST OF TABLES

Table 2.1 Stress–Strain Relationship Constants Proposed by Wang et al. (1978a) and Wang et al. (1978b) 2-12
Table 2.2 Parameter t for Different Concrete Strengths 2-18
Table 2.3 Summary of Eccentric Bracket Tests Performed by Other Researchers 2-21
Table 2.4 α_1, β_1, and ε_{cu} Models Proposed by Other Researchers 2-34
Table 2.5 α_1, β_1, and ε_{cu} Models Proposed by Design Codes 2-41
Table 2.6 Summary of Poisson Ratios Obtained by Other Researchers 2-42
Table 3.1 Aggregate Grading 3-2
Table 3.2 Mix Proportions for Target Concrete Strengths 3-3
Table 3.3 Mix Quantities 3-3
Table 4.1 Cube Compressive Strength Results 4-2
Table 4.2 Descriptive Statistical Summary of Cube Data 4-3
Table 4.3 Cylinder (H/D=2) Compressive Strength, Modulus of Elasticity, and Strain Associated with f_{cy} 4-4
Table 4.4 Descriptive Statistical Summary of Cylinder Data 4-6
Table 4.5 Point Estimate of 150 mm Cylinder Poisson Ratio 4-9
Table 4.6 50 mm Cylinder Five Number Summary Obtained from 50 mm Cubes 4-10
Table 4.7 Mix 1, Mix 2,and Mix 3 and Average MSEL Coefficients for Cubes 4-12
Table 4.8 Mix 1, Mix 2, and Mix 3 and Average MSEL Coefficients for Cylinders 4-12
Table 4.9 MSEL Regression Coefficients of Study Results and Results of Yi et al. (2006) 4-13
Table 4.10 Point Estimate of the Flexural Compression Specimens Poisson Ratio 4-18
Table 4.11 Calculated Stress Block Parameters for Flexural Compression Members 4-22
Table 4.12 MSEL Coefficients for $k_3/k_{3ave(20cm)}$ 4-28
Table 4.13 MSEL Coefficients for $k_1k_3/ k_1k_{3ave(20cm)}$ 4-30
Table 4.14 MSEL Coefficients for $\alpha_1/\alpha_{1ave(20cm)}$ 4-32
Table 4.15 MSEL Coefficients for $\varepsilon_{cu}/\varepsilon_{cuave(20cm)}$ 4-33
Table 4.16 Linear Trend Line Coefficients (y=ax+b) for ε_{c0} and ε_{cu} 4-40
Table 5.1 Size Effect Coefficients for Cubes 5-2
Table 5.2 Effect Coefficients for Cylinders 5-2
Table 5.3 Regression Coefficients of Study Results and Results of Yi et al. (2006) 5-2
Table 5.4 MSEL Coefficients for $k_3/k_{3ave(20cm)}$ 5-3

© University of Pretoria

Preference

Table 5.5 MSEL Coefficients for k_1k_3/ $k_1k_{3ave(20cm)}$ 5-3
Table 5.6 MSEL Coefficients for $\alpha_1/\alpha_{1ave(20cm)}$ 5-3
Table 5.7 MSEL Coefficients for $\varepsilon_{cu}/\varepsilon_{cuave(20cm)}$ 5-3
Table 5.8 Linear Trend Line Coefficients (y=ax+b) for ε_{c0} and ε_{cu} 5-5
Table A.1 Hognestad et al. (1955) A-1
Table A.2 Sargin et al. (1971) A-1
Table A.3 Nedderman (1973) A-1
Table A.4 Kaar et al. (1978a) A-2
Table A.5 Kaar et al. (1978b) A-2
Table A.6 Swartz et al. (1985) A-2
Table A.7 Pastor (1986) A-3
Table A.8 Schade (1992) A-3
Table A.9 Ibrahim (1994) A-3
Table A.10 Tan & Nguyen (2005) A-3
Table A.11 Mertol et al. (2008) A-3
Table A.12 Khadiranaikar & Awati (2012) A-4
Table A.13 Komendant et al. (1978), Perenchio & Klieger (1978), and Carrasquillo et al. (1981) A-4
Table A.14 Swartz et al. (1985), Jerath & Yamane (1987), Radain et al. (1993), and Iravani (1996) A-4
Table A.15 Logan (2005) and Methol et al. (2008) A-5
Table A.16 Yi et al. (2006) A-6

LIST OF SYMBOLS

f_c= The compressive stress in the concrete at a given level of strain
$f_c^{'}$= The cylinder compressive strength
$f_c^{''}$= The flexural compressive strength
ε_c= The strain in the concrete due to the applied external load
ε_{c0}= The strain at the peak compressive strength
ε_{cu}= The ultimate compressive strain
C= The applied external compressive force
M= The applied external moment
b, c= The width (b) and depth (c) of the flexural compression specimen

© University of Pretoria

CHAPTER 1

REPORT INTRODUCTION

1.1 BACKGROUND

Concrete is the most widely used construction material in the world and a vital component of infrastructure. Concrete's popularity derives from its high stiffness, excellent compressive strength, low cost, and ability to be cast into any structural form, the most basic of which are flexural and flexural compression members (beams and columns). The design of these sections is based on the equilibrium of internal forces and moments, generated from the tensile force in the steel reinforcing and a compressive force in the concrete. The compressive force is the resultant of the stress in the compression zone of the reinforced concrete element. This stress distribution, has been a major subject of investigation ever since its inception in the early 20th century, when the ground-breaking work published by Hognestad et al. (1955), proposed the use of a 127 x 203 mm "C-shaped" specimen to simulate the strain distribution in the compression zone of reinforced concrete flexural and flexural compression memebers. These strains, when combined with the load and numerical integration, enable the stress-strain behaviour in flexural compression to be obtained. Subsequent investigations done by Nedderman (1973), Kaar et al. (1978a), Kaar et al. (1978b), Swartz et al. (1985), Pastor (1986), and Ibrahim (1994), all utilised the "C-Shaped" specimen, with different concrete strengths, specimen dimensions and shapes, aggregate type, and the effect of confinement, being among the variables investigated. Researchers such as Soliman & Yu (1967), Sargin et al. (1971), Schade (1992), Tan & Nguyen (2005), Mertol et al. (2008), and Khadiranaikar & Awati (2012) investigated similar variables, but used detachable steel lever arms to apply the secondary load to concrete column sections. Thus, while the influence of compressive strength has been investigated to a degree, the simulated stress block depth (specimen size) has remained unaltered to a large extent.

The design of reinforced concrete flexural and flexural compression members requires the determination of the neutral axis depth, which varies depending on the magnitude of the applied action and the section dimensions. If the load action is small, the internal bending moment can be equilibrated with a reduced neutral axis depth, however, current design models do not consider the influence of a reduction in neutral axis depth (specimen size) on the compressive strength. Being a quasibrittle material, concrete fails through the formation and propagation of cracks, induced by stresses caused by external loads and/or environmental changes. The formation and propagation of cracks release strain energy, and thus the size of the specimen i.e. the depth of the neutral axis, among other things, will have an influence on its flexural behaviour. Even though comprehensive studies on the influence of specimen size on the uniaxial compressive strength has been done by Kim et al. (1998) and Kim et

© University of Pretoria

al. (1999), the influence of size on the *flexural compressive behaviour* has been neglected to some extent. Work done by Kim et al. (2001) concluded that the ratio between the average flexural stress and the strength of a 100 x 200 mm cylinder, as well as the ultimate strain in flexural compression, should increase for specimen sizes smaller than 200 mm. As a typical beam will have the compressive force (caused by flexure) resisted by a relatively shallow compressive stress block, the use of the standard cylinder compressive strength in conjunction with the known stress block parameter models, could result in a significant underestimation of the strength in flexural compression. Thus, since the size effect cannot be ignored, it would be prudent to determine the influence of specimen size and concrete compressive strength on the compressive stress block parameters of concrete by testing twenty-seven concrete specimens (nine for each specimen size) in flexural compression. Understanding this influence may lead to more economical designs.

1.2 OBJECTIVES OF THE STUDY

The aim of this investigation was to determine the effect of both compressive strength and specimen size on the compressive stress block parameters of concrete. The main objectives of this project are to asses and evaluate experimentally:

- The influence of specimen size on the cube strength, cylinder strength, and stress block parameters.
- The Poisson ratio for 150 x 300 mm cylinders (subjected to uniaxial compression) and eccentric specimens (subjected to flexural compression).
- Whether the size effect of the stress block parameters can be eliminated by using the associated cylinder strength as opposed to the conventional 150 x 300 mm cylinder strength in calculations.
- Whether the design assumptions regarding the stress block parameters proposed by the BS 8110-1 (1997), SANS 0100-1 (2000), ACI-318 (2014), and EN 1992-1-1 (2004) codes, are applicable for the analysis and design of concrete containing South African materials.
- Whether the uniaxial stress-strain curve can be used to represent the flexural stress-strain curve, and if the flexural stress-strain curves can be modelled by using a uniaxial stress-strain model and parameter estimates obtained from the study results.

1.3 SCOPE OF THE STUDY

A vast number of covariates influence the flexural deformation of concrete. This study focuses on the deformations and loads induced in flexural compression, with changes in specimen size and concrete strength being the only variables. As the aggregate size and aggregate type directly or indirectly influences the strength of concrete, the same aggregate was used for all mixes. Furthermore, the increased variability associated with a reduced specimen size was not taken into consideration in selecting the quantity of flexural compression members to be tested.

1.4 METHODOLOGY

The influence of specimen size on the cube strength, cylinder strength, and stress block parameters, was established by considering three mix designs (cylinder target strengths of 40 MPa, 65 MPa, and 80 MPa), four cube and cylinder sizes, and three eccentric specimen sizes. The cubes (50 mm, 100 mm, 150 mm, and 200 mm)

© University of Pretoria

and cylinders (50 x 100 mm, 100 x 200 mm, 150 x 300 mm, and 200 x 400 mm) were used to establish the specimen size effect in uniaxial compression. The size effect in flexural compression, i.e. for the stress block parameters, was established by subjecting 50 x 50 x 300 mm, 100 x 100 x 500 mm, and 200 x 200 x 1000 mm specimens to a flexural compression load. Strain gauges, mounted on the surface of the concrete specimen, were used to monitor the distribution of flexural compressive strain when the specimen was loaded with a major force P_1 (applied through the centroid of the section) and a minor force P_2 (applied eccentrically). The combined influence of these loads were used to maintain a condition of zero strain in the back face of the flexural compression specimen, while increasing the strain in the extreme compression fibre. The strain in the extreme compression fibre, the known load applied to the member, and the processes of numerical integration, can be used to calculate the stress-strain curve in flexural compression. With the strength in uniaxial compression of the cubes and cylinders, as well as the stress block parameters known, the Modified Size Effect Law can be used to describe the effect of specimen size on the cube strength, cylinder strength, and stress block parameters, with different equations being generated for each of the respective mixes.

A comparison of the error between the predicted Moment-Axial force (M-N) interaction diagram, obtained by using the BS 8110-1 (1997), SANS 0100-1 (2000), ACI-318 (2014), and EN 1992-1-1 (2004) codes, and the actual M-N interaction diagram, obtained from the experimental points, were made and conclusions regarding their applicability for the design of concrete containing South African materials drawn. Lastly, the flexural stress-strain behaviour was modelled, and a comparison made between the calculated and actual stress block parameters.

1.5 REPORT ORGANISATION

The report consists of the following chapters and appendices:

- Chapter 1 serves as introduction to the report
- Chapter 2 contains a technical introduction based on a literature study.
- Chapter 3 describes the materials and experimental procedures used to obtain the field observations.
- Chapter 4 describes the analysis and detailed description of the field observations.
- Chapter 5 provides the final conclusions and recommendations of the study
- Chapter 6 contains a list of references
- Appendix A contains the data obtained by other researchers used in this report

© University of Pretoria

CHAPTER 2

LITERATURE REVIEW

2.1 INTRODUCTION

This chapter provides a brief background the composition of concrete, and the factors influencing its compressive strength, modulus of elasticity, and flexural compressive strength. Special consideration is given to the compressive stress-strain models and previous methods used to estimate flexural stress-strain distribution and stress block parameters. Finally, the influence of specimen size and shape on the uniaxial compressive strength and flexural compressive strength is discussed in detail.

2.2 CONCRETE COMPOSITION AND FACTORS INFLUENCING ITS BEHAVIOUR

Concrete is a multiphase material consisting mainly of a mixture of cement, water, fine aggregate, and coarse aggregate. After mixing, the cement and water undergo a series of chemical hydration reactions resulting in the cement hardening, so binding the aggregate to form a complex three dimensional structure. In the early stages subsequent to mixing, the cement is consuming water. As the volume originally occupied by the mix constituents progressively reduce, a gradual decrease in the cement paste volume occurs (Domone & Illston, 2010). The reduction in volume, or shrinkage, is restrained by the more dimensionally stable aggregate, inducing tensile strains and corresponding tensile stresses. Once these tensile stresses exceed the tensile capacity of the concrete micro-cracks are formed in the transition zone between aggregates and the cement paste matrix. Within the hardened cement paste, two types of pores, denoted as the gel and capillary pores, exists. These pores are the remains of the space originally occupied by water in the fresh paste that prior to the setting of the paste were all connected. In its densest state the cement gel in the hydrated cement paste is about one third pores and two thirds solids (Ownes, 2009). Thus, unlike most structural materials, concrete contains micro-cracks even before being loaded. These micro-cracks, coupled with the pores present in the hardened cement paste matrix, have significant influence on both the compressive strength and the stiffness (Mehta, 1986). In general, there exists an inverse relationship between porosity and strength given by Equation 2.1 (Mehta, 1986):

$$\sigma = \sigma_0 \times e^{-k \times P} \qquad 2.1$$

Where:

σ= The strength of the material at a given porosity p

© University of Pretoria

σ_0= The intrinsic strength at a porosity of zero

k= A constant

For mortar and hardened cement paste, the porosity is indeed related to strength, but the same cannot be said for concrete. The presence of micro-cracks makes concrete too complex a material for predicting of strength by using the simple strength porosity relationship. However, the validity of the strength porosity relationship still needs to be respected, as the porosity of the component phases will most likely turn out to be the strength limiting factor. From a practical point of view, the measurement of the porosity of the aggregate, transition zone, and cement matrix is not feasible. However, enough research has been done to provide information about the influence of copious factors on compressive strength (Park & Paulay, 1975). According to Mehta (1986), the factors that influence the compressive strength of concrete may broadly be divided into three categories namely: characteristics of materials and mix proportions, curing conditions, and testing parameters. A summary of the interaction between parameters and factors influencing concrete strength is shown in Figure 2.1, with an explanation of the relevant variables being provided in the subsequent sections.

2.2.1 WATER/CEMENT RATIO

The water/cement ratio, more accurately the water/binder ratio, is the ratio between the volume of water present in the concrete mix and the mass of cement or binder material present in the mix. As the water/cement ratio is directly coupled to the amount of water present in the mix, it influences numerous intrinsic and behavioural characteristics including workability, durability, strength, and stiffness. The influence of the water/cement ratio on concrete strength is due to of the progressive weakening of the cement paste matrix caused by an increase in porosity. This does, however, not provide an explanation for the effect of water/cement ratio on the transition zone (boundary layer between the hardened cement paste and aggregate). For low-and-medium strength concrete containing normal density aggregate, both the matrix and transition zone porosity determine the strength, with a direct relationship between water/cement ratio and concrete strength.

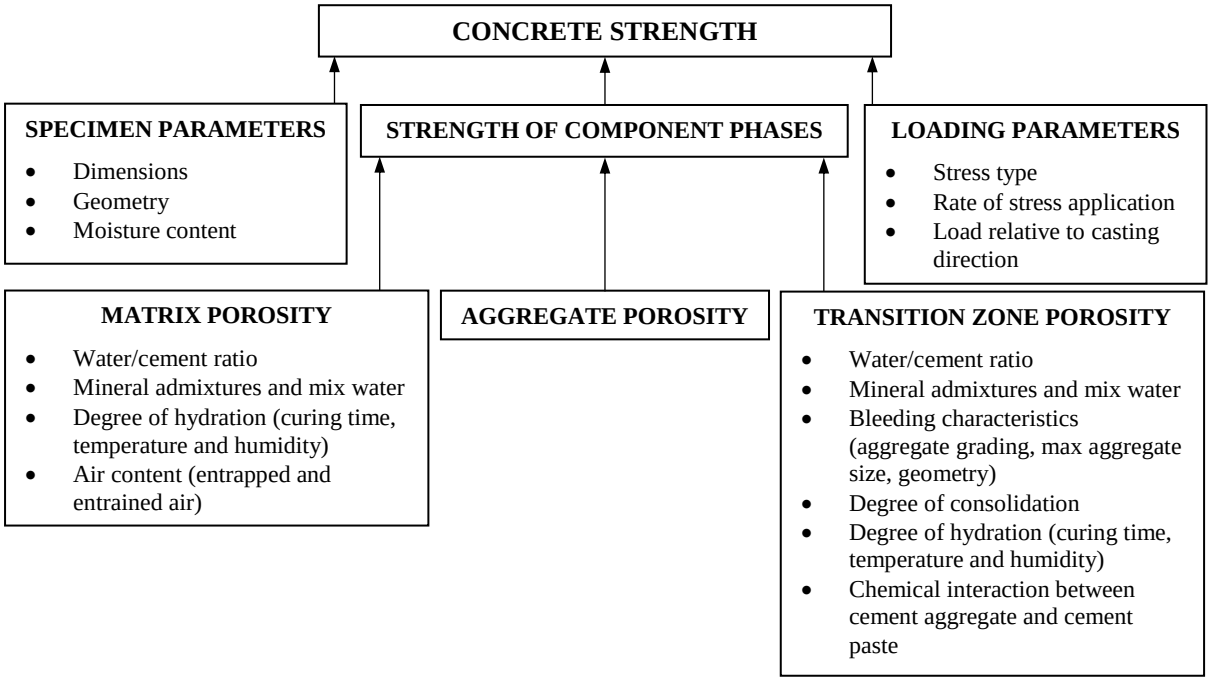

Figure 2.1 Factors Influencing Concrete Strength Adapted from Mehta (1986)

© University of Pretoria

For high strength concrete, however, a disproportional increase in compressive strength can be achieved with a small reduction in water/cement ratio. This phenomenon can be attributed to the significant improvement in transition zone strength (Mehta, 1986). Figure 2.2, illustrates the relationship between water/cement ratio and concrete strength.

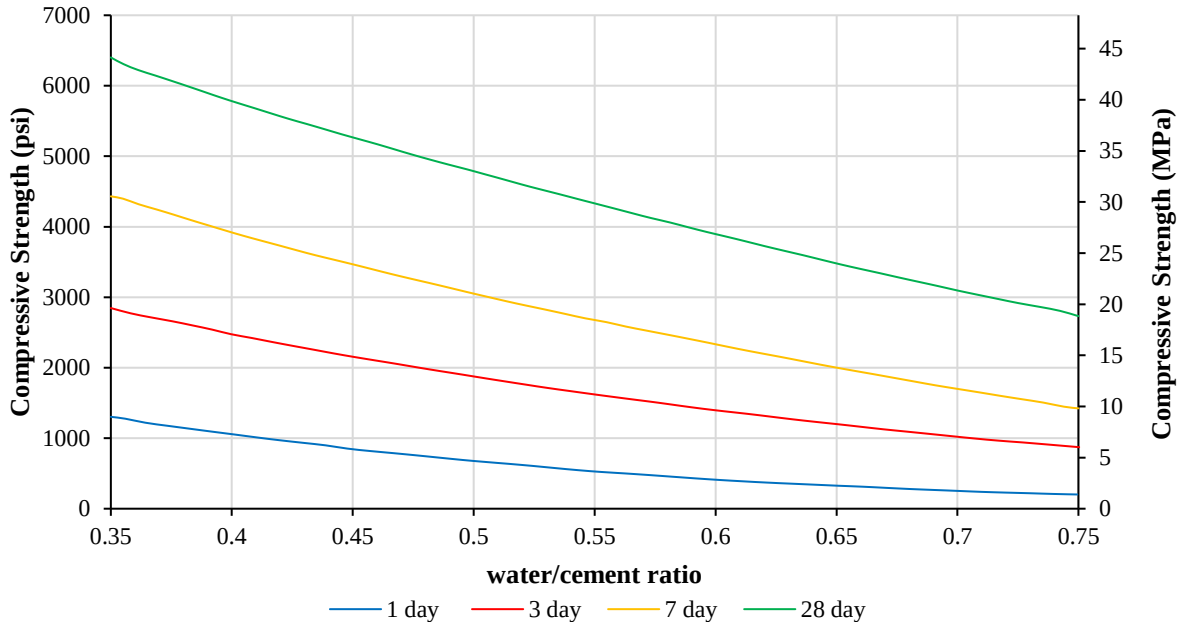

Figure 2.2 Influence of Water/Cement Ratio on Concrete Compressive Strength Adapted from Mehta (1986)

2.2.2 CEMENT TYPE AND ADDITIONS (CEMENT EXTENDERS)

The type of cement has an effect on both the strength that can theoretically be achieved and the rate of strength gain. Depending on the cement designation, the rate of strength development may either be rapid or normal. Cement can also be partially replaced with cement extenders. Cement extenders or additions are materials that undergo a pozzolanic reaction when mixed with alkalis in the presence of moisture. A material is referred to as pozzolanic if it contains active silica (SiO_2), is not cementitious by itself, and will in the presence of moisture react with calcium hydroxide to form cementitious compounds. Ground Granulated Blast furnace Slag (GGBS), Fly Ash (FA), and Micro Silica also called Condensed Silica Fume (CSF), are some of the commercially available extenders in South Africa. Cement extenders are all by-products and has found an increased use, especially in the manufacturing of high strength concrete.

2.2.2.1 GROUND GRANULATED BLAST FURNACE SLAG AND FLY ASH

Ground Granulated Blast Furnace Slag (GGBS or GGBFS), is a by-product of the iron smelting industry. The slag is obtained by rapidly cooling scum formed during the iron smelting process with one of two techniques known as Granulation and Palatalization. The GGBS granulates are then dried, and grounded to a fineness similar to the fineness of cement (Domone & Illston, 2010).

When burned, the pulverised coal used to fire gas power stations, produce exhaust gasses that can be captured before being discharged to the atmosphere. Only some of the ash has the recommended particle size and composition, which after isolation can be sold as FA (Ownes, 2009).FA has a noticeable effect on a number of properties of both fresh and hardened concrete including a reduction in porosity, permeability, potential for alkali

© University of Pretoria

aggregate reaction, heat of hydration, creep, shrinkage, as well as an *increase* in freeze/thaw resistance, strength, and rate of strength development. The partial replacement of Ordinary Portland Cement with FA, will slow down the rate of early strength development. However, the long term strength may be greater if adequate moisture is available for cement hydration at later stages.

2.2.2.2 CONDENSED SILICA FUME

Condensed Silica Fume also called Micro Silica is a by-product condensed from waste gases exerted in the manufacturing of silicon metal. The main advantages of CSF is a reduction in porosity and correspondingly the permeability and bleeding. However, the use of CSF will result in a higher water demand, lower workability, but most importantly, a significant increase in the strength and rate of strength development. This improvement in strength is markedly more than that of concrete containing equal amounts of FA or GGBS, which has resulted in CSF being a primary ingredient in the manufacturing of high strength concrete with strengths in excess of 80.0 MPa (11.61 ksi) (AfriSam Technical Reference Guide, 2013).

2.2.3 ADMIXTURES

Chemical admixtures are materials (soluble and insoluble) other than the four basic constituents of concrete which when added to mortar, grout, or concrete during mixing, modifies one or more of its properties. The fresh concrete properties that can be modified include workability, settling time, segregation potential, pumpability, and bleeding, while the modifiable hardened properties include an inprovement in the rate of early age strength development, 28 day strength, and durability at a constant cement content. Commercially available admixtures, established to have an influence on concrete strength, include air entrainers, plasticising or water-reducing admixtures, high range water reducers or super-plasticising admixtures, retarders, and accelerators (Ownes, 2009).

2.2.3.1 ENTRAINED AND ENTRAPPED AIR

The most important factor influencing the porosity of the cement paste matrix, at a given degree of hydration, is the water/cement ratio. However, the incorporation of air voids into the system, due to either inadequate compaction or through the addition of air entraining admixtures, also increases the porosity with a corresponding reduction in specimen strength. The extent of strength loss, as a result of entrained air, depends not only on the water/cement ratio, but also on the cement content, with the strength reduction more prominent as the cement content increases, as would commonly be the case for high strength concrete (Mehta, 1986). The reduction in compressive strength due to entrained air may be offset with a reduction in water/cement ratio. The small air bubbles acts as a lubricant, increasing the workability whilst also reducing the volume of fine aggregate required to achieve a specified consistence.

2.2.3.2 PLASTICISERS OR WATER REDUCERS

Plasticisers, similar to some air-entrainers, exhibit surface activity and functions by physical absorption onto the surface of the aggregate and cement grain particles. The absorption of water reducers on to the surface of the cement particles has a dispersive effect, but the cement retains its hydrophillicity. As a result, it is possible to achieve an improved workability at the same water/cement ratio and a small acceleration in rate of strength development (due to the cement conglomerates breaking up) potential (Ownes, 2009).

© University of Pretoria

2.2.4 AGGREGATE

For most natural aggregates, the strength of the aggregate is barely utilised as failure is governed by the other two phases. There are however aggregate characteristics such as the size, shape, surface texture, particle size distribution, mineralogy, and density, which are known to affect the concrete strength and stiffness (Mehta, 1986).

2.2.4.1 SIZE

The maximum size of the coarse aggregate has two opposing effects on the strength of the concrete. Water, not only reacts with cementations materials, but provides the lubrication necessary to achieve a good workability. In general, the smaller the particle size of the aggregate and cementations materials, the greater the surface to be lubricated by the water and the lower the workability. With all other mix variables left unaltered, concrete mixes containing large coarse aggregate particles requires less mixing water than those containing smaller aggregates. However, larger aggregate particles tend to form weaker transition zones due to excessive bleed water being trapped under the aggregate, increasing the transition zone porosity, and reducing the strength of the aggregate paste interface (Mehta, 1986).

2.2.4.2 GRADING

The bleeding characteristics of a concrete mix are influenced by the particle size distribution of the cementations materials, fine aggregate, and coarse aggregate. With the water/cement ratio and the coarse aggregate size constant, it has been found that a change in aggregate grading produces a significant change in the bleeding characteristics and consistency of concrete (Mehta, 1986). This change in consistency either result in improper compaction (due to the low workability) or segregation (if an insufficient amount of fine material is present), both of which reduce the concrete strength and stiffness.

2.2.4.3 TEXTURE

Similar to aggregate size, aggregate texture also has an affect on the strength of concrete. With all other mix variables constant, rough textured aggregates (crushed aggregates), as opposed to smooth textured aggregate, show a higher early age strength, with a stronger physical bond between the aggregate and cement paste assumed to be responsible for this difference. For mature concrete, these differences become less pronounced. On the other hand, smooth textured aggregates require less mixing water than rough textured aggregates to achieve the same workability. Thus, the reduction in early age strength, obtained by using smooth textured aggregates, can be offset by reducing the water/cement ratio (Mehta, 1986).

2.2.5 CURING CONDITIONS

Proper curing is dependent on the time, humidity, and temperature, and is essential for the hydration of the cement and cement extenders, and optimal strength development.

Time: The time strength relationship for concrete assumes that the concrete is cured at normal temperatures and under moist conditions. If it can be assumed that the hydration of the cement particles are continuing, then the longer the curing time, the higher the concrete strength.

© University of Pretoria

Humidity: According to Mehta (1986), the continuously moist cured strength of concrete is three times the continuous air cured strength. A minimum curing period of 7 days is generally recommended for concrete containing Ordinary Portland cement. The use of blended cements or mineral admixtures lengthens the curing time. Moist curing is provided by spraying, ponding, curing membranes, plastic wrapping, or by covering the surface of the concrete with wet cotton mats, sawdust, or sand.

Temperature: For a temperature range between 4˚C and 46˚C, moist cured concrete cast and cured at a constant temperature, generally shows an improved early age strength development up to 28 days. The 28 day strength of concrete cast and cured at 4.5˚C, is about 80% of that cast and cured at 21˚C to 46˚C. It should however be noted that the ultimate strength could reduce for curing times in excess of 28 days (Mehta, 1986).

2.2.6 SPECIMEN PARAMETERS

Specimen Dimension and Specimen Geometry: As concrete is a brittle material, the apparent strength and the variability in the results decreases as the physical size of the specimen increases. In the United States of America, the compressive strength of concrete is determined by crushing 152 x 305 mm (6 x 12 in.) cylinders, while in South Africa the compressive strength of concrete is determined by crushing either 100 mm or 150 mm cubes. Mehta (1986) concluded that the larger the diameter of the concrete specimen, the lower its strength (maintaining a height/diameter ratio of two). In general, the effect of a change in specimen geometry (height/diameter ratio) is that the larger the height/diameter ratio becomes, the lower the strength of the concrete specimen (Mehta, 1986). A more exhaustive discussion regarding the effect of size on the cube compressive strength, cylinder compressive strength, and flexural compressive strength of unconfined concrete can be found in section 2.6.

Moisture Content: According to Ownes (2009), a reduction in moisture content would produce an increase in concrete strength. The compression of the water in the hardened cement paste matrix pores raises the internal pressure, which is uniform in all directions (including the direction of lateral tensile expansion). This reduces the compressive strength due to an increased tensile stress in the direction perpendicular to testing.

2.2.7 LOADING CONDITIONS

Loading rate: The compressive strength of concrete is obtained by crushing a concrete specimen in uniaxial compression at a given loading rate. According to SANS 5863 (2006), the rate of compressive load application needs to be 0.3 MPa/s ± 0.1 MPa/s (44 psi/s ± 15 psi/s) until the specimen fails. Similarly, ASTM C39/C39M (2015) specifies a loading rate of 0.24 MPa/s ± 0.05 MPa/s (35 psi/s ± 7 psi/s) until failure. The slower the rate of loading, the lower the apparent compressive strength.

Specimen Casting Direction: The direction in which the specimen is cast and subsequently tested has a marked influence on the compressive strength. As mentioned before, South Africa use cubes while the United States of America use cylinders to evaluate the compressive strength of concrete. Both cube and cylinder specimens are cast in a vertical direction, with bleed water migrating to the top of the section. A portion of the bleed water is trapped under the aggregate particles, increasing the porosity of the transition zone. Once the concrete cube and cylinder has hardened, it is demoulded and cured until the appropriate age for testing. However, the direction of testing for a cube and cylinder is not the same. According to SANS 5863 (2006), concrete cubes are crushed

© University of Pretoria

perpendicular to the casting direction. ASTM C39/C39M (2015) on the other hand specifies that the cylinders should be capped/grinded and tested in the same direction as originally cast.

2.3 COMPRESSIVE STRENGTH OF CONCRETE

The development of plasticisers and the subsequent development of large range water reducers (superplasticisers), has catapulted the compressive strength of concrete to new extremes. Today, concrete may be classified as normal or high strength. According to Newman & Choo (2003), high strength concrete may be classified as concrete with a compressive strength greater than the current design codes and standards, which, in South Africa, will change from a cube strength of 60.0 MPa to 105.0 MPa (5.8 ksi to 13.1 ksi) with the adoption of EN 1992-1-1 (2004).

In a compression test, a test specimen is assumed to have failed if there is no sign of external fracture, but internal fracture has advanced to such an extent that the specimen cannot carry a numerically larger load. In South Africa, the compressive strength of concrete was traditionally measured by crushing either 100 mm or 150 mm concrete cubes. However, with the introduction of EN 1992-1-1 (2004), the compressive strength should be obtained by crushing either 150 mm cubes or 150 x 300 mm cylinders. Even though it may be the same concrete mix being tested, there is a notable difference between the cylinder and cube compressive strengths.

Cylinder compressive strengths are referred to as either a confined or unconfined compressive strength. Figure 2.3, shows the typical stress-strain curves obtained from *unconfined* cylinders loaded in uniaxial compression. From Figure 2.3, it can be deduced that the stress-strain curves are linear to about half the compressive strength, with a sharp peak for high strength concrete and a flatter top for medium strength concrete when the maximum compressive strength is reached. The region prior to the maximum strength is referred to as the ascending portion of the stress-strain curve, and the region after the peak strength the descending portion of the curve. Figure 2.3 also shows that the shape of the stress-strain curve does not stay constant.

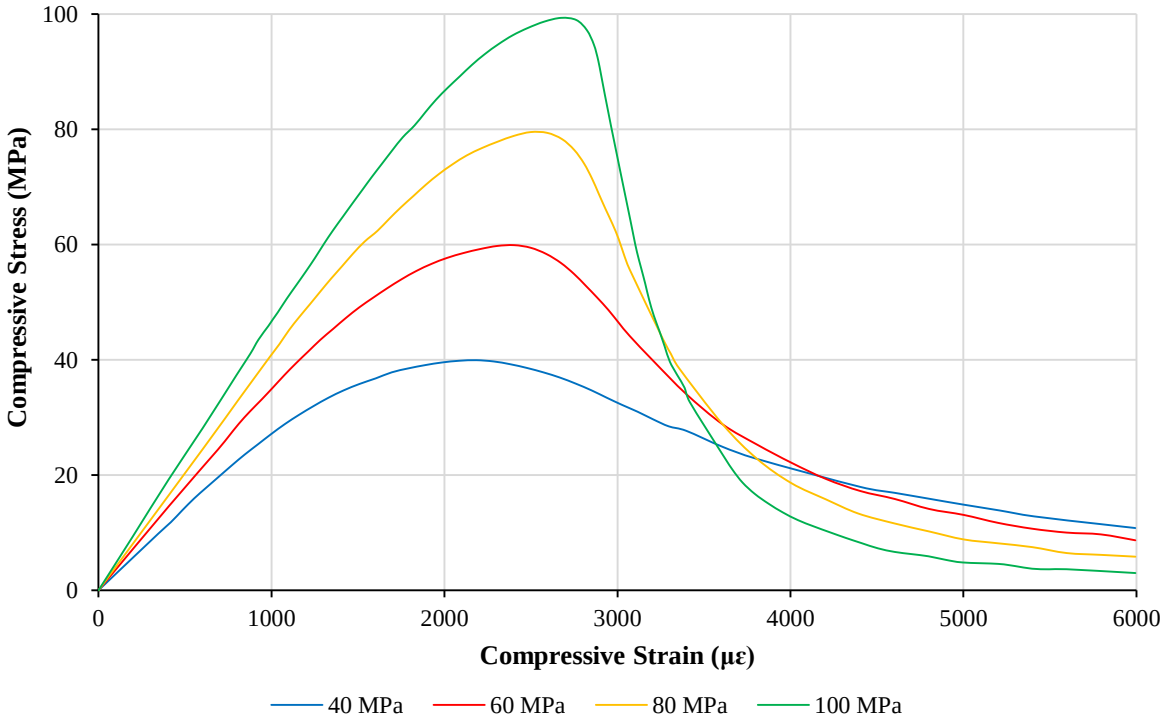

Figure 2.3 Uniaxial Compression Stress-Strain Curves Adapted from Ho et al. (2002)

© University of Pretoria

Tests performed by Rusch (1960), concluded that the shape of the stress-strain curve, before the maximum stress, is dependent on the compressive strength of the concrete. Also, depending on the compressive strength, the strain at maximum compression will vary between 0.002 and 0.003 (Rusch, 1960).

The linearity of any structural material is dependent on the elastic modulus (modulus of elasticity). There are two forms of elastic moduli, the tangential modulus, which is slope of the tangent to the curve at any particular stress, and the secant modulus, which is the slope of the line connecting the origin of the stress-strain curve to a selected stress level. For stress levels not exceeding 30% to 40% of the ultimate strength, the stress-strain behaviour may be regarded as being effectively linear. The slope of the tangent to the stress-strain curve at the origin is referred to as the initial tangent modulus (Ownes, 2009).

2.3.1 NONLINEARITY OF STRESS-STRAIN BEHAVIOUR

As mentioned before, the presence of micro-cracks in the transition zone, and the subsequent development and interlinking of micro-cracks in the cement paste matrix, influence both the strength and the stiffness of concrete. Based on the work done by Hsu et al. (1963), Figure 2.4 confirms that the stress-strain behaviour, more specifically the stiffness of concrete, lies between that of the aggregate and the hardened cement paste.

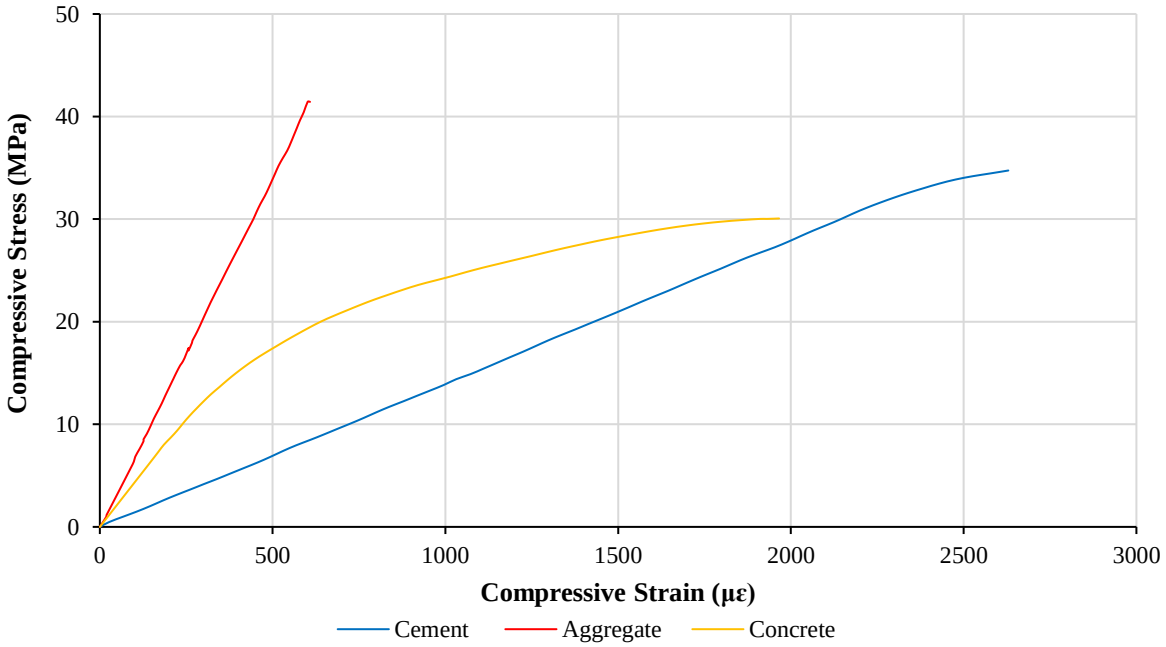

Figure 2.4 Stress-Strain Curves of Cement Paste, Aggregate, and Concrete Adapted from Hsu et al. (1963)

Mehta (1986) states that below 30% of the ultimate compressive strength, the stress-strain behaviour remains linear, with the transition zone cracks considered to remain stable. Between 30% and 50% of the ultimate strength, the number, width, and length of micro-cracks in the transition zone start to increase, and the curve starts to deviate from a straight line. This system of micro-cracks is, however, still assumed to be stable. For load levels between 50% and 60% of the ultimate load, micro-cracks start to form in the hardened cement paste matrix, and at 75% of the ultimate compressive strength, the crack system in the transition zone becomes unstable. Thus, beyond 75% of the ultimate compressive strength, the crack system becomes continuous and causes the failure of the specimen once interlinked. Since the stress-strain behaviour of concrete plays such an intricate role in its design, it comes as no surprise that various models have been developed to describe the stress-strain behaviour.

© University of Pretoria

2.3.2 STRESS-STRAIN MODELS FOR THE COMPRESSION ZONE OF CONCRETE

The compressive stress-strain relationship may be obtained by subjecting either a confined or unconfined cylinder to a uniaxial stress, or subjecting a concrete member to a flexural compression load and monitoring force and deformation characteristics. Numerous mathematical models have been developed to describe the stress-strain behaviour, however, only the unconfined stress-strain relationships obtained in uniaxial and flexural compression will be considered and presented in this section.

2.3.2.1 JENSEN (1943) MODEL

The first model used to describe the compressive stress-strain relationship was that proposed by Jensen (1943) and had a trapezoidal form. Derived by performing flexural tests, the stress-strain curve consists of two parts (Equation 2.2 and Equation 2.3) providing the elastic and the plastic regions of the stress-strain relationship. It should be noted that Jensen (1943) employed the concept of the plasticity ratio (β) to calculate the ultimate compressive strain.

$$f_c = f_c^{'} \frac{\varepsilon_c}{\varepsilon_{c0}} \text{ for } \varepsilon_c \leq \varepsilon_{c0} \quad \textbf{2.2}$$

$$f_c = f_c^{'} \text{ for } \varepsilon_{c0} < \varepsilon_c \leq \varepsilon_{cu} \quad \textbf{2.3}$$

With:

$$\beta = 1/(1 + (f_c^{'}(\text{ksi})/4)) \quad \textbf{2.4}$$

$$E_c(\text{ksi}) = 30000/5 + 10/f_c^{'}(\text{ksi}) \quad \textbf{2.5}$$

$$\varepsilon_{c0} = f_c^{'}(\text{ksi})/E_c(\text{ksi}) \quad \textbf{2.6}$$

$$\varepsilon_{cu} = f_c^{'}(\text{ksi})/((1\text{-}\beta)E_c(\text{ksi})) + \varepsilon_{c0} \quad \textbf{2.7}$$

Where:

- f_c= The compressive stress in the concrete at a given level of uniaxial strain
- ε_c= The compressive strain in the concrete due to the applied external load
- $f_c^{'}$= The cylinder compressive strength
- ε_{c0}= The strain at the cylinder compressive strength
- ε_{cu}= The ultimate compressive strain
- β= The plasticity ratio
- E_c= The secant modulus of elasticity of concrete

2.3.2.2 HOGNESTAD (1951) MODEL

One of the first widely used approximations was proposed by Hognestad (1951). Equation 2.8 provides the second degree polynomial used to approximate the flexural stress-strain behaviour of the ascending portion of the curve, and Equation 2.9 the relationship used to describe the descending part of the curve. The connection between the maximum stress in flexure ($f_c^{''}$) and the cylinder compressive strength ($f_c^{'}$) was provided through a factor k_3. In total, 120 specimens were tested, ninety of which were square with side lengths of 254 mm (10 in.), and thirty

© University of Pretoria

305 mm (12 in.) diameter cylindrical specimens. The main test variables were the volume of reinforcing, eccentricity of the load, and three target strengths of 13.8 MPa, 24.1 MPa, and 34.5 MPa (2 ksi, 3.5 ksi, and 5 ksi). The extent of the falling branch is dependent on the limit of useful concrete strain.

$$f_c = k_3 f_c' \left[\frac{2\varepsilon_c}{\varepsilon_{c0}} - \left(\frac{\varepsilon_c}{\varepsilon_{c0}}\right)^2\right] \text{ for } \varepsilon_c \leq \varepsilon_{c0} \quad \textbf{2.8}$$

$$f_c = k_3 f_c' - \left[\left(0.1275 f_c'\right)\frac{(\varepsilon - \varepsilon_{c0})}{(\varepsilon_{cu} - \varepsilon_{c0})}\right] \text{ for } \varepsilon_{c0} < \varepsilon_c \leq \varepsilon_{cu} \quad \textbf{2.9}$$

With:

$$E_c(\text{psi}) = 1800000 + 460 f_c'(\text{psi}) \quad \textbf{2.10}$$

$$\varepsilon_{c0} = 2 \times k_3 f_c'(\text{psi}) / E_c(\text{psi}) \quad \textbf{2.11}$$

$$\varepsilon_{cu} = 0.0038 \quad \textbf{2.12}$$

Where:

k_3= The ratio between the maximum flexural strength and strength of a uniaxialy loaded cylinder

2.3.2.3 DESAYI & KRISHNAN (1964) MODEL

Desayi & Krishnan (1964) used the accending-cuve stress-strain relationship proposed by Hognestad (1951) to describe both the ascending and descending portions of the stress-strain curve. This relationship, presented in Equation 2.13, is based on short term loading tests, and utilises the same relationships for E_c, ε_{c0}, and ε_{cu} as origionaly proposed by Hognestad (1951).

$$f_c = \frac{(2 f_c'/\varepsilon_{c0}) \times \varepsilon_c}{(1 + (\varepsilon_c/\varepsilon_{c0})^2)} \quad \textbf{2.13}$$

2.3.2.4 SARGIN & HANDA (1969) MODEL

The second degree rational equation proposed by Sargin & Handa (1969), sought to describe the descending portion of the stress-strain curve more accurately. The influence of the modulus of elasticity, compressive strength, lateral reinforcement, strain gradient, and core-gross area ratio on the behaviour of concrete are considered by this model (Equation 2.14). It should be noted that the parameter B was introduced with the sole intention of describing the slope of the descending portion of the stress-strain curve more accurately.

$$f_c = k_3 f_c' \times \left[\frac{A(\varepsilon_c/\varepsilon_{c0}) + (B\text{-}1)(\varepsilon_c/\varepsilon_{c0})^2}{1 + (A\text{-}2)(\varepsilon_c/\varepsilon_{c0}) + B(\varepsilon_c/\varepsilon_{c0})^2}\right] \quad \textbf{2.14}$$

With:

$$E_c(\text{psi}) = 72000\sqrt{f_c'(\text{psi})} \quad \textbf{2.15}$$

$$\varepsilon_{c0} = 0.0021 \quad \textbf{2.16}$$

$$A = E_c(\text{psi})\varepsilon_{c0} / k_3 f_c'(\text{psi}) \quad \textbf{2.17}$$

$$B = 0.65\text{-}5 \times 10^{-5} f_c'(\text{psi}) \quad \textbf{2.18}$$

© University of Pretoria

2.3.2.5 KENT & PARK (1971) MODEL

Kent & Park (1971) based their model on the parabolic relationship proposed by Hognestad (1951). This model describes the stress-strain relationship for both confined and unconfined concrete. The post peak behaviour, or the falling branch of the stress-strain curve, was modelled more accurately by setting $\varepsilon_{c0} = 0.002$ and replacing $0.85f_c^{''}$ with $f_c^{'}$. The expressions describing the ascending and descending branches are given by Equation 2.19 and Equation 2.20 respectively. Equation 2.20 is a line, the slope of which is a function of compressive strength and the percentage reinforcing (which for unconfined concrete is zero). It should be noted that Equation 2.19 assumes that the presence of confining steel in the compression zone, has no affect on the stress-strain properties until the point at which the maximum concrete stress is reached.

$$f_c = f_c^{'}\left[\frac{2\varepsilon_c}{\varepsilon_{c0}} - \left(\frac{\varepsilon_c}{\varepsilon_{c0}}\right)^2\right] \text{ for } \varepsilon_c \leq \varepsilon_{c0} \quad \textbf{2.19}$$

$$f_c = f_c^{'}[1\text{-}Z(\varepsilon_c\text{-}\varepsilon_{c0})] \text{ for } \varepsilon_{c0} < \varepsilon_c \leq \varepsilon_{cu} \quad \textbf{2.20}$$

With:

$$Z = 0.5/(\varepsilon_{50u}\text{-}\varepsilon_{c0}) \quad \textbf{2.21}$$

$$\varepsilon_{c0} = 0.002 \quad \textbf{2.22}$$

$$\varepsilon_{50u} = \left(3 + 0.002f_c^{'}(\text{psi})\right)/\left(f_c^{'}(\text{psi})\text{-}1000\right) \quad \textbf{2.23}$$

Where:

ε_{50u}= Is the strain corresponding to a stress of $0.5f_c^{'}$

2.3.2.6 POPOVICS (1973) MODEL

Equation 2.24 illustrates the simplicity of the model proposed by Popovics (1973) that requires only three parameters $f_c^{'}$, ε_{c0}, and n to describe the ascending and descending branches of the stress-strain curve. The power n is expressed as a function of the compressive strength for normal density aggregate. For concrete strengths lower than 55.0 MPa (8 ksi), Popovics' (1973) model provides accurate results; however, for strengths in excess of 55.0 MPa (8 ksi), this model does not describe the post peak behaviour accurately.

$$f_c = f_c^{'} \times \left[\frac{n(\varepsilon_c/\varepsilon_{c0})}{(n\text{-}1) + (\varepsilon_c/\varepsilon_{c0})^n}\right] \quad \textbf{2.24}$$

With:

$$n = 4 \times 10^{-4} f_c^{'}(\text{psi}) + 1.0 \quad \textbf{2.25}$$

$$\varepsilon_{c0} = f_c^{'}/E_c\,(n/(n\text{-}1))=2.7 \times 10^{-4}\sqrt[4]{f_c^{'}(\text{psi})} \quad \textbf{2.26}$$

2.3.2.7 WANG et al. (1978A) & WANG et al. (1978B) MODEL

Wang et al. (1978a) set up a relatively simple experiment to determine the uniaxial stress-strain curve for normal weight and lightweight concrete, with strengths ranging between 21.0 MPa and 77.0 MPa (3.05 ksi and 11.18 ksi) and 21.0 MPa and 56.0 MPa (3.05 ksi and 8.13 ksi) respectively. For the experiment, 76 x 152 mm (3 x 6 in.)

© University of Pretoria

cylinders were used to obtain the stress-strain behaviour, and similar sized cylinders crushed on the day of testing to obtain the cylinder compressive strength. Equation 2.27 was used to describe the ascending and descending branches of the stress-strain curve, with the coefficients being obtained from the relevant boundary conditions. The accuracy of this model can be improved by using separate sets of coefficients (A, B, C, and D) for the ascending and descending branches of the curve, as shown in Table 2.1.

$$f_c = f_c^{'} \times \left[\frac{A(\varepsilon_c/\varepsilon_{c0}) + B(\varepsilon_c/\varepsilon_{c0})^2}{1 + C(\varepsilon_c/\varepsilon_{c0}) + D(\varepsilon_c/\varepsilon_{c0})^2}\right] \quad \textbf{2.27}$$

For the ascending branch, the following operations are performed to obtain the constants. E_c represents the secant modulus of elasticity at $f_c = 0.45f_c^{'}$:

$$\left\{\begin{array}{c} \left(\frac{df_c}{d\varepsilon_c} = \frac{E_c}{E_i}\middle|\frac{f_c}{f_c^{'}} = 0 \text{ for } \frac{\varepsilon_c}{\varepsilon_{c0}} = 0\right) \\ \left(\frac{df_c}{d\varepsilon_c} = \frac{E_c}{E_i}\middle|\frac{f_c}{f_c^{'}} = 0.45 \text{ for } \frac{\varepsilon_c}{\varepsilon_{c0}} = \frac{0.45}{E_c/E_o}\right) \\ \left(\frac{df_c}{d\varepsilon_c} = \frac{E_c}{E_i}\middle|\frac{f_c}{f_c^{'}} = 1 \text{ for } \frac{\varepsilon_c}{\varepsilon_{c0}} = 1\right) \\ \left(\frac{df_c}{d\varepsilon_c} = 0\middle|\frac{f_c}{f_c^{'}} = 1 \text{ for } \frac{\varepsilon_c}{\varepsilon_{c0}} = 1\right) \end{array}\right\}$$

For the descending branch, the conditions for determining the four constants are:

$$\left\{\begin{array}{c} \frac{f_c}{f_c^{'}} = 1 \text{ for } \frac{\varepsilon_c}{\varepsilon_{c0}} = 1 \\ \left(\frac{df_c}{d\varepsilon_c} = 0\middle|\frac{f_c}{f_c^{'}} = 1 \text{ for } \frac{\varepsilon_c}{\varepsilon_{c0}} = 1\right) \\ \frac{f_c}{f_c^{'}} = \frac{f_i}{f_c^{'}} \text{ for } \frac{\varepsilon_c}{\varepsilon_{c0}} = \frac{\varepsilon_i}{\varepsilon_{c0}} \\ \frac{f_c}{f_c^{'}} = \frac{f_{2i}}{f_c^{'}} \text{ for } \frac{\varepsilon_c}{\varepsilon_{c0}} = \frac{\varepsilon_{2i}}{\varepsilon_{c0}} \end{array}\right\}$$

Where:

E_i= The tangential modulus of elasticity or the slope of a tangent line to the curve at the origin

ε_i= The strain at the inflection point of the curve

f_i= The stress at the inflection point of the curve

ε_{2i}= The strain at a point on the stress-strain curve such that ε_{2i}-$\varepsilon_i = \varepsilon_i$-$\varepsilon_{c0}$

f_{2i}= The stress at a point on the stress-strain curve corresponding to the strain ε_{2i}

Table 2.1 Stress–Strain Relationship Constants Proposed by Wang et al. (1978a) and Wang et al. (1978b)

		Ascending				Descending			
$f_c^{'}$(MPa) (ksi)	**ε_{c0}**	**A**	**B**	**C**	**D**	**A**	**B**	**C**	**D**
20.7 (3)	0.00267	1.597	-0.352	-0.403	0.648	-1.2758	1.4795	-3.2758	2.4795
27.6 (4)	0.0028	1.4434	-0.6425	-0.5566	0.3574	0.1153	0.3064	-1.8847	1.3064
34.5 (5)	0.00292	1.3648	-0.759	-0.6352	0.242	0.3264	0.048	-1.6736	1.048
41.3 (6)	0.00305	1.3237	-0.8095	-0.6763	0.1905	0.3659	-0.0507	-1.6341	0.9493
48.2 (7)	0.00317	1.304	-0.832	-0.696	0.168	0.3576	-0.0956	-1.6424	0.9415
55.1 (8)	0.0033	1.2977	-0.8388	-0.7023	0.1612	0.3326	-0.1163	-1.6674	0.8837
62.0 (9)	0.00342	1.3004	-0.836	-0.6996	0.164	0.3019	-0.1244	-1.6981	0.8756
68.9 (10)	0.00355	1.3092	-0.8261	-0.6908	0.1739	0.2697	-0.1253	-1.7303	0.8747
75.8 (11)	0.00367	1.3227	-0.8107	-0.6773	0.1893	0.238	-0.1218	-1.762	0.8782
82.7 (12)	0.0038	1.3395	-0.7904	-0.6605	0.2096	0.2078	-0.1154	-1.7922	0.8846
89.6 (13)	0.00392	1.359	-0.7657	-0.641	0.2343	0.1796	-0.1071	-1.8204	0.8929

© University of Pretoria

2.3.2.8 TOMASZEWICZ (1984) MODEL

Tomaszewicz (1984) aimed to develop a relationship capable of accurately encompassing the stress-strain behaviour of high strength concrete, by modifying the expression proposed by Popovics (1973) through the addition of a parameter k. The relationship shown in Equation 2.28, is limited to compressive strengths of 85 MPa (12.34 ksi) because the denominator for Equation 2.30 becomes zero.

$$f_c = f_c^{'}\left[\frac{n(\varepsilon_c/\varepsilon_{c0})}{(n\text{-}1) + (\varepsilon_c/\varepsilon_{c0})^{k\times n}}\right] \quad \textbf{2.28}$$

With:

$$\varepsilon_{c0} = 0.7\left(f_c^{'}(MPa)\right)^{0.31}/1000 \quad \textbf{2.29}$$

$$n = 8.32/(8.32\text{-}\left(f_c^{'}(MPa)\right)^{0.475}) \quad \textbf{2.30}$$

$$k = \begin{Bmatrix} (1|\varepsilon_c \le \varepsilon_{c0}) \\ (f_c^{'}(MPa)/20 \,|\, \varepsilon_c > \varepsilon_{c0}) \end{Bmatrix} \quad \textbf{2.31}$$

Utilising the same equation as Tomaszewicz (1984) for the stress-strain relationship, Collins & Porasz (1989) proposed Equation 2.32 and Equation 2.33, and Collins et al. (1993), Equation 2.34 and Equation 2.35, defining new relationships for n and k.

$$n = 0.8 + f_c^{'}(ksi)/2.5 \quad \textbf{2.32}$$

$$k = 0.67 + f_c^{'}(ksi)/9 \ge 1 \quad \textbf{2.33}$$

$$n = 0.8 + f_c^{'}(MPa)/17 \quad \textbf{2.34}$$

$$k = \begin{Bmatrix} (1|\varepsilon_c \le \varepsilon_{c0}) \\ (0.7 + f_c^{'}(MPa)/20|\varepsilon_c > \varepsilon_{c0}) \end{Bmatrix} \quad \textbf{2.35}$$

2.3.2.9 CARREIRA & CHU (1985) MODEL

Carreira & Chu (1985) proposed the use of Equation 2.36 to describe the complete stress-strain curve of unconfined concrete. The strain at the cylinder compressive strength was found to be dependent on the moisture condition of the specimen at the time of testing, and is obtained using Equation 2.37. If *only* the cylinder compressive strength is known, β may be established by using the third order relationship proposed in Equation 2.38. However, if the initial tangential modulus or the modulus of elasticity (obtained according to the ASTM C469/C469M (2014) test procudure) is avalible, β may be established by using the relationship presented in Equation 2.39 or Equation 2.40. Naturaly, estimates of the modulus of elasticity can be made as given by Equation 2.41.

$$f_c = f_c^{'} \times \left[\frac{\beta(\varepsilon_c/\varepsilon_{c0})}{\beta\text{-}1 + (\varepsilon_c/\varepsilon_{c0})^{\beta}}\right] \quad \textbf{2.36}$$

With:

$$\varepsilon_{c0} = \begin{Bmatrix} ((0.00488 f_c^{'}(psi) + 168) \times 10^{-5} | \text{moist cylinders}) \\ (0.002 | \text{dry cylinders}) \end{Bmatrix} \quad \textbf{2.37}$$

$$\beta = \left(f_c^{'}(ksi)/4.7\right)^3 + 1.55 \quad \textbf{2.38}$$

© University of Pretoria

$$\beta = 1/\left[1\text{-}f_c^{'}/(\varepsilon_{c0}E_i)\right] \quad \textbf{2.39}$$

$$\left(0.4\frac{f_c^{'}}{\varepsilon_{c0}E_c}\right)^{\beta}\text{-}\beta\left(\frac{f_c^{'}}{\varepsilon_{c0}E_c}\text{-}1\right)\text{-}1 = 0 \quad \textbf{2.40}$$

$$E_c(psi) = 33\gamma^{1.5}\sqrt{f_c^{'}(psi)} \quad \textbf{2.41}$$

Where:

γ= Unit weight of concrete in lb/ft^3

2.3.2.10 AHMAD & SHAH (1985) MODEL

Ahmad & Shah (1985) proposed the use of both the fractional equation (Equation 2.42) or the combined power and exponential equations (Equation 2.43 for the ascending portion and Equation 2.44 for the descending portion) to represent the stress-strain curve.

$$f_c = f_c^{'} \times \left[\frac{A(\varepsilon_c/\varepsilon_{c0}) + (B\text{-}1)(\varepsilon_c/\varepsilon_{c0})^2}{1 + (A\text{-}2)(\varepsilon_c/\varepsilon_{c0}) + B(\varepsilon_c/\varepsilon_{c0})^2}\right] \quad \textbf{2.42}$$

$$f_c = f_c^{'} \times \left[1\text{-}\left(1\text{-}\frac{\varepsilon_c}{\varepsilon_{c0}}\right)^{A}\right] \text{ for } \varepsilon_c \le \varepsilon_{c0} \quad \textbf{2.43}$$

$$f_c = f_c^{'} \times \exp(\text{-}k(\varepsilon_c\text{-}\varepsilon_{c0})^{1.15}) \text{ for } \varepsilon_{c0} < \varepsilon_c \le \varepsilon_{cu} \quad \textbf{2.44}$$

With:

$$A = E_c(psi)\varepsilon_{c0}/f_c^{'}(psi) \quad \textbf{2.45}$$

$$B = 0.88087\text{-}0.57 \times 10^{\text{-}4}f_c^{'}(psi) \quad \textbf{2.46}$$

$$k = 0.17f_c^{'}(psi) \quad \textbf{2.47}$$

$$\varepsilon_{c0} = 0.001648 + 1.14 \times 10^{\text{-}7}f_c^{'}(psi) \quad \textbf{2.48}$$

$$E_c(psi) = 27.55\gamma^{1.5}\sqrt{f_c^{'}(psi)} \quad \textbf{2.49}$$

2.3.2.11 TSAI (1988) MODEL

Tsai (1988) proposed a generalised form of the Popovics (1973) and the Desayi & Krishnan (1964) model. The introduction of two parameters m and n meant that Tsai's model had greater control over both the pre-and-post peak behaviour. The proposed stress-strain relationship is given by Equation 2.50. The parameter n is used to control the descending branch, while the variable m adjusts the modular ratio, which in turn controls the steepness of the ascending part of the curve. It is interesting to note that if $m = n/(n\text{-}1)$, Equation 2.50 yields the model proposed by Popovics (1973), while $n = 2$ yields the relationship proposed by Desayi & Krishnan (1964).

$$f_c = f_c^{'} \times \left[\frac{m(\varepsilon_c/\varepsilon_{c0})}{1 + [m + n/(n\text{-}1)] \times (\varepsilon_c/\varepsilon_{c0}) + (\varepsilon_c/\varepsilon_{c0})^{n}/(n\text{-}1)}\right] \quad \textbf{2.50}$$

With:

$$n = f_c^{'}(MPa)/6.68\text{-}1.85 \quad \textbf{2.51}$$

$$m = 17.9/f_c^{'}(MPa) + 1 \quad \textbf{2.52}$$

© University of Pretoria

2.3.2.12 HSU & HSU (1994) MODEL

Hsu & Hsu (1994) sought to obtain the complete compressive stress-strain curve of high strength concrete by loading 76 x 152 mm (3 x 6 in.) concrete cylinders to failure. The stress-strain curve for unconfined concrete with strengths not exceeding 68.9 MPa (10 ksi) is given by Equation 2.53 and Equation 2.54. Note that Equation 2.53 is indeed a modified form of the equation originally proposed by Carreira & Chu (1985) with the parameter n being added.

$$f_c = f_c' \times \left[\frac{n\beta(\varepsilon_c/\varepsilon_{c0})}{n\beta\text{-}1 + (\varepsilon_c/\varepsilon_{c0})^{n\beta}}\right] \text{ for } 0 \leq (\varepsilon_c/\varepsilon_{c0}) < (\varepsilon_c/\varepsilon_{c0})_d \quad \textbf{2.53}$$

$$f_c = 0.3 \times (\varepsilon_c/\varepsilon_{c0})_d \times \exp\left[-0.8\left((\varepsilon_c/\varepsilon_{c0}) - (\varepsilon_c/\varepsilon_{c0})_d\right)^{0.5}\right] \text{for } (\varepsilon_c/\varepsilon_{c0}) \geq (\varepsilon_c/\varepsilon_{c0})_d \quad \textbf{2.54}$$

With:

$$\beta = 1/(1\text{-}f_c'/(\varepsilon_{c0}E_i)) \geq 1 \quad \textbf{2.55}$$

It is possible to obtain the parameters f_c', ε_{c0}, n, β, and E_i from uniaxial compressive tests under a constant strain rate. These relationships are presented in Equation 2.56 to Equation 2.59. The parameter n is used to describe the descending portion of the curve (which is dependent on the strain level).

$$\beta = (f_c'(\text{ksi})/9.460)^3 + 2.59 \quad \textbf{2.56}$$

$$E_i(\text{ksi}) = 124.31 \times f_c'(\text{ksi}) + 3283.12 \quad \textbf{2.57}$$

$$\varepsilon_{c0} = 8.9 \times 10^{-5} f_c'(\text{ksi}) + 2.114 \times 10^{-3} \quad \textbf{2.58}$$

$$\left\{\begin{array}{c} (n = 1 \,|\, 0 \leq (\varepsilon_c/\varepsilon_{c0}) < 1) \\ \left(n = 1 \,|\, \varepsilon_{c0} \leq (\varepsilon_c/\varepsilon_{c0}) < (\varepsilon_c/\varepsilon_{c0})_d \text{ and } 0 \leq f_c' < 62 \text{ MPa (9 ksi)}\right) \\ \left(n = 2 \,|\, \varepsilon_{c0} \leq (\varepsilon_c/\varepsilon_{c0}) < (\varepsilon_c/\varepsilon_{c0})_d \text{ and } 62 \text{ MPa (9 ksi)} \leq f_c' < 76 \text{ MPa (11 ksi)}\right) \\ \left(n = 3 \,|\, \varepsilon_{c0} \leq (\varepsilon_c/\varepsilon_{c0}) < (\varepsilon_c/\varepsilon_{c0})_d \text{ and } 76 \text{ MPa (11 ksi)} \leq f_c' < 90 \text{ MPa (13 ksi)}\right) \\ \left(n = 5 \,|\, \varepsilon_{c0} \leq (\varepsilon_c/\varepsilon_{c0}) < (\varepsilon_c/\varepsilon_{c0})_d \text{ and } 90 \text{ MPa (13 ksi)} \leq f_c'\right) \end{array}\right\} \quad \textbf{2.59}$$

Where:

$(\varepsilon_c/\varepsilon_{c0})_d$= The strain ratio at a stress of $0.3f_c'$ in the descending portion of the stress-strain curve

2.3.2.13 WEE et al. (1996) MODEL

Wee et al. (1996) aimed to establish whether the concrete composition had a significant affect on the stress-strain response, to asses the accuracy of existing analytical models by using current test data, and lastly to develop a stress-strain model for concrete strengths ranging between 50.0 MPa and 120.0 MPa (7.26 ksi and 17.4 ksi). Twenty-one normal weight concrete mixes constituting 163 (100 x 200 mm (3.94 x 7.87 in.)) cylinder specimens were used, which were further divided into five subsets according to their water/binder ratio. Different portions of cement extenders were added for each water/binder ratio thus altering the mix composition. The compressive stress-strain curve was characterised using the compressive strength, the initial tangential modulus, and the strain associated with the peak compressive strength. Based on previous experimental results, it was found that the ascending branch of the curve could most accurately be described by using the model proposed by Carreira & Chu (1985), and the descending branch modelled more accurately with the addition of two factors k_4 and k_5

© University of Pretoria

(Equation 2.60). The relationships for k_4 and k_5 are presented in Equation 2.61 and Equation 2.62. For strengths lower than 50.0 MPa (7.25 ksi) k_4 and k_5 should be taken as 1, resulting in the same expression proposed by Carreira & Chu (1985).

$$f_c = f_c' \times \left[\frac{k_4\beta(\varepsilon_c/\varepsilon_{c0})}{k_4\beta\text{-}1 + (\varepsilon_c/\varepsilon_{c0})^{k_5\beta}}\right] \quad \textbf{2.60}$$

With:

$$k_4 = \begin{Bmatrix} \left(1 \,\middle|\, f_c' \leq 50\text{ MPa (7.25 ksi)}\right) \\ \left((50/f_c'(\text{MPa}))^3 \,\middle|\, 50\text{ MPa (7.25 ksi)} < f_c'\right) \end{Bmatrix} \quad \textbf{2.61}$$

$$k_5 = \begin{Bmatrix} \left(1 \,\middle|\, f_c' \leq 50\text{ MPa (7.25 ksi)}\right) \\ \left((50/f_c'(\text{MPa}))^{1.3} \,\middle|\, 50\text{ MPa (7.25 ksi)} < f_c'\right) \end{Bmatrix} \quad \textbf{2.62}$$

$$E_i(\text{MPa}) = 10200 \times (f_c'(\text{MPa}))^{1/3} \quad \textbf{2.63}$$

$$\varepsilon_{c0} = 0.00078 \times (f_c'(\text{MPa}))^{1/4} \quad \textbf{2.64}$$

2.3.2.14 ATTARD & SETUNGE (1996) MODEL

Attard & Setunge (1996) experimentally determined the complete stress-strain curve of five mixes by loading 100 x 200 mm (3.94 x 7.87 in.) concrete cylinders to failure. Three Australian aggregate types (Rhyodacite, Hornfels, and Vesicular Basalt) were investigated, and analytical stress-strain models established. The analytical models are applicable for strengths ranging between 20.0 MPa and 130.0 MPa (2.90 ksi and 18.86 ksi), with the cylinder compressive strengths varying between 60.0 MPa and 130.0 MPa (8.70 ksi and 18.86 ksi). The model proposed by Sargin & Handa (1969) (see Equation 2.65) was extended to this study, with separate coefficients (A, B, C, and D) determined for the ascending and descending branches of the curve.

$$f_c = f_c' \times \left[\frac{A(\varepsilon_c/\varepsilon_{c0}) + B(\varepsilon_c/\varepsilon_{c0})^2}{1 + C(\varepsilon_c/\varepsilon_{c0}) + D(\varepsilon_c/\varepsilon_{c0})^2}\right] \quad \textbf{2.65}$$

Using the boundary conditions below, the values of A, B, C, and D for the ascending branch are given by Equation 2.66 to Equation 2.69:

$$\begin{Bmatrix} \left(\frac{df_c}{d\varepsilon_c} = E_i \,\middle|\, f_c = 0\right) \\ \left(\frac{df_c}{d\varepsilon_c} = 0 \,\middle|\, f_c = f_c'\right) \\ \left(\varepsilon_c = \varepsilon_{c0} \,\middle|\, f_c = f_c'\right) \\ \left(\varepsilon_c = f_c/E_c \,\middle|\, f_c = f_{pl}\right) \end{Bmatrix}$$

$$A = E_i\varepsilon_{c0}/f_c' \quad \textbf{2.66}$$

$$B = \frac{(A\text{-}1)^2}{\alpha(1\text{-}f_{pl}/f_c')} + \frac{A^2(1\text{-}\alpha)}{\alpha^2(f_{pl}/f_c')(1\text{-}f_{pl}/f_c')}\text{-}1 \quad \textbf{2.67}$$

$$C = (A\text{-}2) \quad \textbf{2.68}$$

$$D = (B + 1) \quad \textbf{2.69}$$

Using the boundary conditions below, the values of A, B, C, and D for the descending branch are given by Equation 2.70 to Equation 2.73:

© University of Pretoria

$$\left\{\begin{array}{c}\left(\frac{df_c}{d\varepsilon_c}=0\middle|f_c=f_c^{'}\right)\\ \left(\varepsilon_c=\varepsilon_{c0}\middle|f_c=f_c^{'}\right)\\ \left(\varepsilon_c=\varepsilon_{ci}\middle|f_c=f_{ci}\right)\\ \lim_{\varepsilon_c\to\infty} f_{resid}=f_c^{'}(B/(B+1))=0\end{array}\right\}$$

$$A=\frac{f_{ci}(\varepsilon_{ci}-\varepsilon_c)^2}{\varepsilon_{ci}\times\varepsilon_c\times(f_c-f_{ci})} \quad \textbf{2.70}$$

$$B=0 \quad \textbf{2.71}$$

$$C=A-2 \quad \textbf{2.72}$$

$$D=1 \quad \textbf{2.73}$$

Emperical correlations relating the modulus of elsticity and strain at the cylinder compressive strength, to the cylinder compressive sterngth, are shown in Equation 2.74 and Equation 2.75. Note that the modulus of elasticity for normal stregth concrete is obtained from the relationship proposed by ACI-318 (2014), while for high strength concrete the model proposed by ACI Committee 363 (1992) is used. A distinction is also made between crushed and gravel aggregates, in calculating the strain at the cylinder compressive strength.

$$E_c(MPa)=\left\{\begin{array}{c}\left(0.0043\rho^{1.5}\sqrt{f_c^{'}(MPa)}\middle|\text{ normal strength concrete }\right)\\ \left((3320\sqrt{f_c^{'}(MPa)}+6900)(\rho/2320)^{1.5}\middle|\text{ high strength concrete }\right)\end{array}\right\} \quad \textbf{2.74}$$

$$\varepsilon_{c0}=\left\{\begin{array}{c}\left(4.26\left(f_c^{'}(MPa)\right)^{0.75}/E_c(MPa)\middle|\text{Crushed Aggregate}\right)\\ \left(3.78\left(f_c^{'}(MPa)\right)^{0.75}/E_c(MPa)\middle|\text{Gravel Aggregate}\right)\end{array}\right\} \quad \textbf{2.75}$$

Where:

$f_{pl}=$ $0.45f_c$

$E_c=$ The second modulus measured at the stress of f_{pl}

$\alpha=$ E_i/E_c

$f_{resid}=$ The residual strength as the strain becomes large, with B derived for the descending branch

$\rho=$ The density of the concrete in kg/m^3

2.3.2.15 VAN GYSEL & TAERWE (1996) MODEL

Van Gysel & Taerwe (1996) used the stress-strain model proposed by CEB-FIB Model Code (1990) and Sargin & Handa (1969) to describe the ascending and the descending portions of the stress-strain curve. For these two relationships, shown in Equation 2.76 and Equation 2.77, the strain at the peak stress (ε_{c0}) is obtained by using a slightly modified form of the relationship proposed by Tomaszewicz (1984) (Equation 2.76). Note that for the descending branch, the values for t are shown in Table 2.2.

$$f_c=f_c^{'}\times\left[\frac{(E_i/E_c)(\varepsilon_c/\varepsilon_{c0})-(\varepsilon_c/\varepsilon_{c0})^2}{1+((E_i/E_c)-2)(\varepsilon_c/\varepsilon_{c0})}\right] \text{ for } \varepsilon_c\le\varepsilon_{c0} \quad \textbf{2.76}$$

$$f_c=\frac{f_c^{'}}{1+\left(\frac{(\varepsilon_c/\varepsilon_{c0})-1}{\eta_2-1}\right)^2} \text{ for } \varepsilon_{c0}<\varepsilon_c\le\varepsilon_{cu} \quad \textbf{2.77}$$

© University of Pretoria

With:

$$\varepsilon_{c0} = \begin{Bmatrix} (0.0022 | f_c' \leq 40.2 \text{ MPa } (5.38 \text{ ksi})) \\ ((0.7(f_c'(\text{MPa}))^{0.31}/1000 \, | f_c' > 40.2 \text{ MPa } (5.38 \text{ ksi})) \end{Bmatrix} \quad \textbf{2.78}$$

$$\eta_2 = \varepsilon_{c0} + t/\varepsilon_{c0} \quad \textbf{2.79}$$

Table 2.2 Parameter t for Different Concrete Strengths

f_c' (MPa) (ksi)	50 (7.25)	60 (8.70)	70 (10.15)	80 (11.60)	90 (13.05)	100 (14.50)
t (%)	0.807	0.579	0.388	0.221	0.07	0.015

2.3.2.16 OZTEKIN et al. (2003) MODEL

Oztekin et al. (2003) developed a modified form of the stress-strain model proposed by Hognestad (1951) for the ascending portion of the curve. Equation 2.80 illustrates this model, with experimental verification being done by testing 150 x 300 mm (5.91 x 11.81 in.) concrete cylinders in compression. For the final relationship, ε_{c0} was assumed equal to ε_{cu}, and the expression for ε_{c0} (or ε_{cu}) obtained from the CEB-FIB Model Code (1990), with modifications being made to better suit the experimental results.

$$f_c = f_c' \left[\frac{k\varepsilon_c}{\varepsilon_{cu}} - (k-1) \left(\frac{\varepsilon_c}{\varepsilon_{cu}} \right)^2 \right] \text{ for } \varepsilon_c \leq \varepsilon_{cu} \quad \textbf{2.80}$$

With:

$$k = 2 - [(f_c'(\text{MPa}) - 40)/70] \text{ for } 64 \text{ MPa } (9.29 \text{ ksi}) \leq f_c' \leq 94 \text{ MPa } (13.64 \text{ ksi}) \quad \textbf{2.81}$$

$$\varepsilon_{cu} = [2.2 + 0.015(f_c'(\text{MPa}) - 40)] 10^{-3} \text{ for } 64 \text{ MPa } (9.29 \text{ ksi}) \leq f_c' \leq 94 \text{ MPa } (13.64 \text{ ksi}) \quad \textbf{2.82}$$

As the stress-strain relationship need to be used by design engineers, it seems practical to consider only the stress-strain relationships capable of describing the behaviour with a single equation. Furthermore, by correlating existing single equation stress-strain models to the experimental results will enable the accurate description of the experimental stress-strain behaviour and the subsequent prediction of the stress block parameters.

2.4 FLEXURAL BEHAVIOUR OF CONCRETE

A beam or a pure flexural member may be defined as an element that transfers loads, applied normal to its longitudinal axis, to support points (Mahachi, 2013). When a reinforced concrete member is incrementally loaded to failure, it exhibits four distinct behaviours shown schematically in Figure 2.5.

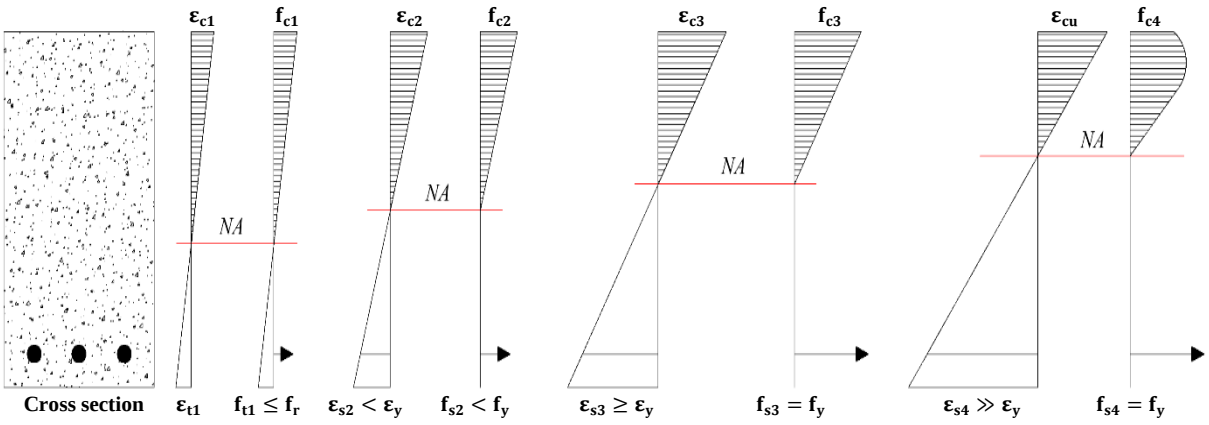

Figure 2.5 Four Stages of Stress-Strain Distribution in a Reinforced Concrete Flexural Member

© University of Pretoria

The first of these four regions ranges from zero load to the load level at which the stress in the tension zone of the beam (bottom of section in the sketch) reaches the modulus of rupture stress (f_r). For this stress range, the load is resisted by a couple moment between tensile stress in both the concrete below the neutral axis and the steel, and the compressive stress in the concrete above the neutral axis. Stage two is initiated once the tensile stress exceeds the modulus of rupture stress, at which time cracks are formed at the extreme tensile fibre and the tensile stress is assumed to be resisted by the steel only. The incremental increase in load sees the neutral axis progressively shifting upwards and the continual propagation of cracks towards the neutral axis.

Stage three is initiated by the yielding of the steel, with the steel assumed to behave in an elasto-plasitic manner. At the same time, the peak concrete compressive strain has not been reached, and as the strain in the extreme compression fibre increases, the compressive stress in the section increases. In order to maintain internal equilibrium, the neutral axis needs to move up to accommodate the increase in average concrete compressive stress and the constant tensile force in the steel. The fourth stage is reached when the section reaches its ultimate flexural strength capacity, initiated when the strain in the extreme compression fibre achieves the ultimate compressive strain (ε_{cu}). The design of a section, or the calculation of the ultimate strength, requires four basic assumptions to be made (Hognestad et al., 1955):

- Plane sections before bending remain plane after bending. This assumption implies that the longitudinal strain in either the concrete or the steel (at various points in the cross section) is proportional to the distance from the neutral axis.
- The stress-strain curve for steel is known, and the strain in the steel and concrete at the same depth of the cross section is assumed the same. For prestressed concrete this assumption is valid in pre-tensioned and bonded post-tensioned systems.
- The tensile strength of the concrete below the neutral axis may be neglected as both the force and the lever arm are small.
- The stress-strain curve of concrete, defining the magnitude and distribution of the compressive stress, is known and is a function of the strain only.

The combination of these four assumptions allows the stress block parameters to be calculated by using the distribution of flexural compressive stress in the concrete member. These stress block parameters in turn allow for the analysis and design of reinforced and prestressed concrete flexural elements at the ultimate limit state.

Thus, for design, the values of the stress block parameters are assumed based on the cylinder compressive strength, and the depth of the neutral axis subsequently calculated. The fact that the depth of the neutral axis varies between shallow, for small load actions, and deep, for large load actions, means that the size effect will have to be considered, a more detailed discussion of which will be given in section 2.6.

2.4.1 STRESS BLOCK PARAMETERS

At the maximum moment, the stress-strain distribution in the compression zone of concrete may mathematically be defined with three parameters k_1, k_2, and k_3 for a rectangular section with a width “b” and a depth “d”. According to Mattock et al. (1961), the three stress block parameters (and k_1k_3) are defined as:

© University of Pretoria

k_1= Ratio between the average and the maximum flexural compressive stress

k_2= Ratio between the position of the resultant compressive force and the depth of the neutral axis

k_3= Ratio between the maximum flexural compressive stress and the cylinder strength

k_1k_3= Ratio between the average flexural compressive stress and the cylinder strength

k_1k_3 and k_2 are obtained by simultaneously satisfying both external and internal equilibrium. Furthermore, by assuming $k_3=f_c''/f_c'$ (with f_c'' representing the maximum stress in flexural compression), the summation of horizontal forces, and the equilibrium of external and internal moments, yields Equation 2.83 and Equation 2.84:

$$C = k_1k_3f_c'bc \rightarrow k_1k_3 = C/f_c'bc \quad \textbf{2.83}$$

$$M = k_1k_3f_c'bc(d-k_2c) \rightarrow k_2 = d/c - M/(k_1k_3f_c'bc^2) \quad \textbf{2.84}$$

As shown in Figure 2.6, the three parameter stress block may be simplified to an equivalent rectangular stress block, provided that the magnitude and the position of the compressive force remains unchanged. According to Mattock et al. (1961), this mathematical simplification was first introduced by Emperger in 1904, and has been improved through the contributions of numerous researchers. The α_1 and β_1 factors are obtained from Equation 2.85 and 2.86 respectively.

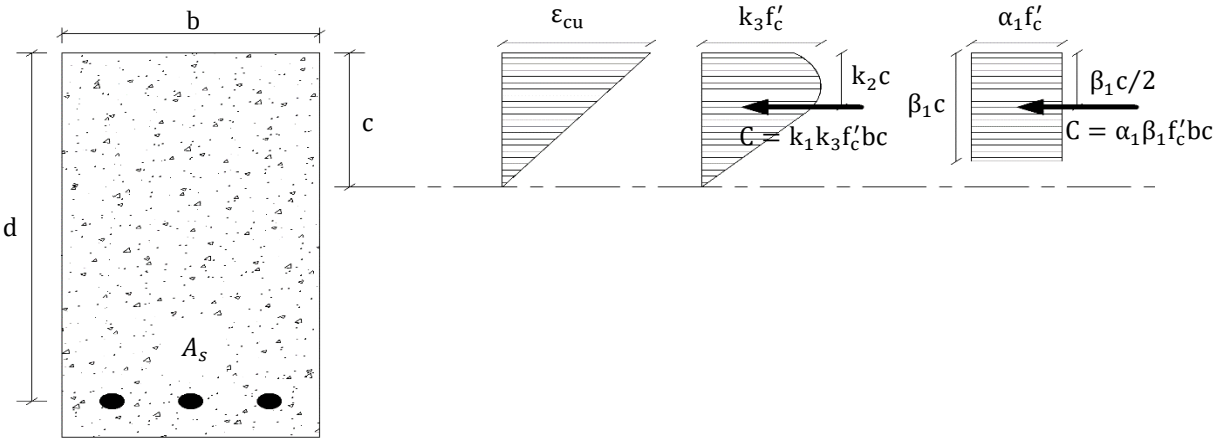

Figure 2.6 Strain, Three Parameter, and Two Parameter Equivalent Rectangular Stress Block

$$C = \alpha_1\beta_1f_c'bc = k_1k_3f_c'bc \rightarrow \alpha_1 = k_1k_3/2k_2 \quad \textbf{2.85}$$

$$k_2c = \beta_1c/2 \rightarrow \beta_1 = 2k_2 \quad \textbf{2.86}$$

It is difficult to determine the flexural stress-strain behaviour of concrete through experimentation. The strains in the section can easily be obtained through direct measurement; however, the stress distribution requires numerical differentiation while satisfying the equilibrium equations. To determine the flexural strain distribution, several researchers has proposed variations of the same test, details of which will be provided in the next section.

2.4.2 ECCENTRIC SPECIMEN TESTS

The stress-strain distribution of concrete has been the subject of investigation ever since the 20th century. The ground breaking work published by Hognestad et al. (1955) meant that the strain distribution and ultimate compressive strain in the cross section could be obtained in an efficient manner. Over the years variations of this test has been developed most of which were much more efficient from an experimental point of view. Table 2.3 summarises these experiments, followed by a detailed description of each researchers experimental procedure.

© University of Pretoria

Table 2.3 Summary of Eccentric Bracket Tests Performed by Other Researchers

Investigator	N.o.S	f_c'(MPa)	Cross Section	Length of Testing Region	Type of Testing Region	Cylinder Dimentions Used
Hognestad et al. (1955)	20	5.3 - 52.4	R: 127 x 203 mm	406 mm	UR	152 x 305 mm
Soliman & Yu (1967)	16	-	R: 1 - 76 x 152 mm, 14 - 102 x 152 mm, 1 - 127 x 152 mm	508 mm	R	-
Sargin et al. (1971)	14	20.6 - 32.3	R: 127 x 127 mm	254 mm	4 - UR, 10 - R	152 x 305 mm
Nedderman (1973)	13(9)	79.2 - 97.5	R: 127 x 203 mm	406 mm	UR	152 x 305 mm
Kaar et al. (1978a)	34	24.5 - 102.4	R: 127 x 203 mm	406 mm	UR	152 x 305 mm
Kaar et al. (1978b)	17	19.2 - 46.5	R: 6 - 127 x 203 mm, 11 - 254 x 406 mm	406 mm, 813 mm	3 - UR, 14 - R	152 x 305 mm
Swartz et al. (1985)	10	57.9 - 77	R: 1 - 127 x 203 mm, 9 - 127 x 127 mm	406 mm	UR	76 x 152 mm
Pastor (1986)	13(10)	17.9 - 79.7	R: 127 x 203 mm	406 mm	UR	152 x 305 mm
Schade (1992)	12	105.8 - 109.6	R: 152 x 152 mm	610 mm	6 - UR, 6 - R	102 x 203 mm
Ibrahim (1994)	15	59.3 - 129.3	R: 200 x 300 mm	1200 mm	3 - UR, 12 - R	100 x 200 mm, 152 x 305 mm
	6	81 - 130.6	T: h=240 mm, b=450 mm	1000 mm	2 - UR, 4 - R	
Tan & Nguyen (2004)	17	45.5 - 100.6	R: 200 x 200 mm	800 mm	3 - UR, 14 - R	150 x 300 mm
Mertol et al. (2008)	21	71.7 - 110.2	R: 229 x 229 mm	406 mm	UR	102 x 203 mm
Khadiranaikar & Awati (2012)	18(16)	60.6 – 115.6	R: 150 x 150 mm	900 mm	UR	150 x 300 mm, 100 x 200 mm

N.o.S= Number of Specimens, R= Rectangular, T=Triangular, UR=Unreinforced, R= Reinforced

© University of Pretoria

2.4.2.1 HOGNESTAD et al. (1955) TEST PROCEDURE

Hognestad et al. (1955) aimed to develop a test method capable of providing a quantitative understanding of the flexural compression stress-strain behaviour and stress block parameters. The scope of the investigation included the quality and the age of the concrete, along with five water cement ratios (1.0, 0.67, 0.5, 0.4, and 0.33), producing uniaxial cylinder strengths ranging between 5.3 MPa and 52.4 MPa (0.775 ksi and 7.6 ksi). The uniaxial compression stress-strain behaviour and compressive strength for each specimen was attained by testing three or four concrete 152 x 305 mm (6 x 12 in.) cylinders at 7, 14, 28, and 90 days.

The details of the "C-shaped" specimen, which were cast horizontally and tested vertically, are show in Figure 2.7. The central portion of the specimen was unreinforced and suitable tension and compression reinforcing was provided in the end brackets to ensure that failure would occur in the unreinforced test region. The test was performed by first levelling the test specimen in the machine and then applying a major thrust (P_1) through a 5 mm (3/16 in.) steel roller mounted on the loading platen of the testing machine. The minor thrust (P_2) was introduced with a hydraulic jack through one or two tie rods, and the magnitude of the force was measured using a calibrated electric strain gauge. P_1 was applied at a constant rate from zero load to failure during a testing period of approximately 15 minutes. By operating the hydraulic pump, P_2 could be adjusted to keep the strain at the back face of the section zero (within 5 x 10^{-6} strain). The strain was monitored at the extreme compression fibre and neutral axis using two 152 mm (6 in.) electric strain gauges, and single strain gauges located at the mid-depth of each of the two sides.

The the flexural stress-strain behaviour was established by combining the strain distribution, loads in flexural compression, and numerical differentiation. Numerical integration of the flexural stress-strain distribution, and the known uniaxial cylinder compressive strength, were used to determine the stress block parameters.

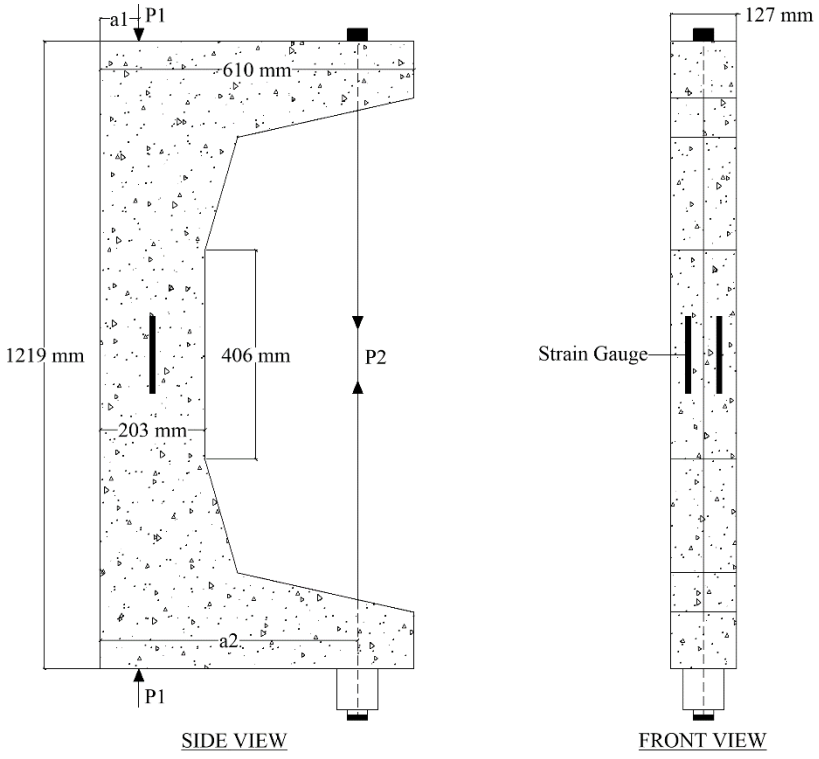

Figure 2.7 Hognestad et al. (1955) Test Specimen

© University of Pretoria

2.4.2.2 NEDDERMAN (1973) TEST PROCEDURE

Several investigators employed the same "C-Shaped" specimen test method used by Hognestad et al. (1955). One of the first of these investigations, done by Nedderman (1973), considered the influence of compressive strength on the stress block parameters. Thirteen specimens with compressive strengths ranging between 79.2 MPa and 97.5 MPa (11.49 ksi and 14.14 ksi) were cast of which nine were successfully tested. The only slight variation to this test procedure was the fact that the end brackets were not reinforced. As a result, large clamps made from 13 mm (0.5 in.) round steel bars and 19 mm (0.75 in.) steel plates, were used to reinforce the end regions and to ensure that failure would occur in the central unreinforced region of the specimen. P_1 was applied to the test specimen through a ball and socket type loading head bearing on a 9.5 mm (3/8 in.) masonite pad, and a 1270 mm^2 (50 $in.^2$) aluminium plate. The load was applied in decreasing increments as the specimen neared failure. P_2 was applied after each major load increment with the aid of a 270 kN (60 kip) hydraulic jack. The load was applied through four 19 mm (0.75 in.) round steel rods, and its magnitude measured using a pressure dial gauge attached to the hydraulic jack. Failure typically took place after 30 to 45 minutes corresponding to loading rates in the region of 1.1 to 1.7 με/s on the extreme compression face.

The uniaxial cylinder strength was measured using 152 x 305 mm (6 x 12 in.) cylinders, which, in some instances, did not fail due to the compressive strength of the cylinders exceeding the machine capacity. After the machine capacity had been reached, the load was maintained, with compressive failure taking place shortly after. It was felt that the cylinders were sufficiently close to failure when the machine capacity had been reached.

2.4.2.3 KAAR ET AL. (1978A) TEST PROCEDURE

Kaar et al. (1978a) investigated the influence of concrete compressive strength and the type of coarse aggregate on the stress block parameters. Both normal density and lightweight aggregate were used, with the design compressive strength ranging between 44.8 MPa and 102.4 MPa (6.5 ksi and 14.85 ksi) and 24.5 MPa to 86.1 MPa (3.56 ksi to 12.49 ksi) respectively. Three normal density aggregate and two lightweight aggregate concretes were investigated, and the specimens were cast horizontally and tested vertically. Apart from slight variations in test instrumentation (length of the strain gauges and type of displacement transducers) the test method and analysis procedure used to obtain the stress block parameters was the same as that proposed by Hognestad et al. (1955). The 152 x 305 mm (6 x 12 in.) cylinder strength was once again used to characterise the uniaxial compressive strength. The results indicated that for lightweight aggregate concrete with a compressive strength of less than 55.0 MPa (8 ksi), the β_1 factor should be reduced.

2.4.2.4 KAAR ET AL. (1978B) TEST PROCEDURE

Still utilising the same shape specimen, Kaar et al. (1978b) investigated the influence of rectangular concrete hoop reinforcing on the stress-strain behaviour of concrete with the compressive strength, quantity of longitudinal reinforcing, hoop spacing, and specimen size being the four variables. Although the "C-Shaped" specimen was still utilised, there was a large variation in the specimen dimensions. Of the seventeen specimens produced, six had the same cross section dimensions and testing region length as originally proposed by Hognestad et al. (1955), while eleven specimens had a cross section of 254 x 406 mm (10 x 16 in.) and a test region length of 813 mm (32 in.). The test specimen dimensions are illustrated in Figure 2.8.

© University of Pretoria

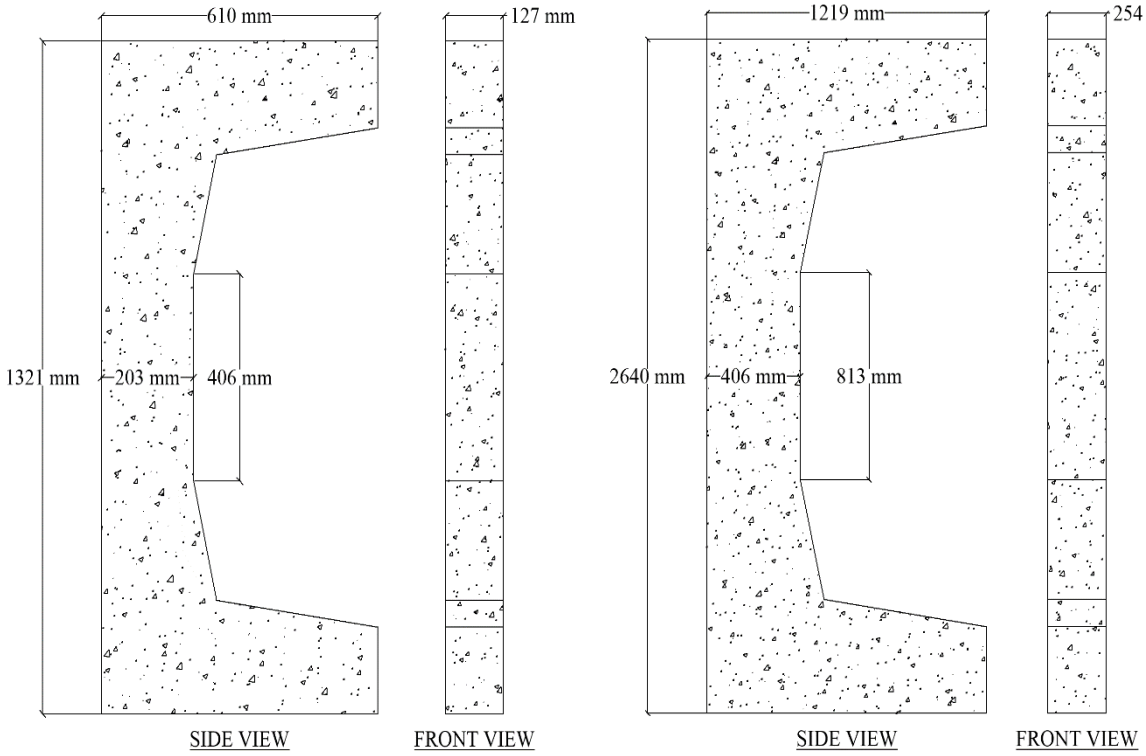

Figure 2.8 Kaar et al. (1978b) Test Specimens

The same measurement instrumentation proposed by Kaar et al. (1978a) was used by Kaar et al. (1978b), with three 152 x 305 mm (6 x 12 in.) concrete cylinders being crushed to determine the compressive strength of each specimen. The compressive strengths ranged between 19.2 MPa and 46.5 MPa (2.78 ksi and 6.75 ksi), and it was concluded that specimens reinforced with hoop reinforcing could accommodate larger strains than identical unreinforced specimens. In addition, it was found that the amount of hoop reinforcing was the single most important factor influencing the stress-strain behaviour of confined concrete, with no clear conclusion being drawn for the other variables due to experimental scatter.

2.4.2.5 SWARTZ ET AL. (1985) TEST PROCEDURE

Swartz et al. (1985) investigated the influence of compressive strength and cross section size on the flexural stress-strain behaviour of high strength concrete. Ten eccentric bracket specimens, with 3 x 6 in (76 x 152 mm) cylinder strengths ranging between 57.9 MPa and 77.0 MPa (8.4 ksi and 11.2 ksi), were tested in flexural compression. One of the specimens had a cross section of 127 x 203 mm (5 x 8 in.) and the remainder a cross section of 127 x 127 mm (5 x 5 in.). Changes in the "C-shaped" section dimensions are illustrated in Figure 2.9. The eccentric bracket specimens were once again cast horizontally and tested vertically. In addition to the eccentric bracket specimens, four concrete rectangular beams with compressive strengths between 79.3 MPa and 84.9 MPa (11.5 ksi and 12.3 ksi) and reinforcement ratios of $0.5\rho_b$ and $1.5\rho_b$ were cast. Where ρ_b represents the reinforcing ratio at balanced failure, i.e. the amount of reinforcement theoretically required to ensure that both the extreme concrete compressive fibre and the steel achieves their respective limiting strains at the same time. It was concluded that the extreme fibre compressive strain at failure was less than 0.003 with a design value of 0.0025 being suggested for future use. Furthermore, it was found that the compressive stress block at failure could be represented by a parabola, and that a similar stress-strain relationship is applicable for both beams and cylinders.

© University of Pretoria

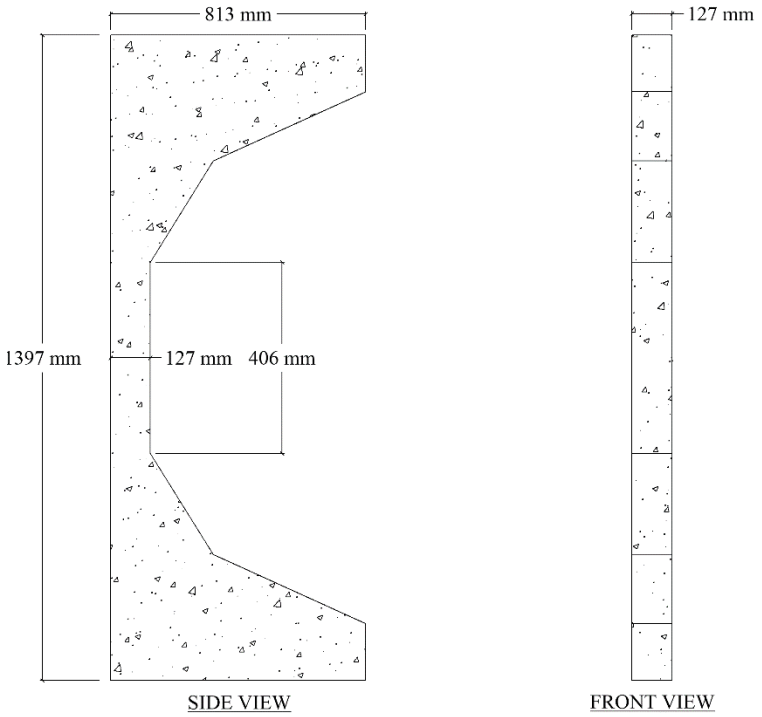

Figure 2.9 Swartz et al. (1985) Test Specimen

2.4.2.6 PASTOR (1986) TEST PROCEDURE

Pastor (1986) used the "C-shaped" specimen to investigate the influence of compressive strength on the stress-strain behaviour of concrete. The 152 x 305 mm (6 x 12 in.) cylinder compressive strengths ranged between 17.9 MPa and 79.7 MPa (2.60 ksi and 11.57 ksi), with ten out of the thirteen eccentric bracket specimens tested successfully (honeycombing and handling problems prohibiting the testing of the remaining three). The casting and testing direction were both vertical, and the only slight variation to the Hognestad et al. (1955) test procedure was the manner in which P_1 and P_2 was applied. Two 127 x 203 x 76 mm (5 x 8 x 3 in.) bearing plates combined with 25 mm (1 in.) rollers were used to apply P_1, and a scaled down version of this load application system used to apply P_2.

2.4.2.7 IBRAHIM (1994) TEST PROCEDURE

Ibrahim (1994) aimed to establish whether the rectangular stress block is applicable for rectangular and triangular high strength and ultra-high strength concrete sections. For this purpose twenty-one "C-shaped" specimens, fifteen rectangular (three plain and twelve reinforced) and six triangular (two plain and four reinforced) specimens were tested in combined flexure and compression. For the rectangular sections, the cylinder compressive strengths ranged between 59.3 MPa and 129.3 MPa (8.6 ksi and 18.75 ksi), and for the triangular specimens between 81.0 MPa and 130.6 MPa (11.75 ksi and 18.94 ksi). The age at testing ranged between 42 days and 186 days, and the test variables included concrete compressive strength, specimen size, as well as the spacing, diameter, and volumetric ratio of the confining steel reinforcing. The specimen details are provided in Figure 2.10, and all specimens were cast and tested vertically. For the rectangular section, the length and cross section of the central test region was 1200 mm (47.24 in.) and 200 x 300 mm (7.87 x 11.81 in.). For the triangular specimens, the length, perpendicular height, and side length of the test region were 1000 mm (39.37 in.), 240 mm (9.45 in.), and 450 mm (17.71 in.) respectively. A 6600 kN (1500 kip) MTS testing machine was used to apply P_1, while a

© University of Pretoria

540 kN (120 kip) hydraulic jack was employed to apply P_2. The deformations of the specimens were measured with both 25 mm and 102 mm (1 in. and 4 in.) strain gauges and linear variable differential transducers (LVDT's).

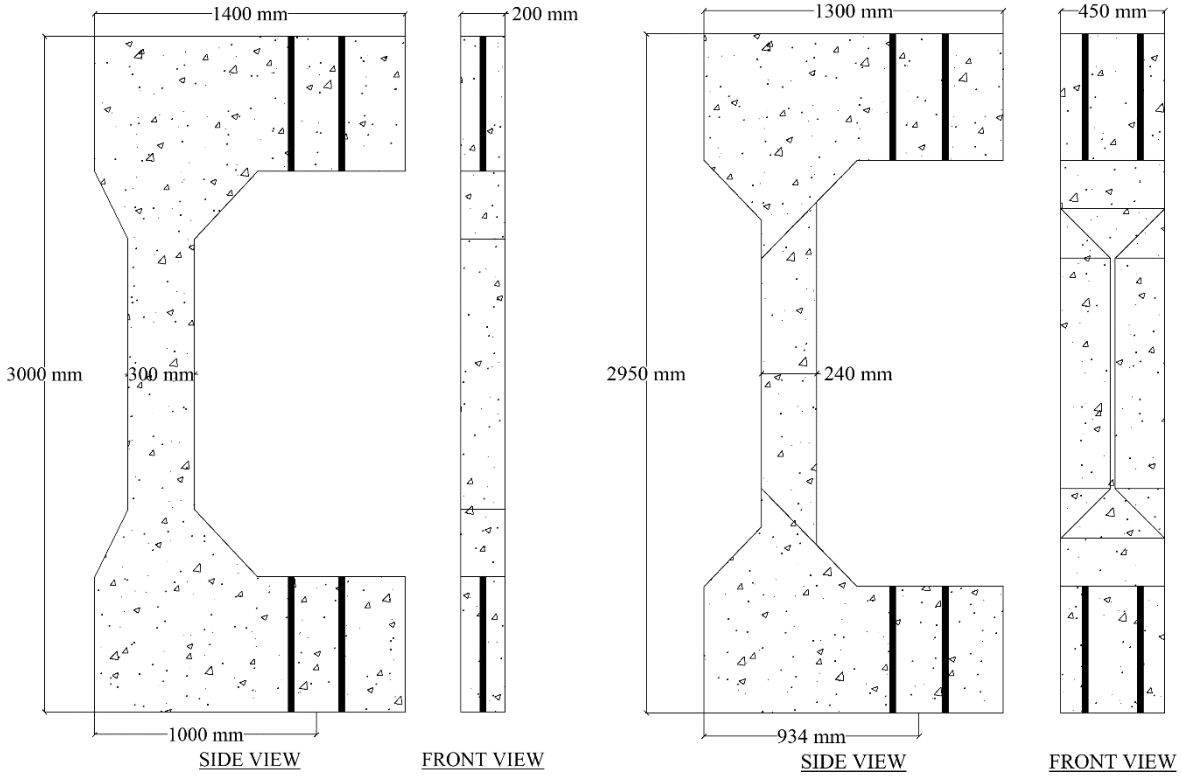

Figure 2.10 Ibrahim (1994) Test Specimens

The compressive strength was obtained by crushing 100 x 200 mm (3.94 x 7.87 in.) and 152 x 305 mm (6 x 12 in.) cylinders for each specimen. Among other things, the most important conclusions were that well confined high strength concrete showed a ductile behaviour, and that owing to the larger amount of concrete located close to the neutral axis, a triangular compression zone exhibits a much more ductile behaviour.

2.4.2.8 SOLIMAN & YU (1967) TEST PROCEDURE

Soliman & Yu (1967) investigated the stress-strain behaviour of confined concrete in order to understand the plastic deformation capacity of concrete reinforced with longitudinal and transverse reinforcing. The test variables included the size, type, and spacing of the transverse reinforcing as well as the concrete cover. Furthermore, three specimen cross sections (76 x 152 mm (3 x 6 in.), 102 x 152 mm (4 x 6 in.), and 127 x 152 mm (5 x 6 in.)) were tested to investigate the effect of specimen width on the flexural stress-strain relationship. Figure 2.11, illustrates the modified test method used by Soliman & Yu (1967). P_2 was applied using two 152 mm (6 in.) steel channel beams, each welded to a 152 x 305 x 19 mm (6 x 12 x ¾ in.) steel plate, which in turn is attached to the specimen via six 20 mm (¾ in.) bolts. The weight of the minor load arrangement was taken off the end of the specimen with the aid of a counterweight connected to the steel section passing over a set of pulleys. The position of the neutral axis was monitored using sixty polyester-based electric strain gauges, while five demountable mechanical strain gauges were used to monitor the strain on the side of the section. Although the specimens were confined, it was concluded that the width of the concrete specimen does not have an affect on the flexural stress-strain relationship. Thus, for a particular concrete section, the assumptions of planar sections remaining plane and strain remaining constant over the width of the section (regardless of section size) appears to be valid.

© University of Pretoria

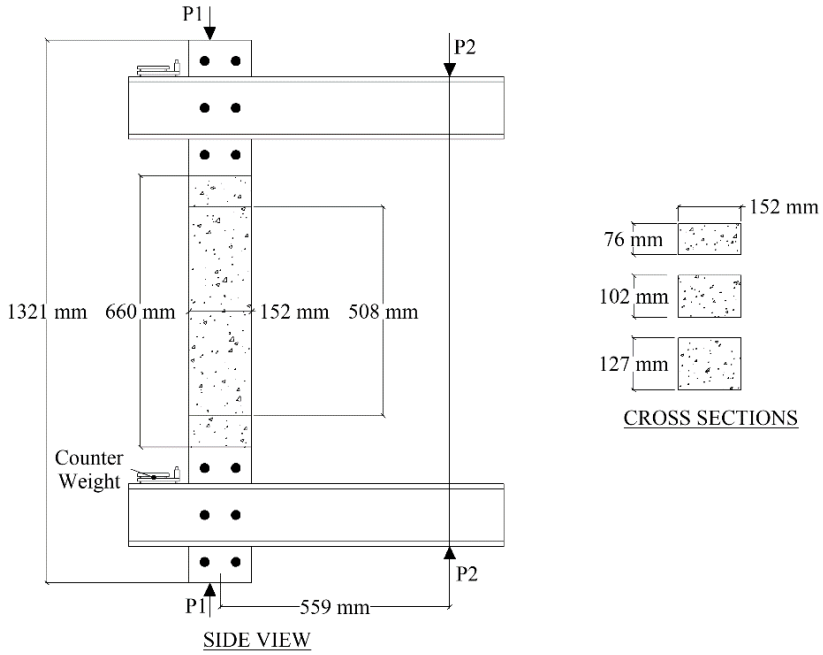

Figure 2.11 Soliman & Yu (1967) Test Setup and Specimen Dimensions

2.4.2.9 SARGIN et al. (1971) TEST PROCEDURE

To explain the complete stress-strain behaviour of concrete confined by rectangular reinforcing, Sargin et al. (1971), proposed the use of the test setup shown in Figure 2.12. The test variables included the grade, spacing, and size of the lateral reinforcing, as well as the enclosed core cover thickness, concrete compressive strength, strain gradient, and the casting direction. In total, sixty-three specimens were cast of which fourteen eccentric bracket specimens were tested. Four of the fourteen specimens were unreinforced (unconfined), and ten reinforced or confined. The 152 x 305 mm (6 x 12 in.) cylinder compressive strengths ranged between 20.6 MPa and 32.3 MPa (2.99 ksi and 4.68 ksi).

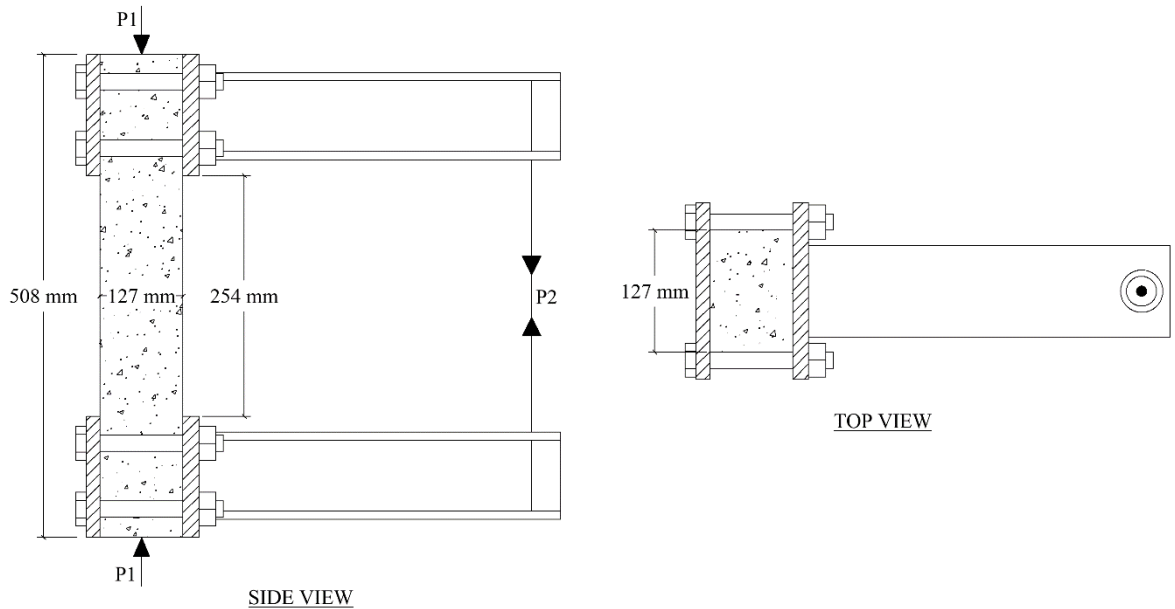

Figure 2.12 Sargin et al. (1971) Test Setup and Specimen Dimensions

From Figure 2.12, it can be seen that the central test region had a length of 254 mm (10 in.) and a cross section of 127 x 127 mm (5 x 5 in.). For the 125 mm (4.92 in.) lengths at the end of the specimen, the spacing of the ties was

© University of Pretoria

reduced to target the effect of stress concentrations. One of the test specimens was cast vertically while the remaining thirteen were cast horizontally. P_1 was applied with the aid of an 890 kN (200 kip) press bearing on cylindrical rollers and grooved plates. The top roller not only served as the point of load application but also acted as a load cell. P_2 was applied with a 45 kN (10 kip) hydraulic jack, and a 90 kN (20 kip) load cell used to measure its magnitude. The I-beams were connected to the end of the specimen with four 22 mm (7/8 in.) high tensile steel bolts at each end. Displacement transducers were used to measure the longitudinal strain on the opposite faces of the specimen, and the test durations varied between 45 and 90 minutes. Once the concrete strength capacity is reached, a sudden release of energy takes place. If the stiffness of the testing machine is inadequate, it is not possible to accurately measure the descending branch of the flexural stress-strain curve. Since the test machine used by Sargin et al. (1971) did not have an adequate stiffness, a spring system was used to accommodate the sudden release in energy, making it possible to monitor the post peak behaviour. In their conclusion, Sargin et al. (1971) found that the amount of confinement provided by the reinforcing was dependant on the spacing, grade, type (rectangular or spiral), and volumetric ratio of the lateral reinforcement as well as the concrete strength.

2.4.2.10 SCHADE (1992) TEST PROCEDURE

In order to not only confirm previous findings in terms of similarities between the stress-strain distribution and bending properties, but also minimise experimental costs, Schade (1992) proposed the use of the test procedure illustrated in Figure 2.13. The only variable was the concrete compressive strength, with six unreinforced specimens (76 x 152 mm (3 x 6 in.) cylinder compressive strengths of 105.8 MPa (15.36 ksi)), and six reinforced concrete specimens (76 x 152 mm (3 x 6 in.) cylinder compressive strengths of 109.6 MPa (15.9 ksi)) being tested. All specimens were cast and tested vertically with an average testing time of 10 min and a loading rate of 5 to 6 με/s. The new type of bracket connection employed two 76 x 51 x 5 mm (3 x 2 x 0.2 in.) hollow structural steel lever arms to apply P_2 to the rectangular column specimen. The column specimen had a test region length of 610 mm (24 in.) and a cross section of 152 x 152 mm (6 x 6 in.).

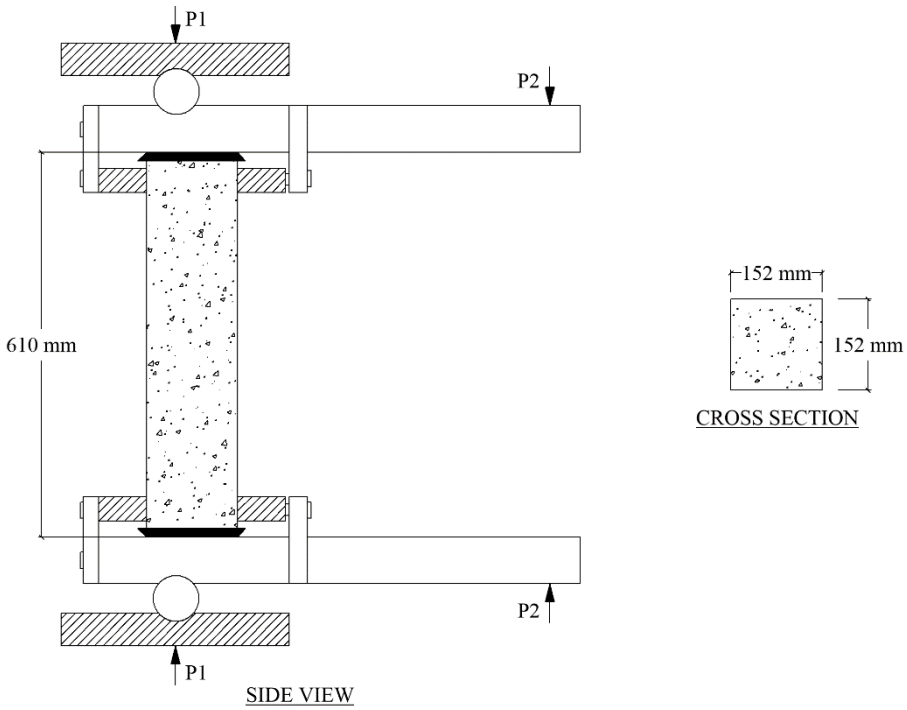

Figure 2.13 Schade (1992) Test Setup and Specimen Dimensions

© University of Pretoria

P_1 was applied through a ball and socket arrangement using a MTS machine with a capacity of 2000 kN (450 kip), and P_2 was once again applied with a hydraulic jack and the load measured with a load cell. Brass target points, a strain gauge based displacement transducer, and a mechanical strain indicator, was used to confirm the 51 mm (2 in.) electrical strain gauge readings, with one strain gauge being placed on each side of the specimen. Schade (1992) also measured the strain in the steel with 0.2 in (5 mm) strain gauges. The stress-strain relationship and numerical values, which characterised the properties of the stress block, was obtained and it was concluded that planer sections do indeed remain plane during bending and the maximum compressive strain at failure exceeded 0.003.

2.4.2.11 TAN & NGUYEN (2005) TEST PROCEDURE

Tan & Nguyen (2005) investigated the effect of confinement produced by lateral reinforcement on the stress-strain behaviour of high strength concrete, as well as whether the equivalent rectangular stress block proposed by the ACI-318, could be replaced with a one parameter equivalent rectangular stress block. The primary test variables included the concrete compressive strength, ranging between 45.5 MPa and 100.6 MPa (6.60 ksi and 14.60 ksi), and the volumetric percentage of the confinement reinforcing (ranging from 0.7% to 2.4%). For the investigation, thirty 200 mm (7.87 in.) square sections were subjected to three different loading schemes. Five of these specimens were subjected to concentric compression, seventeen to eccentric compression (with the position of the neutral axis fixed), and the remaining eight specimens to an eccentric compression with a fixed eccentricity. The test layout is shown in Figure 2.14.

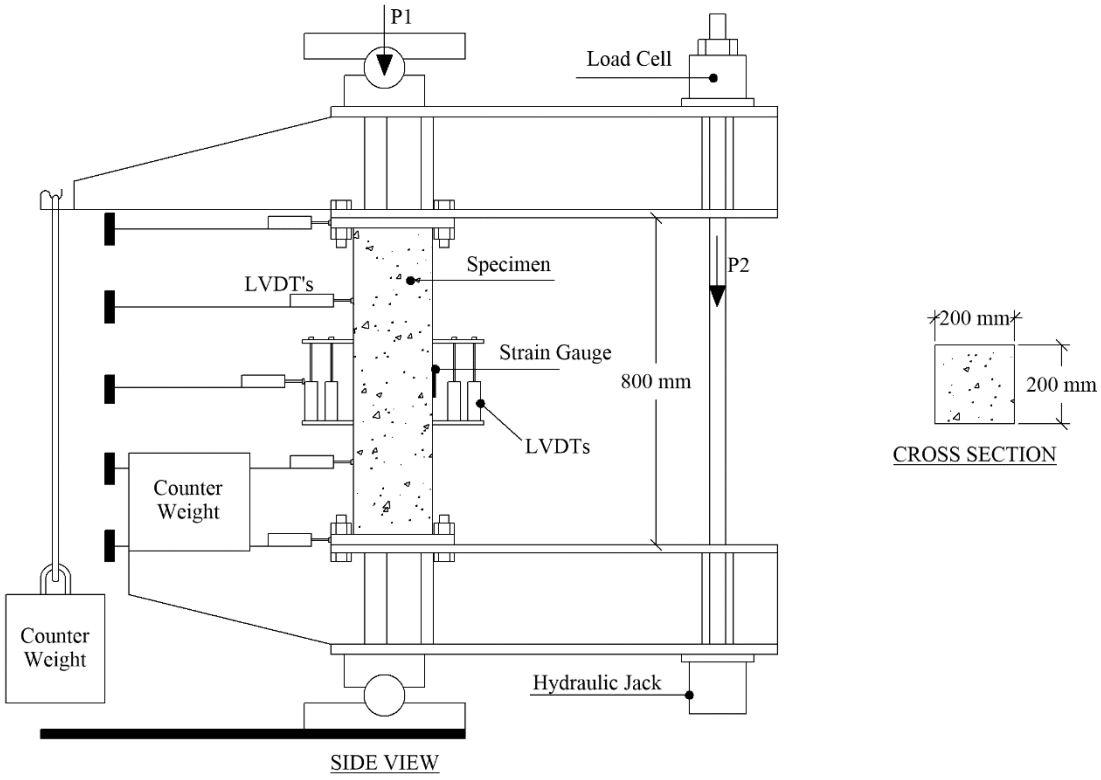

Figure 2.14 Tan & Nguyen (2005) Test Setup and Specimen Dimensions

In this report only the results of the three (unreinforced) eccentrically loaded specimens are presented. For each specimen three 150 x 300 mm (5.91 x 11.81 in.) cylinders were tested and the new one parameter stress block was proposed. Similar to many researchers before them, Tan & Nguyen (2005) concluded that the confinement

© University of Pretoria

produced by lateral reinforcing improved the flexural strength and ductility of reinforced concrete columns. It was also found that high-yield-steel was more effective in confining high strength concrete than lower-yield-steel, and that the concrete compressive strength is the primary variable influencing the flexural stress block parameters.

2.4.2.12 MERTOL et al. (2008) TEST PROCEDURE

Mertol et al. (2008) developed an experimental program to investigate and describe the fundamental characteristics of the compressive stress distribution in high strength flexural compression members. The main test variable was the compressive strength, with three target strengths of 68.9 MPa, 96.5 MPa, and 124.0 MPa (10 ksi, 14 ksi, and 18 ksi). A total of twenty-one specimens, with a length of 1016 mm (40 in.) and cross section of 229 x 229 mm (9 x 9 in.), were tested in flexural compression, five specimens for the target strength of 68.9 MPa (10 ksi), six for 96.5 MPa (14 ksi), and ten for 124.0 MPa (18 ksi). The strength of each specimen at the time of testing was established by testing three 102 x 203 mm (4 x 8 in.) cylinders, and additional cylinders were tested to establish the 28 day compressive strength. Figure 2.15, illustrates a cross section view of the specimen. To prevent localised failure, three longitudinal U shaped reinforcing bars and three transverse reinforcing bars were placed in the end brackets. Additional strength was provided through confinement, with 13 mm (1/2 in.) thick, 254 mm (10 in.) long rectangular hollow sections being cast into the end regions of the section. For each load increment, P_1 was applied to a predetermined level with an 8900 kN (2000 kip) load controlled compression machine, and P_2 applied subsequently with a 540 kN (120 kip) hydraulic jack to develop the strain gradient. P_2 was transferred to the specimen with the aid of two lever arms each consisting of two 610 mm (24 in.) long C 8 x 11.5 channel sections welded to two 229 x 25 x 610 mm (9 x 1 x 24 in.) steel plates at the top and bottom. The steel plates in turn were connected with six threaded rods extending through the concrete and rectangular hollow sections. The steel lever arms were strengthened with 13 mm (½ in.) stiffeners. End restrictions (produced by the applied load) were eliminated with the two specially designed roller connections consisting of two curved plates and six 25 mm (1 in.) diameter rollers.

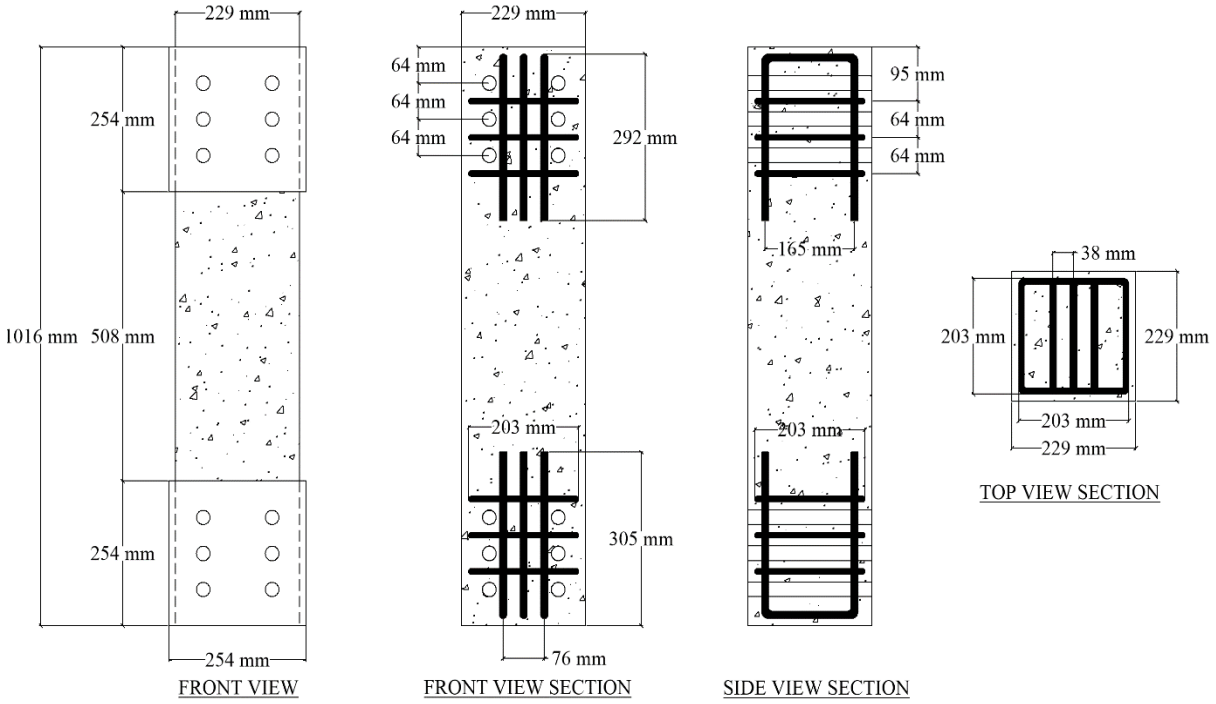

Figure 2.15 Mertol et al. (2008) Test Specimen

© University of Pretoria

From the test setup shown in Figure 2.16, it can be seen that three Linear Variable Differential Transformers (LVDT) were placed at the top, bottom, and mid-height of the section, with nine strain gauges being used to measure the strain distribution (two in the longitudinal direction of each face, and one additional perpendicular strain gauge on the compression face to enable the calculation of the Poisson ratio). Mertol et al. (2008) concluded that for concrete strengths up to 124.0 MPa (18 ksi), plane sections remain plane during bending and the ultimate compressive strain of 0.003 is still applicable.

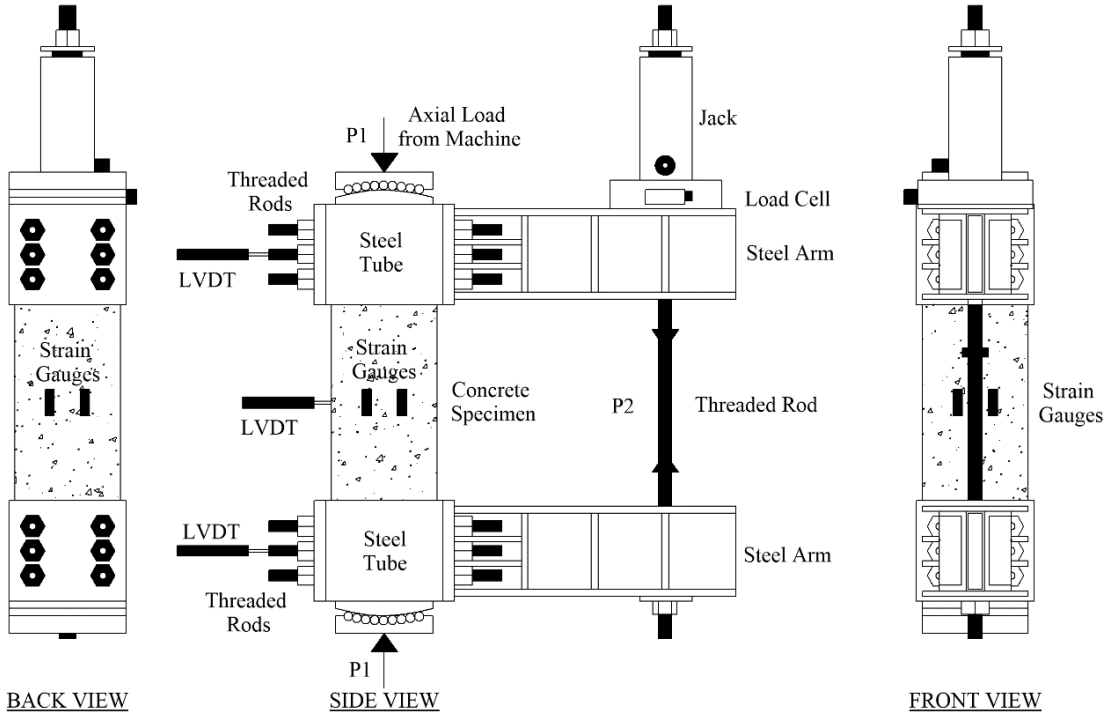

Figure 2.16 Mertol et al. (2008) Test Setup

2.4.2.13 KHADIRANAIKAR & AWATI (2012) TEST PROCEDURE

Khadiranaikar & Awati (2012) developed an experimental program to investigate and describe the fundamental characteristics of the compressive stress distribution in high strength flexural compression members. This study considered a series of three specimen types, fourteen of which were square column sections subjected to eccentric compression, four rectangular beams in pure flexure, and eighteen square columns tested with a fixed neutral axis. The only test variable for the eighteen flexural compression specimens (of which only sixteen were tested successfully) was the compressive strength, ranging between 60.6 MPa and 115.6 MPa (8.8 ksi and 16.78 ksi). For the 60 MPa, 80 MPa, and 100 MPa (8.7 ksi, 11.6 ksi, and 14.5 ksi) target strengths, the uniaxial compressive strength was evaluated by testing three 150 mm (5.91 in.) cubes and three 150 x 300 mm (5.91 x 11.81 in.) cylinders. For the 120 MPa (17.4 ksi) target strength, the uniaxial compressive strength was evaluated by testing 100 mm cubes (3.94 in.) and 100 x 200 mm (3.94 x 7.87 in.) cylinders. The eighteen rectangular column sections had a size of 150 x 150 x 900 mm (5.9 x 5.9 x 35.4 in.). To prevent the localised failure, four 12 mm (0.47 in.) diameter longitudinal reinforcing bars along with adequate transverse reinforcing were placed in the end regions of the specimen. In addition, both ends of the specimen were confined with 12 mm (0.47 in.) steel tubes to reduce the tendency towards failure in the end regions. For each load increment, P_1 and P_2 were monolithically increased to ensure the strain on the back face remains equal to zero. P_2 was transferred to the specimen with the aid of two lever arms each having a depth approximately equal to the depth of the concrete beam. The specimen assembly

© University of Pretoria

was levelled in the compression testing machine on a roller connection. Another roller connection was placed on top of the specimen, followed by a 2000 kN (450 kip) load cell. Similar to Mertol et al. (2008), Khadiranaikar & Awati (2012) used threaded rods extending through the specimen to attach the lever arms. P_1 was applied at a rate of 0.005 mm/s (0.0002 in./s) through a compression testing machine with a 3000 kN (675 kip) capacity. The strain in the section was measured using PI-Gauges (strain-based transducers), and the lateral displacement measured with LVDT's located at the top, middle, and bottom of the section. The test setup is shown in Figure 2.17.

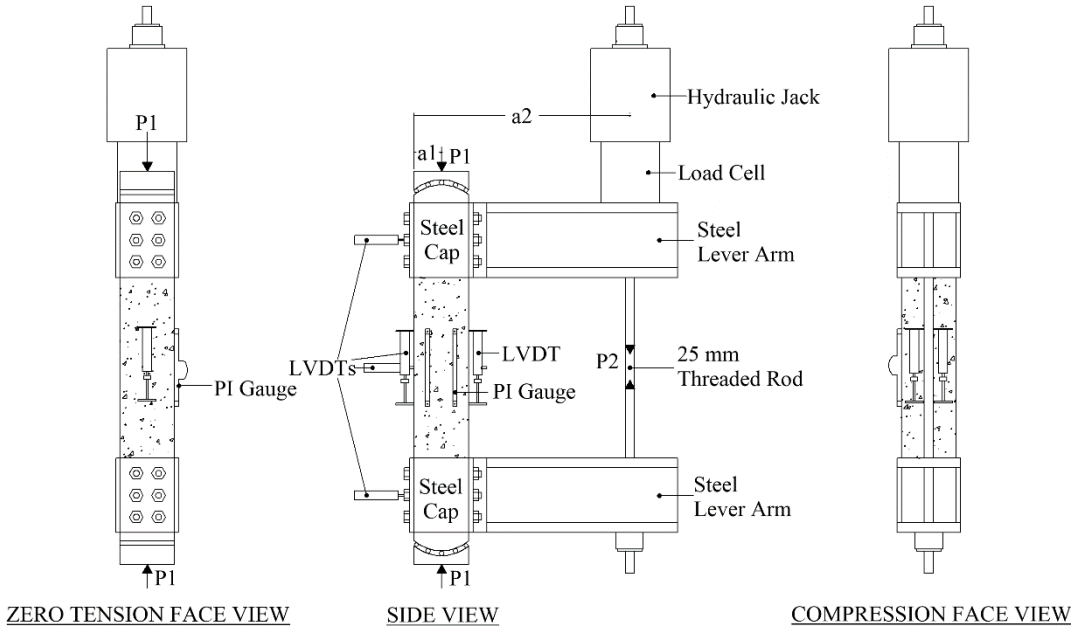

Figure 2.17 Khadiranaikar & Awati (2012) Test Setup

2.4.3 PREVIOUS TEST RESULTS

Although a brief summary of work done by other researchers was provided in the previous section, the stress block parameters that were reported by these researchers are presented in this section. It should be noted that only some the researchers presented all of the parameters. Figure 2.18 to Figure 2.24 illustrate the stress block parameters k_1, k_2, k_3, k_1k_3, α_1, β_1, and ultimate compressive strain (ε_{cu}) obtained by previous researchers.

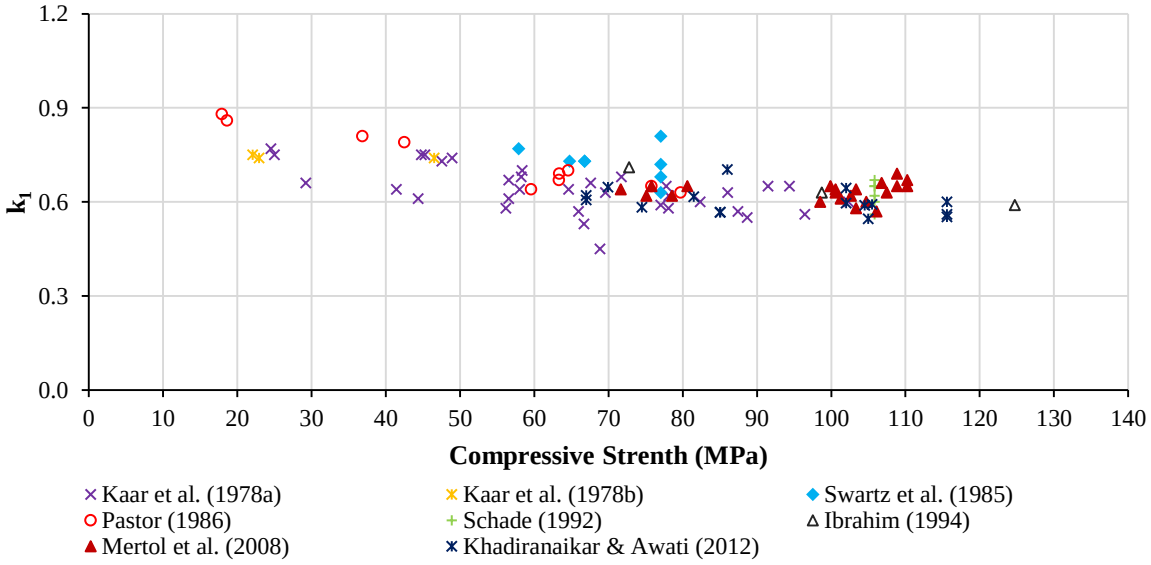

Figure 2.18 k_1 Factor from Previous Research

© University of Pretoria

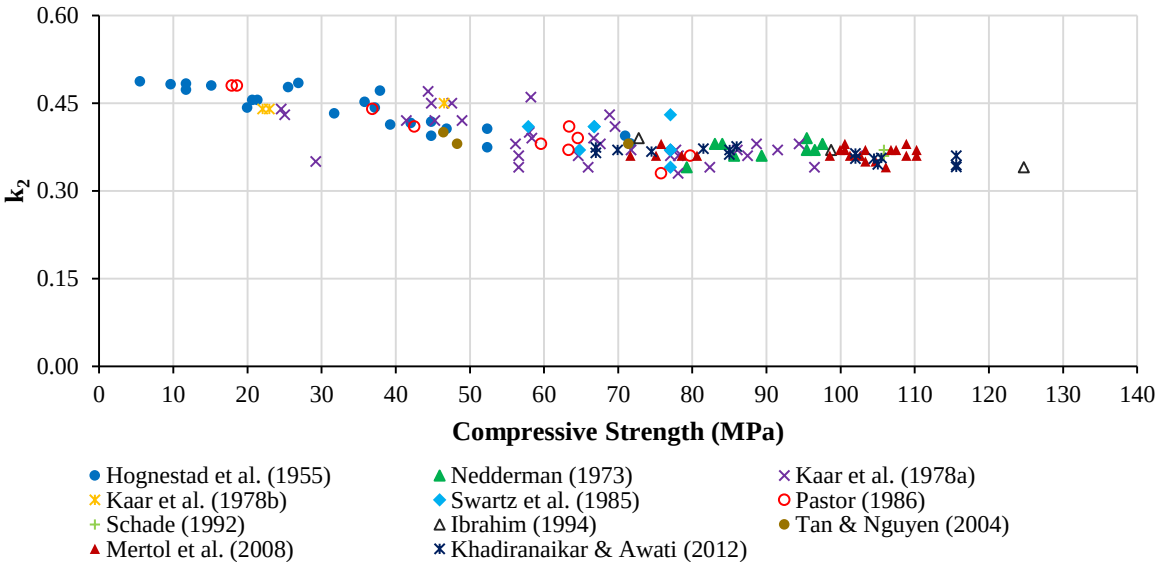

Figure 2.19 k_2 Factor from Previous Research

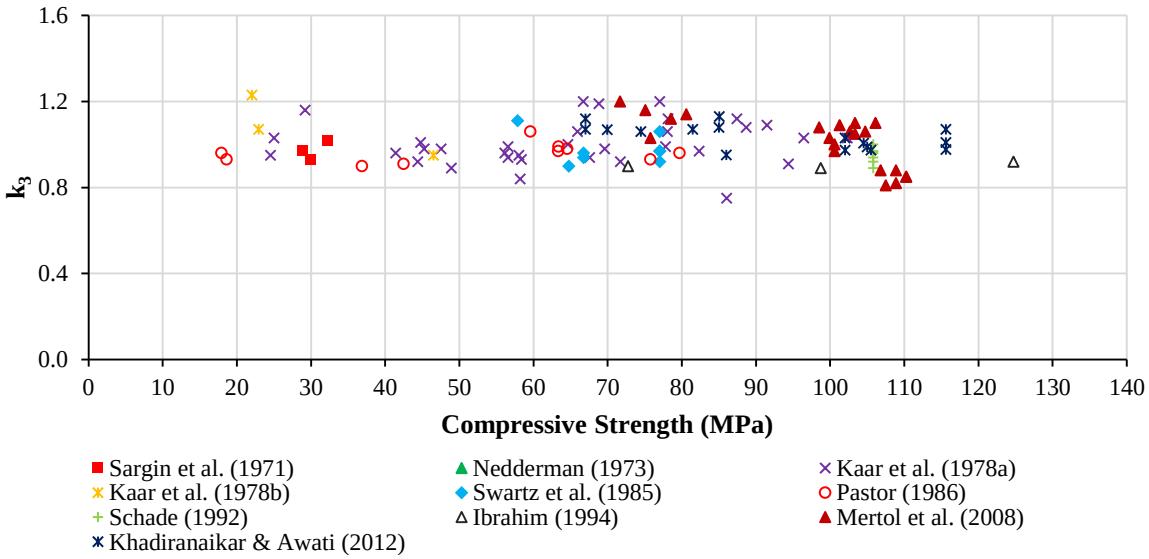

Figure 2.20 k_3 Factor from Previous Research

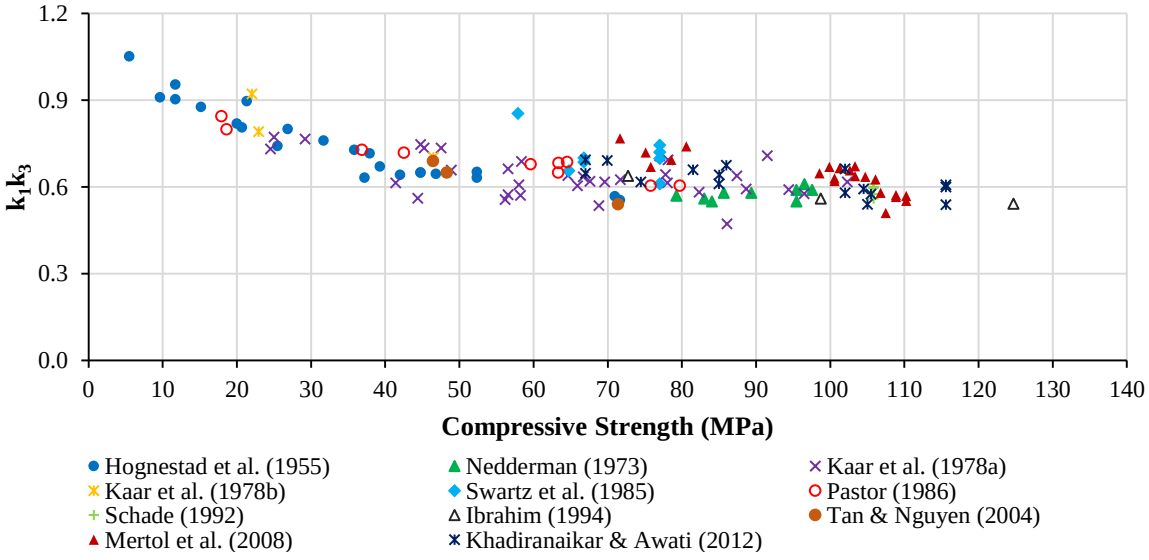

Figure 2.21 k_1k_3 Factor from Previous Research

© University of Pretoria

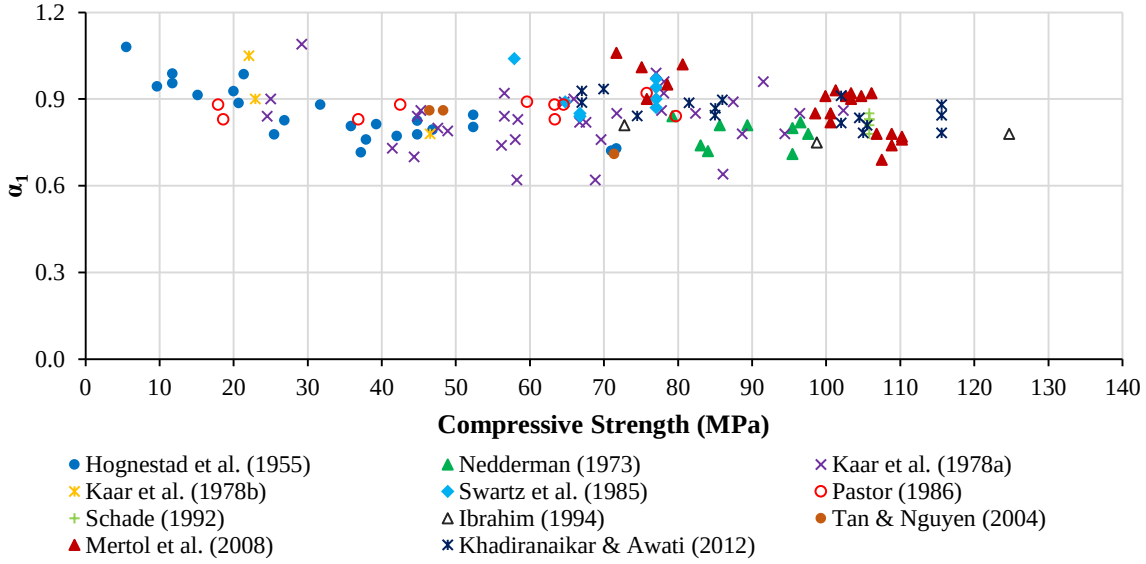

Figure 2.22 α_1 Factor from Previous Research

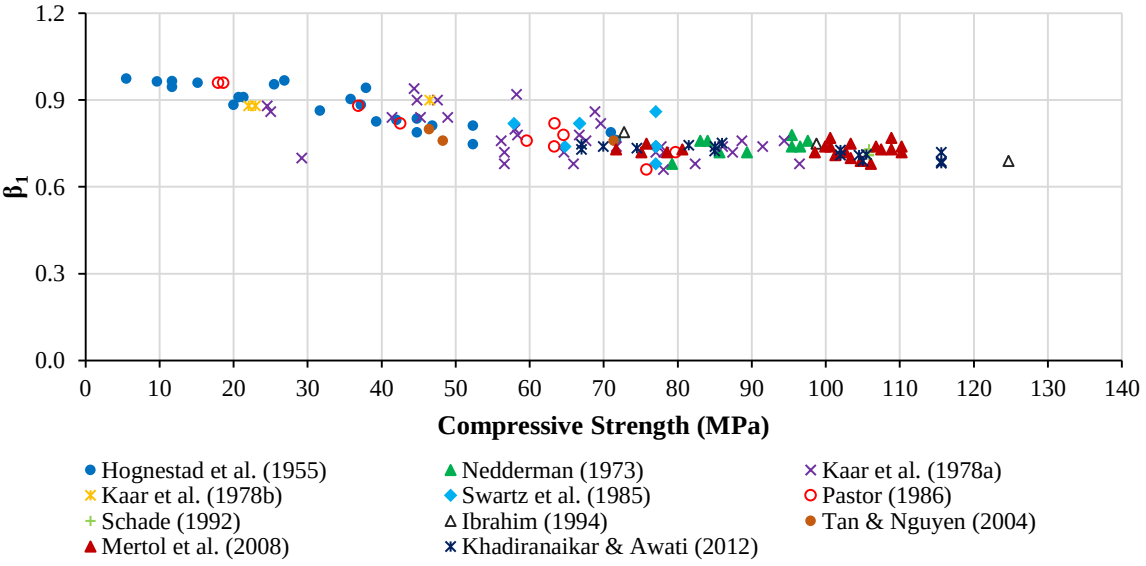

Figure 2.23 β_1 Factor from Previous Research

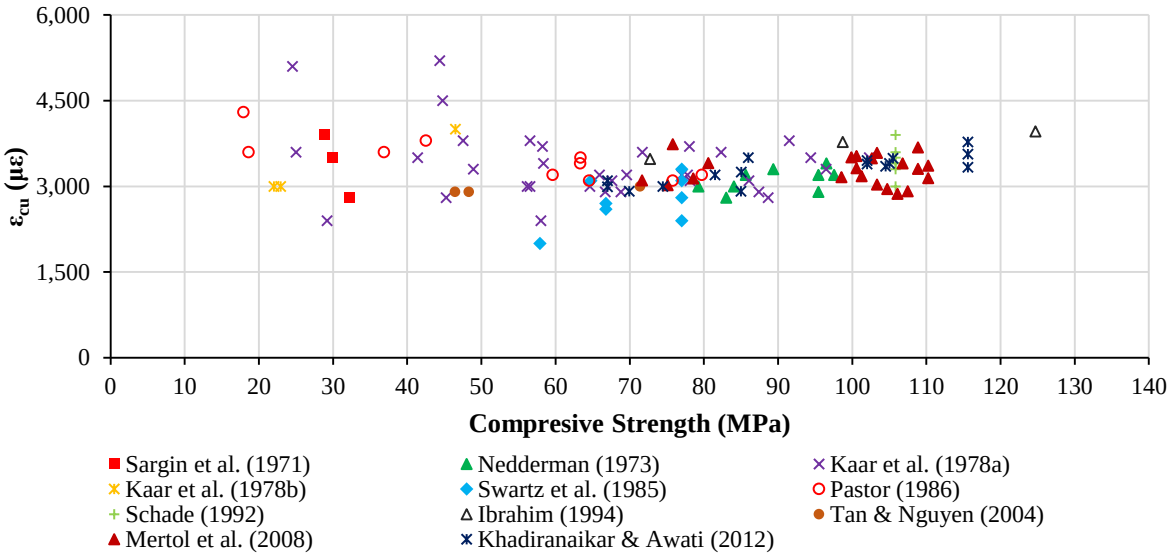

Figure 2.24 Ultimate Concrete Strain from Previous Research

© University of Pretoria

With reference to Figure 2.18, Figure 2.19, Figure 2.21, Figure 2.22, and Figure 2.23 it can be seen that as the compressive strength increases k_1, k_2, k_1k_3, α_1, and β_1 reduces. On the other hand, Figure 2.20 illustrates that the k_3 seems to be independent of the compressive strength and hovers about the value of one. With reference to Figure 2.24, it is also worth wile mentioning that the ultimate compressive strain tends to reduce with an increase in compressive stress; however, it is difficult to accurately estimate this reduction, due to the extreme variability associated with the data. It is for this reason that most researchers and design codes either assumes an ultimate compressive strain equal to the average compressive strain or a suitable lower bound estimate.

2.4.4 HISTORY OF RECTANGULAR STRESS BLOCK PARAMETERS

The concept of the equivalent rectangular stress block was proposed in section 2.4.1, and the experimentally determined values for α_1, β_1, and ε_{cu} were presented in the previous section. This section presents the models proposed by previous researchers used to describe these factors as functions of the concrete compressive strength. The models for α_1, β_1, and ε_{cu} are presented in Table 2.4 with the exception of the model proposed by Whitney (1937) and Zia (1983). Figure 2.25 and Figure 2.26, at the end of this section visually illustrates the models presented in Table 2.4.

2.4.4.1 WHITNEY (1937) MODEL

Whitney (1937) was the first to propose a replacement of the actual compressive stress-strain behaviour of concrete with an equivalent rectangular stress block. Without performing experimental investigations, Whitney (1937) proposed a value of α_1=0.85 while β_1 varied according to reinforcement ratio of the beam. For an under-reinforced section β_1/d (with d the depth of the steel reinforcing), ranged between 0 for unreinforced beams to 0.537 at the balanced steel ratio. A constant value of 0.537 is assumed for over-reinforced sections.

2.4.4.2 MATTOCK et al. (1961) MODEL

Mattock et al. (1961) proposed stress block parameters (based on the experimental work done by previous researchers) which to this day are being used in the ACI-318 design code. It should be noted that no lower bound limit was originally placed on the value of β_1, which at a later stage caused some inaccuracies between numerical predictions and experimental results.

2.4.4.3 ZIA (1983) MODEL

Based on previous experimental studies, Zia (1983) proposed modifications to the then current ACI-318 code with regard to provisions for the design of high strength concrete. Since concrete loses its plasticity and becomes more brittle with an increase in compressive strength, the idealised trapezoidal stress-strain curve proposed by Jensen (1943) was used as the basis for the derivation of the stress-strain response. The values of α_1, β_1 are given in by Equation 2.87 and Equation 2.88 below.

$$\alpha_1 = \frac{3(1+\beta)^2}{4(1+\beta+\beta^2)} \qquad \textbf{2.87}$$

$$\beta_1 = \frac{2(1+\beta+\beta^2)}{3(1+\beta)} \qquad \textbf{2.88}$$

© University of Pretoria

With:

$$E_c(psi) = 57000\sqrt{f_c'(psi)} \quad \textbf{2.89}$$

$$\varepsilon_{cu} = 0.003 \quad \textbf{2.90}$$

$$\beta = 1 - f_c'(psi)/(E_c(psi)\varepsilon_{cu}) \quad \textbf{2.91}$$

2.4.4.4 LI (1993) MODEL AND REGAN (1999) MODEL

Figure 2.3 presented the stress-strain behaviour for various concrete strengths. Li (1993) and Regan (1999) observed that for high strength concrete the shape of the stress-strain curve was similar to that of a triangle with a peak stress of f_c' corresponding to the ultimate compressive strain of 0.003. Assuming k_3=1, both Li (1993) and Regan (1999) established that α_1=0.75 and β_1=0.667 for high strength concrete, and derived stress block coefficients tending to these lower bound estimates.

2.4.4.5 IBRAHIM (1994) MODEL

As part of the same investigation presented in section 2.4.2.7, Ibrahim (1994) provided relationships for the determination of α_1 and β_1. In the previous section the results obtained by Ibrahim (1994) was illustrated, from which the parameter of α_1 was found to reduce with an increase in the cylinder compressive strength and that the ACI-318 code recommendations for the value of $\beta_1/2$ overestimated the internal lever arm, and hence the moment capacity of the section. A new recommended value for β_1 was obtained by preforming a linear regression analysis of the data. For compressive strengths in excess of 100.0 MPa (14.5 ksi) constant values of α_1=0.725 and β_1=0.7 were assumed.

2.4.4.6 PENDYALA & MENDIS (1998) MODEL

Pendyala & Mendis (1998) concluded that the current rectangular stress block models proposed by the then current AS 3600 (1994) code, were incapable of describing the behaviour of concrete with a strength range between 57.0 MPa and 100.0 MPa (8.27 ksi and 14.50 ksi) and new α_1 and β_1 relationships were suggested for this stress range.

2.4.4.7 ATTARD & STEWART (1998) MODEL

Attard & Stewart (1998) proposed new rectangular stress block parameters based on the “mean” probabilistic analysis result for high strength concrete stress-strain curves. The stress stain curve proposed by Attard & Setunge (1996) was used, estimates of the variability of the input parameters made, and a sensitivity analysis performed to establish the uncertainty associated with a particular input parameter. Two values of α_1 and β_1 are provided in Table 2.4, one for specimens not subjected to sustained loading and the other subjected to sustained loading.

2.4.4.8 BAE & BAYRAK (2003) MODEL

As part of their experimental program, Bae & Bayrak (2003) aimed to incorporate the influence of concrete cover spalling on the stress block parameter of high strength concrete. By considering 224 columns, it was concluded that with an increase in concrete compressive strength the ACI-318 stress block parameters leads to a progressive

© University of Pretoria

overestimate of the moment capacity. The proposed stress block parameters and ultimate compressive strains incorporating the effect of early cover spalling are once again presented in Table 2.4. It is important to note that the values of α_1 and β_1 were based on an ultimate compressive strain of 0.0025.

2.4.4.9 SUN et al. (2003) MODEL

Sun et al. (2003) aimed to model the stress-strain relationship of reinforced concrete members with a design strength in excess of 68.9 MPa (10 ksi). A modification to the ACI-318 codes rectangular stress block parameters was proposed to allow the modelling of members with concrete strengths up to 110.2 MPa (16 ksi). For concrete strengths in excess of 68.9 MPa (10 ksi), the proposed stress block parameters resulted in a normalised area which was in close agreement with the results obtained by Popovics (1973).

2.4.4.10 OZTEKIN et al. (2003) MODEL

Oztekin et al. (2003) used regression analysis to establish the relationship between the cylinder compressive strength and α_1, β_1, and ε_{cu}. A modified form of the ultimate compressive strain relationship, originally proposed by the CEB-FIB Model Code (1990) was used to obtain the ultimate compressive strain.

2.4.4.11 OZBAKKALOGLU & SAATCIOGLU (2004) MODEL

Ozbakkaloglu & Saatcioglu (2004) used the stress-strain relationship proposed by Popovics (1973) to derive the stress block parameters of α_1 and β_1. These models, based on the experimental work performed by other researchers, are applicable for eccentrically loaded high strength and normal strength compressive members with compressive strengths ranging between 20.0 MPa and 130 MPa (2.90 and 18.87 ksi).

2.4.4.12 TAN & NGUYEN (2005) MODEL

Tan & Nguyen (2005) suggested a one parameter equivalent rectangular stress block, which was compared to the rectangular stress block proposed by the ACI-318 code. Both α_1 and β_1 can be estimated from experimental data and will still be accurate and safe to use in design. β_1 was kept as close as possible to the experimental data and the product of $\alpha_1\beta_1$ was chosen smaller than the test values. For strengths less than 102.0 MPa (14.8 ksi) a linear relationship between cylinder compressive strength and α_1 and β_1 was obtained. For compressive strengths in excess of 100.0 MPa (14.51 ksi) α_1 and β_1 are both equal to 0.7.

2.4.4.13 MERTOL et al. (2008) MODEL

Mertol et al. (2008) concluded that the α_1 stress block parameter, proposed by the ACI-318, should be reduced for concrete strengths between 68.9 MPa and 124.0 MPa (10 ksi and18 ksi), but the current ACI-318 value of β_1=0.65 was satisfactory for strengths up to 124.0 MPa (18 ksi).

2.4.4.14 KHADIRANAIKAR & AWATI (2012) MODEL

Khadiranaikar & Awati (2012) proposed a modification of the Indian Standard code (IS 456), as the code proposed values are only applicable for concrerte strengths up to 55 MPa. The newly proposed model was applicable for concrete strengths ranging between 40 MPa and 120 MPa (5.8 ksi and 17.4 ksi). Similar to other researchers, the ultimate compressive strain was assumed to be 0.003.

© University of Pretoria

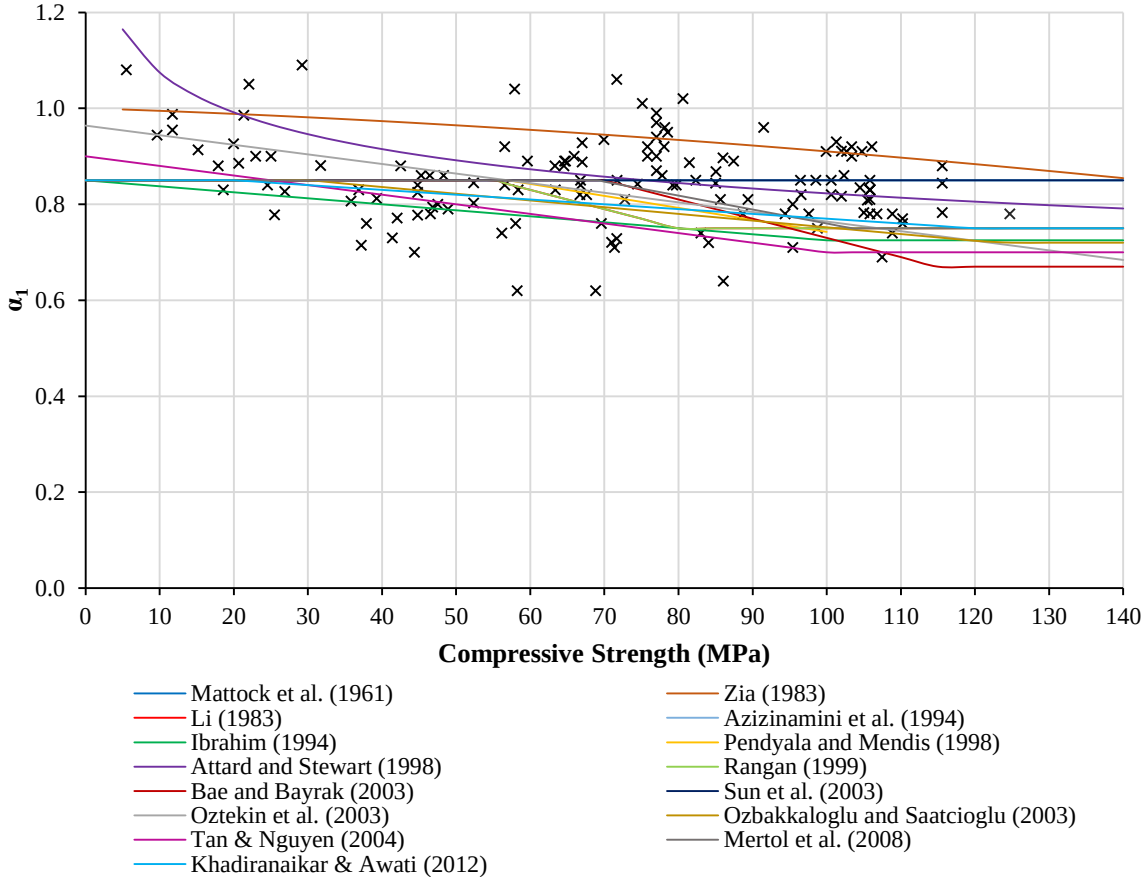

Figure 2.25 α_1 Models from Previous Research

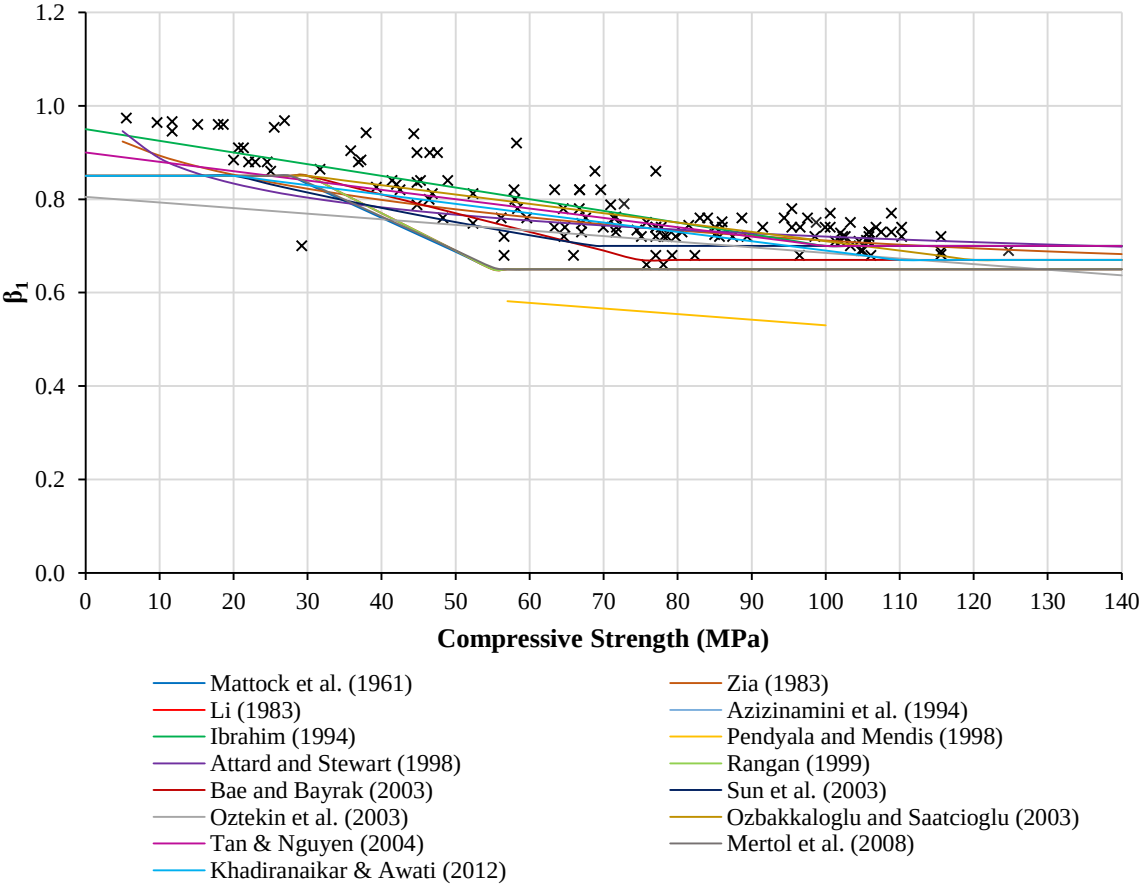

Figure 2.26 β_1 Models from Previous Research

© University of Pretoria

Table 2.4 α_1, β_1, and ε_{cu} Models Proposed by Other Researchers

Investigator	α_1	β_1	ε_{cu}
Mattock et al. (1961)	0.85	$\begin{cases} 0.85 \text{ for } f_c' \le 27.6 \text{ MPa} \\ 0.85\text{-}0.007257(f_c'\text{-}27.6) \text{ for } f_c' > 27.6 \text{ MPa} \end{cases}$	0.003
Li (1993)	$\begin{cases} 0.85 \text{ for } f_c' \le 55 \text{ MPa} \\ 0.85\text{-}0.004(f_c'\text{-}55) \ge 0.75 \text{for } f_c' > 55 \text{MPa} \end{cases}$	$\begin{cases} 0.85 \text{ for } f_c' \le 30 \text{ MPa} \\ 0.85\text{-}0.008(f_c'\text{-}30) \ge 0.65 \text{ for } f_c' > 30 \text{ MPa} \end{cases}$	0.003
Azizinamini et al. (1994)	$\begin{cases} 0.85 \text{ for } f_c' \le 69 \text{ MPa} \\ 0.85\text{-}0.007257(f_c'\text{-}69) \ge 0.60 \text{for } f_c' > 69 \text{ MPa} \end{cases}$	$\begin{cases} 0.85 \text{ for } f_c' \le 30 \text{ MPa} \\ 0.85\text{-}0.008(f_c'\text{-}30) \ge 0.65 \text{for } f_c' > 30 \text{ MPa} \end{cases}$	0.003
Ibrahim (1994)	$0.85\text{-}0.00125f_c' \ge 0.725$	$0.95\text{-}0.0025f_c' \ge 0.7$	0.003
Pendyala & Mendis (1998)	$0.85\text{-}0.0025(f_c'\text{-}57)$ for $57\text{MPa} \le f_c' \le 100\text{MPa}$	$0.65\text{-}0.0012(f_c'\text{-}57)$for $57\text{MPa} \le f_c' \le 100\text{MPa}$	0.003
Attard & Stewart (1998)	$\begin{cases} 1.4037(f_c')^{-0.116} \ge 0.71 \text{ for non-sustained loading} \\ 0.6292(f_c')^{0.0324} \ge 0.58 \text{ sustained loading} \end{cases}$	$1.0276(f_c')^{-0.00785} \ge 0.67$	0.003
Rangan (1999)	$\begin{cases} 0.85 \text{ for } f_c' \le 55 \text{ MPa} \\ 0.85\text{-}0.004(f_c'\text{-}55) \ge 0.75 \text{ for } f_c' > 55 \text{ MPa} \end{cases}$	$\begin{cases} 0.85 \text{ for } f_c' \le 30 \text{ MPa} \\ 0.85\text{-}0.008(f_c'\text{-}30) \ge 0.65 \text{for } f_c' > 30 \text{ MPa} \end{cases}$	0.003
Bae & Bayrak (2003)	$\begin{cases} 0.85 \text{ for } f_c' \le 70 \text{ MPa} \\ 0.85\text{-}0.004(f_c'\text{-}70) \text{ for } 0.67 \le \alpha_1 < 0.85, f_c' > 70 \text{ MPa} \end{cases}$	$\begin{cases} 0.85 \text{ for } f_c' \le 30 \text{ MPa} \\ 0.85\text{-}0.004(f_c'\text{-}30) \ge 0.67 \text{ for } f_c' > 30 \text{ MPa} \end{cases}$	$\begin{cases} 0.003 \text{ for } f_c' \le 55 \text{ MPa} \\ 0.0025 \text{ and } f_c' > 55 \text{ MPa} \end{cases}$
Sun et al. (2003)	0.85	$\begin{cases} 0.85 \text{ for } f_c' \le 20 \text{ MPa} \\ 193/(207 + f_c') \ge 0.70 \text{for } f_c' > 20 \text{ MPa} \end{cases}$	$\begin{cases} 0.003 \text{ for } f_c' \le 27.6 \text{ MPa} \\ 0.2274/(48 + f_c') \ge 2.2\text{E-}3 \text{ for } f_c' > 27.6 \text{ MPa} \end{cases}$
Oztekin et al. (2003)	$0.964\text{-}0.002(f_c')$	$0.805\text{ -}0.0012f_c'$	$[2.2 + 0.015(f_c'\text{-}40)]10^{-3}$ for $64 \le f_c' \le 94$ MPa
Ozbakkaloglu & Saatcioglu (2004)	$\begin{cases} 0.85 \text{ for } f_c' \le 30 \text{ MPa} \\ 0.85\text{-}0.0014(f_c'\text{-}30) \ge 0.72 \text{ for } f_c' > 30 \text{ MPa} \end{cases}$	$\begin{cases} 0.85 \text{ for } f_c' \le 30 \text{ MPa} \\ 0.85\text{-}0.0020(f_c'\text{-}30) \ge 0.67 \text{ for } f_c' > 30 \text{ MPa} \end{cases}$	0.003
Tan & Nguyen (2005)	$\begin{cases} 0.9\text{-}0.002f_c' \text{ for } f_c' < 100 \text{ MPa} \\ 0.7 \text{ for } f_c' \ge 100 \text{ MPa} \end{cases}$	$\begin{cases} 0.9\text{-}0.002f_c' \text{for } f_c' < 100 \text{ MPa} \\ 0.7 \text{ for } f_c' \ge 100 \text{ MPa} \end{cases}$	0.003
Mertol et al. (2008)	$\begin{cases} 0.85 \text{ for } f_c' \le 68.9 \text{ MPa} \\ 0.85\text{-}0.0029(f_c'\text{-}69) \ge 0.75 \text{ for } f_c' > 68.9 \text{ MPa} \end{cases}$	$\begin{cases} 0.85 \text{ for } f_c' \le 27.6 \text{ MPa} \\ 0.85\text{-}0.007252(f_c'\text{-}28) \ge 0.65 \text{ for } f_c' > 27.6 \text{ MPa} \end{cases}$	0.003
Khadiranaikar & Awati (2012)	$0.85\text{-}0.001(f_c'\text{-}20)$ for $0.75 \le \alpha_1 \le 0.85$	$0.85\text{-}0.002(f_c'\text{-}20)$ for $0.75 \le \beta_1 \le 0.85$	0.003
f_c'= Cylinder Compressive Strength (MPa)			

© University of Pretoria

2.4.5 RECTANGULAR STRESS BLOCK PARAMETERS: DESIGN CODES

As mentioned before, the rectangular stress block is applicable at the ultimate limit state, and is characterised by the two coefficients α_1 and β_1. The results obtained by some of the researchers, mentioned in the previous section, served as a basis for the formulation of various design codes. The models proposed by some of these design codes are summarised in Table 2.5, and a graphical illustration provided in Figure 2.27 and Figure 2.28. Note that to ensure a suitable factor of safety against collapse, the models shown in Table 2.5 normally specify the use of the characteristic cylinder strength (f_{ck}) (strength of cylinders with a 95% chance of being exceeded). However, even though f_{ck} is used in *design*, it was *not* used in the *formulation* of these models.

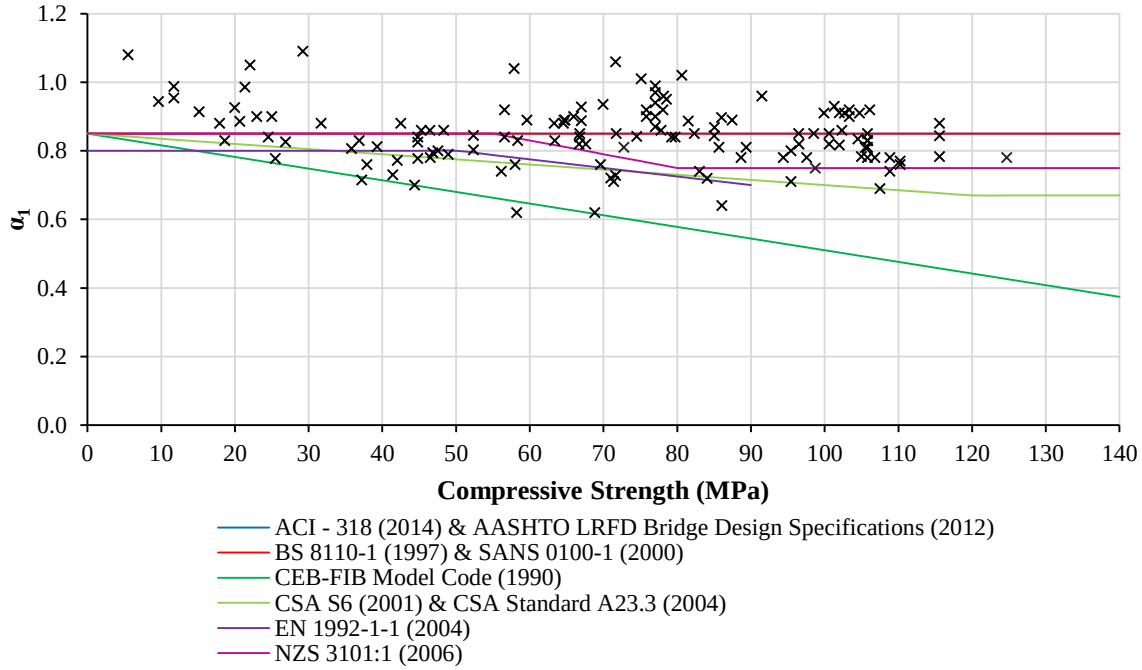

Figure 2.27 α_1 Models from Design Codes

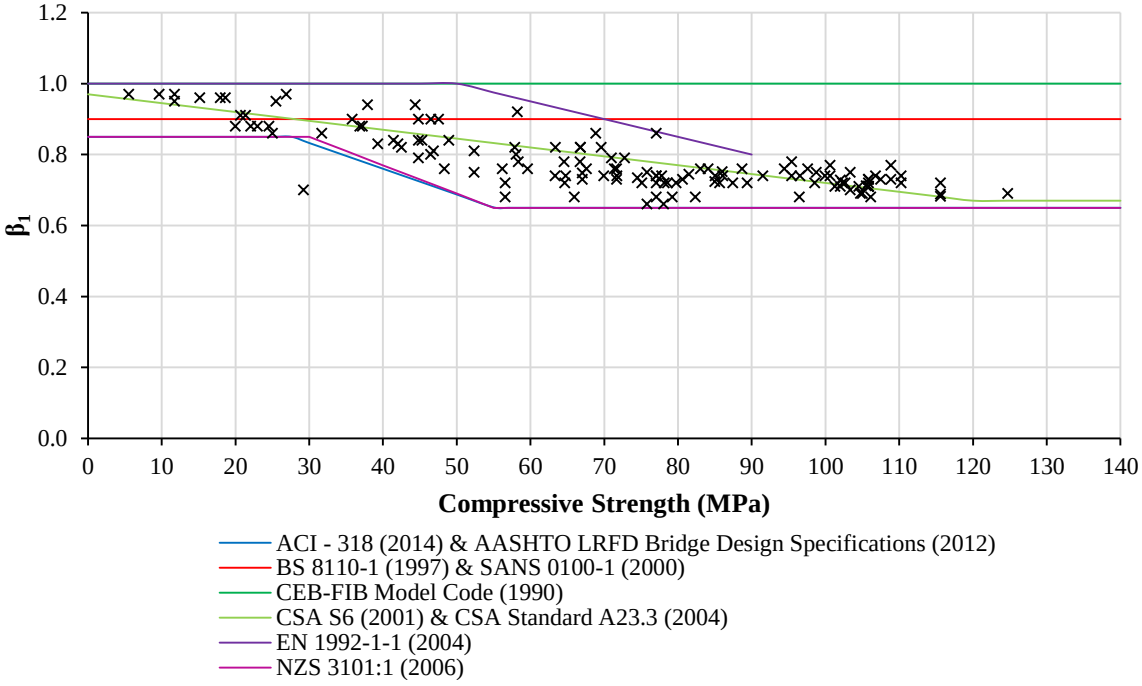

Figure 2.28 β_1 Models from Design Codes

© University of Pretoria

Table 2.5 α_1, β_1, and ε_{cu} Models Proposed by Design Codes

Code	α_1	β_1	ε_{cu}
ACI-318 (2014) & AASHTO LRFD Bridge Design Specifications (2012)	0.85	$\begin{cases} 0.85 \text{ for } f_c' \leq 27.6 \text{ MPa} \\ 0.85\text{-}0.05\left(\frac{f_c'\text{-}27.6}{6.89}\right) \geq 0.65 \text{ for } f_c' > 27.6 \text{ MPa} \end{cases}$	0.003
BS 8110-1 (1997) & SANS 0100-1 (2000)	0.85	0.9	0.0035
CEB-FIB Model Code (1990)	$0.85\left(1\text{-}\frac{f_c'}{250}\right)$	1	$0.004\text{-}\frac{0.002f_c'}{100}$
CSA S6 (2001) & CSA Standard A23.3 (2004)	$0.85 - 0.0015f_c' \geq 0.67$	$0.97 - 0.0025f_c' \geq 0.67$	0.0035
EN 1992-1-1 (2004)	$\begin{cases} 0.8 \text{ for } f_c' \leq 50 \text{ MPa} \\ 0.8\text{-}\left(\frac{f_c'\text{-}50}{400}\right) \text{for } 50\text{MPa} < f_c' \leq 90 \text{ MPa} \end{cases}$	$\begin{cases} 1 \text{ for } f_c' \leq 50 \text{ MPa} \\ 1\text{-}\left(\frac{f_c'\text{-}50}{200}\right) \text{ for } 50 \text{ MPa} < f_c' \leq 90 \text{ MPa} \end{cases}$	$\begin{cases} 0.0035 \text{ for } f_c' \leq 50 \text{ MPa} \\ 0.0026 + 0.035\left(\frac{90\text{-}f_c'}{100}\right)^4 \text{ for } 50 \text{ MPa} < f_c' \leq 90 \text{ MPa} \end{cases}$
*f_c'= Cylinder Compressive Strength (MPa), note f_c' is normally specified as the characteristic strength (f_{ck}) in design codes			

© University of Pretoria

Based on the experimental procedures presented in this section, the practicality of using steel lever arms to apply the secondary load becomes apparent. Although the initial capital investment, i.e. for the construction of the steel lever arms, is more, the long term reduction in concrete and reinforcing costs, along with the fact that existing concrete moulds can be used, means that this test method is more efficient and economical. While various specimen sizes were used, the 127 x 203 mm (4 x 8 in.) flexural compression specimen, used in conjunction with the 152 x 305 mm (6 x 12 in.) cylinder strength, originally proposed by Hognestad et al. (1955), forms the basis of the stress block parameter calculations. This means that the correlation between the stress block parameters obtained for concrete containing South African materials and the stress block parameters obtained by other researchers, can be achieved by using flexural compression specimens and cylindrical specimens with sizes equal to that proposed by Hognestad et al. (1955).

The majority of the stress block parameters presented in this section illustrated a clear dependence on compressive strength. The ability of the stress block parameter models proposed by various design codes to accurately describe the flexural and flexural compressive strength of concrete, is based on a combined plot of the α_1 and β_1 stress block parameters, and not the isolated consideration of these data plots. These models are however incapable of considering the increased compressive strength associated with a reduction in specimen size.

2.5 POISSON RATIO

The Poisson ratio of concrete may be defined as the ratio between the lateral tensile strain and longitudinal compressive strain, and has been measured by numerous researchers either through measurements done on cylinders, or the ratio between the transverse and longitudinal strain gauge readings obtained from eccentric bracket tests. One of the most important features of the Poisson ratio is that it does not remain constant with load. Thus, as the compressive load increases the Poisson ratio will approach a value of 1, signifying the failure of the material.

The finding of previous researchers, shown in Table 2.6, gives the type of specimen tested, range of concrete strengths, and range of Poisson ratios obtained. It should be noted that while researchers such as Ibrahim (1994) specified a range of Poisson ratios for eccentric specimen tests, no point estimate of the Poisson ratio was made. The point estimates of the Poisson ratios are shown in Figure 2.29 below.

Table 2.6 Summary of Poisson Ratios Obtained by Other Researchers

		Range	
Researcher	**Specimen Type**	**Compressive Strength**	**Poisson Ratio**
Komendant et al. (1978)	**152 x 406 mm Cylinder**	43.3 MPa - 72.8 MPa	0.19 - 0.24
Perenchio & Klieger (1978)	**152 x 305 mm Cylinder**	31.5 MPa - 79.8 MPa	0.19 - 0.28
Carrasquillo et al. (1981)	**102 x 203 mm Cylinder**	30.3 MPa - 76.5 MPa	0.19 - 0.24
Swartz et al. (1985)	**Eccentric Bracket Specimen: 127 x 127 x 381 mm**	66.7 MPa - 79.2 MPa	0.13 - 0.23
Jerath & Yamane (1987)	**152 x 305 mm Cylinder**	25.7 MPa - 124.9 MPa	0.1 - 0.24
Radain et al. (1993)	**152 x 305 mm Cylinder**	39.8 MPa - 115.4 MPa	0.1 - 0.2
Ibrahim (1994)	**Eccentric Bracket Specimen: 203 x 305 x 1194 mm**	57.5 MPa - 125.6 MPa	-
Iravani (1996)	**102 x 203 mm Cylinder**	64.3 MPa - 97.4 MPa	0.11 - 0.2
Logan (2005)	**102 x 203 mm Cylinder**	34.9 MPa - 115.8 MPa	0.1 - 0.29
Mertol et al. (2008)	**Eccentric Bracket Specimen: 229 x 229 x 406 mm**	71.7 MPa - 110.2 MPa	0.19 - 0.25

© University of Pretoria

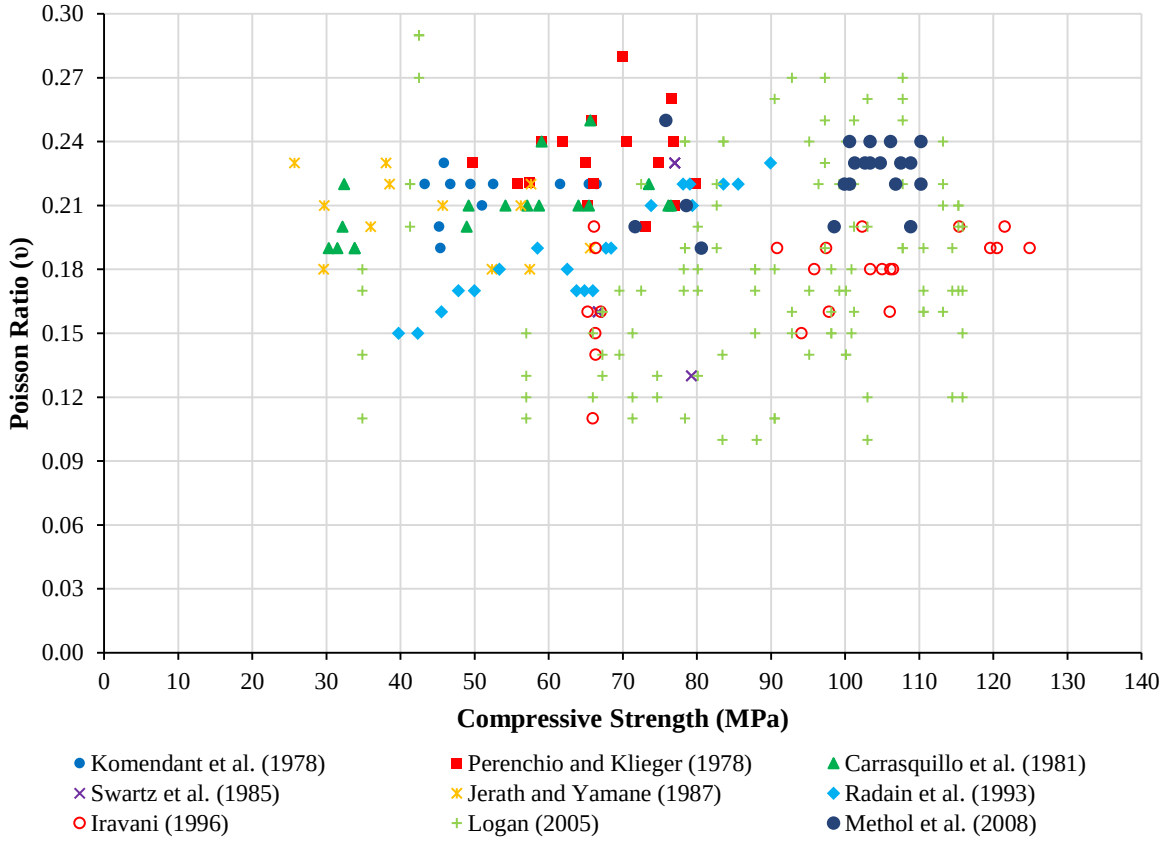

Figure 2.29 Point Estimates of Poisson Ratio Obtained by Other Researchers

The fact that the Poisson ratio of concrete can be determined using both cylinders and flexural compression specimens, together with the data obtained by previous researchers, provides an excellent bases for the comparison of the Poisson ratio obtained for concretes containing South African materials.

2.6 SIZE DEPENDANT BEHAVIOUR OF CONCRETE

2.6.1 BASICS OF SCALING

The size effect is a problem of scaling, which is central to every physical theory. The size effect may be understood as the effect of the characteristic dimension (D) on the nominal strength (σ_n) when geometrically similar structures are compared. It should be noted that the definition of D is arbitrary and can be defined as the size of the cube, the diameter of the cylinder, or the depth of a beam. The basic scaling laws are power laws for which no characteristic size exists, and are in the form of Equation 2.92 (Bazant, 1999). The power laws are applicable for theories such as elasticity with a strength limit, elasto-plasticity, and Linear Elastic Fracture Mechanics (LEFM).

$$f(D) = \left(\frac{D}{c}\right)^{s} \qquad 2.92$$

Where:

f(D)= The response quantity of interest

D= The characteristic size of the geometrically similar structures (in this case any of the structure)

c= Constant always implying a unit of measurement

s= A constant

© University of Pretoria

The exponent "s" is governed by the failure criterion of the material. For elasticity with a strength limit and plasticity (expressed in terms of stresses or strains) $s = 0$. Thus if there is no characteristic dimension, all geometrically similar structures must fail at the same nominal stress. On the other hand, $s = -0.5$ for LEFM, which, when combined with the other scaling law, plots as two lines on a $\log(\sigma_n)$ - $\log(D)$ graph (shown in Figure 2.30). The bridge between these limits represents the behaviour of a quasi-brittle materials, i.e. materials that on a small scale obeys the theory of plasticity (characterised by the material yield strength) and on a large scale obeys LEFM. Note that while plasticity theory and LEFM theory on their own possesses no characteristic length the combination of both does.

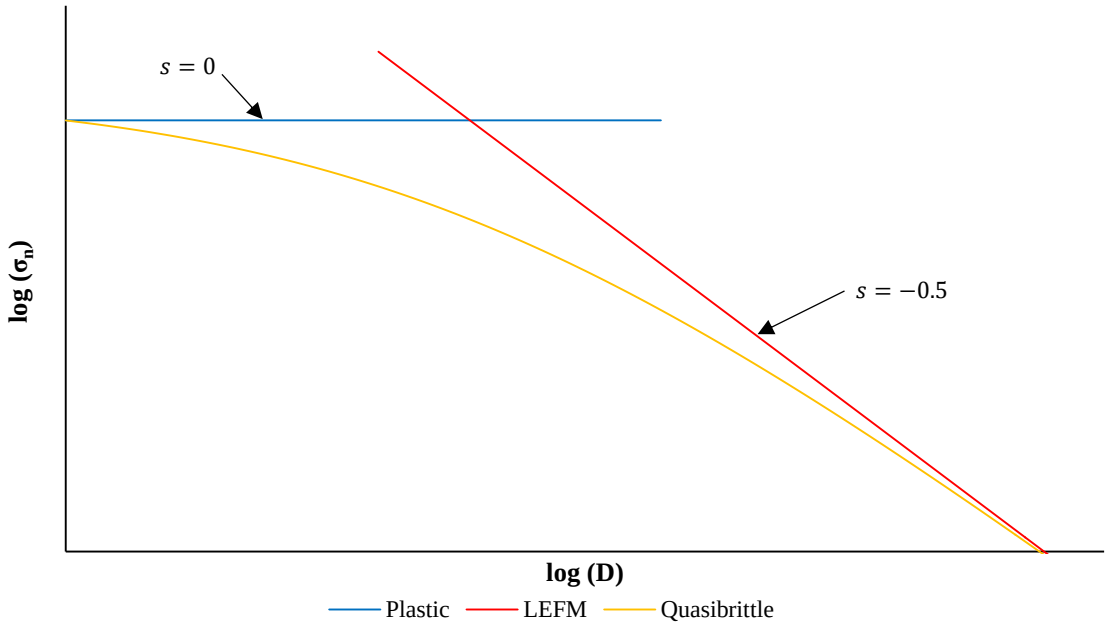

Figure 2.30 Plastic, LEFM, and Quasibrittle Size Effect

Concrete, being a quasi-brittle material, fails through the formation and propagation of cracks induced by external loads and/or environmental changes. The formation and propagation of cracks release strain energy, and the size of the specimen will thus have an influence on its mechanical properties. Bazant (1984) derived the Size Effect Law (SEL) for concrete members subjected to uniaxial tensile stress, by considering the energy balance at the instant of crack propagation. The SEL, indicated in Equation 2.93, assumes that the energy released is proportional to $nd_a a$ with "n" a constant, "a" the crack length, and d_a the maximum aggregate size.

$$\sigma_n = \frac{P}{bD} = \frac{\beta f_t'}{\sqrt{1 + D/(\lambda_0 d_a)}} \qquad \textbf{2.93}$$

Where:

σ_n= Nominal Strength (unit of stress)
P= The maximum load (unit of load)
b= The thickness of the specimen (unit of distance)
D= The characteristic dimension (unit of distance)
f_t'= Direct tensile strength of concrete (unit of stress)
d_a= Maximum aggregate size (unit of distance)
β, λ_0= Empirical Constants

© University of Pretoria

A modified form of the SEL equation, referred to as the Modified Size Effect Law (MSEL) was proposed by Kim & Eo (1990). This formulation assumed that a certain component of strength, represented by $\alpha f_t^{'}$, is independent of specimen size. The MSEL is represented by Equation 2.94.

$$\sigma_n = \frac{\beta f_t^{'}}{\sqrt{1 + D/(\lambda_0 d_a)}} + \alpha f_t^{'} \qquad \textbf{2.94}$$

Where:

α= Empirical Constant

2.6.2 UNIAXIAL COMPRESSIVE STRENGTH

Kim & Eo (1990) proposed a model to predict the uniaxial compression strength of cylindrical specimens (height /diameter ratio of two), by replacing $f_t^{'}$ with $f_c^{'}$ and the value of α assumed to vary between $0.7f_c^{'}$ and $0.85f_c^{'}$. The value of α is a function of $f_c^{'}$ and increases with an increase in $f_c^{'}$. Kim et al. (1999) found that within the practical range of aggregate sizes, the effect of aggregate size was negligible, and that a constant vale of $\alpha = 0.8$ was obtained from statistical analysis. Thus, for the range of concrete strengths it was concluded that Equation 2.95 provided an excellent relationship between the cylinder compressive strength and size.

$$f_0 = \frac{0.4f_c^{'}}{\sqrt{1 + (h\text{-}d)/50}} + 0.8f_c^{'} \qquad \textbf{2.95}$$

Where:

f_0= Compressive strength of cylindrical concrete specimen (MPa)

$f_c^{'}$= Strength of a standard concrete cylinder (MPa)

h, d= Height and diameter of cylindrical specimen (cm)

Yi et al. (2006) investigated the influence of specimen, size, shape, and casting direction on the compressive strength of concrete for 100 x 200 mm (3.94 x 7.87 in.) cylinder compressive strengths ranging between 27.0 MPa and 78.1 MPa (3.92 ksi and 11.34 ksi). Equation 2.96 and Equation 2.97 was obtained by performing a Least Squares Method (LSM) regression analysis on the cylinder and cube data. For a cube, "d" represents the cube side length in centimeters, and the cube size law effect is specified in terms of the standard cylinder compressive strength. The data obtained by Yi et al. (2006) along with Equation 2.96 and Equation 2.97 is shown in Figure 2.31 and Figure 2.32.

$$f_0 = \frac{0.49f_c^{'}}{\sqrt{1 + d/2.6}} + 0.8f_c^{'} \qquad \textbf{2.96}$$

$$f_0 = \frac{1.17f_c^{'}}{\sqrt{1 + d/2.6}} + 0.62f_c^{'} \qquad \textbf{2.97}$$

2.6.3 FLEXURAL COMPRESSION STRENGTH

Due to the fracture based theory of the SEL and MSEL, research has focused more on the pure tension and shear loading condition than on flexural compression. The topic of size effect in flexural compression caries much merit as the flexural strength of an over-reinforced concrete beam is directly related to the concrete strength, while the

© University of Pretoria

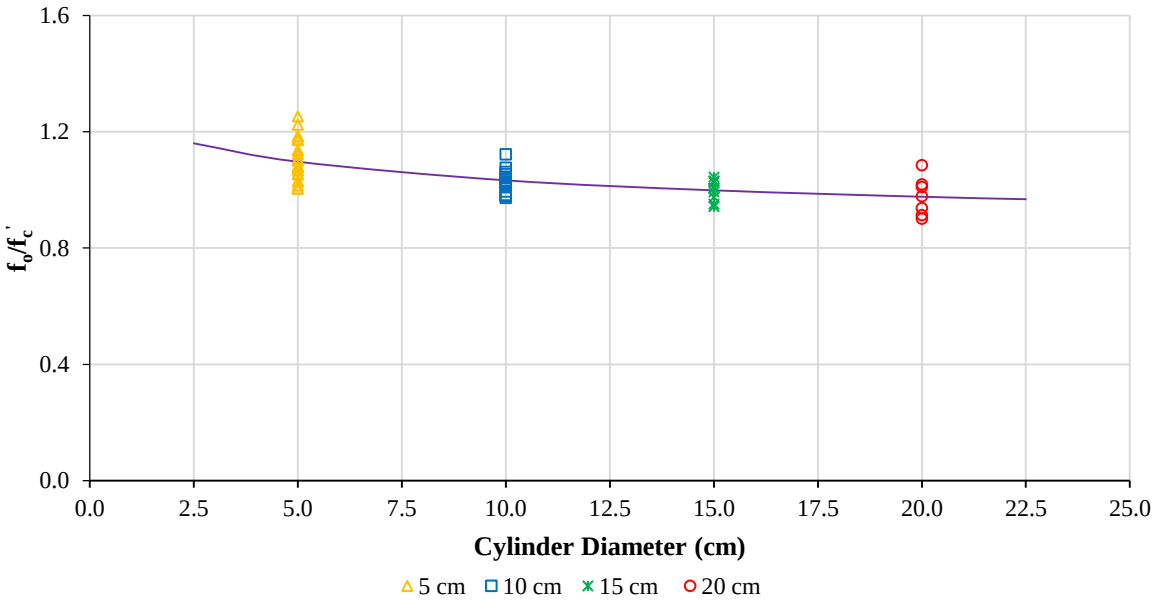

Figure 2.31 Size Effect for Cylinders Adapted from Yi et al. (2006)

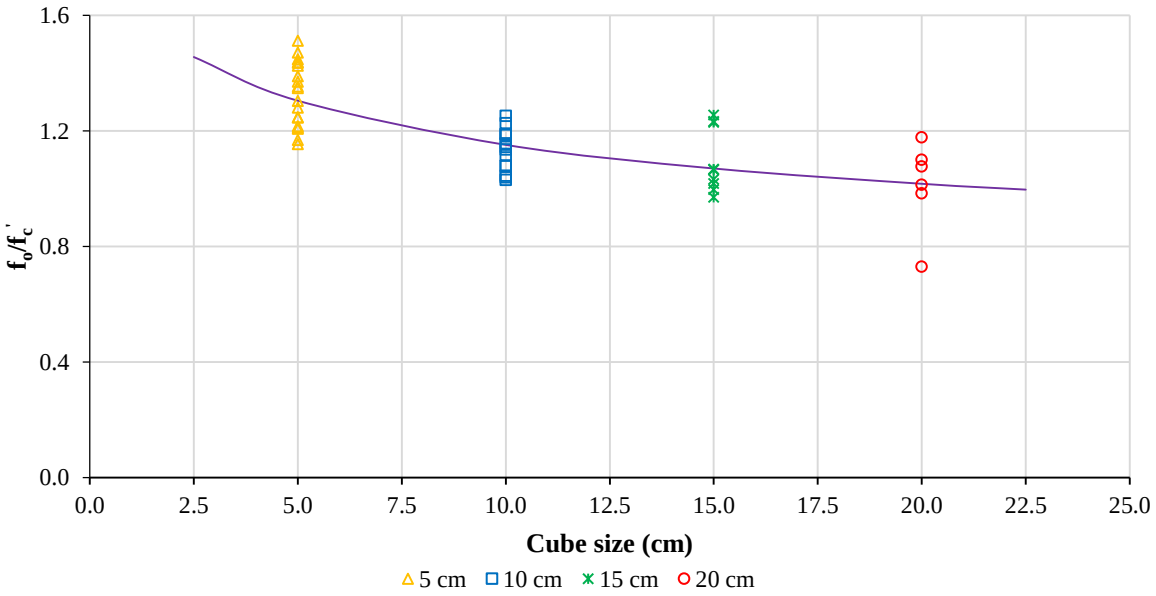

Figure 2.32 Size Effect for Cubes Adapted from Yi et al (2006)

flexural strength of an under-reinforced beam will be dictated by the amount of tensile reinforcing. Thus, for an over-reinforced beam, the size effect for compressive strength is directly related to the flexural compressive strength in the compressive region of the beam, while for an under-reinforced member, the increased flexural compressive strength results in a longer lever arm and thus an increased moment capacity. Even though research on this topic is scarce, researchers such as Kim et al. (2000) attempted to quantify the influence of specimen size on flexural compressive behaviour and the ultimate compressive strain.

The "C-shaped" specimen originally proposed by Hognestad et al. (1955) was used for the experiment by Kim et al. (2000), with the main test variable being the specimen size ratio of 1:2:4. The height h and depth c of the specimens were changed proportionally, but the specimen width 125 mm (4.9 in.) kept constant. The details of these three specimens are shown in Figure 2.33. A total of twenty-one (52.0 MPa (7.55 ksi)) "C-shaped" specimens were cast, six for 1:1 and 1:2 scales and nine for 1:4 scale. Similar to the "C-shaped" specimen used

© University of Pretoria

by Hognestad et al. (1955), the end regions were reinforced to ensure failure in the central un-reinforced section. The "C-shaped" specimens were cast horizontally, demoulded after 24-hours, and subsequently dry cured. Twelve strain gauges, located around the perimeter of the specimen, were used to measure the strain at discrete locations whilst the specimen was being tested. Along with the "C-shaped" specimens, three vertically cast 100 x 200 mm (3.94 x 7.87 in.) cylinders were used to determine $f_c^{'}$, f_{ct} (split cylinder strength), and E_c at the appropriate age.

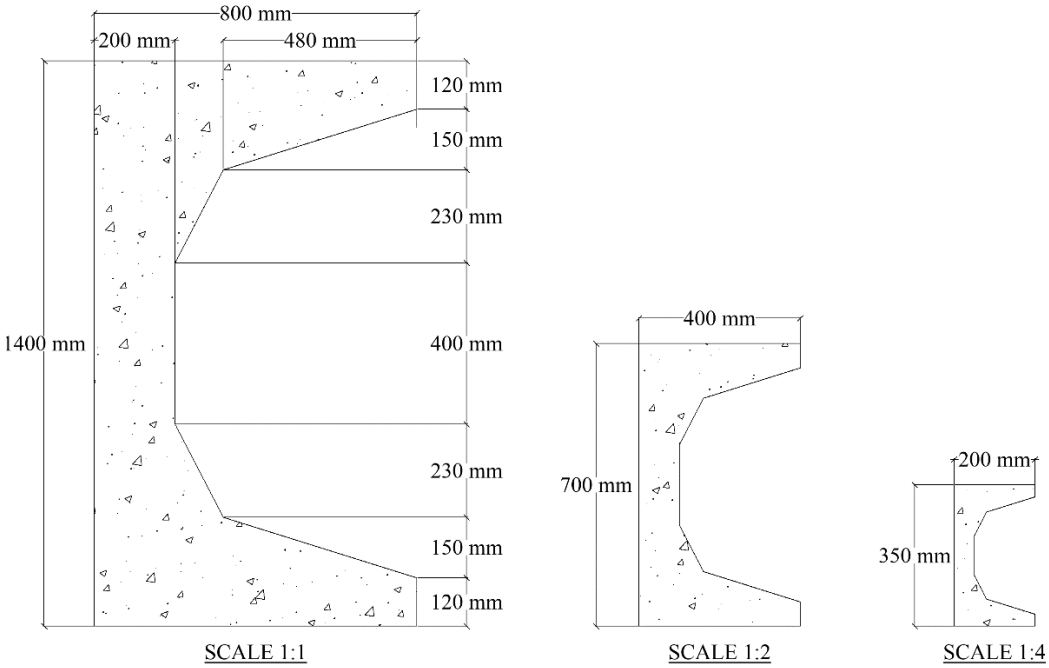

Figure 2.33 Specimen Sizes used by Kim et al. (2000)

P_1 was applied with a 2500 kN (560 kip) universal testing machine under displacement control, and P_2, for the 1:1 and 1:2 scale specimens, using a hand operated hydraulic jack with a 200 kN (45 kip) capacity. For the 1:4 scale specimens, P_2 was applied using a rod and an assembly of bolts and nuts, thus reducing the self-weight of the hydraulic jack. The test procedure consisted of applying P_1 in increments and subsequently increasing P_2 until a zero strain condition was obtained on the back face of the "C-shaped" specimen.

Kim et al. (2000) combined the SEL and the MSEL with LSM regression analysis of the twenty data points to formulate an analytical equation capable of predicting the size effect of the flexural strength of "C-shaped" specimens. The combination of the SEL and LSM regression analysis produced Equation 2.98.

$$\sigma_n = \frac{0.96f_c^{'}}{\sqrt{1 + c/22.27}} \qquad \textbf{2.98}$$

Where:

σ_n= Nominal flexural compressive strength (MPa)

c= Section depth (cm)

Assuming that the crack width could be determined from the empirical correlations mentioned at the start of this section, the combination of the MSEL and LSM regression analysis is given by Equation 2.99.

$$\sigma_n = \frac{0.70f_c^{'}}{\sqrt{1 + c/2.6}} + 0.47f_c^{'} \qquad \textbf{2.99}$$

© University of Pretoria

The ratio between the nominal flexural compressive strength and cylinder compressive strength (σ_n/f_c') is a function of the depth of the of the "C-shaped" section (measured form the compressive edge to the neutral axis of the member). Figure 2.34 illustrates the dependence of strength on section depth.

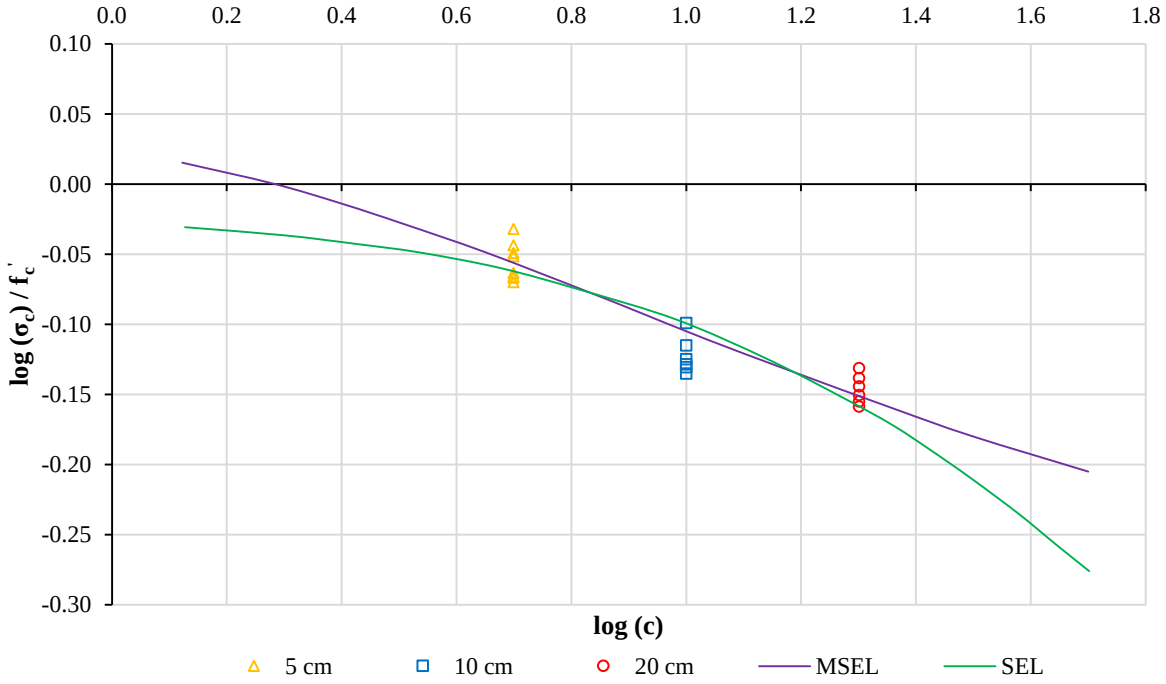

Figure 2.34 Size Effect for Flexural Compressive Stress Adapted from Kim et al. (2000)

Figure 2.35, illustrates the influence of size effect on the normalised ultimate compressive strain. Once again combining the MSEL and LSM regression analysis, Kim et al. (2000) obtained Equation 2.100, which provided the relationship between, $\varepsilon_{cu}/\varepsilon_{cu20}$ and $c/20$ as the 20 cm section can be considered as the reference size.

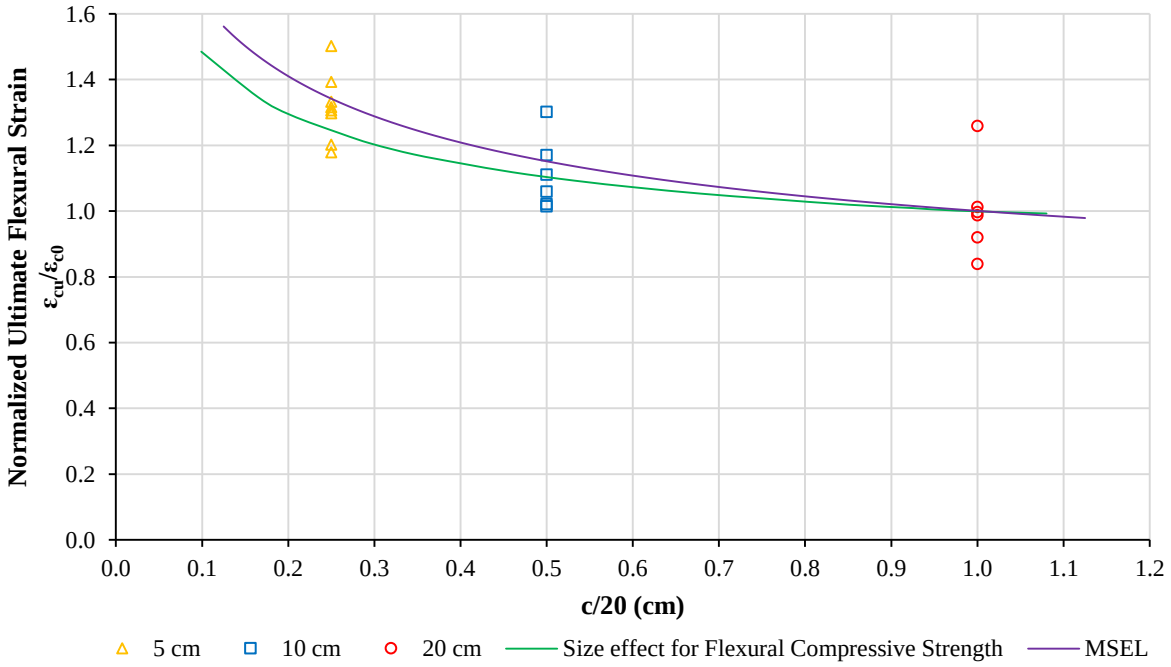

Figure 2.35 Size Effect for Ultimate Compressive Strain Adapted from Kim et al. (2000)

$$\varepsilon_{cu} = \frac{1.70\varepsilon_{cu20}}{\sqrt{1 + 17(c/20)}} + 0.6\varepsilon_{cu20} \qquad \textbf{2.100}$$

© University of Pretoria

Based on Equation 2.100, Kim et al. (2000) concluded that similar to the nominal flexural compressive strength, the ultimate compressive strain of the specimen decreased as the size of the specimen increased. It was also concluded that at high load levels the strain distribution with depth was nonlinear. This nonlinearity was deemed insignificant, and the assumption that plane sections remain plane during bending was concluded to still be valid. From Figure 2.35 it is clear that there is a strong size dependence with the MSEL best describing the experimental results. The reduction in flexural compressive strength with specimen size is more apparent than for pure uniaxial compression.

2.7 SUMMARY OF LITERATURE

In this chapter, background was provided on the factors influencing the compressive behaviour, modulus of elasticity, and the flexural compressive behaviour of concrete. The aim of this investigation is to determine the effect of specimen size and compressive strength on the stress block parameters of concrete. In order for the stress block parameters to be determined in the most accurate way the mix designs needs to be as simple as possible, should contain near similar volumetric portions of aggregate, and consist of a single cement type. Additionally, curing the concrete for 28 days before drying the specimens should result in the smallest possible variation in strength for a particular mix. The rate of loading of the flexural compression specimens should be the same in order for the stress-strain behaviour, obtained for each specimen size to be correlated.

As a lot of research has gone into the development of models capable of accurately describing the stress-strain relationship of concrete, these models can be calibrated using the experimental results obtained in this study. The most suitable relationship can then selected based on both the simplicity of the model and error between calculated and experimental values. Furthermore, while the “C-shaped” specimen, proposed by Hognestad et al. (1955) provided a convenient method of testing specimens in flexural compression, P_2 will be applied by using detachable steel lever arms as this proceure would result in a reduced long term material cost and also enable the use of standard concrete moulds (as opposed to the “C-shaped” specimen moulds needing to be manufactured). The experimental program, used to determine the influence of specimen size and compressive strength on the stress block parameters of concrete will be presented in Chapter 3.

© University of Pretoria

CHAPTER 3

EXPERIMENTAL PROGRAM

3.1 INTRODUCTION

This chapter describes the experimental program developed to study the effects of change in water/cement ratio and specimen size on the uniaxial compressive strength and stress block parameters of concrete. A detailed description is provided of the equipment and procedure used to measure the strain distribution through the depth of the flexural compression sections, along with a less detailed description of the procedures used to measure the various aggregate properties, and the cube and cylinder-compressive strengths.

3.2 MATERIAL SPECIFICATION

3.2.1 CEMENT

PPC CEM I 52.5 N Cement, was used as the sole binder for this experiment. An attractive property of PPC CEM I 52.5 N cement with Relative Density (R.D) of 3.09, is that it can be considered as a pure cement, composed of approximately 95% clinker and 5% gypsum, and complies with the requirements set out in SANS 50197-1 (2000).

3.2.2 AGGREGATE

As aggregate constitutes such a significant volumetric fraction of concrete, its properties will have a major influence on the compressive strength, modulus of elasticity, and the flexural compressive behaviour of the concrete. Dolomite (R.D = 2.83) with a maximum aggregate size of 4.75 mm, constituted the aggregate portion of the mix. Dolomite, or Dolomitic limestone, is a calcareous rock originating from the Griqualand West sequence or alternatively the Chinispoort group of the Transvaal sequence. The Dolomite aggregate used in this study is a product of the Lyttleton Centurion mine, which supplies both coarse and fine aggregate to the construction industry. The reason for the selection of this specific aggregate was:

- Even though smaller aggregate results in an increased water requirement for a specified workability, the increase in compressive strength, especially in the production of high strength concrete, is desirable. The increased water requirement, caused by the reduction in aggregate size and the use of angular particles, was not a problem due to the superior strength development of the cement. Thus, high strength concrete can be obtained without a large reduction in the water/cement ratio.

© University of Pretoria

- The production of high strength concrete requires a specific type of grading curve. For the purposes of this project, the grading of the aggregate was assumed adequate for the production of both high strength and normal strength concrete. The grading characteristics of the Dolomitic aggregate are shown in Table 3.1 and Figure 3.1.
- Seeing that only one aggregate source was used, the influence of mineralogical composition is eliminated. Additionally, Figure 3.1 shows that the Dolomite aggregate does not have any intermediate sizes missing. Thus, for a R.D of 2.83, segregation should theoretically not be a problem.

Table 3.1 Aggregate Grading

Material	Dolomite Aggregate	SANS 1083 (2014) Specification
Sieve Size (mm)	**Percentage Passing (%)**	**Percentage Passing (%)**
6.7	100.0	-
4.75	92.9	90-100%
2.36	56.5	-
1.18	35.2	-
0.6	23.6	-
0.3	16.1	-
0.15	10.1	-
0.075	7.3	≤10

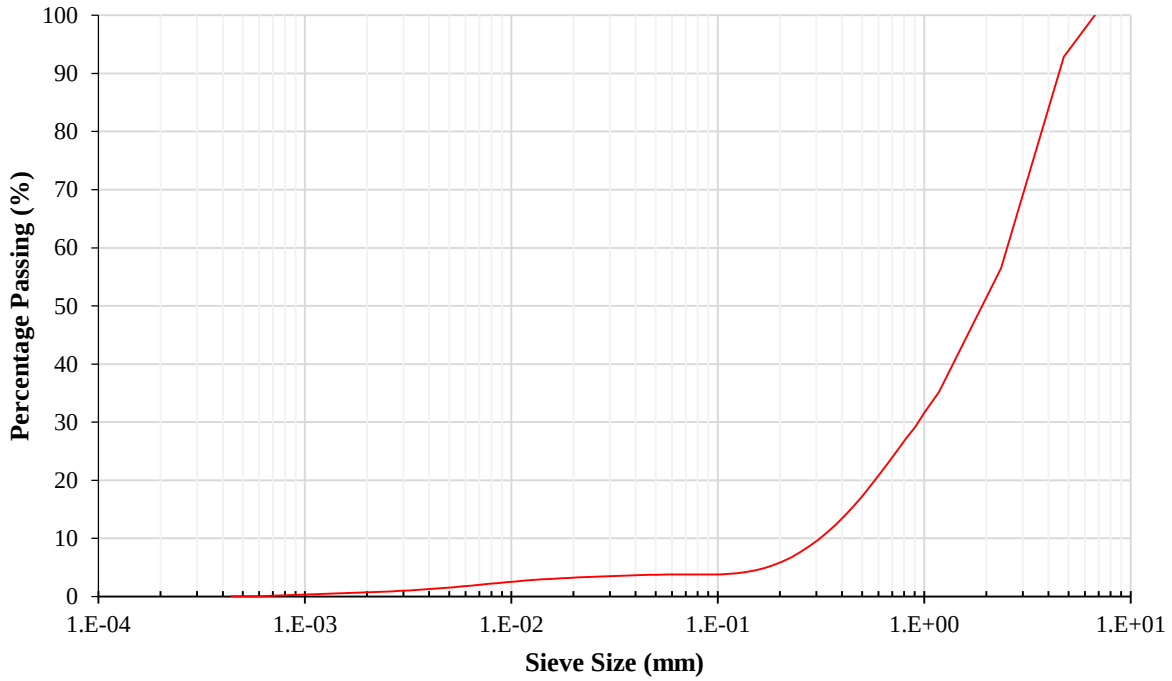

Figure 3.1 Aggregate Grading Curve

3.3 MIX PROPORTIONS, VOLUMES, AND CURING

The mixes, specified in Table 3.2, were aimed at achieving 150 x 300 mm cylinder target strengths of 40 MPa, 65 MPa, and 80 MPa. The elements and their respective quantities cast for each individual mix are shown in Table 3.3. Both cubes and cylinders were tested in order to investigate the influence of size and shape on the uniaxial compressive strength and uniaxial compressive stress-strain relationship. It is worthwhile mentioning that the 150 mm cubes and 150 mm cylinders were chosen to provide an indication of both the standard concrete compressive strength, and the parameter necessary for the Modified Size Effect Law (MSEL).

© University of Pretoria

Table 3.2 Mix Proportions for Target Concrete Strengths

	Target Strength (MPa)		
	40	**65**	**80**
PPC CEM 52.5 N (kg/m^3)	269	400	536
Total Water (kg/m^3)	222	227	231
Dolomite Sand (kg/m^3)	1980	1848	1711
Total Mix Weight (kg/m^3)	2471	2475	2478
Water/Cement	0.8	0.57	0.43

Table 3.3 Mix Quantities

Element		
Designation	**Dimensions**	**Quantity**
Cubes	**50 x 50 x 50 mm**	12
	100 x 100 x 100 mm	12
	150 x 150 x 150 mm	12
	200 x 200 x 200 mm	5
Cylinders	**50 x 100 mm**	12
	100 x 200 mm	12
	150 x 300 mm	12
	200 x 400 mm	5
Flexural Compressive Members	**50 x 50 x 300 mm**	3
	100 x 100 x 500 mm	3
	200 x 200 x 1000 mm	3

Although a reduction in specimen size is known to result in an increase in compressive strength variability, this increase in variability was not considered in selecting the quantity of specimens to be tested for each size. Batching and mixing of materials was done in accordance with SANS 5861:1 (2006) and the specimens prepared in accordance with SANS 5861:3 (2006). After casting, the specimens were covered with a plastic sheet to minimise surface evaporation, and stored in a curing room at a temperature of 23±1℃ and a relative humidity of 65%. 24 hours later, the specimens were demoulded and water cured for 28 days. After 28 days, the specimens were placed in an oven for a period of 2 days at 50˚C to remove any moisture that may cause an increase in the compressive strength.

3.4 EXPERIMENTAL METHOD AND EQUIPMENT

In this section, a description of the equipment, their corresponding accuracies, and in certain cases the dimensions of specialized (nonstandard) equipment used during the course of the experiment is provided. Additionally, the construction procedure of the flexural compression specimens and test setup used to obtain the flexural compression strain distribution, is described.

3.4.1 COMPRESSIVE STRENGTH, MODULUS OF ELASTICITY, AND POISSON RATIO

The 200 mm cubes and 200 mm cylinder moulds were manufactured at the University of Pretoria, and the 50 mm, 100 mm, and 150 mm cube and cylinder mould dimensions were within the tolerances specified by SANS 5860 (2006) and ASTM C470/C470M (2015). A minimum of 14 days after being placed in water, the cylinders were grinded in accordance with SANS 5863 (2006). SANS 5863 (2006) specifies the rate of compressive load application needs to be 0.3 ± 0.1 MPa/s while ASTM C39/C39M (2015) specifies a loading rate of 0.24

© University of Pretoria

± 0.05 MPa/s until failure. Seeing that the rate of loading has an effect on the compressive strength, a loading rate of 0.3 MPa/s was chosen, as it is the average specified in SANS 5863 (2006) and an upper limit for ASTM C39/C39M (2015). The compressive strength of the specimens was tested with a 5000 kN Advantest 9 Controls concrete press, meeting the requirements of BS EN 12390-4 (2000).

For each mix, the cubes were crushed to obtain an indication of the compressive strength, which was subsequently used to select the upper bound load for the secant modulus of elasticity test. The 50 mm, 100 mm, and 150 mm cylinder stress-strain relationships were obtained by using suitable sized compressometers, while the 200 mm cylinder stress-strain relationships were obtained using a Universal Electronic Compressometer. The 150 mm cylinder compressometer measured both longitudinal and transverse deformation, making it possible to calculate the Poisson ratio.

Some of the compressive stress-strain models use parameters such as the initial tangential modulus to define the stress-strain relationship. Thus, as part of the uniaxial cylinder compressive test, each specimen is loaded to the upper stress level (specified for the calculation of the secant modulus of elasticity) and the stress subsequently reduced to a lower bound value. This cycle is repeated three times to ensure that the concrete remains elastic. After the third cycle, the load is increased at the aforementioned rate before failure is finally achieved. Seeing that the stress-strain curve is obtained, the initial tangential modulus and secant modulus of elasticity for the 50 mm, 100 mm, 150 mm, and 200 mm cylinders can be determined in accordance with ASTM C469/C469M (2014).

3.4.2 FLEXURAL COMPRESSION

Chapter 2 illustrated that there are two approaches, utilising either steel or reinforced concrete lever arms to transfer the eccentrically applied load to the flexural compression specimen. For this experiment, the test method employed by Mertol et al. (2008) was modified to provide a more cost effective solution.

3.4.2.1 SELECTION OF FLEXURAL COMPRESSION SECTION

The original “C-Shaped” specimen proposed by Hognestad et al. (1955) had a rectangular cross section, however, Soliman & Yu (1967) concluded that the width of the cross section had no marked influence on the flexural compressive strain distribution. Kim et al. (2000) considered the influence of three specimen sizes on the flexural compressive member (scale 1:1, 1:2, and 1:4), and established that for concrete with a compressive strength of 52 MPa, the influence of specimen size on the average flexural compressive stress and ultimate compressive strain is apparent.

Thus, for the purpose of this experiment, the influence of concrete compressive strength and specimen size on the stress block parameters of concrete was evaluated by considering three concrete strengths 40 MPa, 65 MPa, and 80 MPa for three specimen scales (1:1, 1:2, and 1:4). The 1:1 scale specimens had cross section dimensions of 200 x 200 mm and a length of 1000 mm, and were used to check whether the stress block parameters of concrete containing South African materials correlates with the stress block parameters obtained by other researchers. The depth of the cross section corresponds to the approximate depth originally proposed by Hognestad et al. (1955), and the length to the dimension proposed by Mertol et al. (2008).

© University of Pretoria

3.4.2.2 TEST SPECIMENS REINFORCING LAYOUT AND PREPARATION

The ends of the flexural compression specimens were heavily reinforced with SANS 920 (2011) approved Grade 450 MPa hot rolled high yield steel bars. The reinforcing configuration in the end regions of the concrete sections are illustrated in Figure 3.2. The presence of the longitudinal and shear reinforcing not only promotes the failure of the concrete specimen in the central unconfined region, but also the proper transfer of both the axial load and the bending moment. The longitudinal reinforcing for the 1:1, 1:2, and 1:4 scale specimens consisted of three Y 12, two Y 8, and two Y 5 bars respectively. Transverse reinforcing, used in the 1:1 and 1:2 scale specimens, consisted of three Y 10 and three Y 6 bars respectively, with 2 mm steel wire used to enclose the 1:4 scale specimen cages. As show in Figure 3.3 and Figure 3.4, the longitudinal position of the reinforcing cages were adjusted so that the central unreinforced region was as required. As the specimens were cast horizontally, this provided some difficulty with regards to the attachment of the lever arms. Ideally, the lever arm end plates should be attached to a smooth and even surface, a difficult task considering the casting direction. The flexural compression specimens were therefore grinded, with the 1:2 and 1:4 scale specimens being small enough to have the entire front flexural compression face ground. For the 1:1 scale specimens, grinding was restricted to the top and bottom 300 mm of the flexural compressive face.

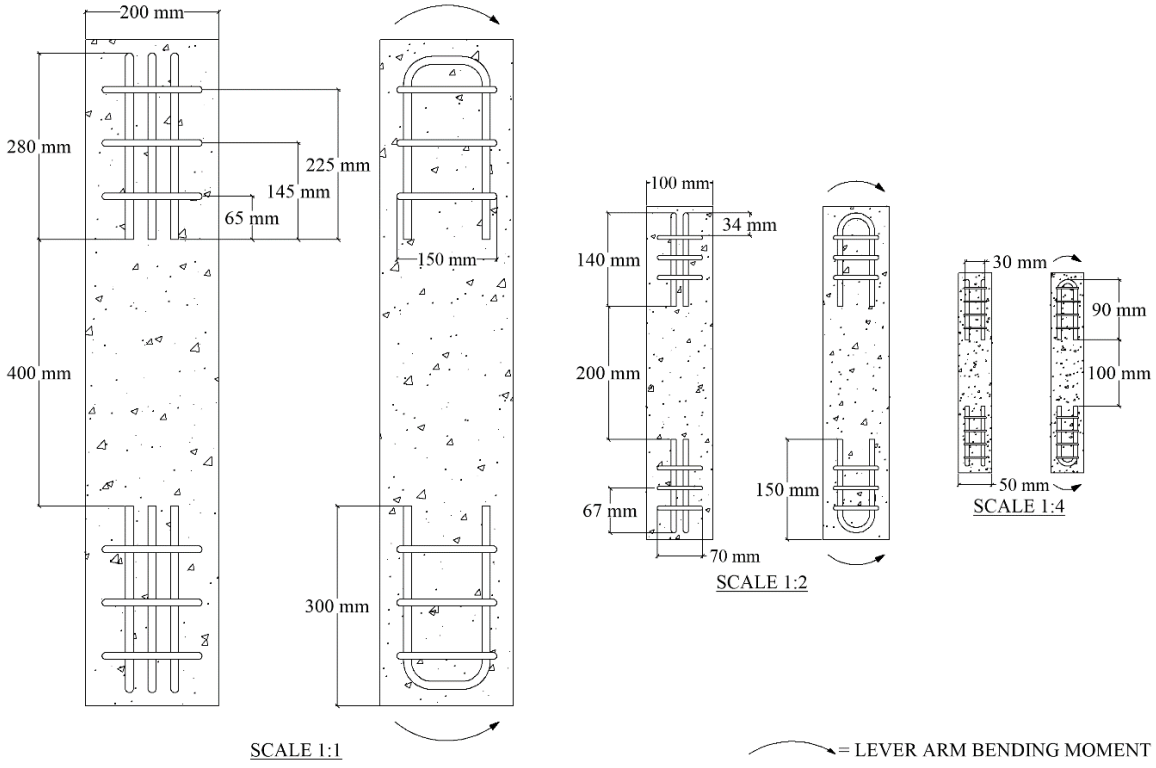

Figure 3.2 Configuration of Longitudinal and Shear Reinforcing in Flexural Compression Members

After the casting and grinding, the compressive flexural members were moved to a constant temperature room and the central concrete region sanded. Pressurised air and Acetone cleaning agent were used to remove the majority of particulate matter and/or any residue present on the specimen surface. The position of the electrical resistance strain gauges (shown in Figure 3.5 to Figure 3.7) was marked on the surface of the specimen, and the strain gauges prepared. Each specimen was instrumented with 30 mm long BK 2/120 strain gauges. Six strain gauges were attached to the 1:2 and 1:4 scale flexural compressive specimens, and nine to the 1:1 scale specimens. All specimens had three strain gauges on the flexural compressive surface, two monitoring the longitudinal

© University of Pretoria

compressive strain and one the transverse tensile strain. X60 bonding agent, a two-component fast curing adhesive consisting of a liquid (component B) and a powder (component A), was used to fasten the strain gauges to the surface of the specimen. After the bonding agent had set, a 4 x 4 grid of electronic stripboard (containing 0.3 mm twin-flex wire) was soldered to each strain gauge, enabling the quick and easy connection of the strain gauges to the monitoring system. The 0.3 mm twin-flex wires were glued to the surface of the concrete specimen, reducing their susceptibility to be impaired during the handling of the specimen both prior to, and during testing.

Figure 3.3 Reinforcing Layout and Fixing System for Scale 1:1 Specimens

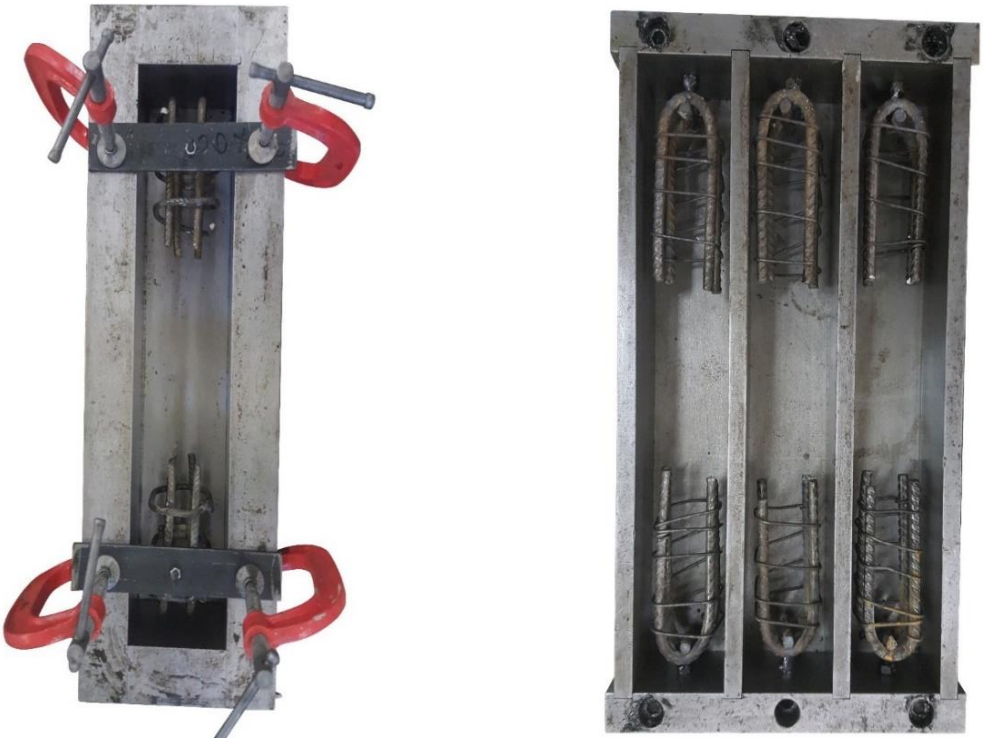

Figure 3.4 Reinforcing Layout and Fixing System for Scale 1:2 (Left) and Scale 1:4 (Right) Specimens

© University of Pretoria

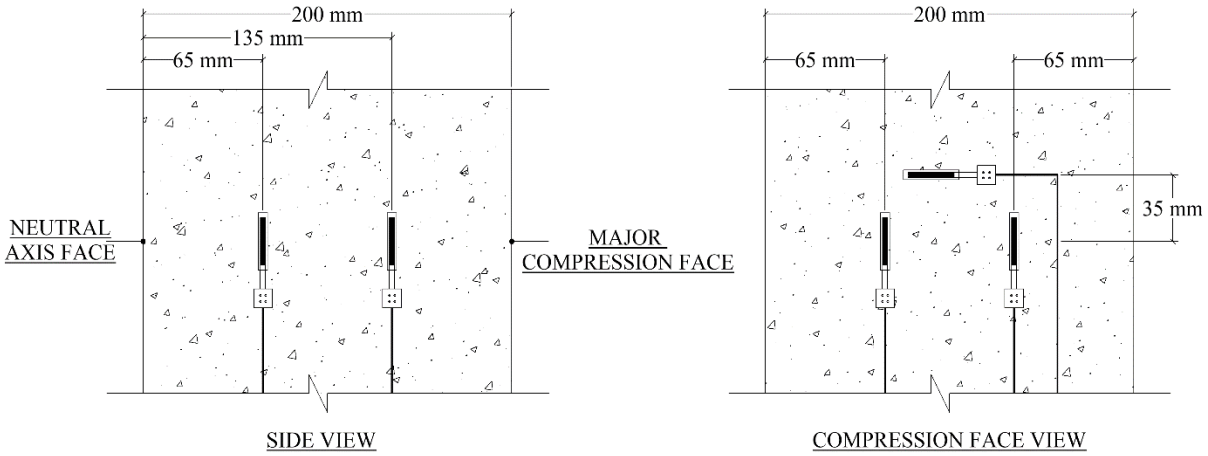

Figure 3.5 Strain Gauge Layout for Scale 1:1 Flexural Compression Specimens

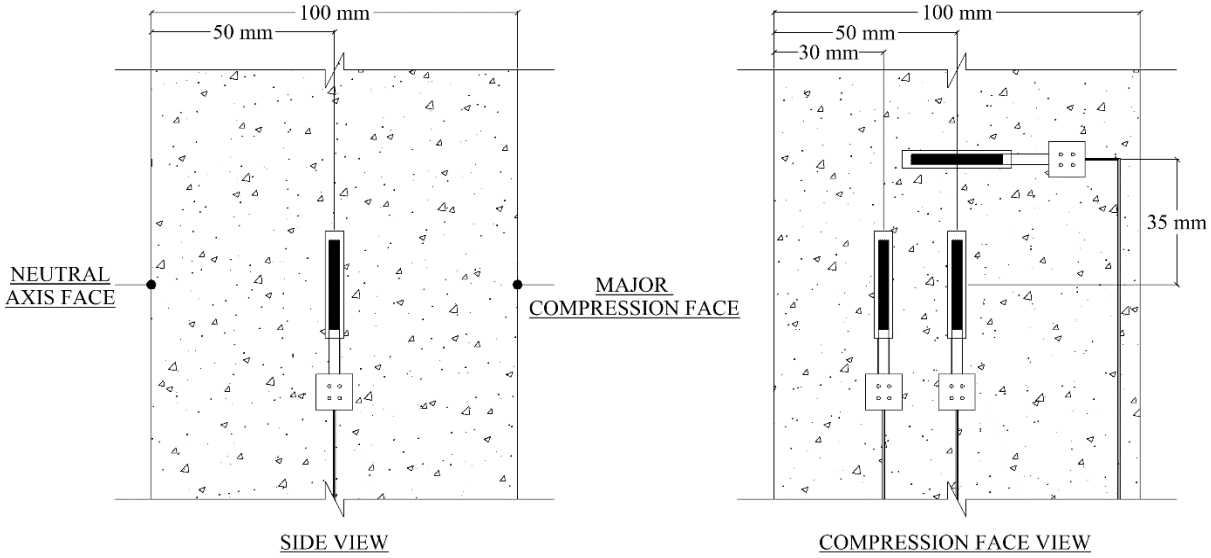

Figure 3.6 Strain Gauge Layout for Scale 1:2 Flexural Compression Specimens

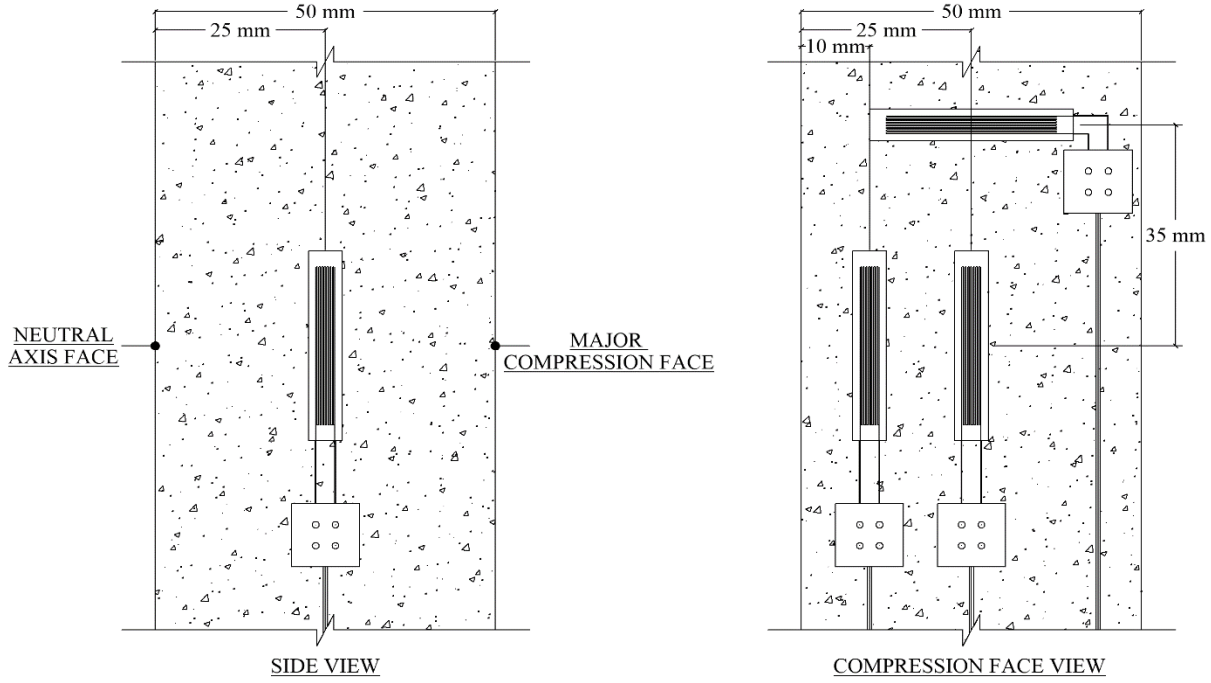

Figure 3.7 Strain Gauge Layout for Scale 1:4 Flexural Compression Specimens

© University of Pretoria

3.4.2.3 ECCENTRIC SPECIMEN LEVER ARMS

Methol et al. (2008), proposed the use of steel tube sections located in the end regions of the flexural compression members, and a bolt assembly system extending through the concrete specimen itself. This experimental procedure was convenient in terms of the design of the lever arm and the backing plate, but the high cost of the square tubing made this approach impractical. A more economical design was obtained by using a bolt assembly system that extended *around* the specimen. The lateral confinement of the concrete located in the end regions were obtained using a frictional system, details of which will be discussed for each specimen size. Thus, the cost of the square tubing sections located in the end regions was eliminated. Detailed drawings of the steel lever arms followed by a general isometric view of the lever arm, back plate assembly, and side confinement plates are shown in Figure 3.8 to Figure 3.14. Note that unless otherwise mentioned all steel was GR 355 JR.

For the 1:1 scale lever arms (shown in Figure 3.8), three web-stiffeners(1) were welded inside each of the two PC 200 x 75 channel sections (2) (see Figure 3.8 and Figure 3.9) to eliminate the possibility of web crippling and/or bulking under the application of the load P_2. The two PC 200 x 75 channel sections were attached to a 400 x 260 x 25 mm steel end plate(3) via a 15 mm welds, and subsequently linked with two 600 x 180 x 8 mm steel plates(4) attached to their top and bottom flanges. Four 178 x 100 x 8 mm triangular steel plates(5) were used to stiffen the end plate and ensure the uniform spread of the bending moment across its width. Holes, 30 mm in diameter, were drilled through the 8 mm steel cover plates (470 mm from the face of the end plate) through which the 26.5 mm prestressing bar, used to apply P_2, passed. Seeing that the stiffness of the system depends on the stiffness of the back end plate, two PC 200 x 75 channel sections(6) were welded to the 400 x 260 x 25 mm back end plate(7) to improve its stiffness. M33 Gr. 8.8 high tensile threaded rods(8) linked the lever arm to the back plate assembly. Finally, the friction generated by tightening the twelve nuts inside the two PC 200 x 75 side channels(9) (milled to reduce the major dimension from 200 mm to 199.5 ± 0.1 mm) provided the necessary confinement.

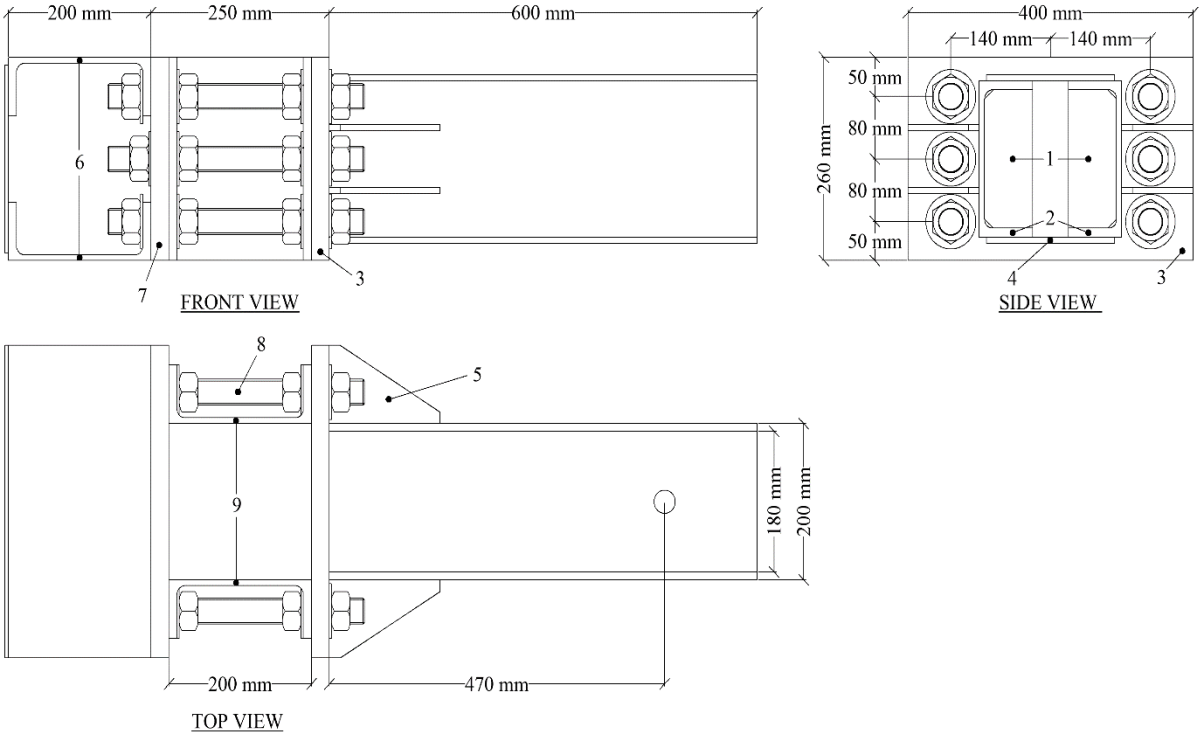

Figure 3.8 Scale 1:1 Detailed Lever Arm Drawing

© University of Pretoria

Figure 3.9 Scale 1:1 Lever Arm, Back Plate, and Confinement Plate

As shown in Figure 3.10 and Figure 3.11, the 1:2 scale lever arms contained three web stiffeners(1), welded inside each of the C 100 x 50 channel sections(2) at the point of application of P_2. The C 100 x 50 channel sections were attached to a 250 x 130 x 20 mm end plate(3) via a 10 mm weld, and subsequently linked using two 400 x 90 x 5 mm steel plates(4) attached to their top and bottom flanges. Two 105 x 65 x 8 mm triangular steel plates(5) were used to stiffen the end plate and ensure the uniform spread of the bending moment across its width. Holes, 14 mm in diameter, were drilled through the 5 mm cover plates (330 mm from the face of the end plate) through which the 9.6 mm seven-wire strand, used to apply P_2, passed. Two C 100 x 50 channel sections(6) (attached to the 250 x 130 x 20 mm steel end plate(7)) improved the stiffness of the back end plate, and thus the stiffness of the system. Two C 100 x 50 channel sections(8) (milled to reduce the major dimension from 100 mm to 99.5 ± 0.1 mm) provided the lateral confinement of the concrete in the end regions, through friction generated by tightening the nuts on the four 16 mm Gr. 8.8 high tensile threaded rods(9) (used to link the lever arm to the back plate assembly).

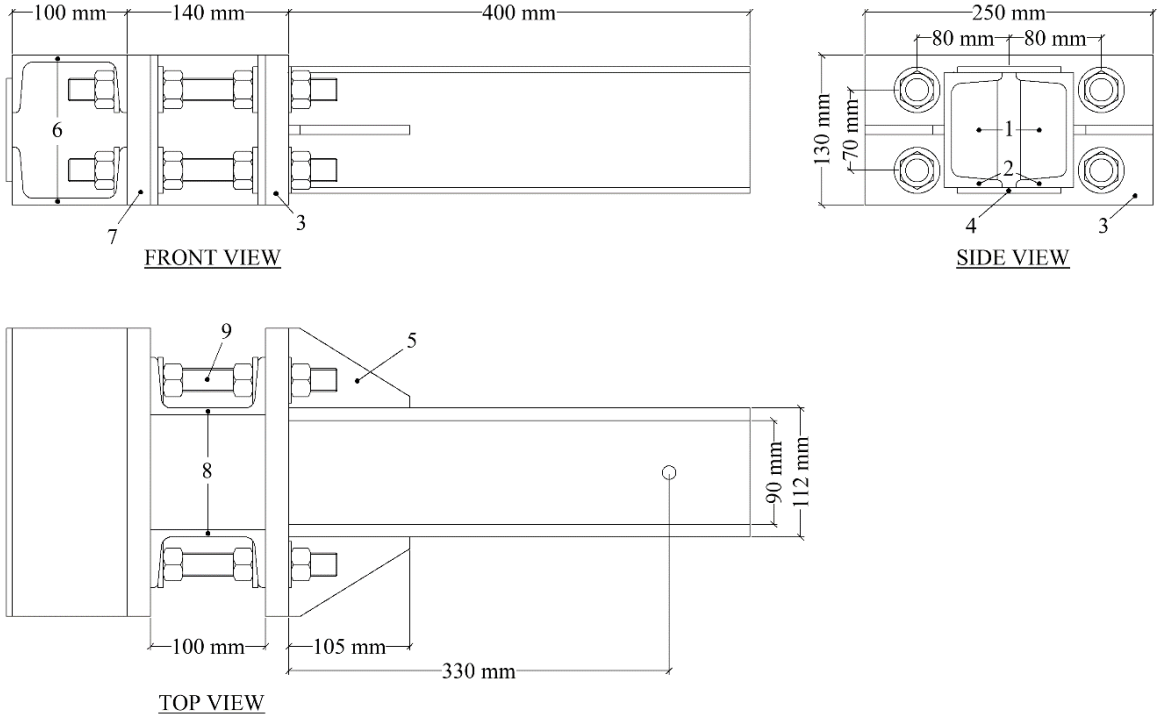

Figure 3.10 Scale 1:2 Detailed Lever Arm Drawing

© University of Pretoria

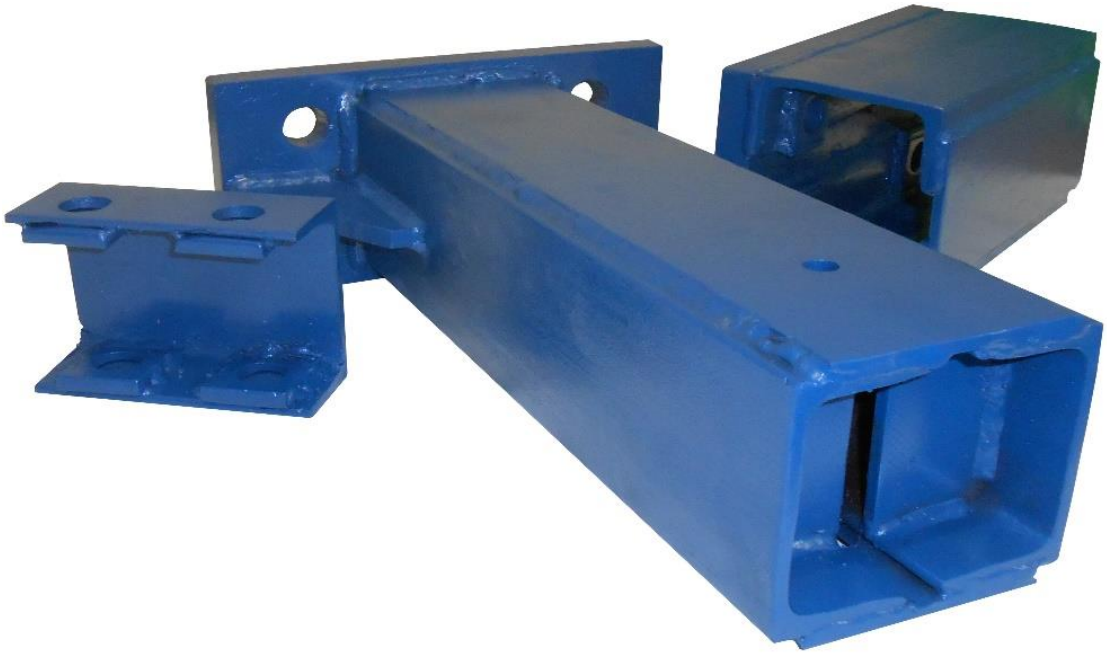

Figure 3.11 Scale 1:2 Lever Arm, Back Plate and Confinement Plate

As shown in Figure 3.12, the 1:4 scale lever arms consisted of a 50 x 50 x 4.5 mm square tubing section(1) attached to a 150 x 85 x 16 mm steel end plate(2) via an 8 mm fillet weld. Holes, 12 mm in diameter, were drilled 170 mm from the face of the 16 mm end plate, through which a 7 mm (1760 MPa) rod used to transfer P_2 passed. Two 50 x 50 x 2.5 mm square hollow sections(3) (milled to reduce the major dimension from 50 mm to 49.5 ± 0.1 mm), coupled with the friction generated by tightening the bolts on the four 16 mm Gr. 8.8 high tensile bolts(4), ensured the lateral confinement of the concrete in the end regions. The steel back plates, lever arm, and confinement plates are shown in Figure 3.13 while a general isometric view of the three lever arms are shown in Figure 3.14

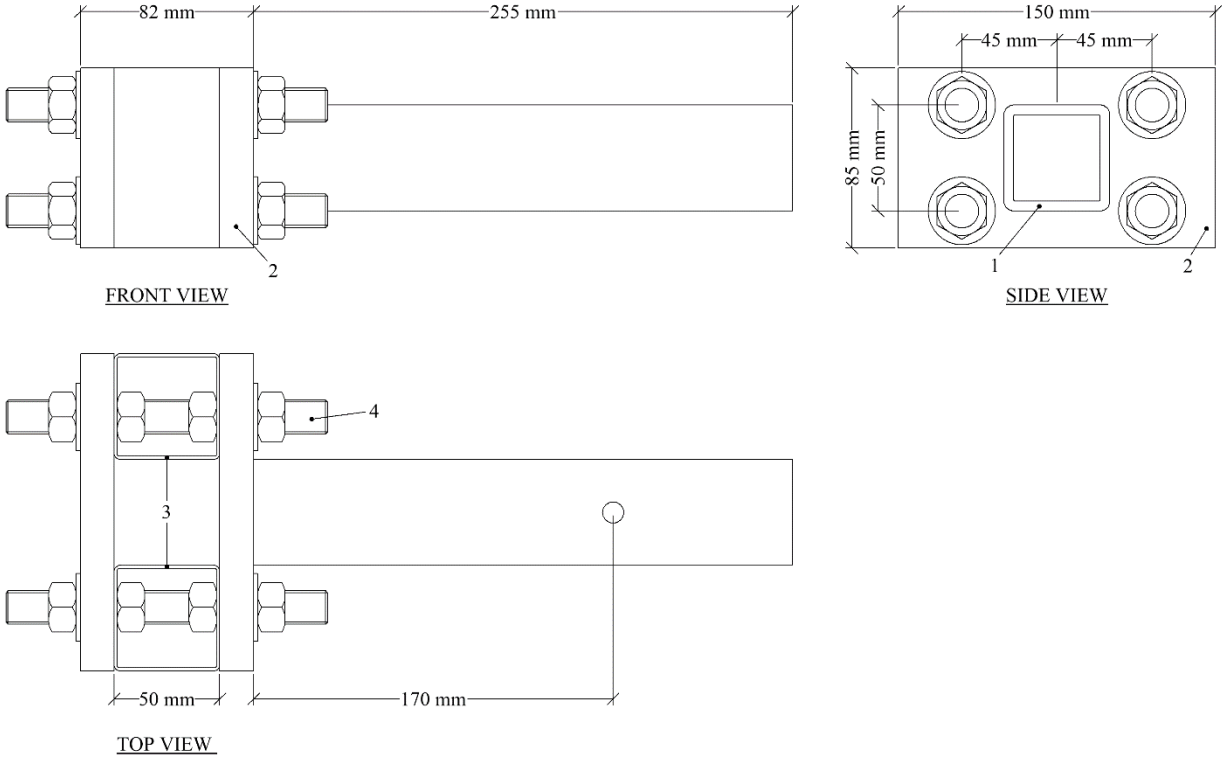

Figure 3.12 Scale 1:4 Detailed Lever Arm Drawing

© University of Pretoria

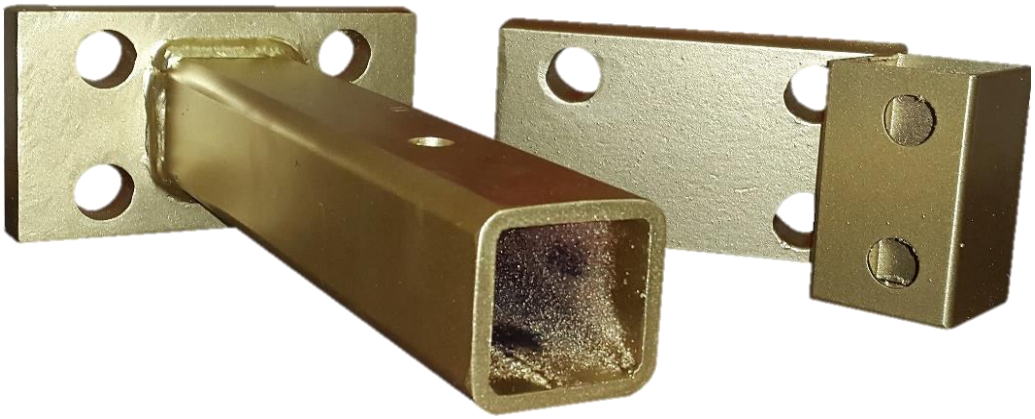

Figure 3.13 Isometric View Scale 1:4 Lever Arm, Back Plate and Confinement Plate

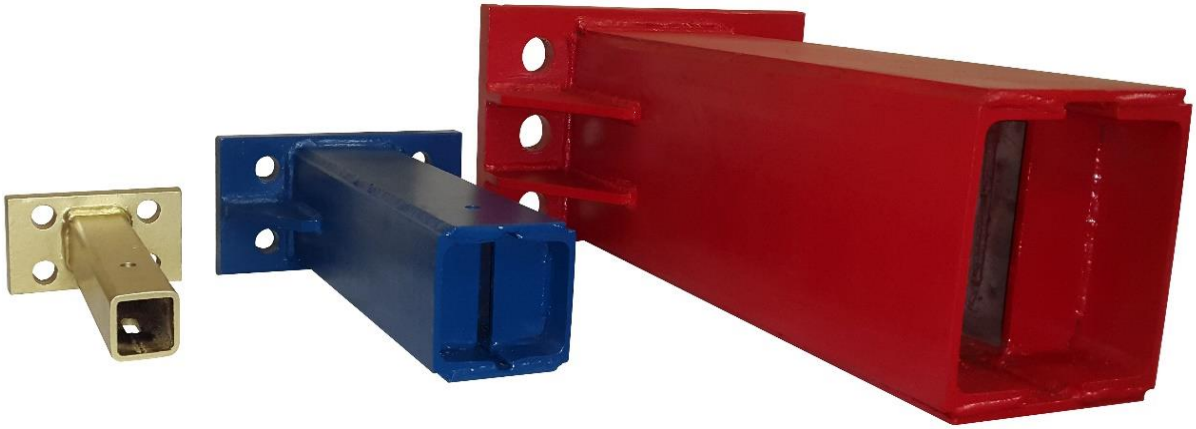

Figure 3.14 Scale 1:4, 1:2, and 1:1 Lever Arms

3.4.2.4 TEST SETUP AND PROCEDURE

The primary axial load (P_1) was applied using a 3000 kN Amsler compression machine for the 1:1 and 1:2 scale specimens, and a 250 kN MTS compression machine for the 1:4 scale specimens. The upper limit of the concrete compressive strength was chosen due to the capacity limitation on the Amsler compression machine. Two ball seatings, located at the top and bottom of the specimen, ensured the unrestricted rotation of the flexural compression member, with the same ball seatings being utilised for the 1:1 and 1:2 scale specimens, and alternative smaller seatings used for the 1:4 scale specimens. The secondary load (P_2) was applied to the 1:1 scale specimens using a 100 ton Simplex Hydraulic jack, while a 10 ton Euro press pack hydraulic jack was used for the 1:2 and 1:4 scale specimens.

For each specimen, the back and side confinement plates was first assembled and gridlines demarcated on the ground to ensure that the lever arms would be attached a fixed distance from the top and bottom of the flexural compression member. Owing to the mass of the 1:1 scale specimens, a hand operated crane was used to lift and place the specimens in the two preassembled back and side confinement plate systems, while the 1:2 and 1:4 scale specimens were moved by hand. The top and bottom leaver arms of the 1:1 scale specimens were lifted with the same crane, and the centre of the end plate holes aligned with the protruding threaded rods. For the 1:2 and 1:4 scale specimens, the lever arms were placed in position by hand. The lever arms were connected to the backing plate by tightening the external nuts on the end plate of the lever arms. The bolts, located inside the side confinement plates, were then tightened to ensure that these plates would remain in position for the duration of

© University of Pretoria

the test. For the 1:1 and 1:2 scale specimens, the assembled system was then placed inside the Amsler compression machine using the crane, while the 1:4 scale assembly could be placed in the MTS testing machine by hand.

The assemblies were subsequently centred and the crosshead lowered until the specimens were subjected to a minor state of compression. The relevant hydraulic jack was then centred over the predrilled hole in the steel lever arm, and the 26.5 mm prestressing bar, 9.6 mm seven-wire strand, or the 7 mm prestressing bar, used for the 1:1, 1:2, or 1:4 scale specimens respectively, inserted through the predrilled holes and the hydraulic jack. For the 1:1 scale specimens, a 170 mm diameter x 20 mm thick circular steel plate provided a bearing surface on the bottom lever arm, and a 170 mm diameter x 40 mm thick circular steel plate was used to span over the hole of the hydraulic jack. This hydraulic jack assembly was fixed in position using two 26.5 mm prestressed reinforcing nuts. For the 1:2 scale specimens, no bearing plates were required, however a for the 1:4 scale specimens a 100 x 100 x 10 mm steel plate (with a 12 mm centrally drilled hole) was used to span over the Euro press pack hydraulic jack. The hydraulic assembly, used to apply the eccentric load for the 1:2 and 1:4 scale specimens, was tied in position using a two 9.6 mm and two 7 mm conical wedge cones respectively. The Linear Variable Differential Transducers (LVDT's) (used to measure the translation of the specimen) were attached to a pre-constructed LVDT frame at the respective heights. With the specimen ready for testing, the 0.3 mm twin-flex strain gauge wires, LVDT's, and the pressure transducers of both the compression machine and the hydraulic hand pump (used to control the hydraulic jack) were connected to the data acquisition system. All the instrument readings were zeroed and P_1 applied at a rate of 2 MPa/min until failure. P_2 was applied with the hydraulic hand pump and hydraulic jack, maintaining a condition of zero strain (within 5 micro strain) on the neutral surface. The data was logged through a data acquisition system at a frequency of 5 Hz, and the test performed until failure.Detailed drawings of the 1:1, 1:2, and 1:4 scale specimens test setups, and the corresponding isometric views, are shown in Figure 3.15 to Figure 3.20.

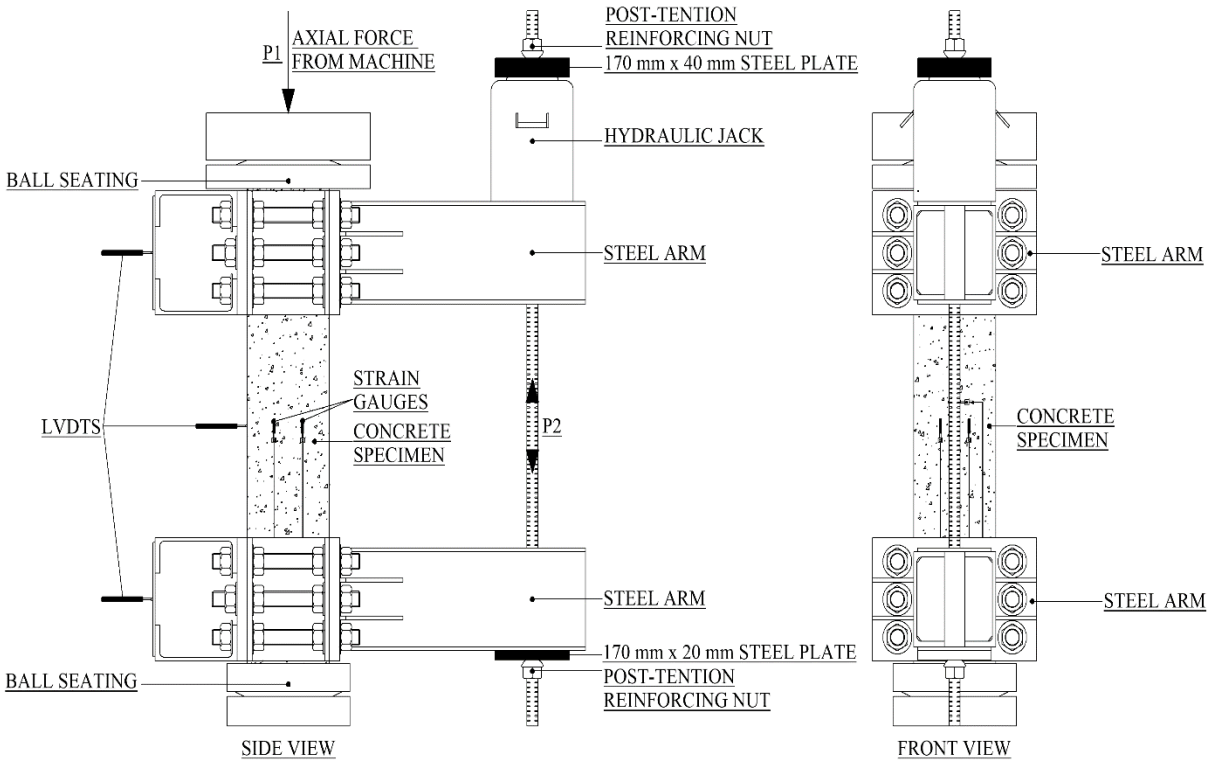

Figure 3.15 Detailed Layout of Scale 1:1 Test Setup

© University of Pretoria

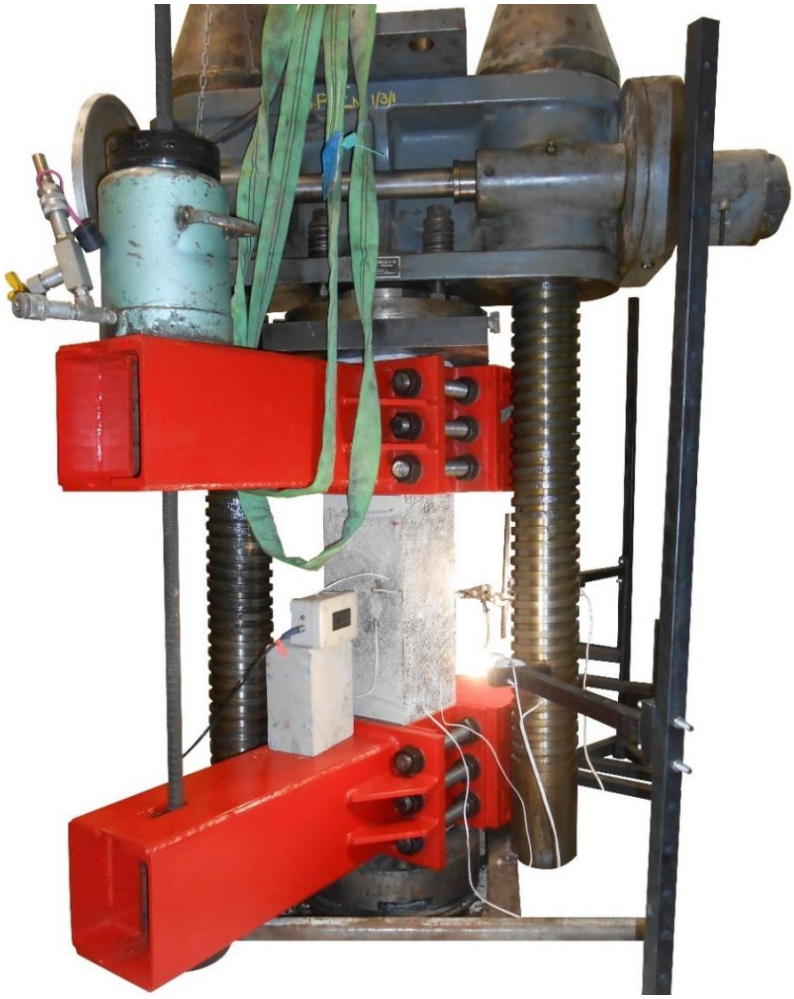

Figure 3.16 Scale 1:1 Specimen Layout Prior to Testing

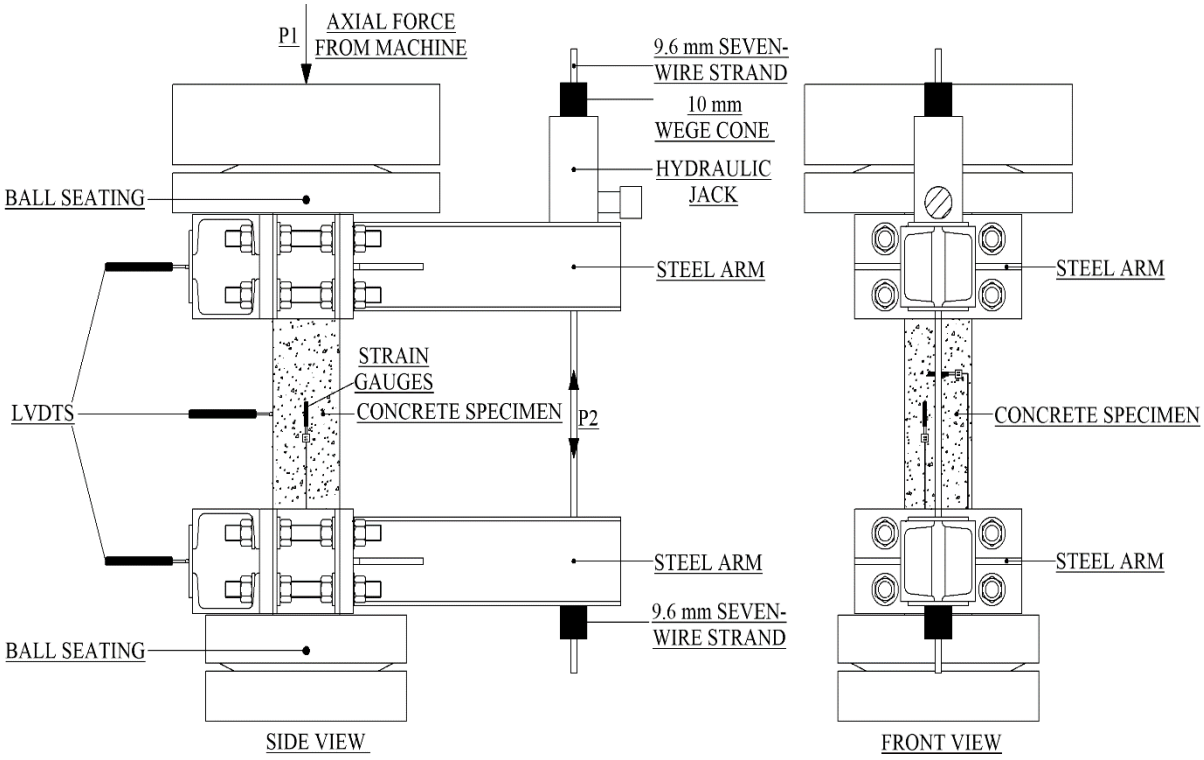

Figure 3.17 Detailed Layout of Scale 1:2 Test Setup

© University of Pretoria

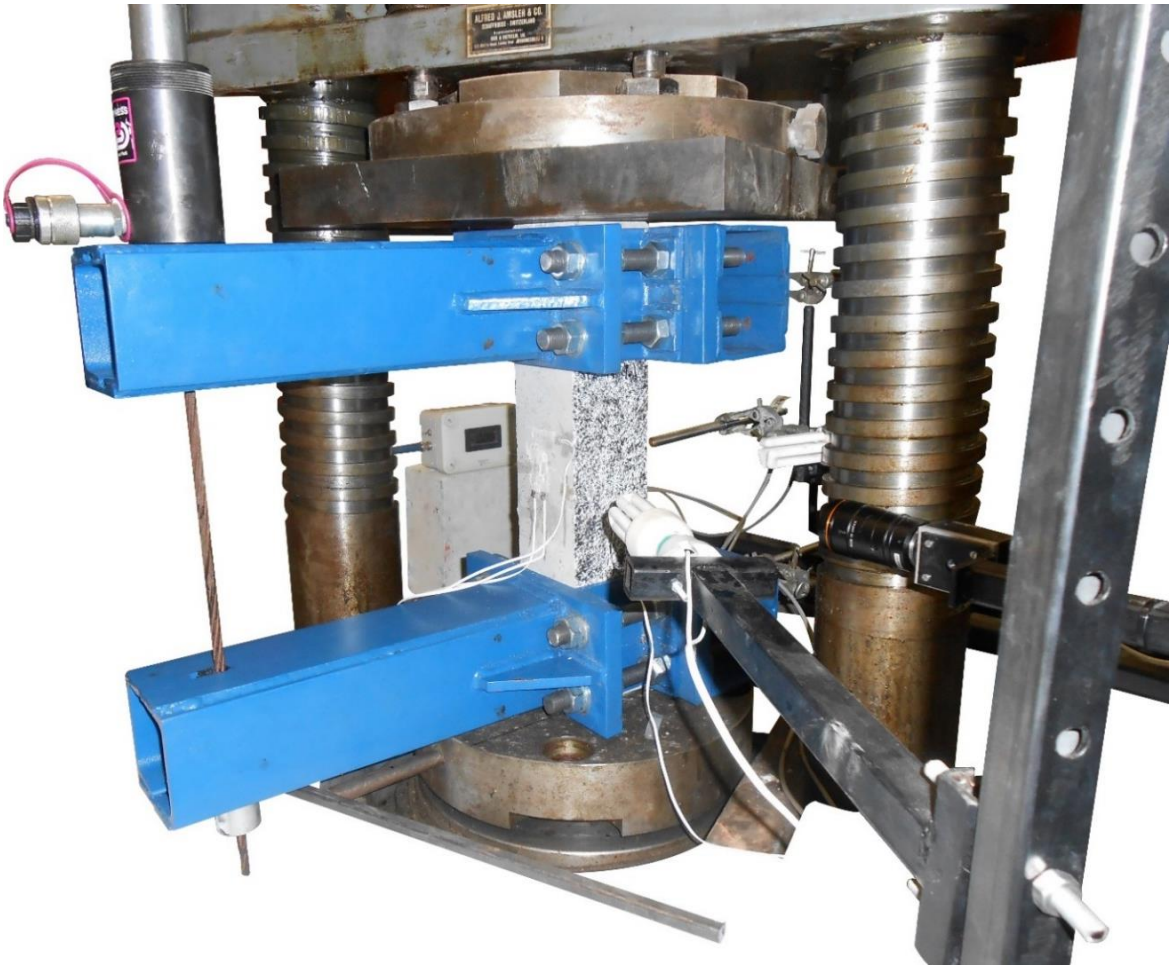

Figure 3.18 Scale 1:2 Specimen Layout Prior to Testing

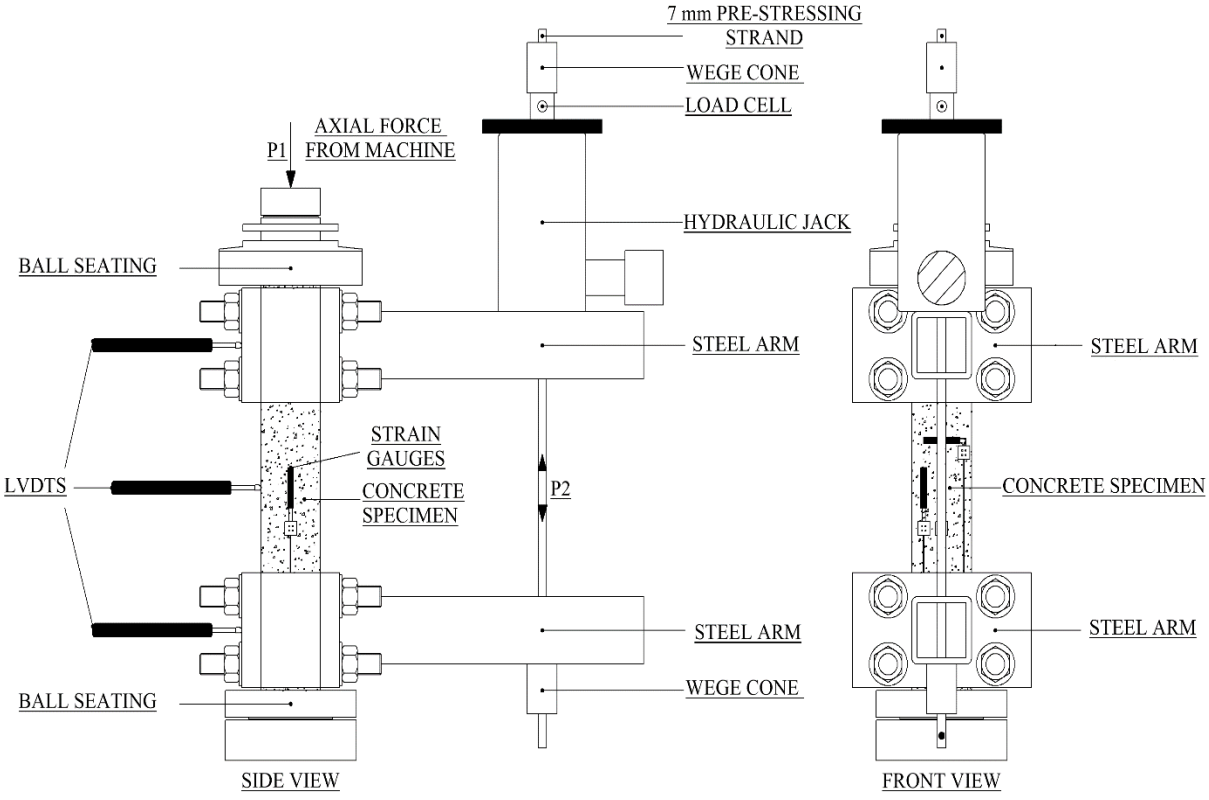

Figure 3.19 Detailed Layout of Scale 1:4 Test Setup

© University of Pretoria

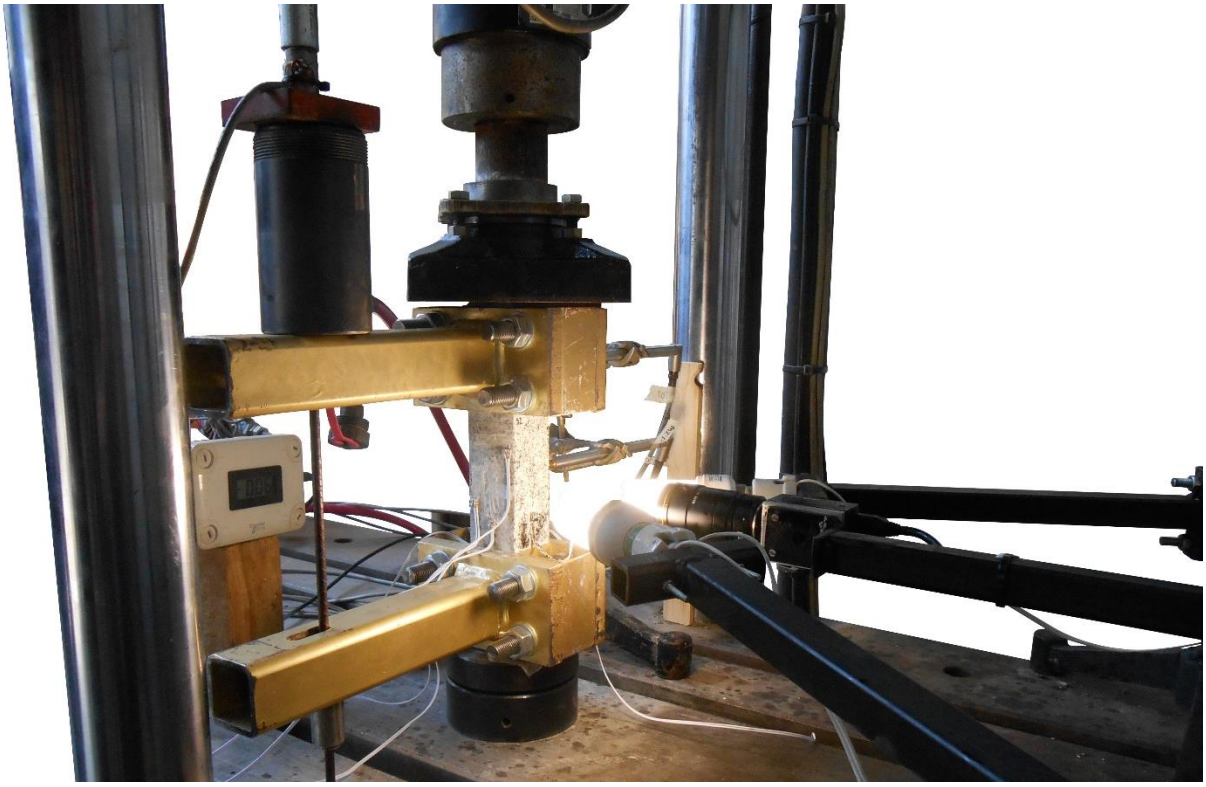

Figure 3.20 Scale 1:4 Specimen Layout Prior to Testing

© University of Pretoria

CHAPTER 4

DISCUSSION AND ANALYSIS OF RESULTS

4.1 INTRODUCTION

In this chapter, the results obtained during the course of the experimental program are presented, analysed, and discussed. The effect of a change in uniaxial compressive strength and specimen size on the flexural compression behaviour of concrete, stress block parameters, ultimate compressive strain, and Poisson ratio are discussed, compared, and conclusions drawn. In addition, the adequacy of various design codes to be used in the analysis and design of concrete containing South African materials is evaluated and discussed. Finally, the flexural stress-strain behaviour is modelled, and a comparison made between the actual and calculated stress block parameters.

4.2 COMPRESSIVE STRENGTH AND MODULUS OF ELASTICITY

Three different 150 mm cylinder target strengths (40 MPa, 65 MPa, and 80 MPa) were chosen for this investigation. For each target strength twelve (of each) 50 mm, 100 mm, and 150 mm cubes and cylinders (height/diameter = 2) were cast along with five 200 mm cubes and cylinders (height/diameter = 2). In this section, the data obtained from the cubes and cylinders are presented and analysed in terms of the strength, modulus of elasticity, and size effect.

4.2.1 CUBE RESULTS

Table 4.1 shows the cube compressive strength results obtained during the course of the investigation. For each cube size, the normality of the data was assessed and outliers identified. Once the outliers (highlighted in red in Table 4.1) had been eliminated, the compressive strength was assumed to be normally distributed. The mean, standard deviation, and five number summary (minimum, 25^{th} percentile (Q_1), 50^{th} percentile (Q_2), 75^{th} percentile (Q_3), and maximum) were subsequently obtained and are presented in Figure 4.1 and Table 4.2.

From the box-and-wisker plot shown in Figure 4.1, it is clear that with an increase in cube size there is a marked reduction in the compressive strength along with a reduction in variability in some instances. A reduction in variability occures when the cube size is increased from 50 mm to 100 mm. For intermediate cube sizes it seems that the variability remains constant, while the transition from 150 mm to the 200 mm cubes again shows an increased variability. The apparent increase in variability of the 200 mm cubes may have something to do with the quality of the concrete moulds. As these moulds were self-manufactured, the water tightness as well as

© University of Pretoria

dimensional tolerances obtained in the standard 50 mm, 100 mm, and 150 mm cube moulds could not be attained. This resulted in some of the finer fraction of the mix seeping out at the interface of the cube mould side walls and base plate, leaving a reduced amount of paste to bind the aggregate particles. It should be noted that this did not happen to every cube, thus the apparent increased variability in 200 mm cube results. Only the bottom 10 mm to 15 mm of some of the 200 mm cubes were affected by the leaching of the finer fraction material, which probably influenced the results.

Table 4.1 Cube Compressive Strength Results

	Mix 1	Mix 2	Mix 3
Cube Size (mm)	**f_{cu} (MPa)**	**f_{cu} (MPa)**	**f_{cu} (MPa)**
50	43.3	53.2	86.8
	44.8	75.3	89.4
	45.9	75.4	94.3
	46.9	76.5	96.9
	47.2	76.6	97.0
	47.4	77.7	97.2
	47.7	80.3	98.4
	48.0	81.0	98.6
	48.8	82.2	99.5
	49.0	82.5	99.6
	49.0	84.6	101.2
	49.2	89.3	101.3
100	41.3	69.9	81.5
	41.4	70.3	83.2
	41.6	70.3	85.4
	41.6	71.6	86.0
	41.9	71.8	86.3
	42.5	73.2	87.8
	44.7	73.8	87.9
	44.9	75.3	87.9
	46.4	75.9	89.4
	46.6	76.8	89.7
	47.9	77.3	90.2
	49.5	79.9	92.4
150	37.6	65.0	76.7
	37.9	65.2	77.7
	38.3	65.3	78.9
	38.5	67.8	79.9
	38.7	68.1	80.5
	39.5	68.7	80.5
	39.6	69.0	81.2
	40.9	70.3	81.9
	41.0	70.6	82.0
	42.1	71.2	83.0
	43.2	72.5	84.4
	43.6	73.3	89.9
200	33.5	55.5	63.1
	36.1	56.9	63.7
	36.9	59.4	72.5
	39.7	64.1	74.4
	41.0	64.5	78.5

© University of Pretoria

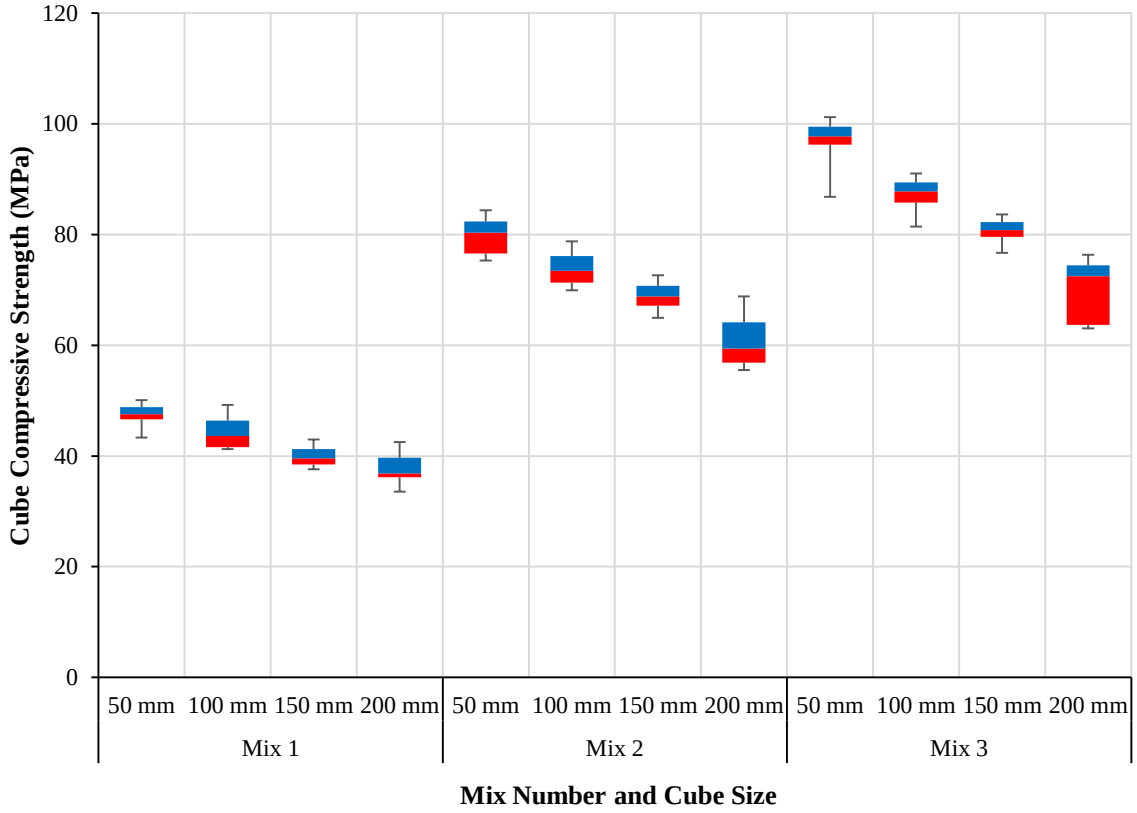

Figure 4.1 Box-and-Whisker Plot of Cube Compressive Strengths

Table 4.2 Descriptive Statistical Summary of Cube Data

Cube Size (mm)	Statistical Parameter	Mix 1	Mix 2	Mix3
50	Sample Mean (X)	47.3	79.2	96.7
	Minimum	43.3	75.3	86.8
	Q_1	46.6	76.6	96.3
	Q_2	47.6	80.3	97.8
	Q_3	48.8	82.4	99.5
	Maximum	49.2	89.3	101.3
	Sample Standard Deviation (S)	1.8	3.3	4.5
100	Sample Mean (X)	44.8	74.6	86.8
	Minimum	41.3	69.9	81.5
	Q_1	41.6	71.3	85.8
	Q_2	43.6	73.5	87.8
	Q_3	46.4	76.1	89.4
	Maximum	49.5	79.9	92.4
	Sample Standard Deviation (S)	2.8	3.0	2.7
150	Sample Mean (X)	40.8	69.7	80.6
	Minimum	37.6	65.0	76.7
	Q_1	38.5	67.2	79.6
	Q_2	39.6	68.9	80.8
	Q_3	41.3	70.8	82.3
	Maximum	43.6	73.3	89.9
	Sample Standard Deviation (S)	1.9	2.4	1.7
200	Sample Mean (X)	37.4	61.2	72.3
	Minimum	36.1	59.4	72.5
	Q_1	36.7	61.8	73.5
	Q_2	38.3	64.1	74.4
	Q_3	40.0	64.3	76.5
	Maximum	41.0	64.5	78.5
	Sample Standard Deviation (S)	3.0	3.7	6.2

© University of Pretoria

4.2.2 CYLINDER RESULTS

Table 4.3 provides a summary of the cylinder compressive strength, modulus of elasticity, and the strain at the associated peak stress (ε_{c0}). Where no *strength* values are indicated, the values were either not obtained or unrealistic. Furthermore, even though the modulus of elasticity was measured for the 100 mm, 150 mm, and the 200 mm cylinders, the same process could not be employed for the 50 mm cylinders, as the strain readings obtained from the 50 mm cylinder compressometer was unrealistic.

Table 4.3 Cylinder (H/D=2) Compressive Strength, Modulus of Elasticity, and Strain Associated with f_{cy}

	Mix 1			Mix 2			Mix 3		
D (mm)	**f_{cy} (MPa)**	**E_c (GPa)**	**ε_{c0} (με)**	**f_{cy} (MPa)**	**E_c (GPa)**	**ε_{c0} (με)**	**f_{cy} (MPa)**	**E_c (GPa)**	**ε_{c0} (με)**
50	31.4	-	3333	57	-	2928	69.4	-	2352
	34.4	-	2859	51.1	-	2764	65.8	-	1947
	32.3	-	3818	48.2	-	2213	71.7	-	1937
	32.8	-	3244	58	-	2224	67.9	-	-
	32.2	-	3213	58.8	-	2817	-	-	-
100	38.1	34.2	3321	67.4	42.5	2531	79.6	43.6	2606
	42	38.6	3275	71.7	40.5	2886	83.5	43.4	2821
	42.5	36.1	3548	70.8	41.5	3044	80.2	42.5	2887
	43.2	38.6	3745	64.1	44	2457	77.2	41.8	2697
	41.9	40.1	3064	70.5	44.3	2551	78.1	44.1	2380
	40.1	37.6	3089	71.5	40.3	3031	76.3	39.5	2454
	40.9	35	3409	67	40.7	2976	82.7	42.6	2976
	43.3	37.5	3298	67.4	39.1	2876	77.1	42	2622
	44.3	35.7	3512	66.4	42.2	2905	71.3	-	-
	41.5	37.6	3391	64	37.5	3055	81.8	-	-
	41.3	34.5	3485	-	-	-	85.7	-	-
	43.2	36	3163	-	-	-	83.5	-	-
150	38.6	37.1	2848	64.3	37.9	2879	83.7	41.8	3186
	40.4	41.2	3108	67.4	42.5	2160	74.8	39	2608
	38	44.2	2630	66	39.4	2648	70.8	43	2287
	42.9	42.9	3118	60.1	35.7	2724	71.2	44.2	2163
	39.2	42	2189	64.3	39.3	2545	78.7	44.4	2529
	40.5	41.3	2846	62.9	37.2	3174	73.7	43.3	2523
	41.5	39.9	2596	65.4	-	-	74.5	-	-
	39.2	38.8	2189	60.3	-	-	78.6	-	-
	41.8	37.5	2365	65.8	-	-	78.8	-	-
	38	39.2	2450	64.9	-	-	74	-	-
	41.3	39.4	2422	62.6	-	-	82.6	-	-
	-	-	-	64.8	-	-	73.9	-	-
200	32.1	32.6	2886	57.9	37.9	2739	67.2	39.1	3006
	39.5	35.5	2618	56	38.1	2443	71.6	41.2	2840
	40.6	36.2	2549	63.1	48.4	2247	63.1	48.1	2247
	39.7	37.1	2620	56.5	42	2199	64.8	39.4	2504
	37.6	33.6	2436	67.2	39.2	3006	69.8	-	-

4.2.2.1 CYLINDER COMPRESSIVE STRENGTH

The cylinder compressive strength, more particularly the 150 mm cylinder strength, may be the most important mechanical property of concrete. Based on Table 4.3, a statistical analysis of the data was performed and the mean, standard deviation, and five number summary were used to construct the box-and-whisker plot as shown in Figure 4.2 (presented in Table 4.4). Figure 4.2 illustrates that with a reduction in cylinder size (at a constant

© University of Pretoria

height/diameter ratio) the compressive strength of concrete does tend to increase, with the exception of the 50 mm specimens. The 50 mm cylinders yielded erratic results and only five of the twelve specimens was tested successfully. After testing, the severed fragments of the 50 mm cylinders were investigated to obtain a possible explanation for the variable and relatively low compressive strength. The common observation was that even though the 50 mm cylinders were compacted on a vibrating table, and the quantity air voids may have been the same as in the other specimens, the size of these air voids meant that the void ratio of the concrete increased. The increased void ratio resulted in a less dense concrete micro-structure and an associated reduction in the compressive strength. This behaviour was not observed in the 50 mm cubes, as the distance which an air bubble needs to travel to reach the top of the specimen is halved, thus entrapping less air.

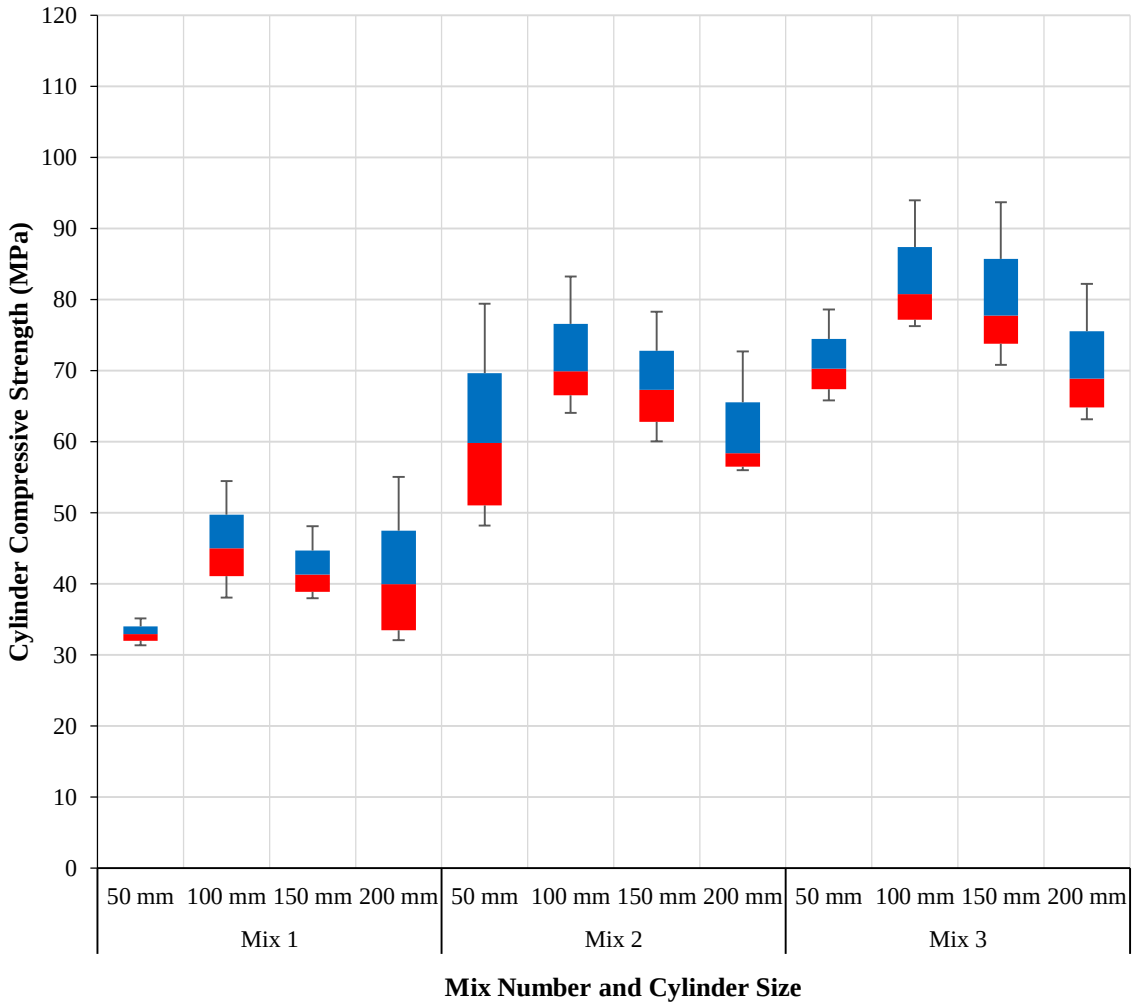

Figure 4.2 Box-and-Whisker Plot of Cylinder Compressive Strengths

Variability in the 50 mm cylinder compressive strength was also introduced during the grinding of the cylinders. During grinding, aggregates located on the edge of the specimen may be dislodged. For a 100 mm, 150 mm, or 200 mm cylinder, the loss of aggregate from the surface of load application, and the resultant reduction in area, has a negligible effect on the compressive stress-strain behaviour. However, for a 50 mm specimen, the dislodged aggregate represents a substantial portion or the cross sectional area. The effect of this reduced area, coupled with the increased porosity of the concrete, meant that the 50 mm cylinder strength would not necessarily provide an accurate prediction of the associated uniaxial compressive strength of the 50 x 50 x 300 mm flexural compression members.

© University of Pretoria

Table 4.4 Descriptive Statistical Summary of Cylinder Data

Cylinder Dimensions	Statistical Parameter	Mix 1	Mix 2	Mix3
50 mm	Sample Mean (X)	32.6	54.6	68.7
	Minimum	31.4	48.2	65.8
	Q_1	32.2	49.7	66.3
	Q_2	32.3	57.0	68.7
	Q_3	32.8	58.4	71.1
	Maximum	34.4	58.8	71.7
	Sample Standard Deviation (S)	1.1	4.7	2.5
100 mm	Sample Mean (X)	41.9	68.1	80.2
	Minimum	38.1	64.0	76.3
	Q_1	41.1	66.6	77.2
	Q_2	42.0	67.4	79.9
	Q_3	42.8	70.7	82.9
	Maximum	43.3	71.7	85.7
	Sample Standard Deviation (S)	1.7	2.9	3.2
150 mm	Sample Mean (X)	40.1	64.1	76.4
	Minimum	38.0	60.1	70.8
	Q_1	38.9	62.8	73.8
	Q_2	40.4	64.5	74.8
	Q_3	41.4	65.5	78.8
	Maximum	42.9	67.4	83.7
	Sample Standard Deviation (S)	1.6	2.2	4.3
200 mm	Sample Mean (X)	36.9	60.2	67.3
	Minimum	32.1	56.0	63.1
	Q_1	33.5	56.5	64.8
	Q_2	38.5	57.9	67.2
	Q_3	39.6	63.1	69.8
	Maximum	40.6	67.2	71.6
	Sample Standard Deviation (S)	3.9	4.9	3.5

4.2.2.2 UNIAXIAL COMPRESSIVE STRESS-STRAIN CURVES

A summary of the cylinder compressive strength, modulus of elasticity, and the strain at the associated peak stress, was provided in the previous section. These values were deduced from the stress-strain curves shown in Figure 4.3 to Figure 4.6.

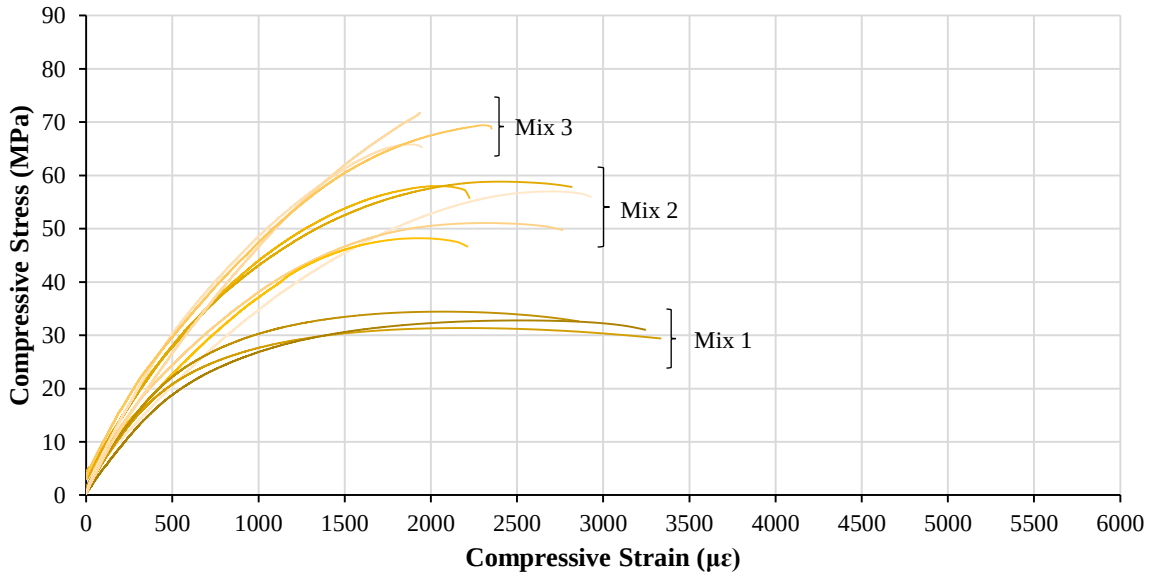

Figure 4.3 50 mm Cylinder Stress-Strain Curves

© University of Pretoria

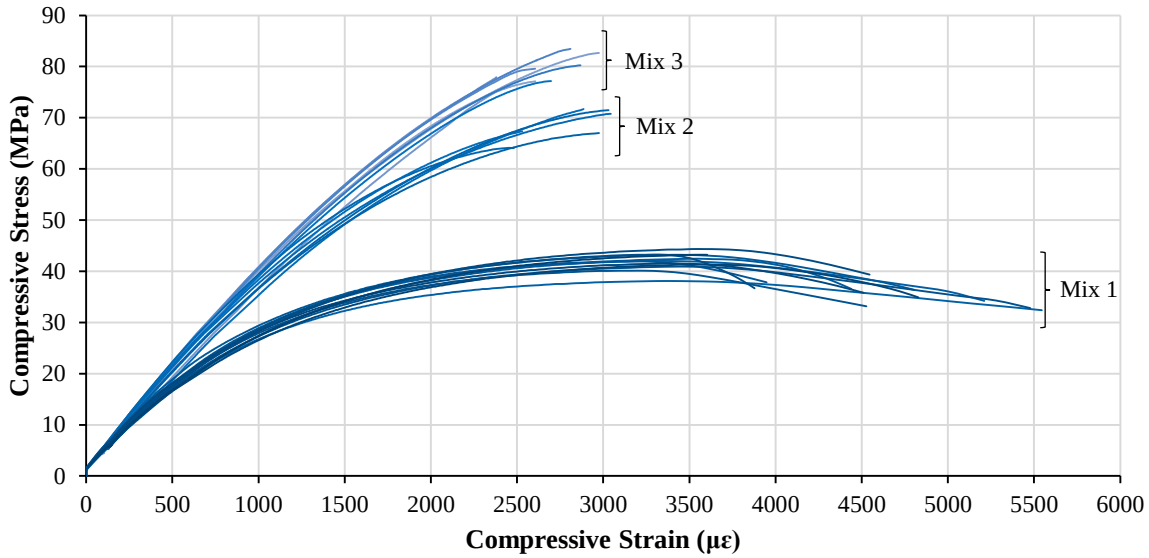

Figure 4.4 100 mm Cylinder Stress-Strain Curves

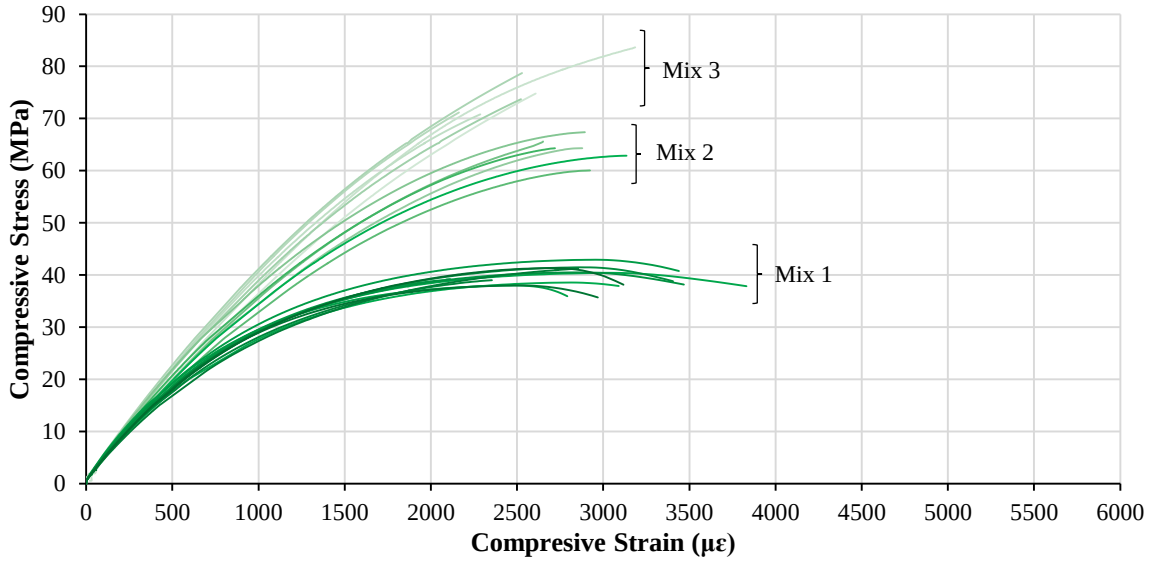

Figure 4.5 150 mm Cylinder Stress-Strain Curves

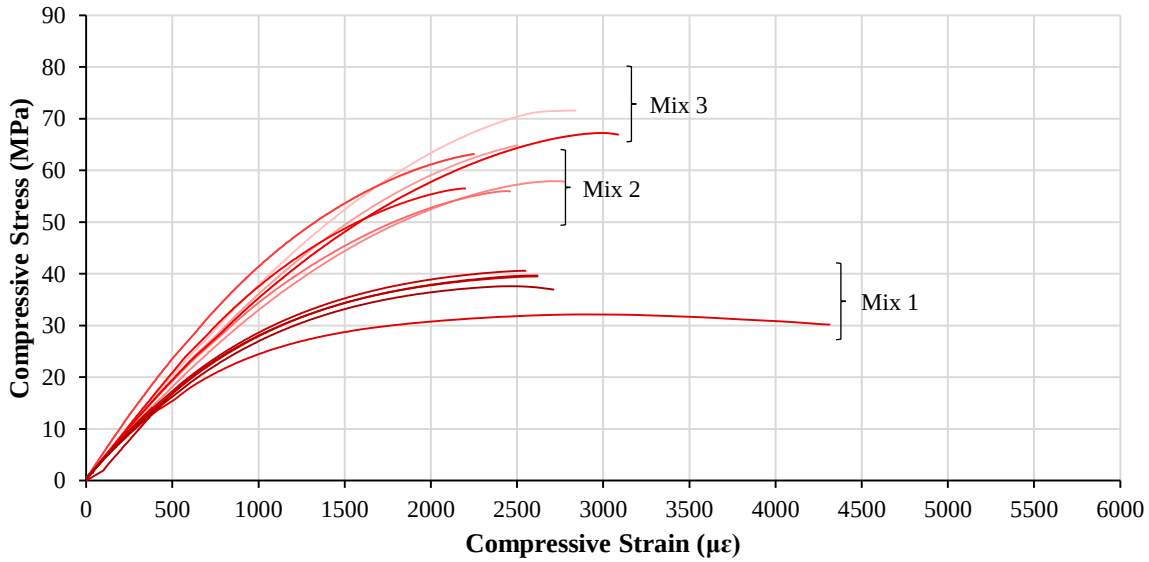

Figure 4.6 200 mm Cylinder Stress-Strain Curves

© University of Pretoria

Figure 4.3 to Figure 4.6 show that the 100 mm cylinders tend to provide the most repeatable results, followed closely by the 150 mm cylinders. The 50 mm cylinders, not only under performs in terms of compressive strength, but also had a profoundly different stress-strain behaviour than the other cylinder sizes. It would therefore not be practical to provide a connection between the uniaxial compressive stress-strain curve and the flexural compressive stress-strain curve for the 50 x 50 x 300 mm flexural compression members.

4.2.2.3 MODULUS OF ELASTICITY

Being a multiphase material, concretes stiffness is a function of the stiffness of its component phases (aggregate, Hardened Cement Paste, and interstitial transition zone). Previous prediction models for the modulus of elasticity all concluded that for a particular aggregate type the increase in compressive strength would result in an associated increase in the modulus of elasticity. Figure 4.7 shows a plot of the modulus of elasticity for the 100 mm, 150 mm, and 200 mm cylinders.

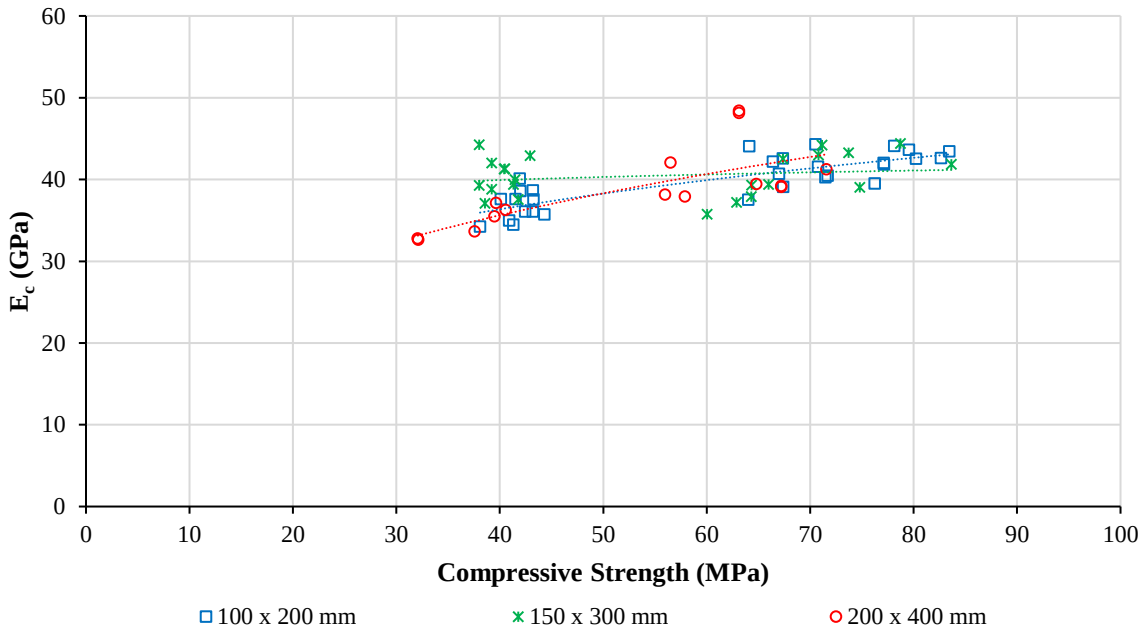

Figure 4.7 Modulus of Elasticity versus Compressive Strength

The slight increase in the modulus of elasticity, with a reduction in water/cement ratio, has to do with the specifically chosen mix designs. Although the paste in Mix 1 is significantly weaker than that of Mix 2 and Mix 3, Mix 1 does contain slightly more aggregate. Thus, as the paste content and paste stiffness increases for Mix 2 and Mix 3, the associated reduction in the volumetric portion of aggregate results in a limited increase in the modulus of elasticity compared to that of Mix 1. Furthermore, Figure 4.7 also illustrates that the modulus of elasticity tends to be independent of the specimen size.

4.2.2.4 POISSON RATIO (150 MM CYLINDERS)

The Poisson ratio of the 150 mm cylinders were obtained by using a standard compressometer, capable of measuring both horizontal and vertical displacements. A plot of the Poisson ratio with respect to the longitudinal compressive strain is shown in Figure 4.8. The axis limits of 500 με and 1500 με were chosen as data below 500 με showed large fluctuations, while data above 1500 με started to exhibit an increased Poisson ratio due to the formation of micro-cracks. By using Figure 4.8, point estimates of the Poisson ratio in uniaxial compression

© University of Pretoria

(shown in Table 4.5) were obtained. These values were compared to the values obtained by previous researchers, as shown in Figure 4.9.

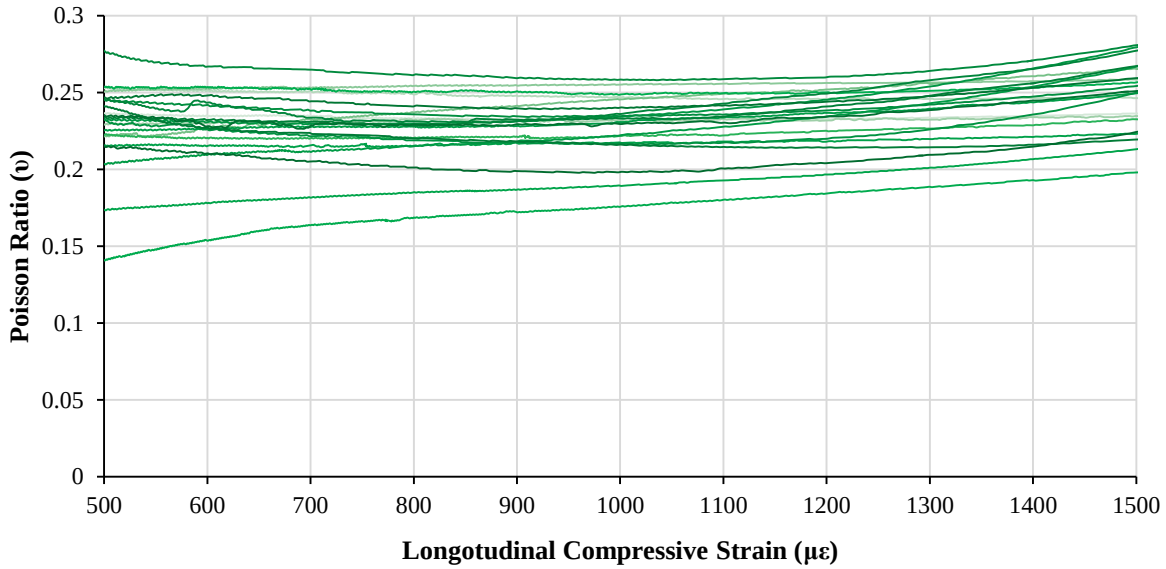

Figure 4.8 Poisson Ratio versus Longitudinal Compressive Strain for 150 mm Cylinders

Table 4.5 Point Estimate of 150 mm Cylinder Poisson Ratio

Mix 1		Mix 2		Mix 3	
f_c' (MPa)	υ	f_c' (MPa)	υ	f_c' (MPa)	υ
38.6	0.22	64.3	0.22	83.7	0.25
40.4	0.24	67.4	0.25	74.8	0.23
38.0	0.22	66.0	0.18	70.8	0.23
42.9	0.24	60.1	0.20	71.2	0.25
39.2	0.26	64.3	0.22	78.7	0.24
40.5	0.24	62.9	0.24	73.7	0.24
41.5	0.23	-	-	-	-
39.2	0.22	-	-	-	-
41.8	0.24	-	-	-	-
38.0	0.23	-	-	-	-
41.3	0.20	-	-	-	-

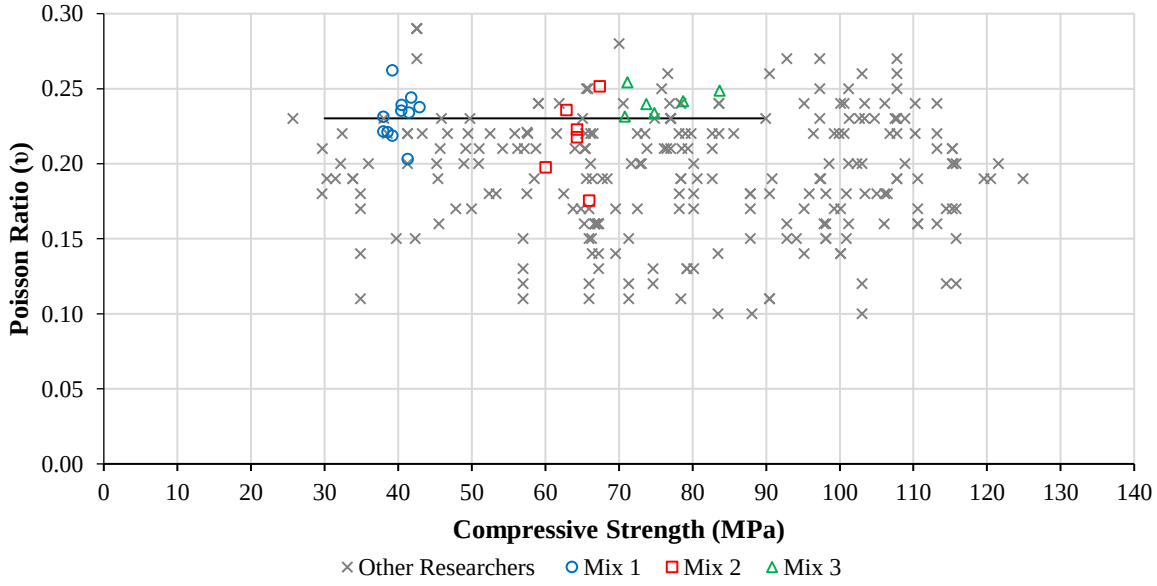

Figure 4.9 Poisson Ratio Point Estimates for 150 mm Cylinders

© University of Pretoria

From Table 4.5 it can be concluded that the Poisson ratio of the 150 mm cylinders (subjected to uniaxial compression) varies between 0.16 and 0.25. A regression analysis shows that the Poisson ratio of the 150 mm cylinders is independent of the compressive strength, and that an average value of 0.23 can be assumed for the three mixes. In addition, Figure 4.9 illustrates that concrete containing Dolomitic aggregate has a Poisson ratio that is high in comparison to the results obtained by other researchers. This means that both a local and global estimate of the Poisson ratio needs to be made.

4.2.3 CUBE VERSUS CYLINDER RESULTS

The extent of confinement for a cube is more prominent than that for a cylinder, resulting in a higher uniaxial cube compressive strength. The ratio between the cylinder and cube strength is generally assumed to vary between 0.7 and 0.9, with an average of 0.8 used by most design codes. Figure 4.10, shows that a plot of the cube five number summary compressive strengths versus cylinder five number summary compressive strengths.

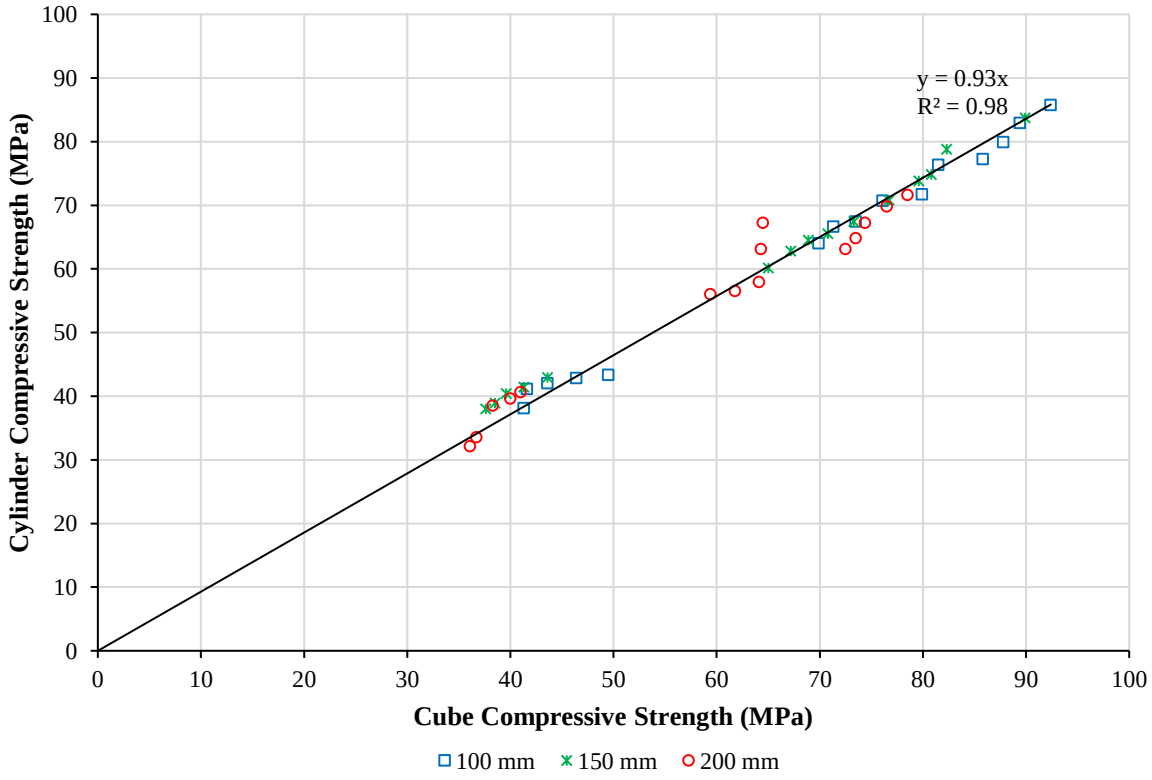

Figure 4.10 Cylinder versus Cube Strength Results

The cylinder to cube strength ratio of 0.93 was used to estimate the 50 mm cylinder compressive strength, to be used in the analysis of the flexural compression specimens. This ratio, along with the 50 mm cubes five number summary, were used to obtain the corresponding five number summary for the 50 mm cylinder strengths. The results of this analysis are shown in Table 4.6.

Table 4.6 50 mm Cylinder Five Number Summary Obtained from 50 mm Cubes

Designation	Mix 1	Mix 2	Mix 3
50 mm	40.3	70.0	80.7
	43.4	71.2	89.5
	44.2	74.7	90.9
	45.4	76.6	92.5
	45.7	83.1	94.2

© University of Pretoria

4.2.4 CUBE AND CYLINDER SIZE EFFECT

The influence of specimen size on compressive strength can be deduced by utilising the Modified Size Effect Law (MSEL) and Least Squares Method (LSM) regression analysis. By assuming $\lambda_0 = 2$, $d_a = 0.475$ cm, and standardizing the compressive strength of both the cylinders and the cubes with respect to the average 150 mm cylinder strength, the remaining regression coefficients presented in the MSEL equation can be estimated. As regression analysis is used, the number of data points used for each specimen size needs to be the same. It was for this reason that the five number summary of the cube and cylinder strengths was used to estimate the regression coefficients. The results obtained for the cube size effect as well as the cylinder size effect are shown in Figure 4.11 and Figure 4.12, with the associated coefficients indicated in Table 4.7 and Table 4.8 respectively.

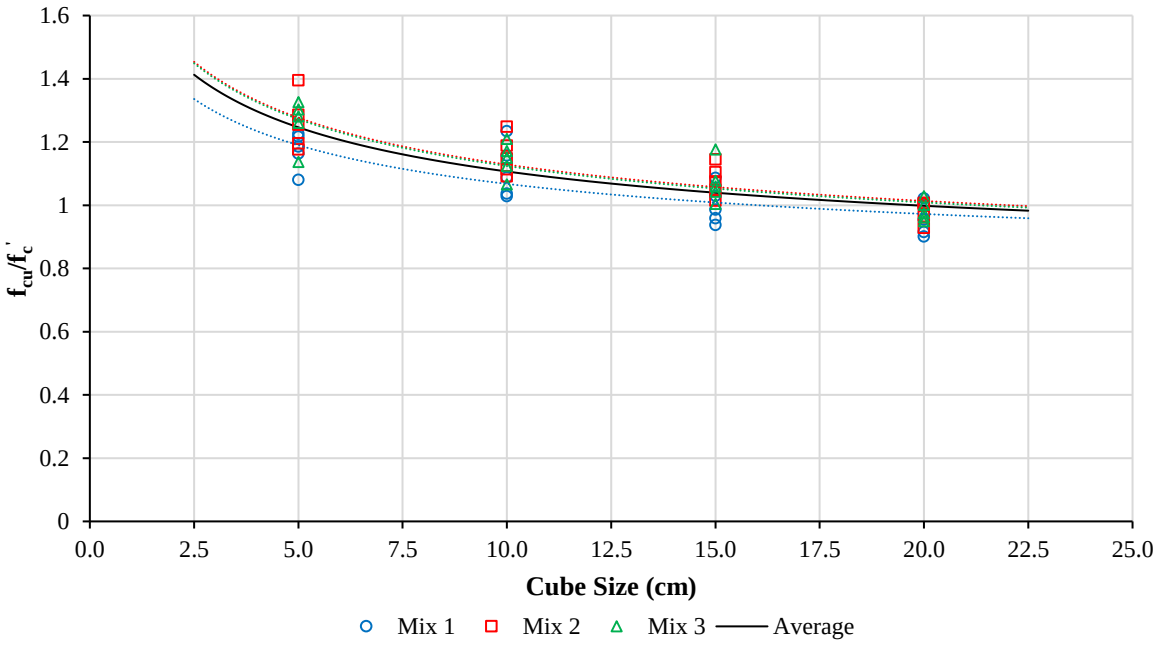

Figure 4.11 Size Effect for Cubes

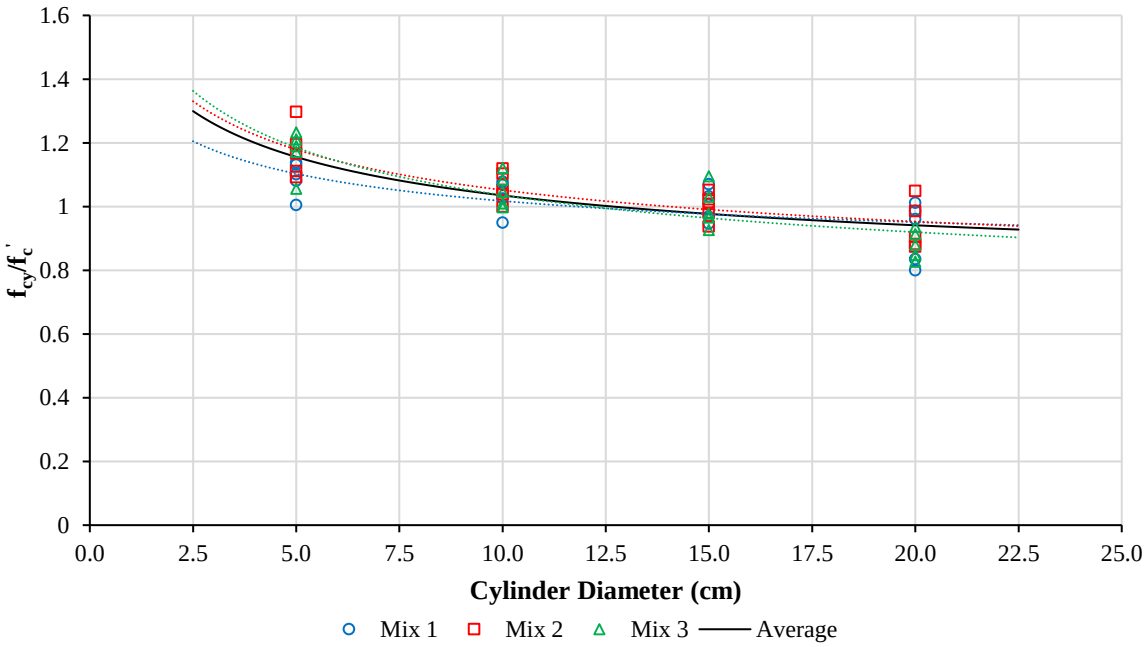

Figure 4.12 Size Effect for Cylinders

© University of Pretoria

Table 4.7 Mix 1, Mix 2,and Mix 3 and Average MSEL Coefficients for Cubes

	Mix 1	Mix 2	Mix 3	Average
β	1.17	1.41	1.41	1.33
$\lambda_0 d_a$	0.95	0.95	0.95	0.95
α	0.72	0.71	0.71	0.72

Table 4.8 Mix 1, Mix 2, and Mix 3 and Average MSEL Coefficients for Cylinders

	Mix 1	Mix 2	Mix 3	Average
β	0.81	1.21	1.42	1.15
$\lambda_0 d_a$	0.95	0.95	0.95	0.95
α	0.78	0.70	0.62	0.70

From Figure 4.11 and Table 4.7, it can be seen that for cubes, β tends to increase with an increase in compressive strength from Mix 1 to Mix 2, but remains fairly constant between Mix 2 and Mix 3. In addition, there is a slight reduction in the α value from Mix 1 to Mix 2, but this reduction may be ignored for all practical purposes. The black line constitutes the average of the cube size effect, indicating that the size independent component of all the cubes is in the region of 0.72.

From Figure 4.12 and Table 4.8, it can be seen that for cylinders a substantial increase in the value of β may be observed along with a recognisable reduction in the α values. These respective increases and decreases have to do with the reduced compressive strength of the 200 mm cylinders, as well as the fact that the ratio between the cylinder and cube strength was used to estimate the strength of the 50 mm cylinders. The average relationship coefficients (shown in the last column of Table 4.8) illustrate that the size independent component of the cylinder strength may be taken as 0.7.

A comparison between the average β value in Table 4.7 and Table 4.8 shows that the size effect is more prominent for the cubes than cylinders. This is because for cubes, a large portion of the stress is concentrated on the edge of the specimen. Furthermore, comparing these results to the results obtained by Yi et al. (2006), the effect of the maximum aggregate size can be observed.

As Yi et al. (2006) made use of a maximum aggregate size of 13 mm, and $\lambda_0 d_a = 2.6$ cm was assumed, this had the effect of altering the coefficients of β and α, theoretically meaning that compatibility in terms of the β and α coefficients, cannot be obtained. Figure 4.13 and Figure 4.14, show plots of the cube and cylinder results obtained from this study along with the results obtained by Yi et al. (2006). Yi et al. (2006) estimated the coefficients of the MSEL equation by using different quantities of test data points for each respective specimen size. The model is therefore weighted towards the 50 mm cylinders and 50 mm cubes. A comparison between the results obtained from this study, and the results obtained by Yi et al. was therefore made based on the five number summary of the results as shown in Figure 4.13 and Figure 4.14.

With all specimen sizes carrying equal weight, the MSEL coefficients obtained from the results of Yi et al. (2006) look vastly different. A comparison between the results obtained by Yi et al. (2006) and the modified results (based on the five number summary) can be seen in Table 4.9. These results combined with Figure 4.13 and Figure 4.14, once again confirms that the MSEL is dependent on the aggregate type. Thus one universal equation relating the size of either a cube or cylinder, to the standard 150 mm cylinder size is not possible.

© University of Pretoria

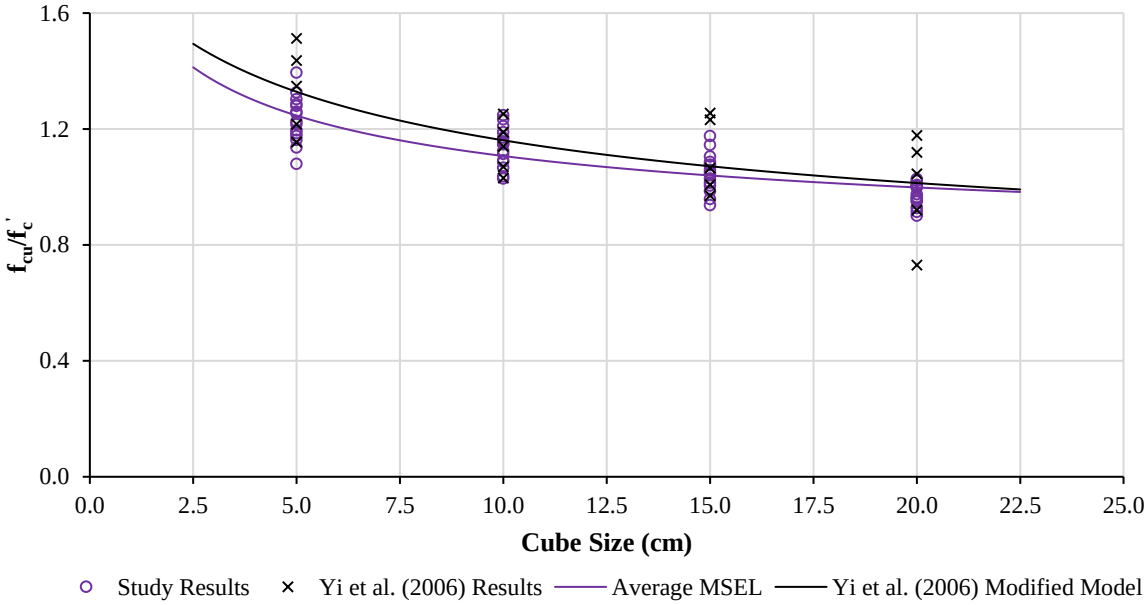

Figure 4.13 Comparison: Study Test Results and Results Obtained by Yi et al. (2006) for Cubes

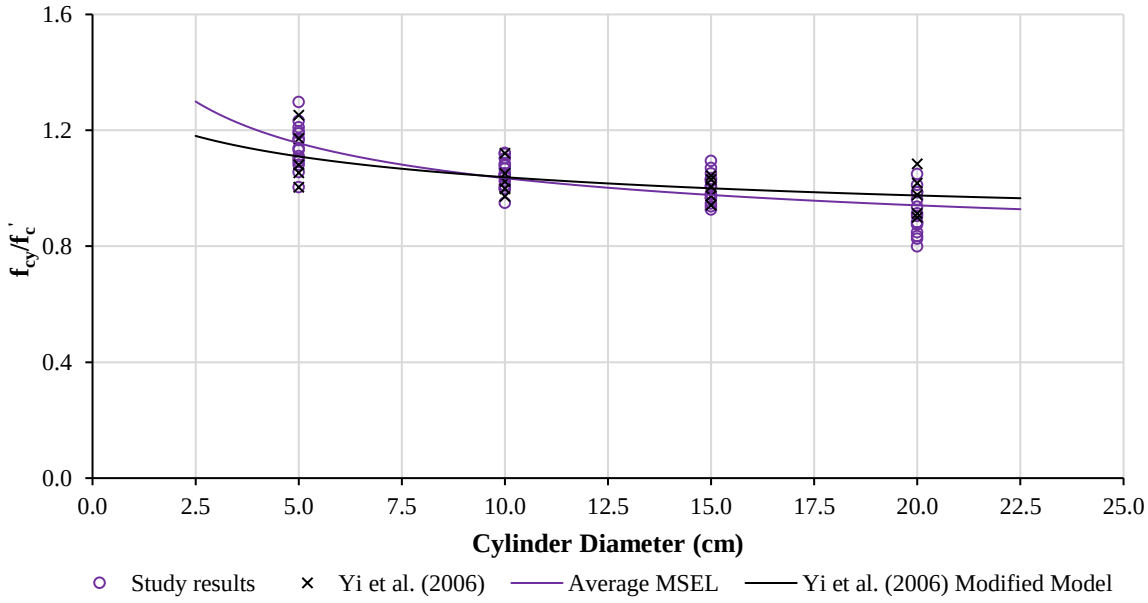

Figure 4.14 Comparison: Study Test Results and Results Obtained by Yi et al. (2006) for Cylinders

Table 4.9 MSEL Regression Coefficients of Study Results and Results of Yi et al. (2006)

	Cubes			Cylinders		
	Average	**Yi et al. (2006)**	**Yi et al. (2006) Modified**	**Average**	**Yi et al. (2006)**	**Yi et al. (2006) Modified**
β	1.33	1.17	1.28	1.15	0.49	0.55
$\lambda_0 d_a$	0.95	2.6	2.6	0.95	2.6	2.6
α	0.72	0.62	0.58	0.7	0.81	0.79

4.3 FLEXURAL STRENGTH

The main objective of this study is to establish the influence of specimen size and compressive strength on the stress block parameters of concrete. This was done by subjecting twenty-seven specimens to a controlled flexural compression load, while maintaining a condition of zero strain on the back face of the specimen.

© University of Pretoria

4.3.1 GENERAL OBSERVATIONS

Throughout the investigation, no significant difficulties were experienced applying either the primary or secondary load. The primary load was applied at a constant rate of 2 MPa/min. This meant that regardless of specimen size, and without considering the size effect, the flexural compression specimens of the same mix should have failed in roughly the same time. For all mix types and specimen sizes, the rate of application of the secondary load was constant while the concrete was in the elastic range, and decreased as the specimen approached failure.

Similarities were observed between the failure of the cubes, cylinders, and the flexural compression members. The increased ductility observed in the uniaxial stress-strain behaviour of the cylinders, was also observed in the flexural compression members. However, unlike the cylinders which only showed this behaviour for the 100 mm specimens of Mix 1, the flexural compression members of Mix 1 behaved the same regardless of specimen size. As expected, the increased ductility resulted in a slow and surprisingly gentile failure of the specimens of Mix 1, but with increased compressive strength failure became increasingly brittle, with large pieces of concrete being hurled perpendicular to the compression face of the specimen and to the surrounding area. Some of the typical failure modes of the 1:1 scale specimens are shown in Figure 4.15 to Figure 4.17 for Mix 1, Mix 2, and Mix 3 respectively. It should be noted that for each mix the same failure behaviour was observed regardless of specimen size.

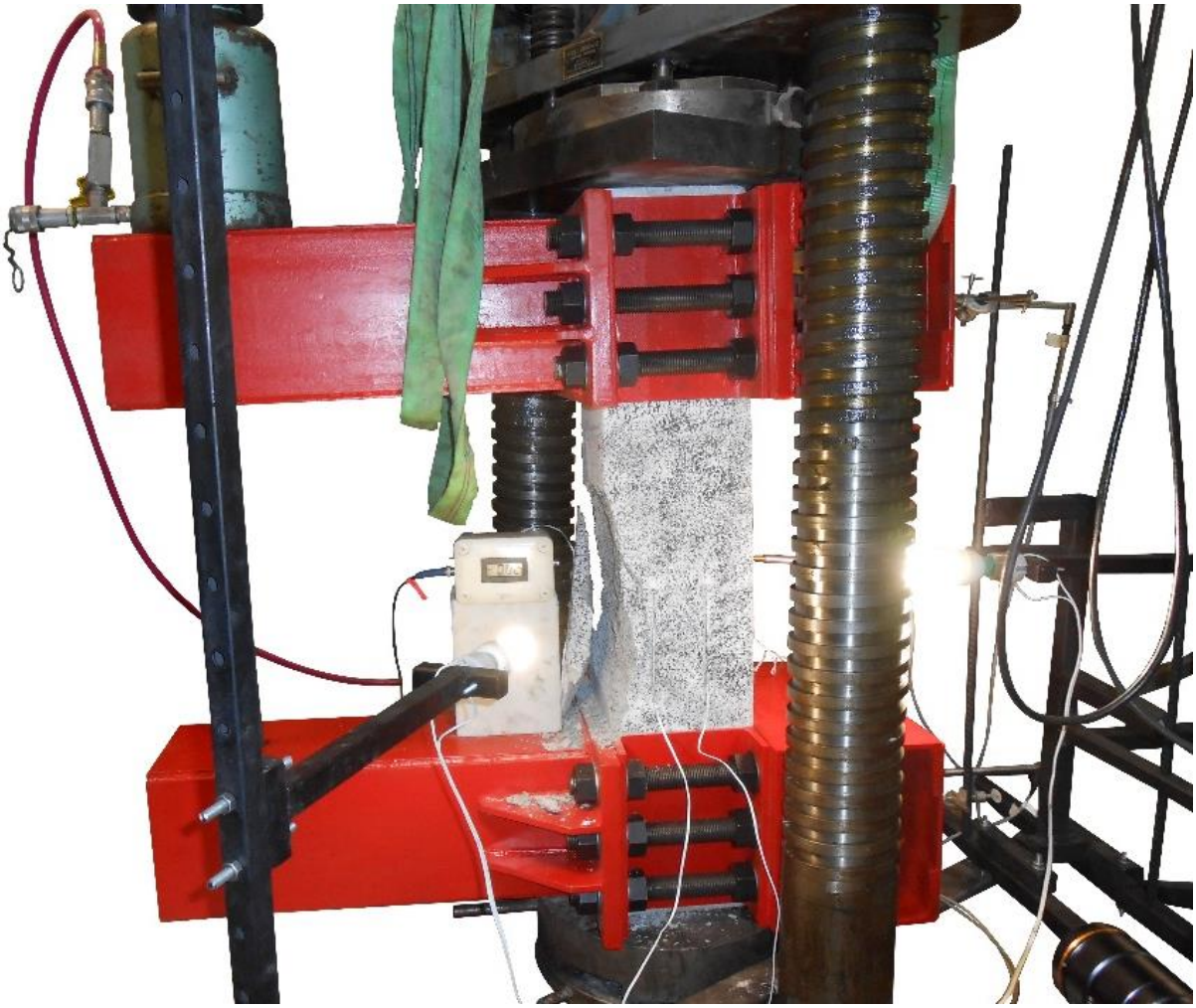

Figure 4.15 Failure Mode of Scale 1:1 Specimen (Mix 1)

© University of Pretoria

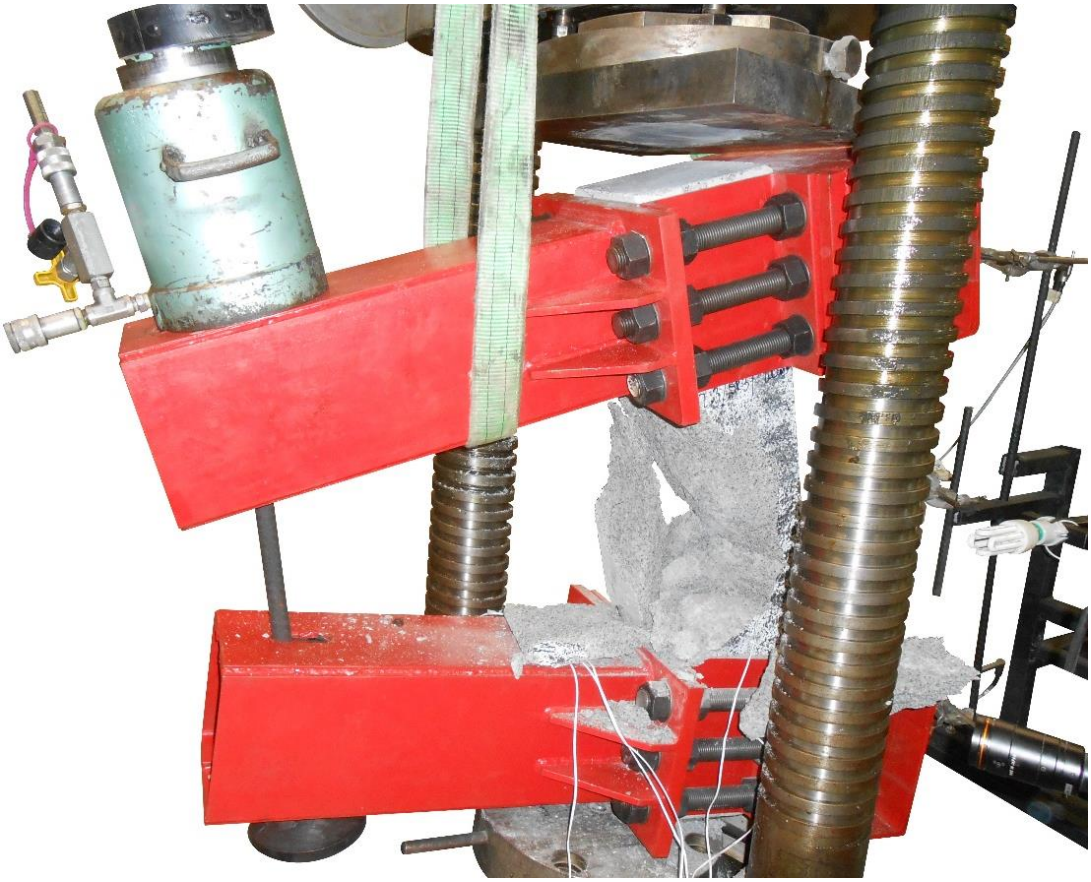

Figure 4.16 Failure Mode of Scale 1:1 Specimen (Mix 2)

Figure 4.17 Failure Mode of Scale 1:1 Specimen (Mix 3)

© University of Pretoria

4.3.2 SURFACE STRAIN MEASUREMENTS

Throughout each of the twenty-seven tests, surface strain gauges continually monitored both the transverse and longitudinal deformations. The purpose of these strain gauges were to facilitate the numerical integration process used to obtain the stress-strain relationship in flexural compression, as well as to confirm the assumption that plane sections remain plane during bending. Figure 4.18 to Figure 4.20 shows the strain gauge readings throughout the depth of one of the flexural compression specimens at an extreme fibre strain of 1000 με, 2000 με, 3000 με, and failure. These figures confirms that the plane sections remain plane during bending assumption is valid for analysis and design. Although the results of only three specimen are presented, the same observation was made for the remaining twenty-four specimens.

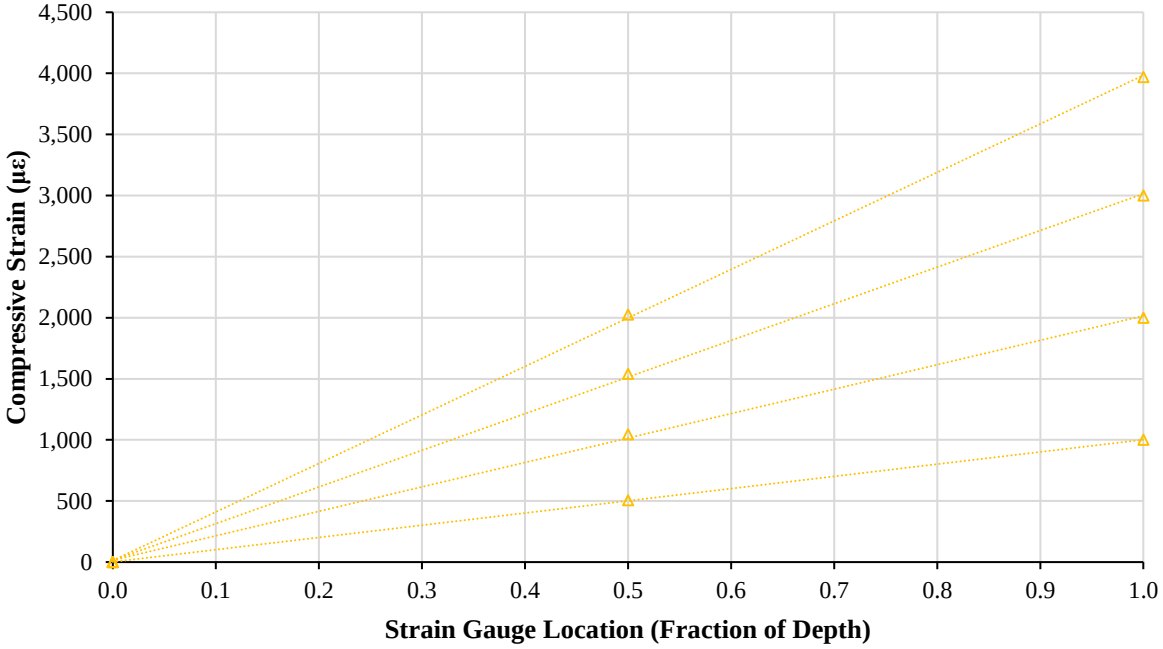

Figure 4.18 Strain Distribution through Depth of M3/50mm/S2

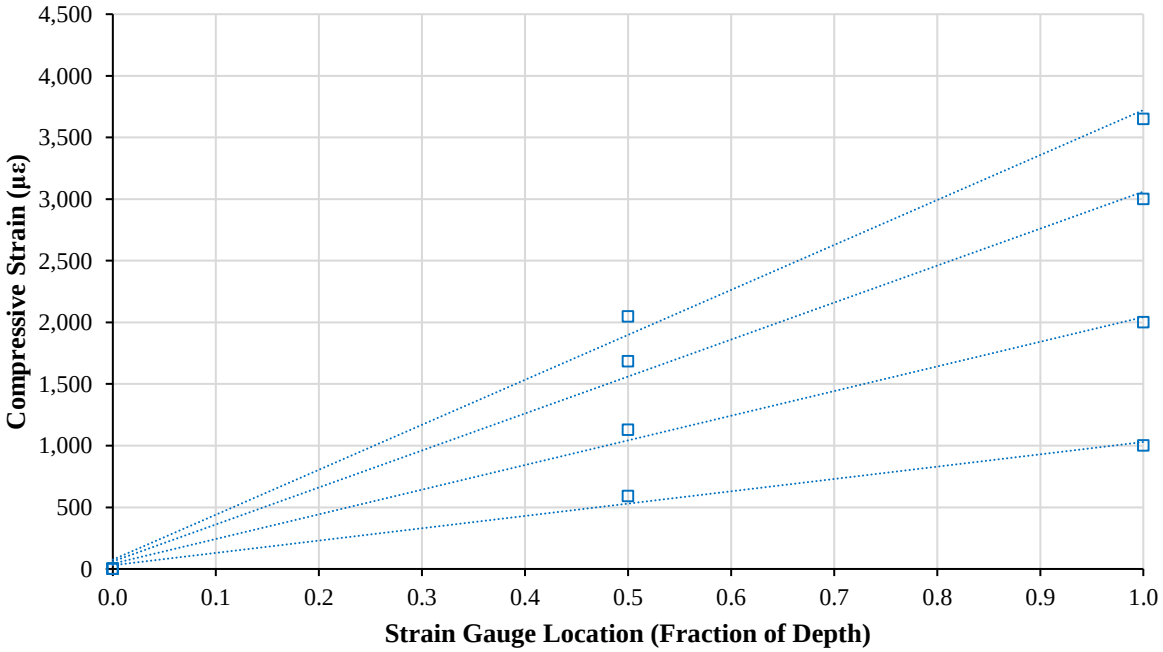

Figure 4.19 Strain Distribution through Depth of M3/100mm/S2

© University of Pretoria

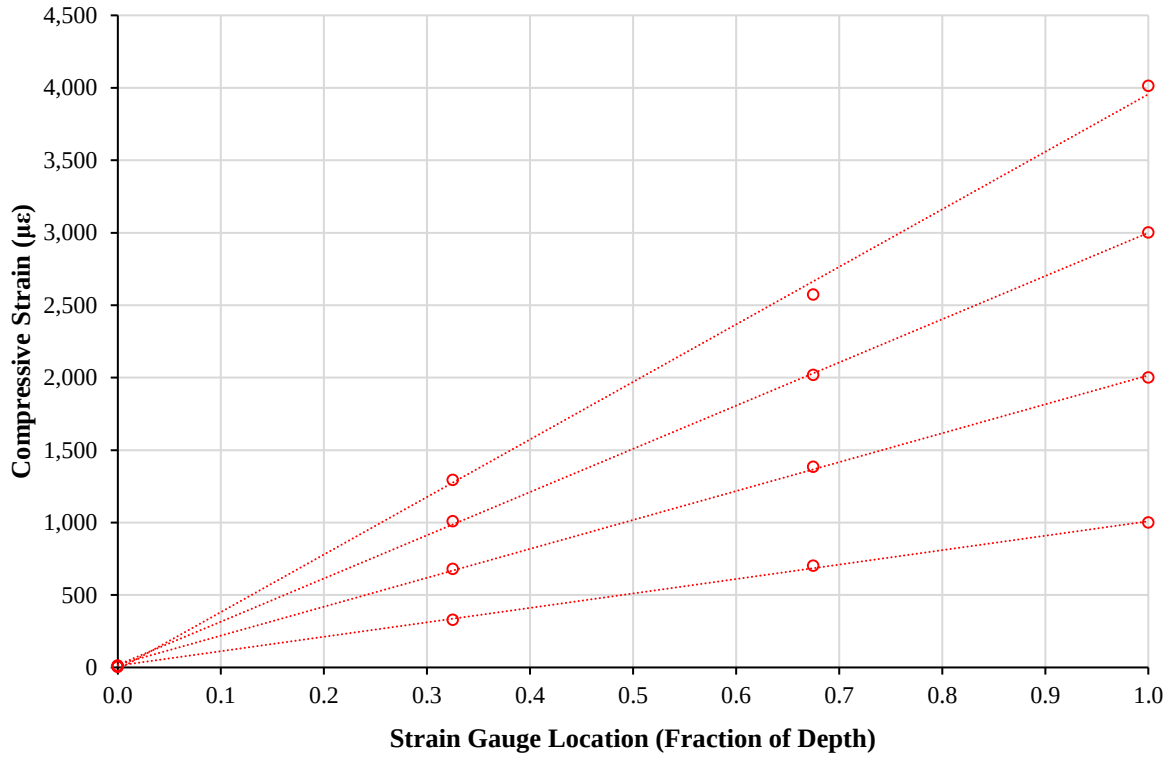

Figure 4.20 Strain Distribution through Depth of M3/200mm/S1

4.3.3 POISSON RATIO (FLEXURAL COMPRESSION)

The strain gauge layout, as indicated in Figure 3.6 to Figure 3.8, showed that each flexural compression specimen had three strain gauges (two longitudinal and one transverse to the loading direction) located on the extreme compression face. The Poisson ratio for the flexural compression members were evaluated by dividing the transverse strain gauge reading, at a particular time interval, by the average of the two longitudinal compressive strain gauge readings. As for the 150 mm cylinders, a plot of the eccentric specimen Poisson ratios (shown in Figure 4.21) was made between 500 με and 1500 με, as data below 500 με once again showed a great deal of fluctuation, and the Poisson ratio above 1500 με started to increase due to the effect of transverse micro-cracks. Figure 4.21 illustrates that regardless of the mix type the 100 mm specimens provides the most consistent results. This comes as no surprise as the surface of the 100 mm flexural compression specimens were ground flat. However, even though the 50 x 50 x 300 mm specimens were ground in a similar fashion, the strain gauge length and the specimen size could have had an effect on the transverse strain gauge readings.

The fact that the transverse strain gauge was positioned in the middle of the specimen, but the tips of the strain gauge were only 10 mm from the corners, could have resulted in the increased variability obtained in the Poisson ratio. For the 200 mm flexural compression specimens, the increased variability in the Poisson ratio can be attributed to the surface finish.

For each of the twenty-seven specimens, point estimates of the Poisson ratio were made by taking the average of the readings between 500 με and 1500 με. These point estimates, grouped according to mix and specimen dimensions, are shown in Table 4.10 and plotted in Figure 4.22, along with the values obtained by other researchers and the results obtained from the 150 mm cylinders (presented in section 4.2.2.4).

© University of Pretoria

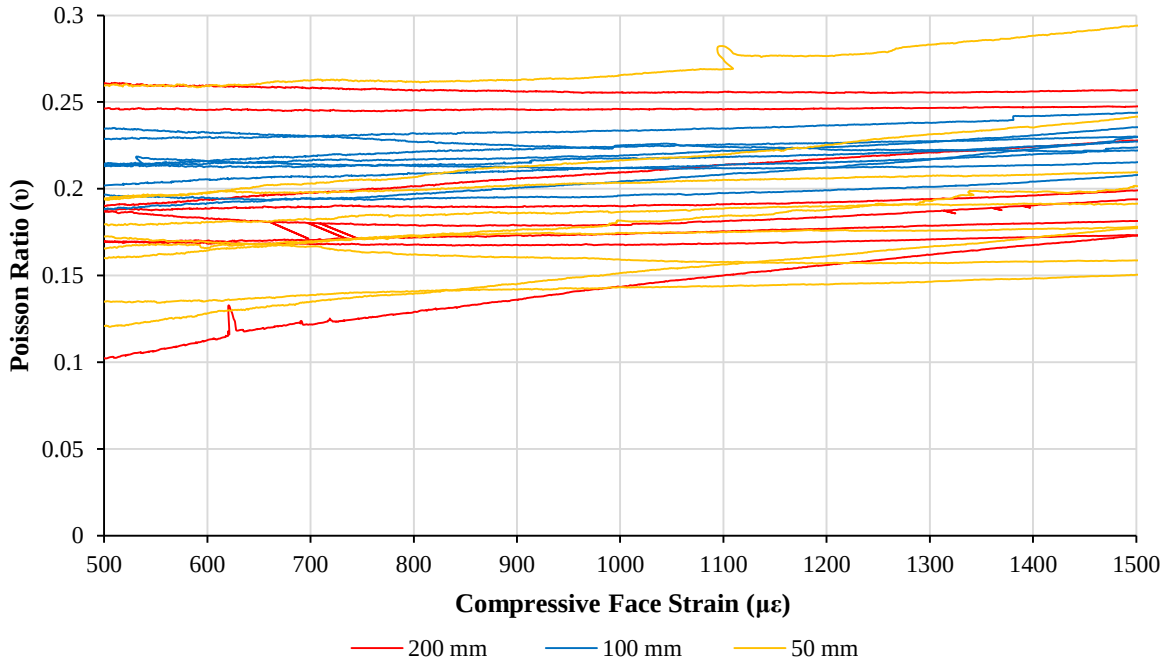

Figure 4.21 Poisson Ratio versus Longitudinal Compressive Strain for Flexural Compression Members

Table 4.10 Point Estimate of the Flexural Compression Specimens Poisson Ratio

	Mix 1		Mix 2		Mix 3	
D (mm)	**f_c' (MPa)**	**υ**	**f_c' (MPa)**	**υ**	**f_c' (MPa)**	**υ**
50	39.0	0.18	65.9	0.23	75.1	0.16
	41.8	0.18	63.2	0.19	72.1	0.18
	40.1	0.17	64.5	0.28	78.7	0.20
100	39.0	0.20	65.9	0.23	75.1	0.21
	41.8	0.20	63.2	0.22	72.1	0.21
	40.1	0.21	64.5	0.23	78.7	0.22
200	39.0	0.19	65.9	0.26	75.1	0.21
	41.8	0.16	63.2	0.20	72.1	0.19
	40.1	0.21	64.5	0.16	78.7	0.25

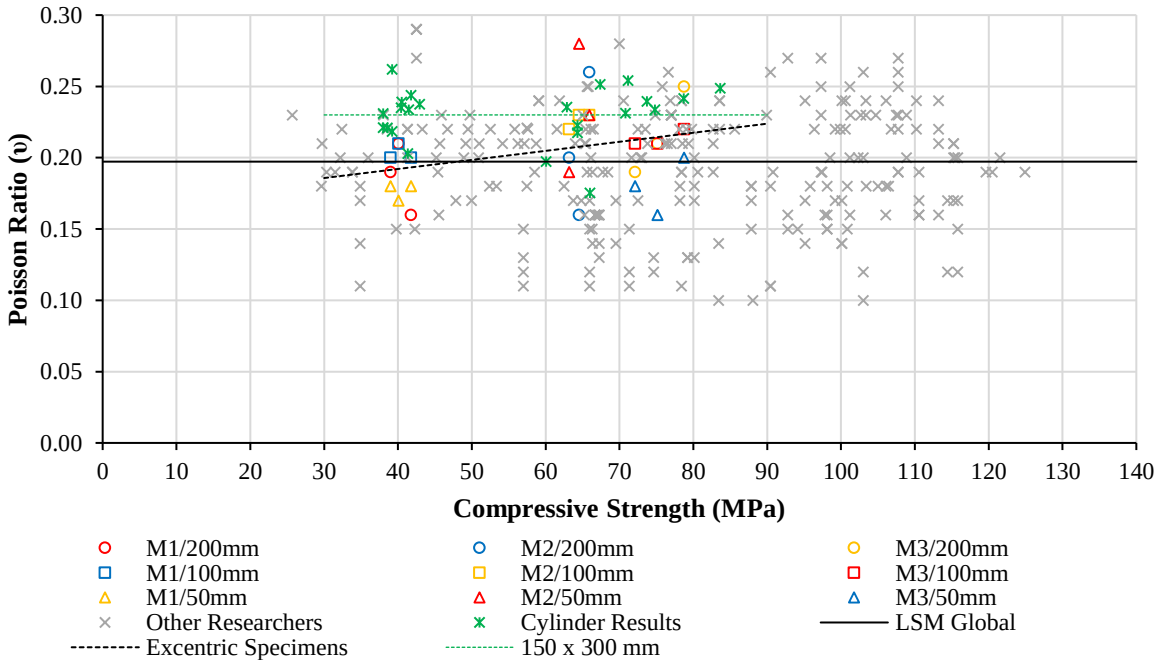

Figure 4.22 Point Estimates of the Poisson Ratios for Flexural Compression Specimens

© University of Pretoria

From Figure 4.22 it can be concluded that the Poisson ratio of the 50 mm and 200 mm flexural compression specimens show more variability than that obtained from the 150 mm cylinders. The 100 mm specimens on the other hand tend to show values that are not only consistent, but also correspond with the Poisson ratios obtained from the 150 mm cylinders. The global estimate of the Poisson ratio indicates that with the addition of the new Poisson ratios obtained in this study, the average Poisson ratio has been increased from 0.191 to 0.197. This increase is not substantial, and confirms the validity of the assumed Poisson ratio of 0.20.

4.3.4 FLEXURAL COMPRESSION STRESS-STRAIN DISTRIBUTION

The same approach originally proposed by Hognestad et al. (1955), was used to determine the stress-strain relationship for each flexural compression member. In this approach, the concrete stress (σ_c) is expressed as a function of the strain at the most extreme fibre (ε_c), and the applied stresses (f_o and m_o). Figure 4.23 shows a free-body diagram of the 1:1 scale eccentric bracket specimen.

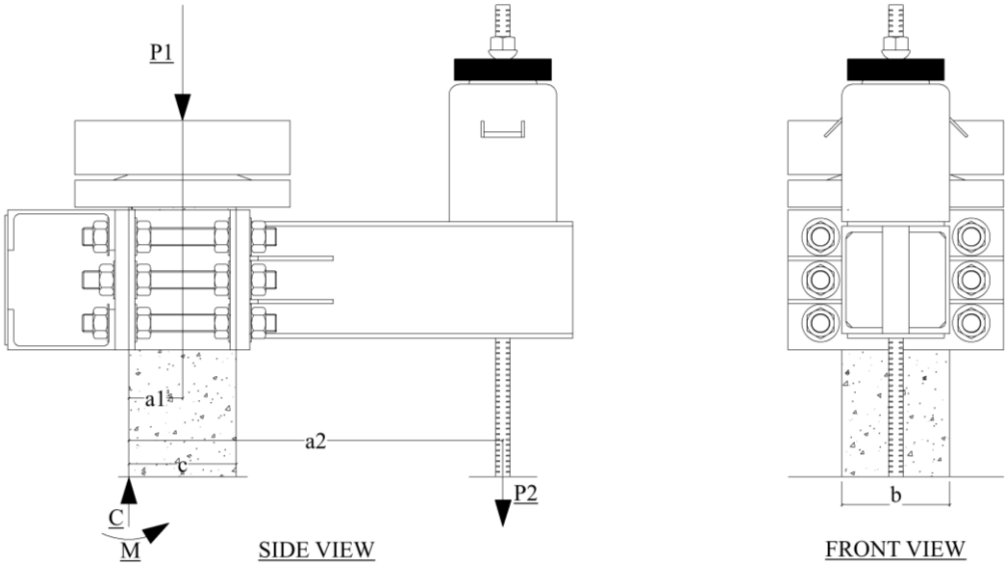

Figure 4.23 Free Body Diagram of Scale 1:1 Eccentric Bracket Specimen

By equating the internal and external forces and moments, and taking the second order moments due to the deflection of the member into consideration, Equation 4.1 to Equation 4.4 can be obtained.

$$C = P_1 + P_2 = f_o bc = \frac{bc}{\varepsilon_c}\int_0^{\varepsilon_c} \sigma_c(\varepsilon_x)d\varepsilon_x \qquad \textbf{4.1}$$

$$M = P_1 a_1 + P_2 a_2 = m_o bc^2 = \frac{bc^2}{\varepsilon_c^2}\int_0^{\varepsilon_c} \sigma_c(\varepsilon_x)\varepsilon_x d\varepsilon_x \qquad \textbf{4.2}$$

With:

$$f_o = \frac{P_1 + P_2}{bc} \qquad \textbf{4.3}$$

$$m_o = \frac{P_1 a_1 + P_2 a_2}{bc^2} \qquad \textbf{4.4}$$

Where:

C= Total externally applied load

© University of Pretoria

M= Total externally applied moment

P_1= Primary axial load

P_2= Secondary axial load

a_1= Primary load eccentricity

a_2= Secondary load eccentricity

b= Width of the section

c= Depth of the section

f_o= Average uniaxial Stress

m_o= Average bending Stress

By differentiating and rearranging the last terms of Equation 4.1 and Equation 4.2 with respect to ε_c, Equation 4.5 and Equation 4.6 are derived, both of which express the stress in the concrete as a function of the extreme fibre strain, and the externally applied stresses f_o and m_o. By using small enough increments, the differentials of $df_o/d\varepsilon_c$ and $dm_0/d\varepsilon_c$ may be approximated by $\Delta f_o/\Delta\varepsilon_c$ and $\Delta m_o/\Delta\varepsilon_c$.

$$\sigma_{c1} = \frac{df_o}{d\varepsilon_c}\varepsilon_c + f_o \qquad \textbf{4.5}$$

$$\sigma_{c2} = \frac{dm_o}{d\varepsilon_c}\varepsilon_c + 2m_o \qquad \textbf{4.6}$$

Equation 4.5 and Equation 4.6 were used to obtain two similar stress-strain relationships for each flexural compression specimen, and the average of the two taken as the stress-strain distribution in the flexural compression member. The stress-strain relationship so obtained tends to increase to a maximum after which it decreases prior to failure. The process of numerical integration in Equation 4.5 and Equation 4.6 tend to amplify experimental scatter. Furthermore, the manual application of P_2 results in erratic fluctuations in the slope. As mentioned by Ibrahim (1994), the simplest method of eliminating the experimental scatter is to fit a 3rd order polynomial function through the f_o and m_o data. By fitting the third order approximation, the final stress-strain curves for the 50 x 50 x 300 mm, 100 x 100 x 500 mm, and 200 x 200 x 1000 mm specimens can be obtained as shown in Figure 4.24 to Figure 4.26. These figures illustrate that the ultimate compressive strain tends to reduce with an increase in the compressive strength, tending to 3000 με for the 200 mm and 100 mm specimens and no clear lower limit for the 50 mm specimens. It is also clear that regardless of the specimen size, the shape of the ascending branch of the stress-strain curve changes with an increase in compressive strength from a parabolic rectangular form to a more triangular form. The most interesting phenomenon is the variability associated with each specimen size. It can be seen that similar to the results obtained from the 200 mm cubes and 200 mm cylinders, the variability in compressive strength increased for the 200 mm flexural compression specimens.

4.3.5 STRESS BLOCK PARAMETERS

For each of the three mixes and sample sizes, the stress-strain relationships were used to calculate the stress block parameters and the ultimate compressive strains presented in Table 4.11. As the stress block parameters are traditionally plotted versus the mean cylinder strength, the stress block parameters were calculated for both the mean 150 mm cylinder strength, and the mean 50 mm, 100 mm, and 200 mm cylinder strength. Plots of these stress block parameters overlaying the results obtained by other researchers, are shown in Figure 4.27 to Figure 4.36.

© University of Pretoria

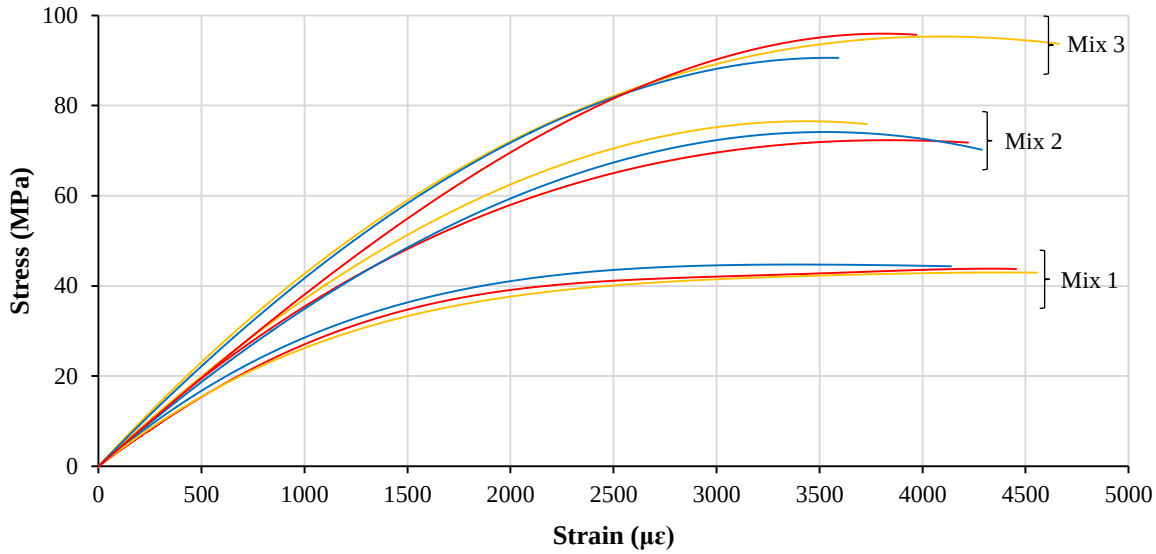

Figure 4.24 50 mm Specimens Flexural Stress-Strain Relationships

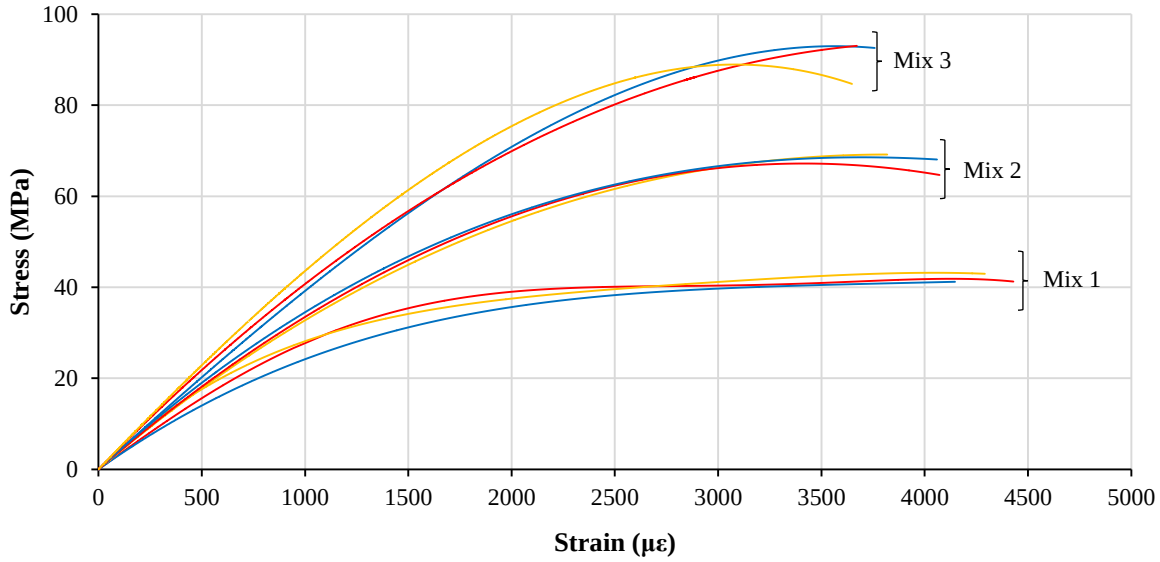

Figure 4.25 100 mm Specimens Flexural Stress-Strain Relationships

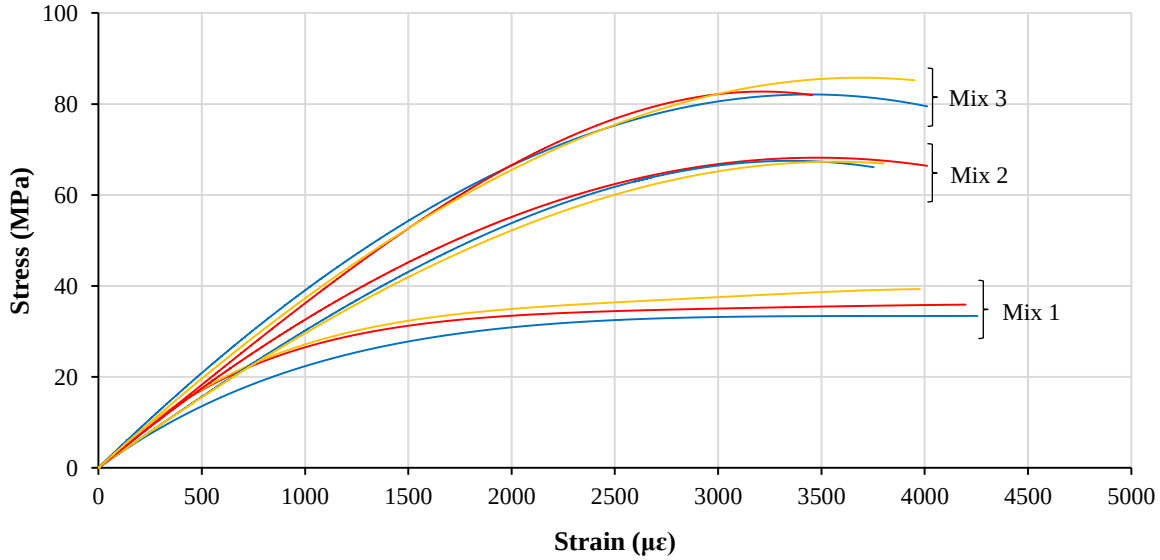

Figure 4.26 200 mm Specimens Flexural Stress-Strain Relationships

© University of Pretoria

Table 4.11 Calculated Stress Block Parameters for Flexural Compression Members

D (mm)	Mix	Specimen	f_c'	f_{cy} (MPa)	k_1	k_2	k_3	k_1k_3	α_1	β_1	ε_{cu} (με)
50	1	1	$f_{c\,(150\ mm)}'$	39.0	0.74	0.41	1.15	0.85	1.03	0.82	4138
			$f_{c\,(50\ mm)}'$	44.1			1.02	0.75	0.91		
		2	$f_{c\,(150\ mm)}'$	41.8	0.77	0.41	1.05	0.81	0.98	0.83	4455
			$f_{c\,(50\ mm)}'$	45.7			0.96	0.74	0.89		
		3	$f_{c\,(150\ mm)}'$	40.1	0.78	0.41	1.07	0.83	1.01	0.83	4556
			$f_{c\,(50\ mm)}'$	44.7			0.96	0.75	0.90		
	2	1	$f_{c\,(150\ mm)}'$	65.9	0.70	0.39	1.10	0.77	0.99	0.78	4288
			$f_{c\,(50\ mm)}'$	74.5			0.97	0.68	0.88		
		2	$f_{c\,(150\ mm)}'$	63.2	0.66	0.39	1.17	0.77	0.99	0.78	4221
			$f_{c\,(50\ mm)}'$	71.6			1.04	0.68	0.88		
		3	$f_{c\,(150\ mm)}'$	64.5	0.66	0.38	1.19	0.79	1.03	0.76	3730
			$f_{c\,(50\ mm)}'$	78.2			0.98	0.65	0.85		
	3	1	$f_{c\,(150\ mm)}'$	75.1	0.64	0.37	1.21	0.77	1.03	0.74	3592
			$f_{c\,(50\ mm)}'$	89.4			1.01	0.64	0.87		
		2	$f_{c\,(150\ mm)}'$	72.1	0.62	0.37	1.33	0.82	1.12	0.73	3970
			$f_{c\,(50\ mm)}'$	89.5			1.07	0.66	0.91		
		3	$f_{c\,(150\ mm)}'$	78.7	0.67	0.39	1.21	0.82	1.05	0.78	4663
			$f_{c\,(50\ mm)}'$	90.5			1.05	0.71	0.91		
100	1	1	$f_{c\,(150\ mm)}'$	39.0	0.73	0.42	1.07	0.78	0.93	0.84	4430
			$f_{c\,(100\ mm)}'$	42.2			0.99	0.72	0.86		
		2	$f_{c\,(150\ mm)}'$	41.8	0.77	0.40	0.99	0.76	0.94	0.81	4147
			$f_{c\,(100\ mm)}'$	41.5			0.99	0.77	0.95		
		3	$f_{c\,(150\ mm)}'$	40.1	0.76	0.42	1.08	0.82	0.98	0.84	4430
			$f_{c\,(100\ mm)}'$	42.7			1.01	0.77	0.92		
	2	1	$f_{c\,(150\ mm)}'$	65.9	0.69	0.38	1.05	0.73	0.96	0.76	3819
			$f_{c\,(100\ mm)}'$	69.9			0.99	0.68	0.90		
		2	$f_{c\,(150\ mm)}'$	63.2	0.67	0.39	1.06	0.71	0.92	0.78	4072
			$f_{c\,(100\ mm)}'$	65.9			1.02	0.68	0.88		
		3	$f_{c\,(150\ mm)}'$	64.5	0.68	0.39	1.06	0.72	0.93	0.78	4060
			$f_{c\,(100\ mm)}'$	68.3			1.00	0.68	0.88		
	3	1	$f_{c\,(150\ mm)}'$	75.1	0.63	0.36	1.24	0.78	1.08	0.73	3672
			$f_{c\,(100\ mm)}'$	79.5			1.17	0.74	1.02		
		2	$f_{c\,(150\ mm)}'$	72.1	0.63	0.38	1.23	0.77	1.02	0.76	3648
			$f_{c\,(100\ mm)}'$	79.4			1.12	0.70	0.93		
		3	$f_{c\,(150\ mm)}'$	78.7	0.62	0.37	1.18	0.73	1.00	0.73	3758
			$f_{c\,(100\ mm)}'$	82.0			1.13	0.70	0.96		
200	1	1	$f_{c\,(150\ mm)}'$	39.0	0.82	0.42	0.86	0.70	0.83	0.84	4256
			$f_{c\,(200\ mm)}'$	32.1			1.04	0.85	1.01		
		2	$f_{c\,(150\ mm)}'$	41.8	0.79	0.43	0.86	0.68	0.79	0.86	4198
			$f_{c\,(200\ mm)}'$	40.0			0.90	0.71	0.82		
		3	$f_{c\,(150\ mm)}'$	40.1	0.75	0.42	0.98	0.74	0.88	0.84	3977
			$f_{c\,(200\ mm)}'$	38.6			1.02	0.77	0.91		
	2	1	$f_{c\,(150\ mm)}'$	65.9	0.66	0.38	1.03	0.68	0.89	0.77	4012
			$f_{c\,(200\ mm)}'$	56.9			1.20	0.79	1.03		
		2	$f_{c\,(150\ mm)}'$	63.2	0.63	0.37	1.07	0.68	0.92	0.73	3753
			$f_{c\,(200\ mm)}'$	59.8			1.13	0.72	0.97		
		3	$f_{c\,(150\ mm)}'$	64.5	0.64	0.37	1.04	0.67	0.90	0.74	3801
			$f_{c\,(200\ mm)}'$	67.2			1.00	0.64	0.86		
	3	1	$f_{c\,(150\ mm)}'$	75.1	0.66	0.38	1.09	0.72	0.94	0.77	4012
			$f_{c\,(200\ mm)}'$	64.0			1.28	0.84	1.10		
		2	$f_{c\,(150\ mm)}'$	72.1	0.62	0.36	1.15	0.71	0.98	0.72	3455
			$f_{c\,(200\ mm)}'$	69.4			1.19	0.74	1.02		
		3	$f_{c\,(150\ mm)}'$	78.7	0.65	0.37	1.09	0.71	0.95	0.75	3950
			$f_{c\,(200\ mm)}'$	76.7			1.12	0.73	0.98		

© University of Pretoria

Figure 4.27 illustrates the variation of k_1 with respect to the 150 mm cylinder strength. The k_1 value is defined as the ratio between the average flexural stress and the maximum flexural stress, and even though the cylinder strength is *not used in the calculation* of k_1, it is still a function of the cylinder compressive strength, decreasing as the compressive strength increases. From Figure 4.27, however, k_1 appears to be only marginally effected by the flexural compression specimen size.

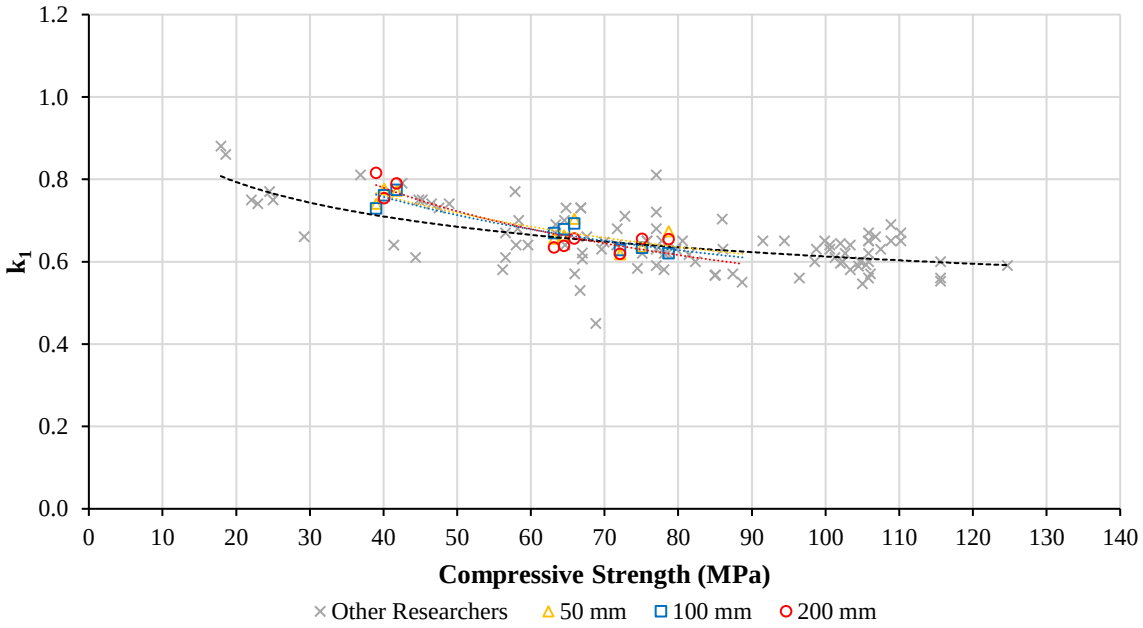

Figure 4.27 Effect of 150 mm Cylinder Compressive Strength on k_1

Figure 4.28 illustrates the variation in k_2 (defined as the ratio between the depth of the resultant compressive force and the position of the neutral axis) with respect to the 150 mm cylinder strength. The k_2 value is determined from the stress-strain distribution and the cylinder strength is not used in its calculation, however, similar to k_1, k_2 will reduce with an increase in compressive strength. Figure 4.28 also indicates that the size of the flexural compression specimen does not seem to have a significant effect on the k_2 values.

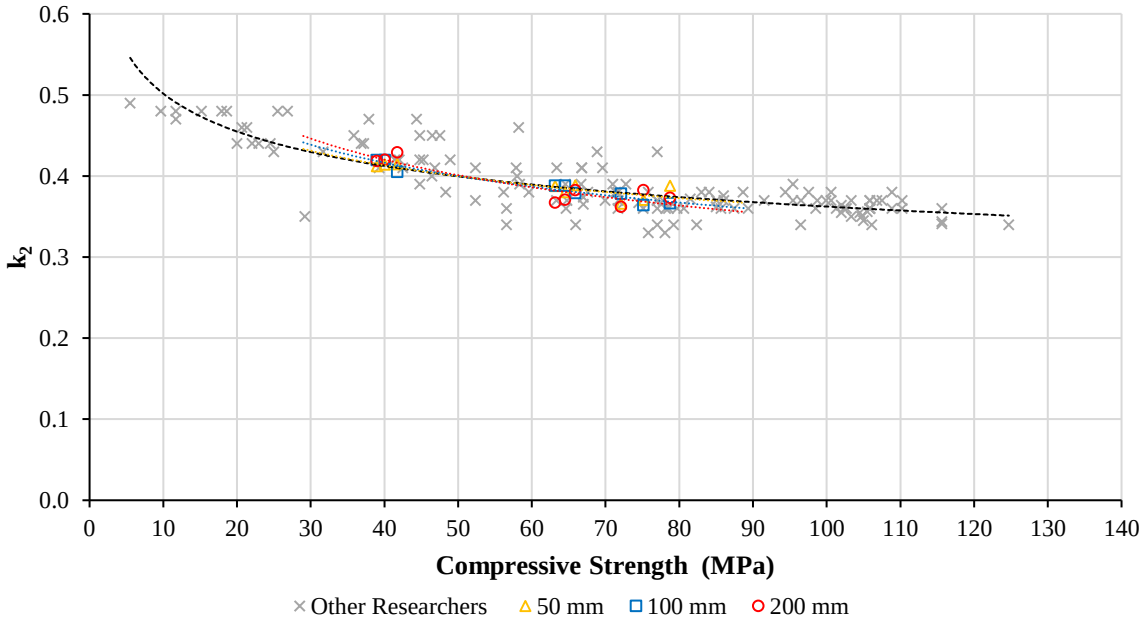

Figure 4.28 Effect of 150 mm Cylinder Compressive Strength on k_2

© University of Pretoria

Figure 4.29 and Figure 4.30, illustrate the effect of cylinder strength on the k_3 value (defined as the ratio between the maximum flexural compressive stress and the 150 mm cylinder compressive strength). Thus, the calculation of k_3 is directly dependant on whether the 150 mm or associated cylinder strength is used. As shown in Figure 4.29, the 200 mm results tend to lie below that of the 100 mm results, and that below the 50 mm results. The k_3 values indicated in Figure 4.29 provides an initial indication of specimen size effect. The k_3 values shown in Figure 4.30, were calculated using the 150 mm cylinder strength for the 200 mm specimens, and the associated cylinder strength for the 50 mm and 100 mm specimens. Based on Figure 4.30, it would seem that if the associated cylinder strength were used to calculate the stress block parameters for the 50 mm and 100 mm specimens, the size effect of k_3 can be eliminated.

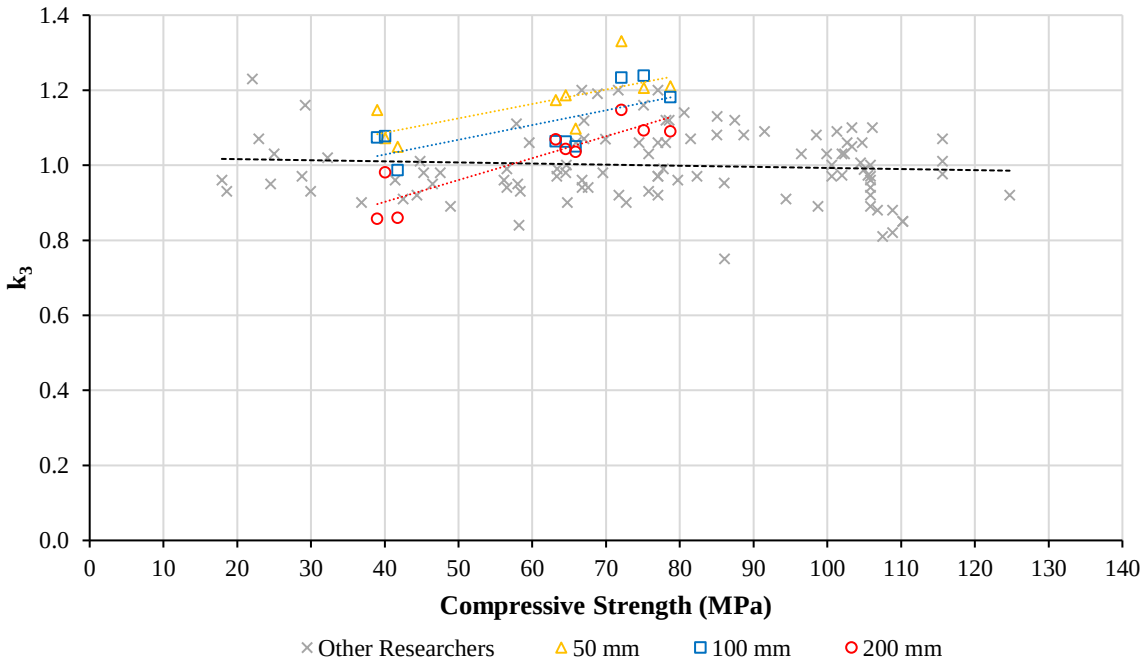

Figure 4.29 Effect of 150 mm Cylinder Compressive Strength on k_3

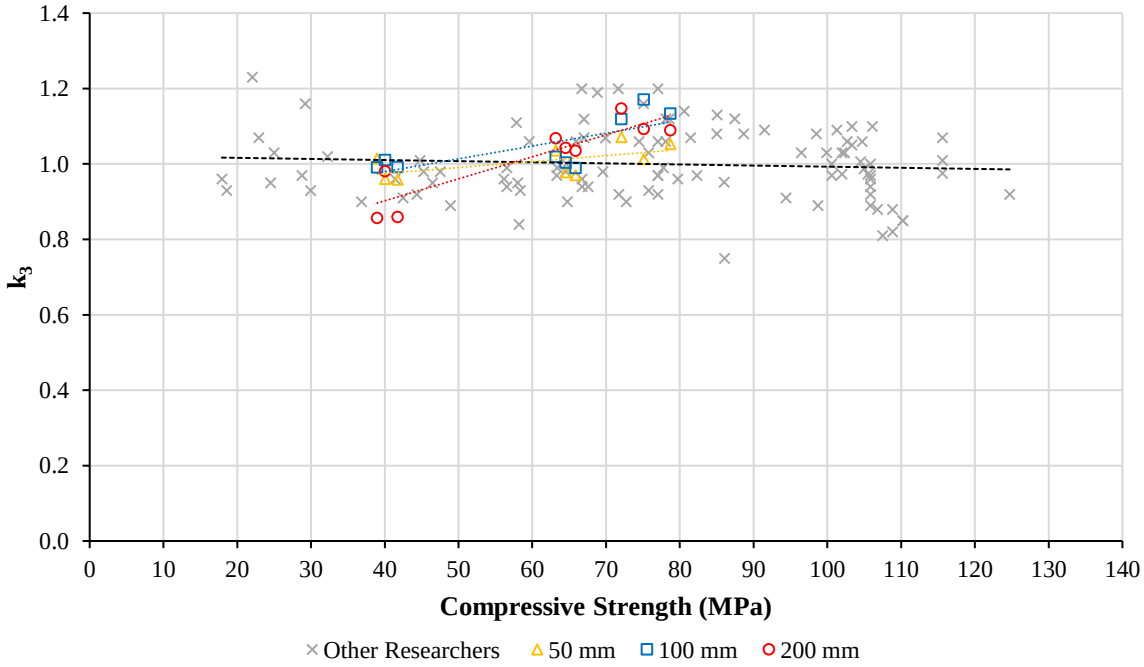

Figure 4.30 Effect of Associated Cylinder Compressive Strength on k_3

© University of Pretoria

Figure 4.31 and Figure 4.32 show the variation in k_1k_3 with respect to the 150 mm cylinder strength. The 50 mm and 100 mm k_1k_3 values, shown in Figure 4.32, were calculated using the associated cylinder strength, and the 200 mm specimen k_1k_3 values, were calculated using the 150 mm cylinder strength. From Figure 4.31, it is clear that the k_1k_3 value of the 200 mm specimen slightly reduces with an increase in compressive strength, with the reduction becoming ever more prominent for the 100 mm and 50 mm specimens. Figure 4.31 shows a specimen size effect for k_1k_3, and from Figure 4.32 it would seem that if the associated cylinder strength is used to calculate k_1k_3 for the 50 mm and 100 mm specimens, this size effect can be eliminated.

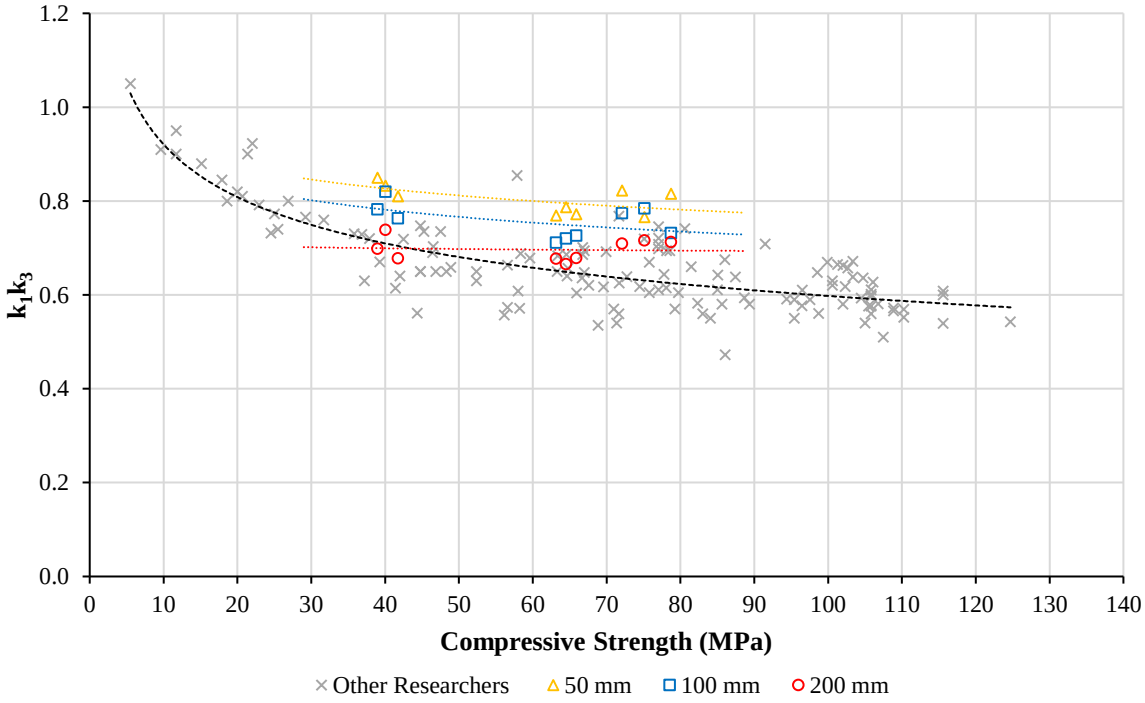

Figure 4.31 Effect of 150 mm Cylinder Compressive Strength on k_1k_3

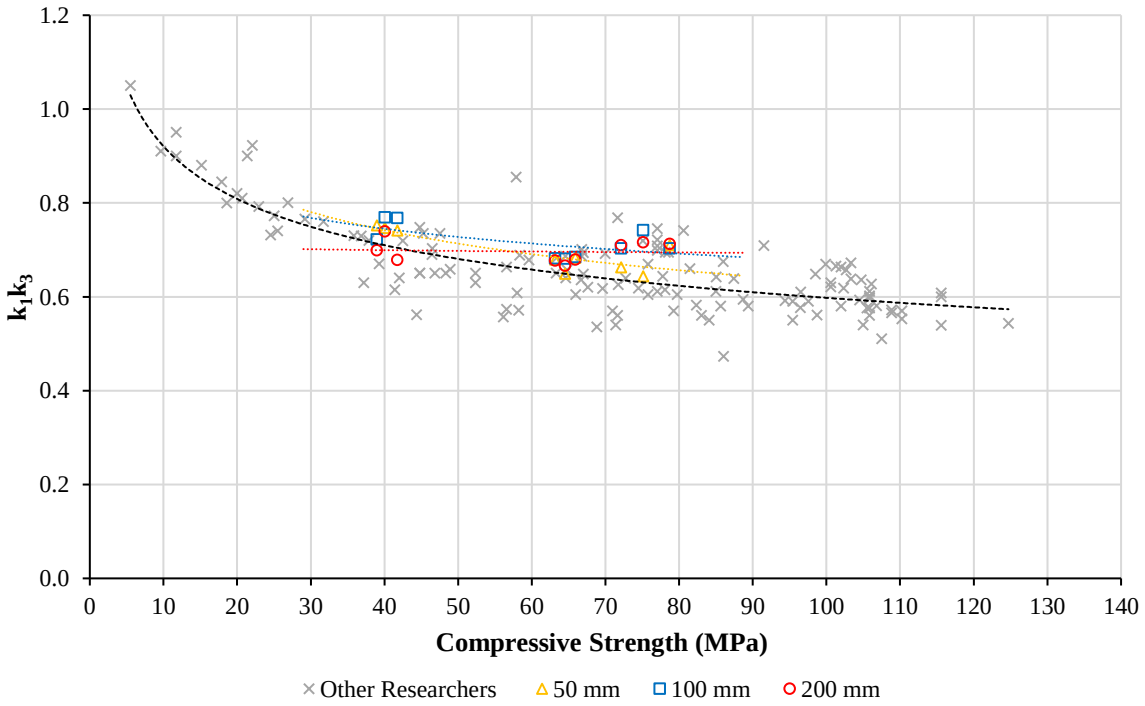

Figure 4.32 Effect of Associated Cylinder Compressive Strength on k_1k_3

© University of Pretoria

Figure 4.33 and Figure 4.34, show the variation of α_1 with respect to the 150 mm cylinder strength. The 50 mm and 100 mm k_1k_3 values, shown in Figure 4.34, were calculated using the associated cylinder strength, and the 200 mm specimen k_1k_3 values were calculated using the 150 mm cylinder strength. As α_1 is calculated as the ratio between k_1k_3 and $2k_2$, the type of the cylinder strength will once again have an effect on the results. Figure 4.33 indicates that the 50 mm and 100 mm specimens plot markedly higher than the 200 mm specimens. If Figure 4.33 and Figure 4.34 are compared, it can be seen that the α_1 values of the 50 mm and 100 mm specimens, shown in Figure 3.34, lie within the cluster of values obtained by previous researchers. Thus, when compared on the basis of the 150 mm cylinder strength, α_1 shows a definite size effect, however, by using the associated cylinder strength for the 50 mm and 100 mm specimen, the size efect can be eliminated.

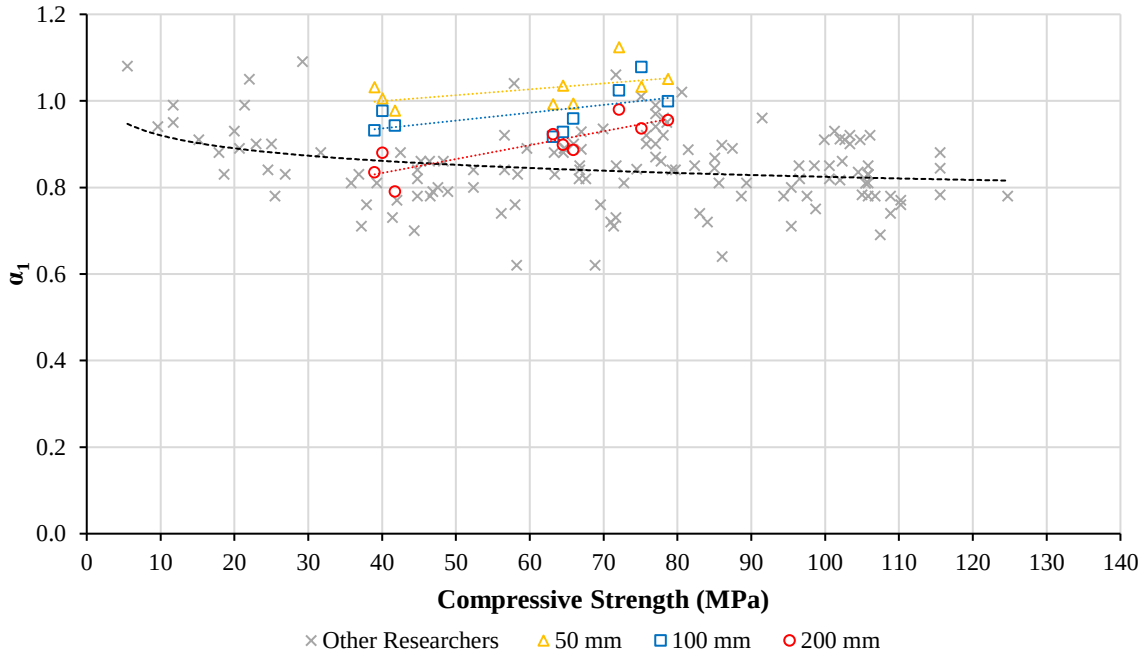

Figure 4.33 Effect of 150 mm Cylinder Compressive Strength on α_1

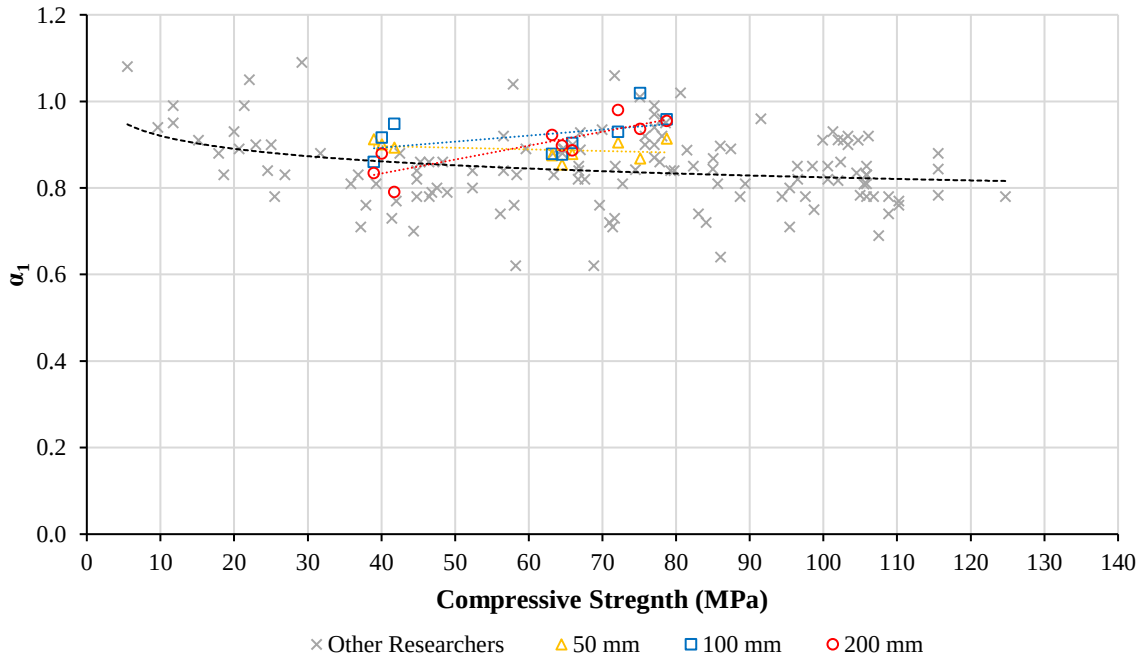

Figure 4.34 Effect of Associated Cylinder Compressive Strength on α_1

© University of Pretoria

Figure 4.35 shows the variation in β_1 with respect to the 150 mm cylinder strength. As β_1 is defined as $2k_2$, and k_2 itself appeared to be independent of the specimen size, the results obtained for β_1 seems to be independent of the cylinder size too.

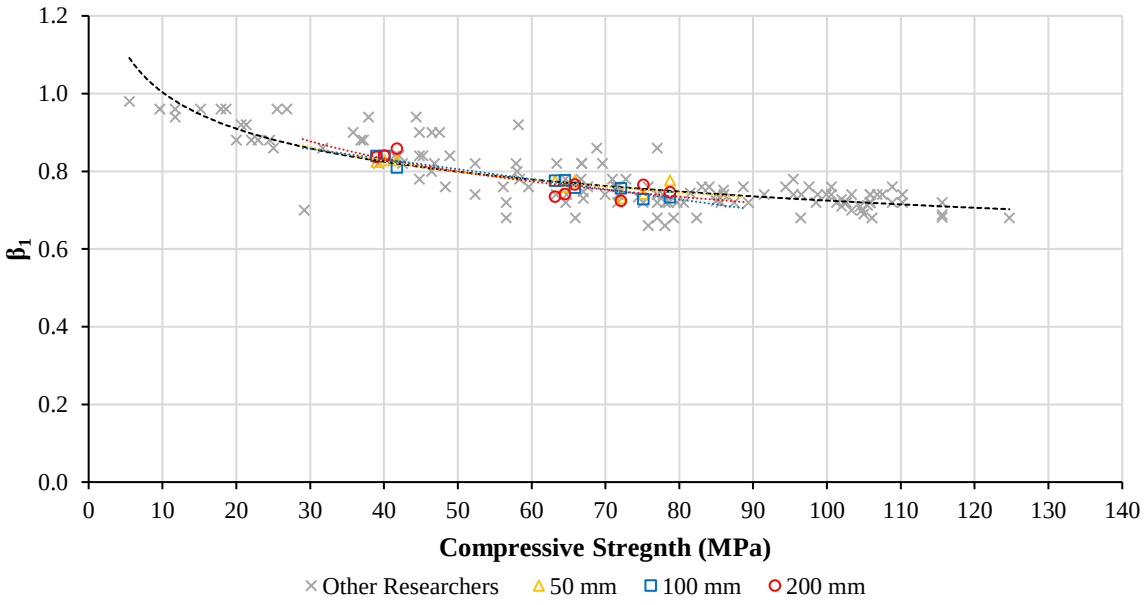

Figure 4.35 Effect of 150 mm Cylinder Compressive Strength on β_1

Figure 4.36 illustrates the ultimate compressive strain with respect to the 150 mm cylinder strength. With an increase in compressive strength, there is a general reduction in the ultimate compressive strain (ε_{cu}), and a definite size effect. Additionally it should be noted that ultimate compressive strain is independent of whether the associated or 150 mm cylinder strength is used.

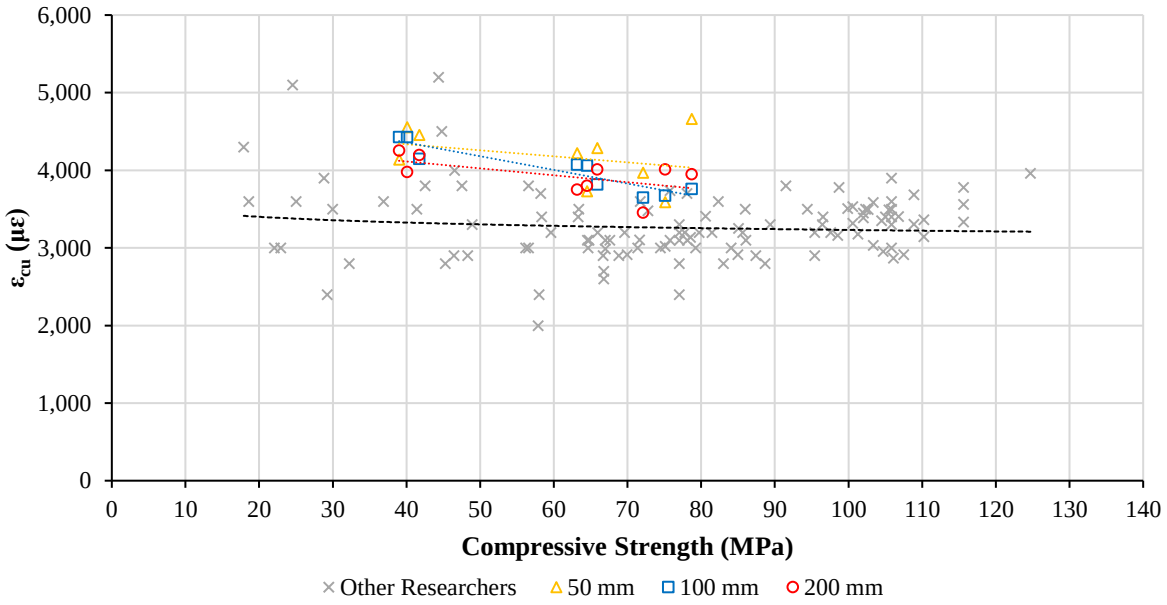

Figure 4.36 Effect of 150 mm Cylinder Compressive Strength on ε_{cu}

With the exception of k_1, k_2, and β_1, Figures 4.27 to Figure 4.36 illustrated a clear difference in the stress block parameters for different specimen sizes, when the parameter of interest was calculated with the 150 mm cylinder strength. It seems, however, that this size effect can easily be eliminated by using the associated cylinder strength for the 50 mm and 100 mm specimens.

© University of Pretoria

4.4 INFLUENCE OF SPECIMEN SIZE ON THE FLEXURAL COMPRESSIVE BEHAVIOUR

For a particular mix, a clear difference in the stress block parameters of the three specimen sizes is notable when the k_3, k_1k_3, and α_1 results are calculated using the 150 mm cylinder compressive strength, and the ultimate compressive strain is plotted with respect to the 150 mm cylinder strength. In this section the magnitude of this influence on the stress block parameters will be established, with the average value of the 200 mm (20 cm) specimen stress block parameter used as the basis of standardization.

The size effect is defined as the effect of the sample dimension on the strength of a specimen if geometrically similar members are compared. Even though the size effect is only applicable for geometrically similar members, the use of the associated cylinder strength may result in the satisfactory elimination of this effect, enabling smaller members (50 x 50 x 300 mm and 100 x 100 x 500 mm), as opposed to the conventional 200 x 200 x 1000 mm specimens, to be used to determine the stress block parameters in future.

4.4.1 SIZE EFFECT FOR k_3

k_3 was originally defined as the ratio between the maximum flexural compressive stress and the 150 mm cylinder strength. Thus, k_3 is the first of the stress block parameters that is calculated using the cylinder strength. Figure 4.37 shows a clear specimen size effect for all three mixes, however, this effect is not as prominent for Mix 2. Utilising the MSEL and LSM regression analysis, the coefficients for each respective mix and the average can be obtained, and are shown in Table 4.12.

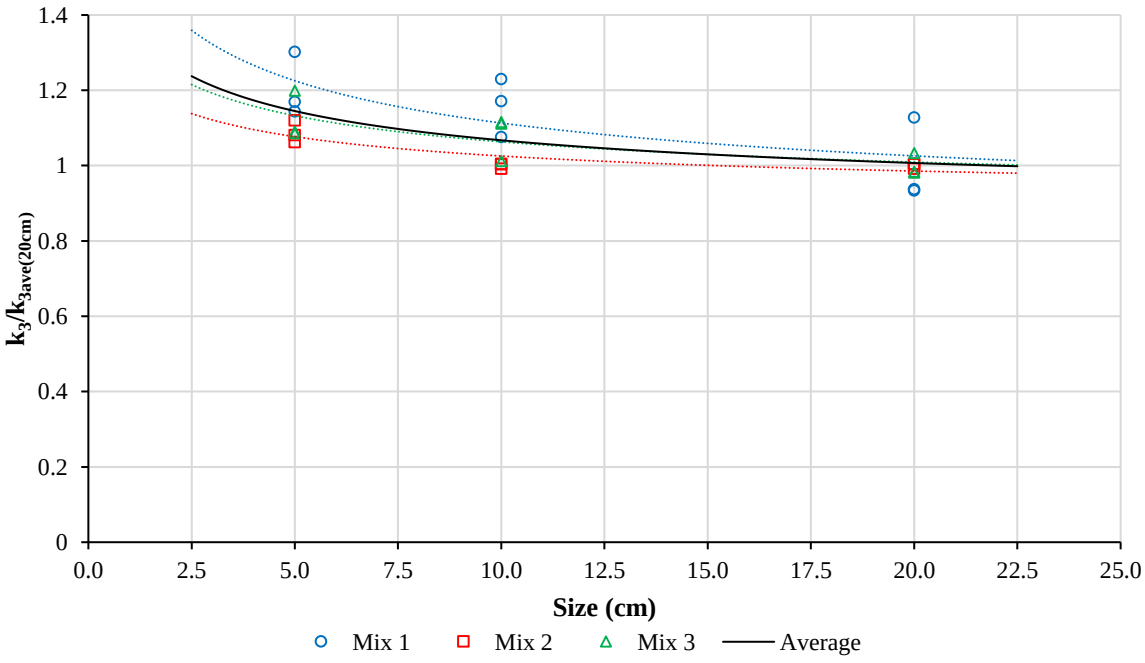

Figure 4.37 Effect of Specimen Size on $k_3/k_{3ave(20cm)}$

Table 4.12 MSEL Coefficients for $k_3/k_{3ave(20cm)}$

	Mix 1	Mix 2	Mix 3	Average
β	1.11	0.49	0.65	0.75
$\lambda_0 d_a$	0.95	0.95	0.95	0.95
α	0.79	0.88	0.88	0.85

© University of Pretoria

It is interesting to note that an increase in compressive strength does not necessarily result in an increase in the size effect of k_3. The average k_3 size effect was used to define the specimen size effect, with the final relationship used to describe this behaviour given in Equation 4.7.

$$k_3 = \frac{0.75k_{3(20cm)}}{\sqrt{1+\frac{c}{0.95}}} + 0.85k_{3(20cm)} \qquad 4.7$$

Where:

k_3= The k_3 for a specific specimen size

$k_{3(20cm)}$= The k_3 of a 200 x 200 x 1000 mm specimen

c= The specimen dimension (cm)

As the k_3 value is dependent on the cylinder compressive strength, and the cylinders themselves conform to the MSEL, it should be possible to largely eliminate the specimen size effect by utilising the associated cylinder rather than the 150 mm cylinder strength in the calculation of k_3. Figure 4.38 shows a plot of the ratio between the k_3 value for each specimen, and the average k_3 value of a 200 mm specimens. Note that the associated cylinder strengths were used to calculate the stress block parameters for the 50 mm and 100 mm specimens, and the 150 mm cylinder strengths used to calculate the stress block parameters for the 200 mm specimens.

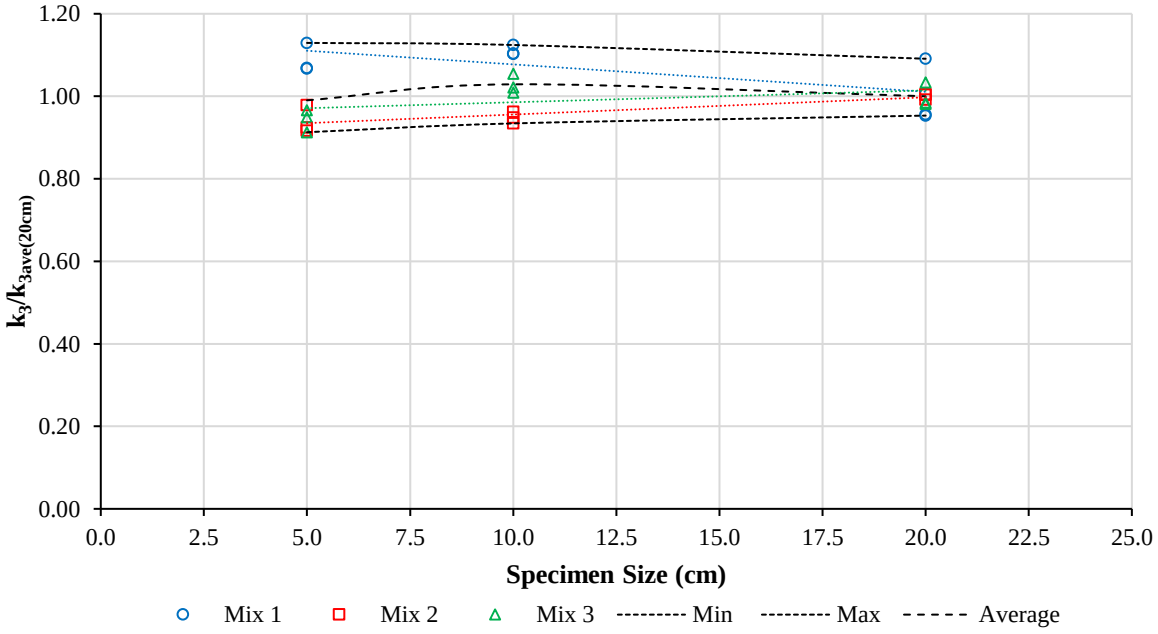

Figure 4.38 Elimination of Size Effect for $k_3/k_{3ave(20cm)}$

Figure 4.38 shows that the $k_3/k_{3ave(20cm)}$ value for the 50 mm specimen varies between 0.91 and 1.15 with an average of 0.99, the 100mm specimen values varies between 0.94 and 1.15 with an average of 1.02. Thus, it can be concluded that the size effect for k_3 can be eliminated if the associated cylinder strength is used for the 50 mm and 100 mm specimens.

4.4.2 SIZE EFFECT FOR k_1k_3

The stress block parameter k_1k_3, is defined as the ratio between the average stress (f_o) and the 150 mm cylinder compressive strength. Similar to k_3, k_1k_3 is directly influenced by the cylinder compressive strength. The influence

© University of Pretoria

of flexural compression specimen size on k_1k_3, based on the standard 150 mm cylinder strength, is shown in Figure 4.39. As expected, there is a definite size effect, the exact extent of which was obtained by performing LSM regression analysis and employing the MSEL equation. The coefficients of the MSLE equation, is shown in Table 4.13.

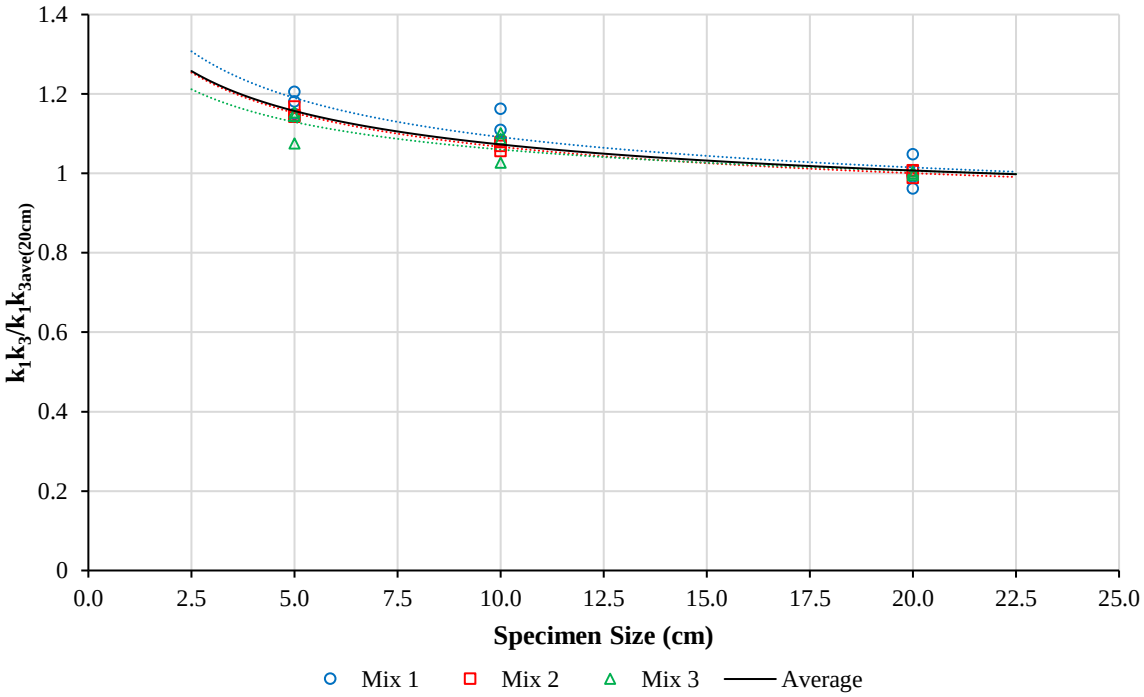

Figure 4.39 Effect of Specimen Size on k_1k_3/ $k_1k_{3ave(20cm)}$

Table 4.13 MSEL Coefficients for k_1k_3/ $k_1k_{3ave(20cm)}$

	Mix 1	Mix 2	Mix 3	Average
β	0.94	0.81	0.66	0.80
$\lambda_0 d_a$	0.95	0.95	0.95	0.95
α	0.82	0.83	0.87	0.84

The coefficients of the MSEL obtained for k_1k_3 are close to the coefficients obtained for k_3. This makes sense as k_1 (for each specimen size and mix) remained relatively constant. Based on the average of all three mixes, the final MSEL relationship for k_1k_3 is shown in Equation 4.8.

$$k_1k_3 = \frac{0.8k_1k_{3(20cm)}}{\sqrt{1+\frac{c}{0.95}}} + 0.84k_1k_{3(20cm)} \qquad \textbf{4.8}$$

Where:

k_1k_3= The k_1k_3 for a specific specimen size

$k_1k_{3(20cm)}$= The k_1k_3 of a 200 x 200 x 1000 mm specimen

c= The specimen dimension (cm)

In an attempt to eliminate the size effect of k_1k_3, the 150 mm cylinder strength was once again used to calculate the stress block parameters of the 200 mm specimens, while the associated cylinder strength is used to calculate the stress block parameters of the 50 mm and 100 mm flexural compression specimens. Figure 4.40, shows that the k_1k_3 value of the 50 mm specimens varies between 0.9 and 1.08 times the average k_1k_3 value of the 200 mm

© University of Pretoria

specimen, with an average of 0.99, while the k_1k_3 value of the 100 mm specimens varies between 0.95 and 1.12, with an average of 1.02 times the average k_1k_3 value of the 200 mm specimens. Figure 4.40 shows that the size effect for k_1k_3 can be eliminated if the 150 mm cylinder strength is used to calculate k_1k_3 for the 200 mm specimens, and the associated cylinder strength used to calculate k_1k_3 for the 50 mm and 100 mm specimens.

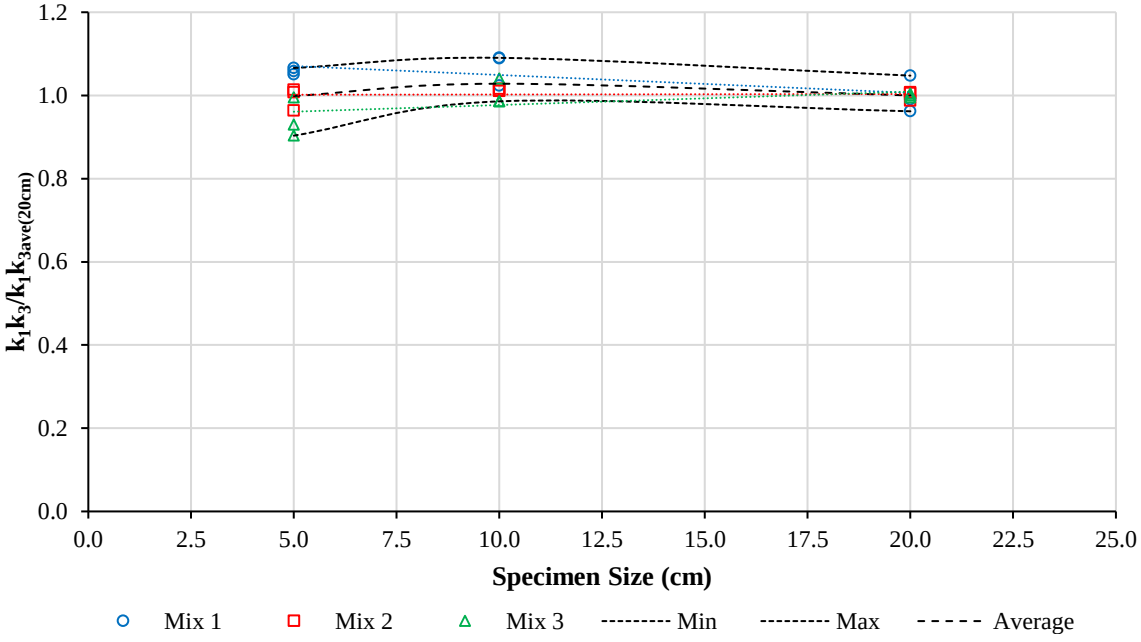

Figure 4.40 Elimination of Size Effect for $k_1k_3/k_1k_{3ave(20cm)}$

4.4.3 SIZE EFFECT FOR α_1

The stress block parameter α_1 is defined as $k_1k_3/2k_2$. Figure 4.41, shows the size effect for $\alpha_1/\alpha_{1ave(20cm)}$, with the coefficients of the MSEL equations obtained for each respective mix and the average relationship shown in Table 4.14. Once again, the coefficients of the MSEL for α_1 are close to the coefficients obtained for k_3 and k_1k_3. The final MSEL relationship for α_1 is shown in Equation 4.9.

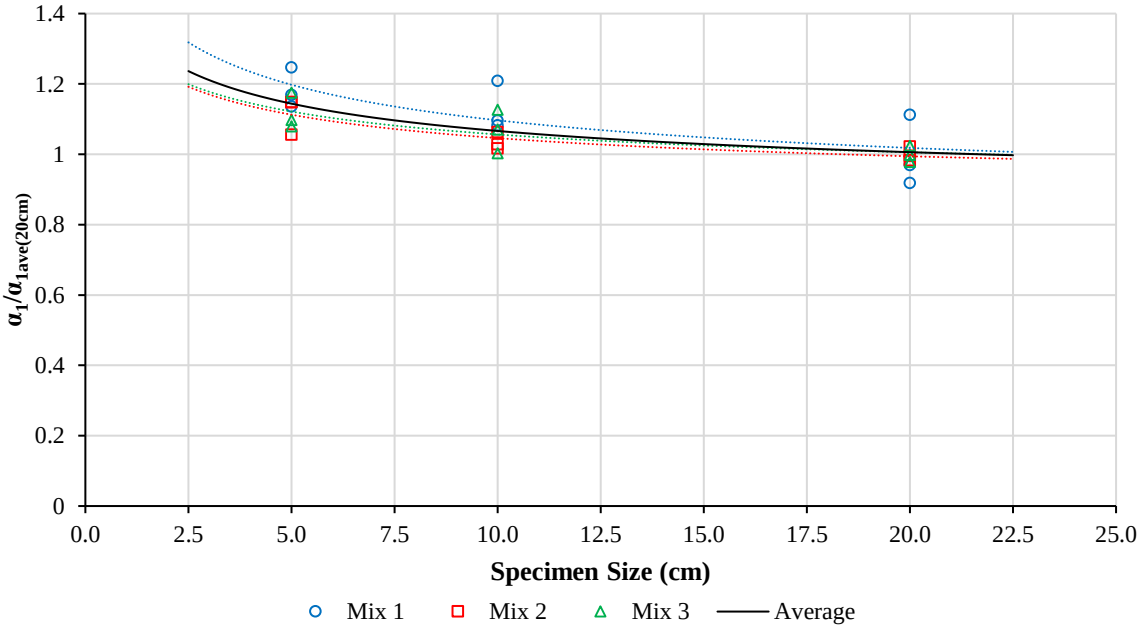

Figure 4.41 Effect of Specimen Size on $\alpha_1/\alpha_{1ave(20cm)}$

© University of Pretoria

Table 4.14 MSEL Coefficients for $\alpha_1/\alpha_{1ave(20cm)}$

	Mix 1	Mix 2	Mix 3	Average
β	1.07	0.63	0.61	0.77
$\lambda_0 d_a$	0.95	0.95	0.95	0.95
α	0.79	0.86	0.88	0.84

$$\alpha_1 = \frac{0.77\alpha_{1(20cm)}}{\sqrt{1+\frac{c}{0.95}}} + 0.84\alpha_{1(20cm)} \qquad \textbf{4.9}$$

Where:

α_1= The α_1 for a specific specimen size

$\alpha_{1(20cm)}$= The α_1 of a 200 x 200 x 1000 mm specimen

c= The specimen dimension (cm)

Figure 4.42 shows that the value of α_1 varies between 0.90 and 1.1 with an average of 0.99, and the 100 mm specimens values varies between 0.96 and 1.13 with an average of 1.02 times the average α_1 value of the 200 mm specimens. Thus, Figure 4.42 again confirms that the size effect for α_1 may be eliminated if the 150 mm cylinder strength is used to calculate α_1 for the 200 mm specimen, and the associated cylinder strength used to calculate α_1 for the 50 mm and 100 mm specimens.

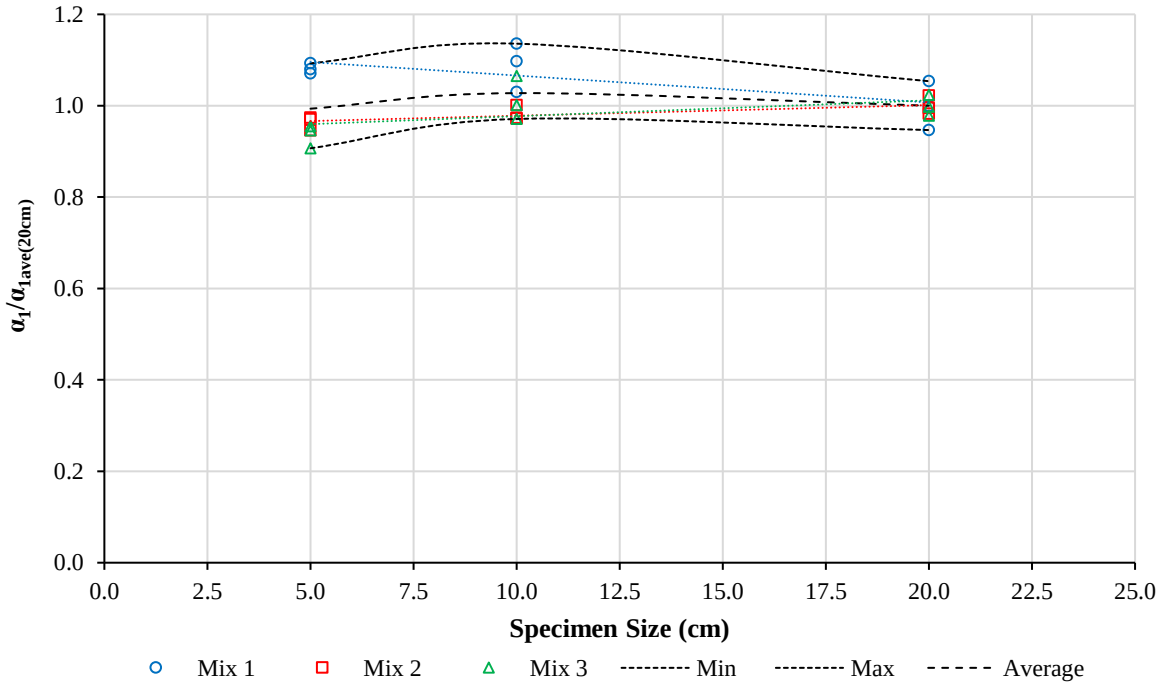

Figure 4.42 Elimination of Size Effect for $\alpha_1/\alpha_{1ave(20cm)}$

4.4.4 SIZE EFFECT FOR ε_{CU}

The ultimate compressive strain in flexural compression is a stress block parameter associated with a great deal of variability. Yi et al. (2006) showed that the ultimate compressive strain in flexural compression tends to increase with a reduction in specimen size. This conclusion, although not as extreme as suggested by Yi et al. (2006), can also be made when considering Figure 4.43 and Table 4.15. The average coefficients were used to provide the influence of specimen size on the ultimate compressive strain (Equation 4.10).

© University of Pretoria

Table 4.15 MSEL Coefficients for $\varepsilon_{cu}/\varepsilon_{cuave(20cm)}$

	Mix 1	Mix 2	Mix 3	Average
β	0.30	0.31	0.41	0.34
$\lambda_0 d_a$	0.95	0.95	0.95	0.95
α	0.94	0.94	0.89	0.92

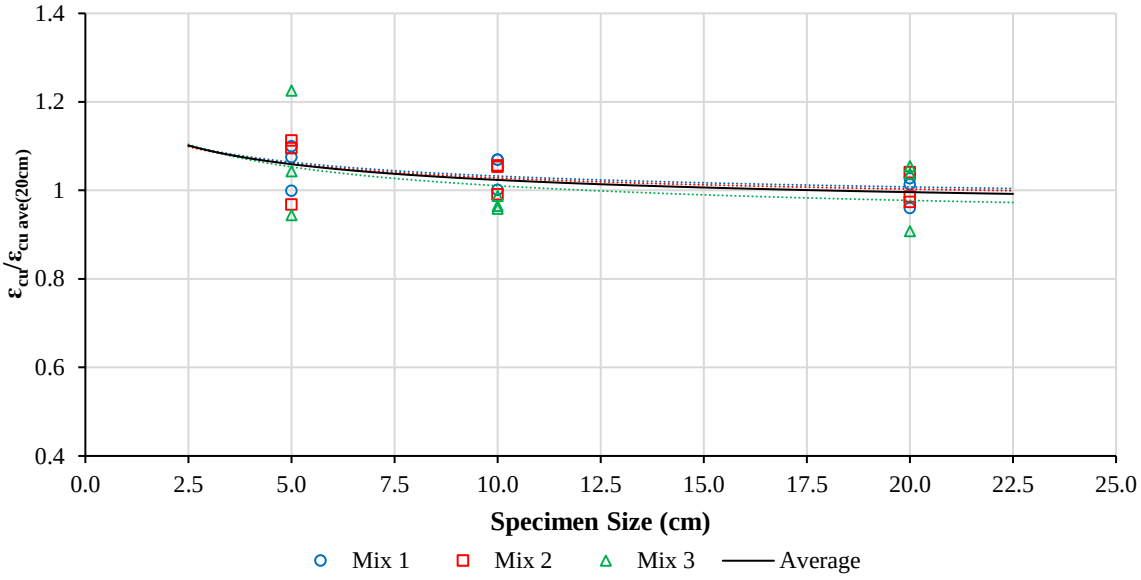

Figure 4.43 Effect of Specimen Size on $\varepsilon_{cu}/\varepsilon_{cuave(20cm)}$

$$\varepsilon_{cu} = \frac{0.34\varepsilon_{cu(20cm)}}{\sqrt{1+\frac{c}{0.95}}} + 0.92\varepsilon_{cu(20cm)} \qquad \textbf{4.10}$$

Where:

ε_{cu}= The ultimate compressive strain for a specific specimen size

$\varepsilon_{cu(20cm)}$= The ultimate compressive strain of a 200 x 200 x 1000 mm specimen

c= The specimen dimension (cm)

The ultimate compressive strain size effect is the only size effect that cannot be eliminated using the associated cylinder strength. It can therefore be concluded that smaller specimens not only possess higher strengths, but produces an increase in the rotational capacity of the flexural compression member. Theoretically, this should result in a reduction in steel percentage for a given moment, and an increase in neutral axis depth at failure.

4.5 ADEQUACY OF DESIGN CODES

In this section the BS 8110-1 (1997), SANS 0100-1 (2000), ACI-318 (2014), and EN 1992-1-1 (2004) design codes will be compared both from a global perspective, and with respect to their ability to predict the flexural behaviour of concrete containing South African materials. The accuracy of any design model can be assessed by evaluating the error, expressed as the percentage difference between the experimental and calculated values, divided by the experimental value. The basis for this calculation is a Moment-Axial force (M-N) interaction diagram, which has been normalised with respect to the section dimensions and the compressive strength. For reinforced concrete, this normalised M-N interaction diagram represents the contribution of the concrete to the load and moment carrying capacity. Each of the experimental points obtained by previous researchers and in this

© University of Pretoria

investigation can be presented by a coordinate pair (m_t, n_t) on the interaction diagram. The position of each point is calculated using Equation 4.11 and Equation 4.12 (obtained from the equilibrium of forces and moments), and represents the maximum capacity of the concrete section in flexural compression. The normalised M-N interaction diagram for the experimental results is shown in Figure 4.44. Note that each point on this plot can also be defined by a radian coordinate system consisting of a radial distance (R_t) and an angle (θ). The value of R_t and θ can be calculated using Equation 4.13 and Equation 4.14.

$$n_t = \frac{C}{bcf_c'} = \zeta_t k_1 k_{3_t} \quad \textbf{4.11}$$

$$m_t = \frac{M}{bc^2 f_c'} = \zeta_t k_1 k_{3_t}(0.5\text{-}\zeta_t k_{2_t}) \quad \textbf{4.12}$$

$$R_t = \sqrt{n_t^2 + m_t^2} \quad \textbf{4.13}$$

$$\tan\theta_t = \frac{1}{0.5\text{-}\zeta_t k_{2_t}} \quad \textbf{4.14}$$

Where:

n_t= Normalised axial load for the test point

m_t= Normalised moment for the test point

ζ_t= The relative position of the neutral axis depth during the test, which in this case ζ_t=1

$k_1k_{3_t}$= The k_1k_3 stress block parameter obtained from research

k_{2_t}= The k_2 stress block parameter obtained from research

R_t= The radial distance from the origin to the test point

θ_t= Angle between the normalised moment axis and the line connecting the origin and test point

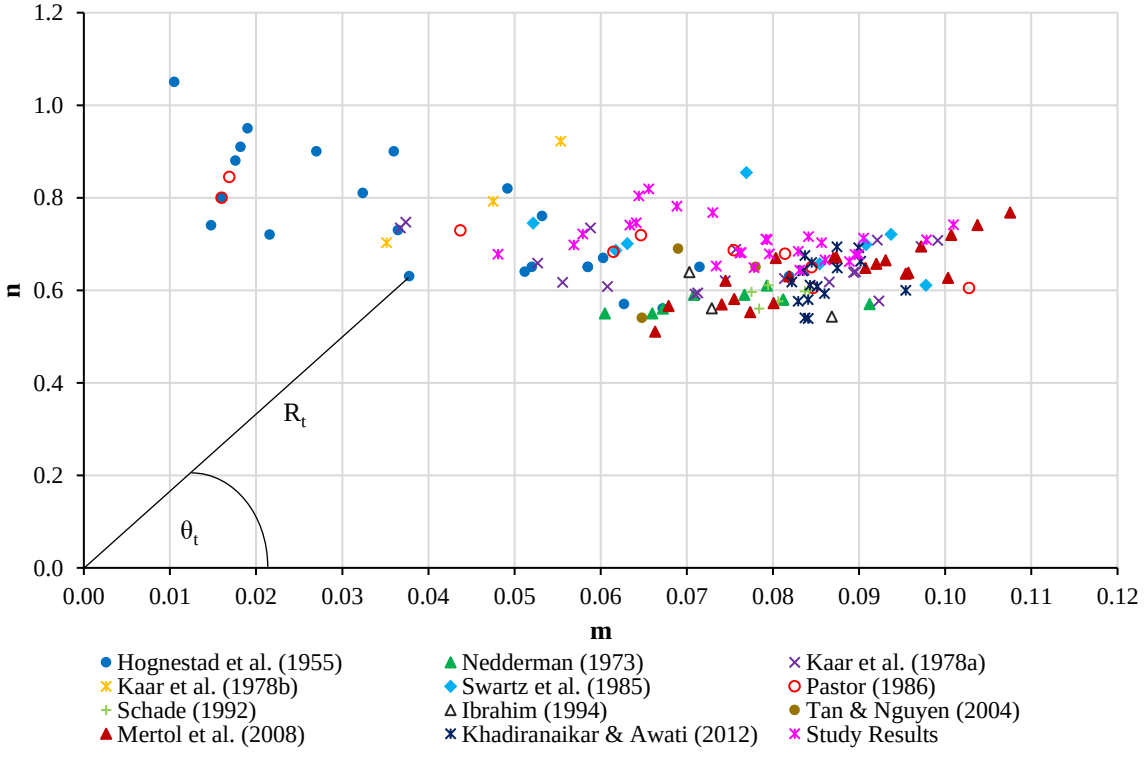

Figure 4.44 Normalised M-N Interaction Diagram Obtained from Experimental Results

© University of Pretoria

The link between design recommendations and experimental results can be obtained by generating normalised M-N interaction diagrams using the recommended design values of the stress block parameters. Equation 4.15 and Equation 4.16, enable the normalised M-N interaction diagram to be generated by using the design values of $k_1k_{3_d}$ and k_{2_d} obtained from the BS 8110-1 (1997), SANS 0100-1 (2000), ACI-318 (2014), and EN 1992-1-1 (2004) codes.

$$n_d = \frac{C}{bcf_c'} = \zeta_d k_1 k_{3_d} \quad \textbf{4.15}$$

$$m_d = \frac{M}{bc^2 f_c'} = \zeta_d k_1 k_{3_d}(0.5\text{-}\zeta_d k_{2_d}) \quad \textbf{4.16}$$

$$R_d = \sqrt{{n_d}^2 + {m_d}^2} \quad \textbf{4.17}$$

$$\tan\theta_d = \frac{1}{0.5\text{-}\zeta_d k_{2_d}} = \frac{1}{0.5\text{-}\zeta_t k_{2_t}} \rightarrow \zeta_d = \frac{\zeta_t k_{2_t}}{k_{2_d}} = \frac{1 \times k_{2_t}}{k_{2_d}} \quad \textbf{4.18}$$

Where:

n_d= Normalised axial load obtained for design recommendations

m_d= Normalised moment obtained for design recommendations

ζ_d= The relative position of the neutral axis depth

$k_1k_{3_d}$= The k_1k_3 stress block parameter obtained from design recommendations

k_{2_d}= The k_2 stress block parameter obtained from design recommendations

R_d= The radial distance from the origin to the point generated using design recommendations

θ_d= Angle between the normalised moment axis and the line connecting the origin and generated point

Equation 4.18 provides the link between the normalised M-N interaction diagram generated for the test points, and the M-N interaction diagrams generated by using the design models. This equation states that the angle between the normalised moment axis and the line connecting the origin to the test point, needs to be the same as the angle between the normalised moment axis and the line connecting the origin to the point generated using the design model. As $\zeta_t = 1$, the value of ζ_d (to be used in Equation 4.15 and Equation 4.16) can be obtained from Equation 4.18, and the normalised M-N interaction diagram using the design recommended values (for the particular concrete strength) generated. As the experimental and recommended design values lie on the same line, the error (δ) between the design and experimental value can be expressed as a percentage of the experimental value by using Equation 4.19. This error gives an indication of the accuracy of the proposed model. Thus, if δ is larger than one, the design recommendations under predict the strength and vice versa. Equation 4.19 was used to generate the δ values for the BS 8110-1 (1997), SANS 0100-1 (2000), ACI-318 (2014), and EN 1992-1-1 (2004) codes. The result of these analysis are shown in Figure 4.45, Figure 4.46, Figure 4.47, and a histogram in Figure 4.48.

$$\delta = \frac{R_t\text{-}R_d}{R_t} \times 100 \quad \textbf{4.19}$$

Where:

δ= Is the percentage difference between experimental and design value expressed as a percentage of the experimental value

© University of Pretoria

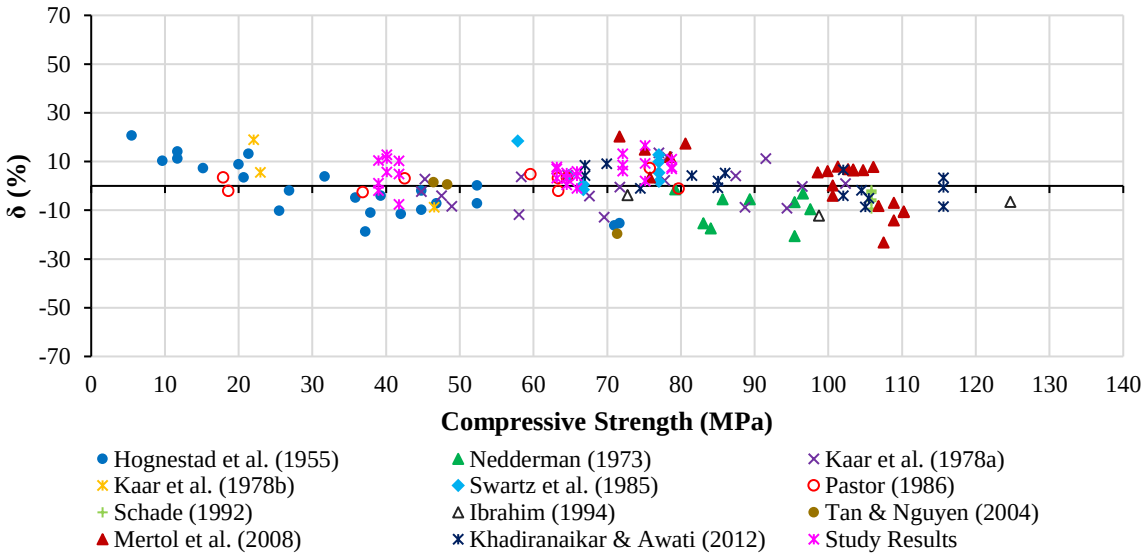

Figure 4.45 Percentage Error: BS 8110-1 (1997) & SANS 0100-1 (2000) and Experimental Results

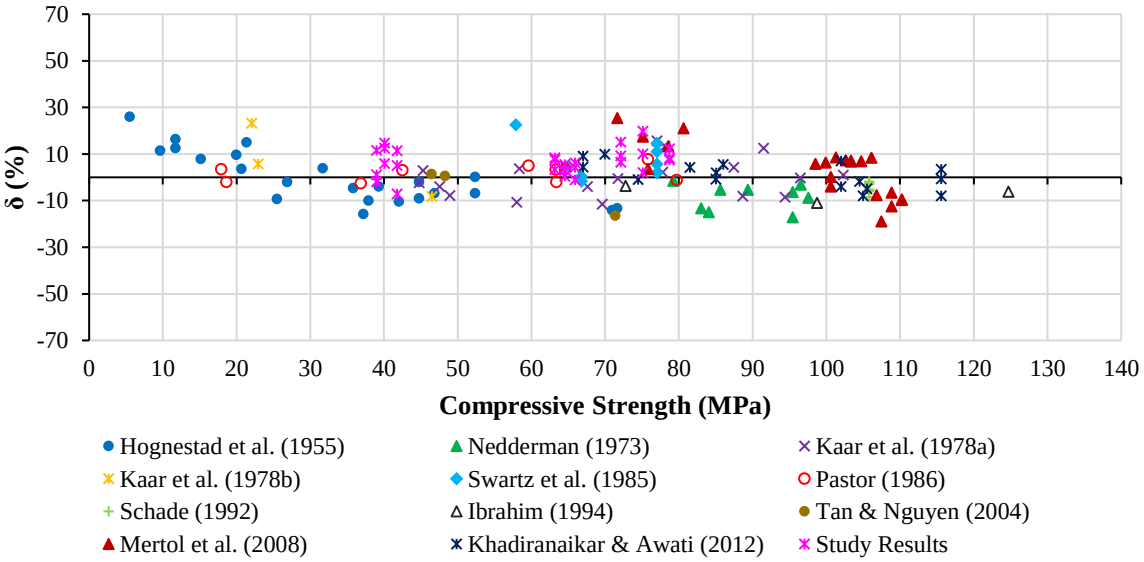

Figure 4.46 Percentage Error: ACI-318 (2014) and Experimental Results

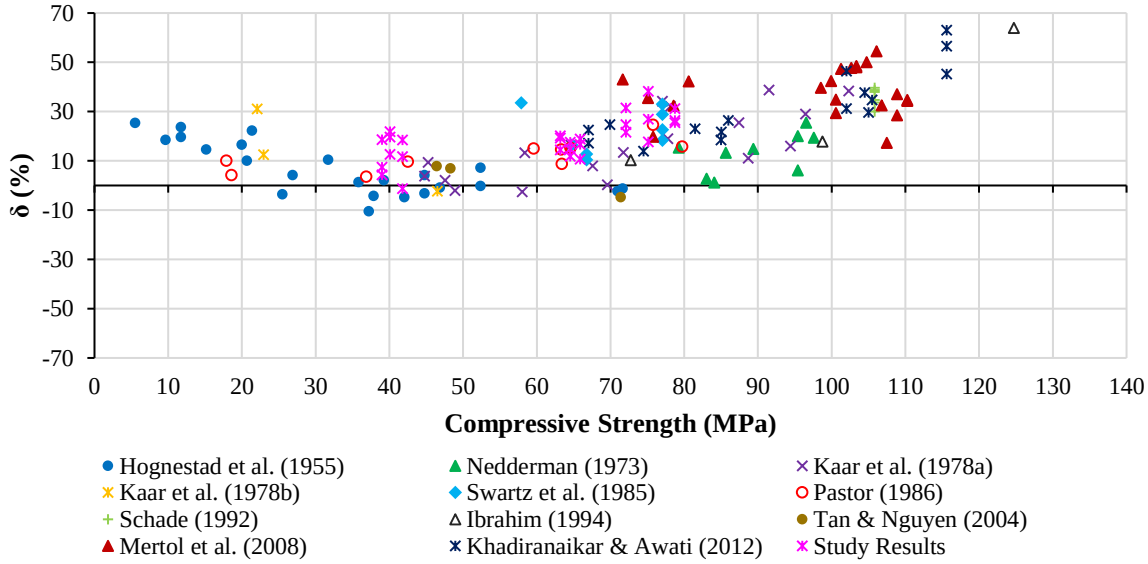

Figure 4.47 Percentage Error: EN 1992-1-1 (2004) and Experimental Results

© University of Pretoria

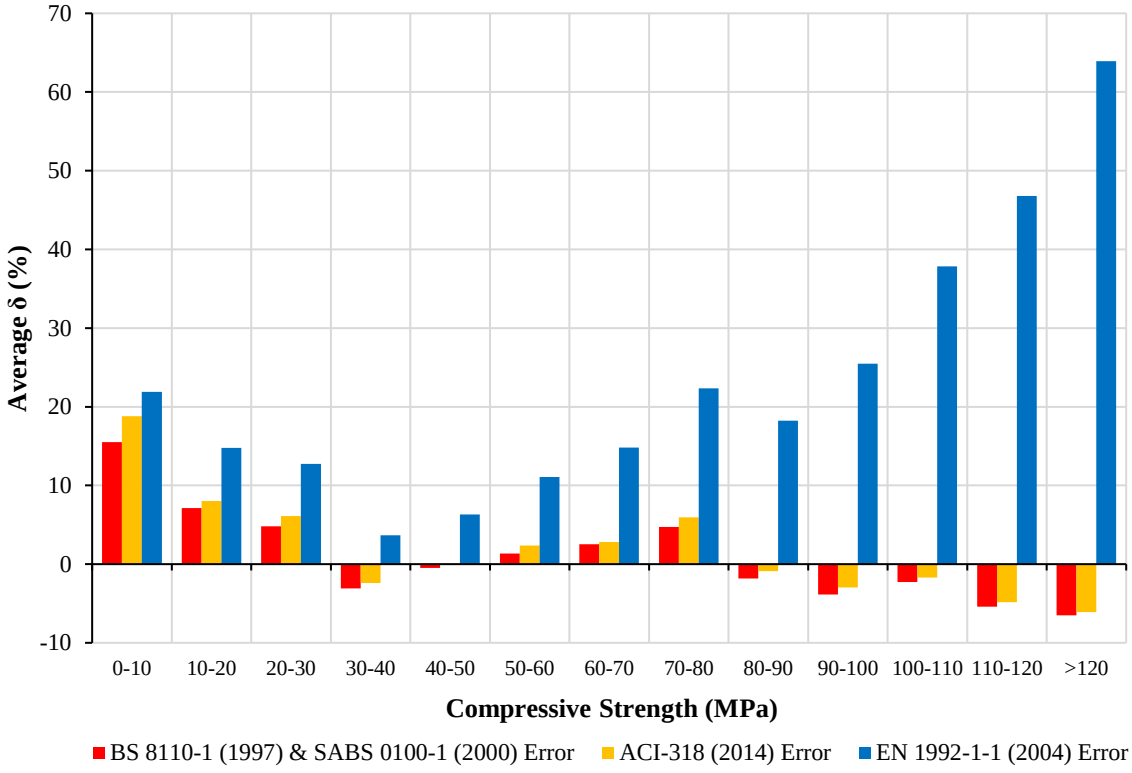

Figure 4.48 Average Percentage Error versus Compressive Strength

Figure 4.45 and Figure 4.48 shows that the BS 8110-1 (1997) and SANS 0100-1 (2000) codes do not provide a constant error, and the prediction becomes less conservative with an increase in compressive strength. On average the BS 8110-1 (1997) and SANS 0100-1 (2000) codes underestimate by 0.8%. For cylinder strengths in excess of 80 MPa, the BS 8110-1 (1997) and SANS 0100-1 (2000) codes overestimates by as much as 6.5%, while for cylinder strengths less than 80 MPa the codes *underestimates* by as much as 15.5%, and *overestimates* by up to 3.3%. In total 48.6% of results were smaller than the code prediction. On average the BS 8110-1 (1997) and SANS 0100-1 (2000) codes underestimates the study results by 5.2%, 4.0%, and 9.0% for Mix 1, Mix 2, and Mix 3 respectively. The study values varied between -7.6% and 16.5%, with 14.8% of study values less than the code prediction.

Figure 4.46 and Figure 4.48 shows that the ACI-318 (2014) code does not provide a constant error, becoming less conservative with an increase in compressive strength. On average, the ACI-318 (2014) code underestimates the experimental values by 1.8%. For cylinder strengths in excess of 80 MPa, the ACI-318 (2014) code overestimates by as much as 6.1%, while for cylinder strengths less than 80 MPa, the code *underestimates* the data by as much as 18.8%, and *overestimates* by up to 2.2%. In total 48.6% of values are smaller than the code prediction. On average, the ACI-318 (2014) code underestimates the study results by 6.0%, 4.3%, and 10.1% for Mix 1, Mix 2, and Mix 3 respectively. The study values vary between -7.0% and 19.9%, with 14.8% of the study values less than the code prediction.

Figure 4.47 and Figure 4.48 shows that the EN 1992-1-1 (2004) code provides a relatively constant error for strengths less than the design limit of 90 MPa, on average underestimating by 18.6%. In total 10.1% of values are smaller than the code prediction. Compared to the study results, the EN 1992-1-1 (2004) code on average underestimates by 12.6%, 16.0%, and 27.1% for Mix 1, Mix 2, and Mix 3 respectively. The study values vary

© University of Pretoria

between -1.2% and 38.2%, with 3.7% of the study values less than the code prediction. If the same values for α_1 and β_1 assumed for f_c'=90 MPa, i.e. α_1=0.70 and β_1=0.8, are assumed for strengths in excess of 90 MPa, the EN 1992-1-1 (2004) code calculations result in an ever increasing error, underestimating by as much as 63.5%.

The BS 8110-1 (1997), SANS 0100-1 (2000), and ACI-318 (2014) codes tends to be less conservative than the EN 1992-1-1 (2004) code for all concrete grades, particularly for concrete with strengths in excess of 80 MPa. As all three design codes are calibrated to provide a suitable factor of safety against collapse, and the study results were mostly underestimated, it can be concluded that the BS 8110-1 (1997), SANS 0100-1 (2000), and ACI-318 (2014) codes can be used for the safe design of flexural members and flexural compression members up to 80 MPa, while EN 1992-1-1 (2004) is suitable for the design of members up to 90 MPa. Furthermore, the EN 1992-1-1 (2004) code can be used for the design of flexural members with strengths in excess of 90 MPa, however, this would require a significant amount of steel in the compression zone of the member, likely resulting in an uneconomical design.

4.6 STRESS-STRAIN BEHAVIOUR

4.6.1 UNIAXIAL COMPRESSION VERSUS FLEXURAL COMPRESSION STRESS-STRAIN CURVES

Figure 4.49 and Figure 4.50 show a comparison between the 100 mm cylinders and 100 mm flexural compression specimens, and the 150 mm cylinders and 200 mm flexural compression specimens stress-strain curves. These figures show that there is a remarkable similarity between the stress-strain behaviours, the only difference being the increased ultimate compressive strain achieved in flexural compression. As flexural compression tests are difficult, expensive, and time consuming to perform, and the stress-strain curves are so similar, it can be concluded that the uniaxial stress-strain curves provides a more than adequate representation of the ascending branch of the flexural compression stress-strain curves.

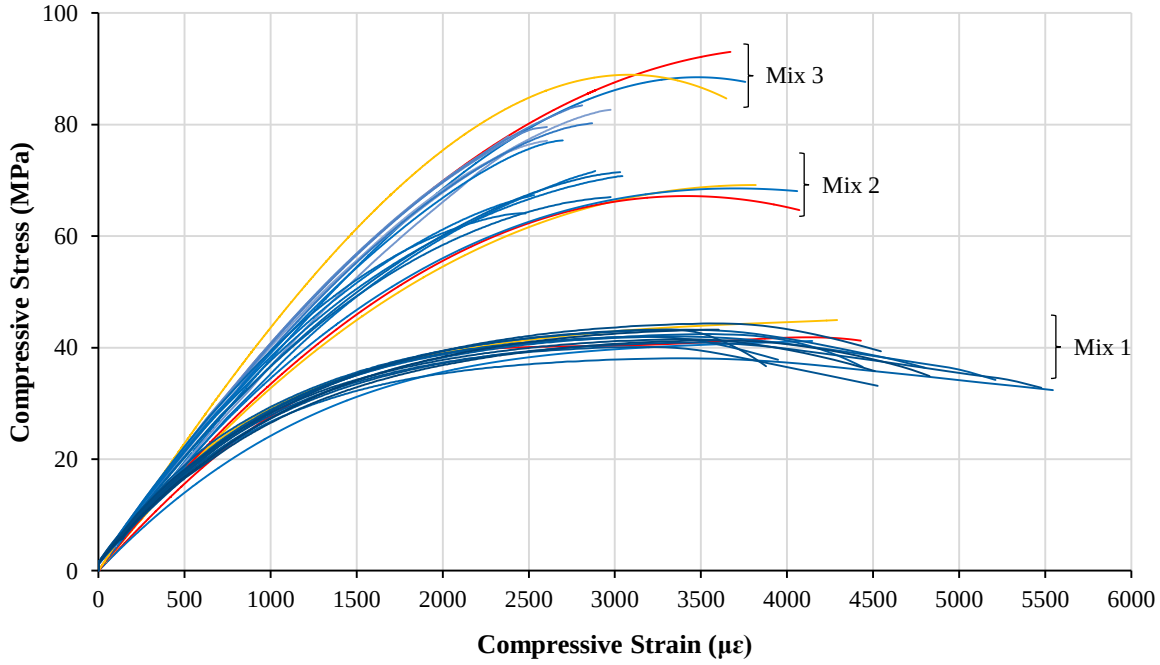

Figure 4.49 100 mm Cylinder and 100 mm Flexural Compression Specimen Stress-Strain Curves

© University of Pretoria

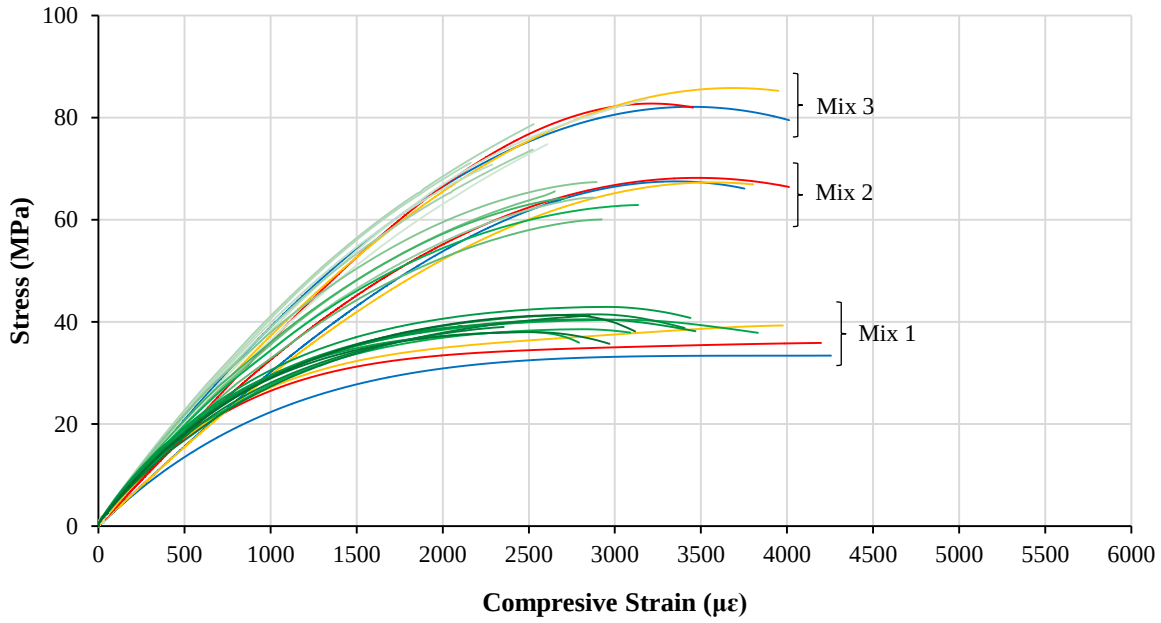

Figure 4.50 150 mm Cylinder and 200 mm Flexural Compression Specimen Stress-Strain Curves

4.6.2 PROPOSED FLEXURAL COMPRESSION STRESS-STRAIN RELATIONSHIP

Even though the uniaxial stress-strain curve can be used to represent the ascending portion of the flexural stress-strain curve, an attempt was made to describe the complete flexural stress-strain curve (ascending and descending portion) using a known stress-strain model. Some of the stress-strain models presented in Chapter 2 consisted of complicated equations and coefficients making them unattractive to most engineers. Thus, only the simplest relationships were used to describe the stress-strain behaviour, and a single stress-strain relationship selected. The relationship proposed by Carreira & Chu (1985) was found to be the most suitable. This relationship, shown in Equation 4.20, is based on a factor of β_2 (Equation 4.21), which is dependent on the strain at the maximum flexural compressive stress, the instantaneous elastic modulus, and the maximum flexural compressive stress.

$$f_c = f_c'' \times \left[\frac{\beta_2(\varepsilon_c/\varepsilon_{c0})}{\beta_2\text{-}1 + (\varepsilon_c/\varepsilon_{c0})^{\beta_2}}\right] \quad \textbf{4.20}$$

With:

$$\beta_2 = 1/(1\text{-}f_c''/(\varepsilon_{c0}E_i)) \quad \textbf{4.21}$$

Where:

f_c= The flexural stress at a given strain ratio

f_c''= The maximum stress in flexural compression

β_2= Is a material parameter that depends on the shape of the stress-strain diagram

$\varepsilon_c/\varepsilon_{c0}$= The ratio between strain at a given instance and the strain at the peak stress

E_i= Is the tangential modulus of elasticity, or the slope of a tangent line to the curve at the origin

Equation 4.20 can be used to predict the stress-strain relationship in flexural compression if estimates are made of all parameters. A global estimate of the initial tangential modulus was made by assuming a power relationship between the maximum flexural compressive stress and the stiffness (shown in Figure 4.51). By assuming a linear

© University of Pretoria

relationship between both ε_{c0} and ε_{cu}, and the maximum flexural compressive stress, separate estimates of these parameters were made for 50 mm, 100 mm, and 200 mm specimens. The separation of these estimates were based on the difference between the achievable ultimate compressive strains of the three specimen sizes. The numerical estimates of the linear trend line coefficients are shown in Table 4.16, with plots of these estimates shown in Figure 4.52 and Figure 4.53.

Table 4.16 Linear Trend Line Coefficients (y=ax+b) for ε_{c0} and ε_{cu}

	50 mm		100 mm		200 mm	
	a	**b**	**a**	**b**	**a**	**b**
ε_{c0} (με)	-5.67	4216	-16.77	4888	-15.86	4680
ε_{cu}(με)	-6.41	4633	-13.44	4905	-7.68	4416.4

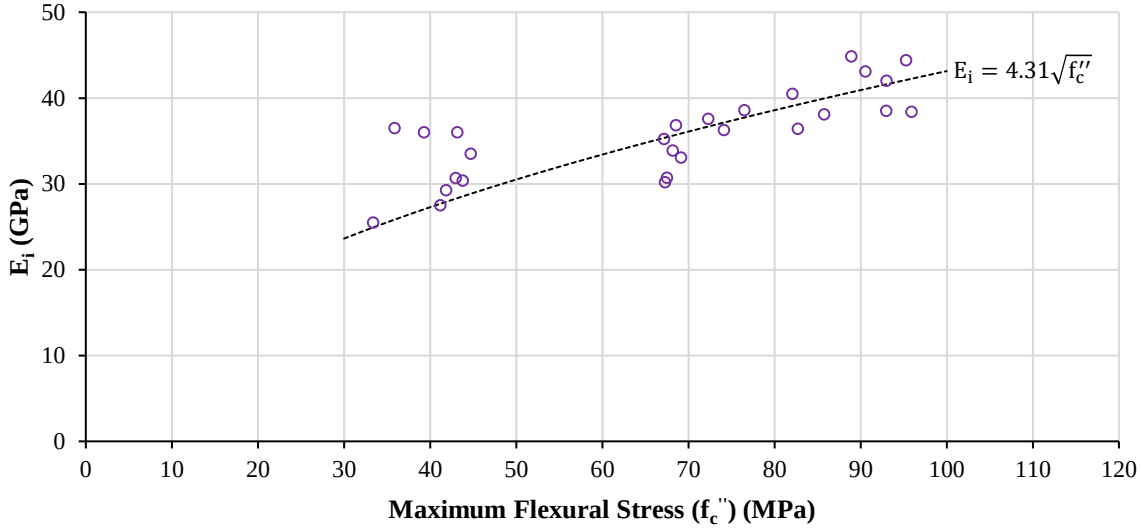

Figure 4.51 Instantaneous Elastic Modulus Estimate

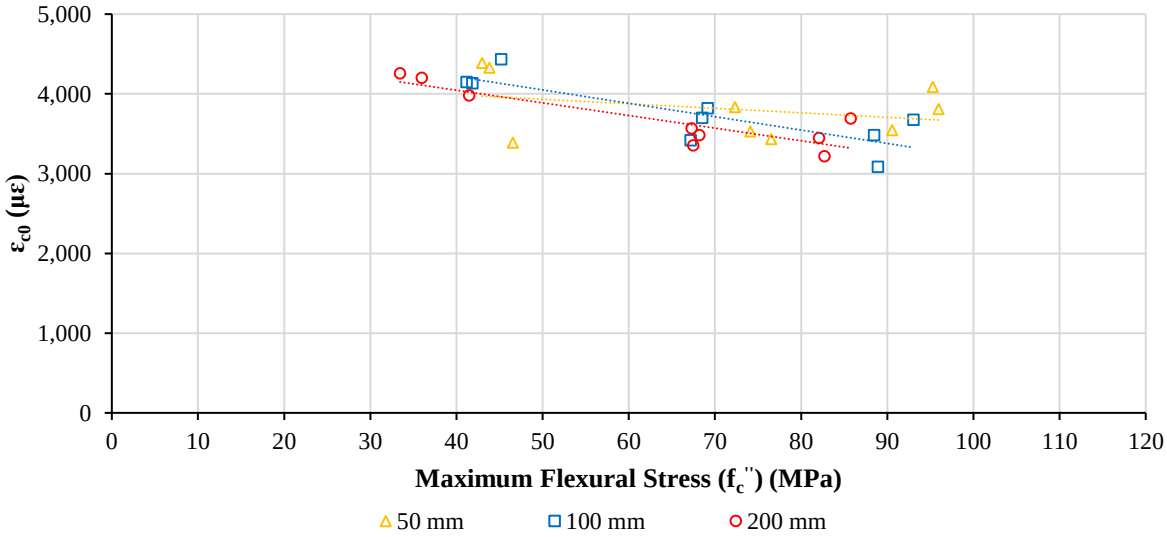

Figure 4.52 Strain Associated with Peak Stress (ε_0) Estimate

Comparison plots between the actual stress-strain relationships and the stress-strain relationships obtained using the model proposed by Carreira & Chu (1985), are shown in Figure 4.54 to Figure 4.56. As the shape of the proposed stress-strain relationships and the actual stress-strain relationships will inevitably differ, the stress block parameters k_1 and k_2, which are directly linked to the shape of the stress-strain relationship, will be affected. The ratio between the actual and calculated values of k_1 and k_2 are shown in Figure 4.57 and Figure 4.58 respectively.

© University of Pretoria

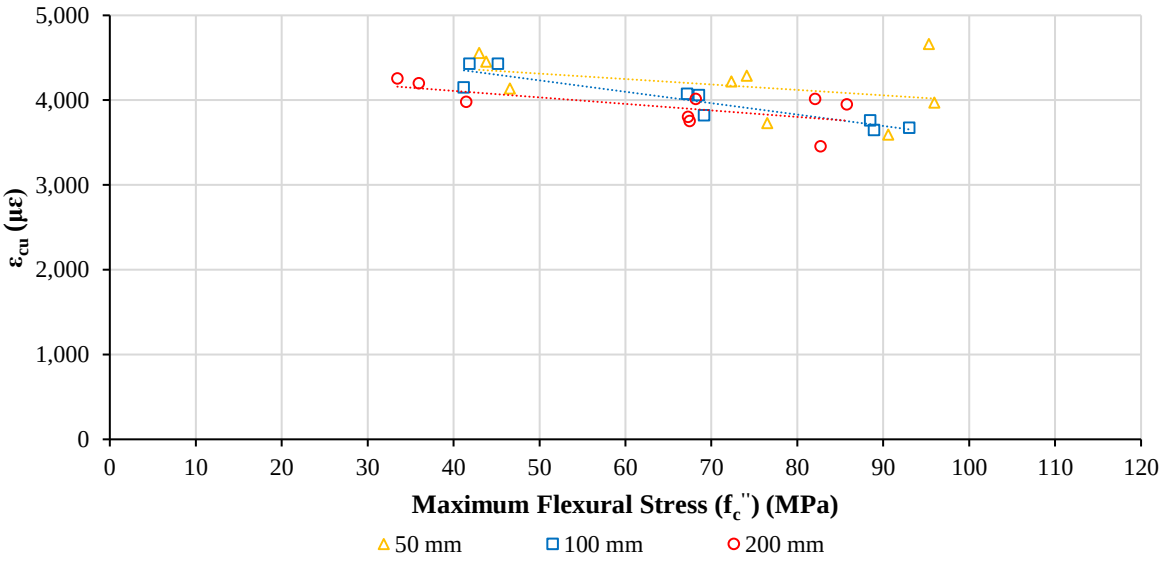

Figure 4.53 Ultimate Compressive Strain Estimate

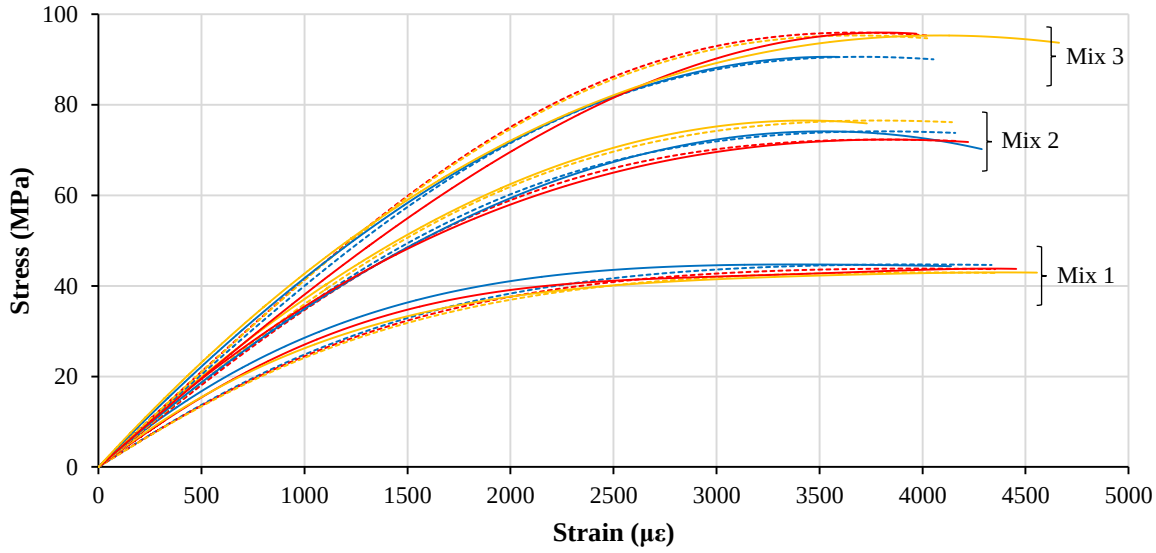

Figure 4.54 Actual and Carreira & Chu (1985) (Dotted Line) Model for 50 mm Specimens

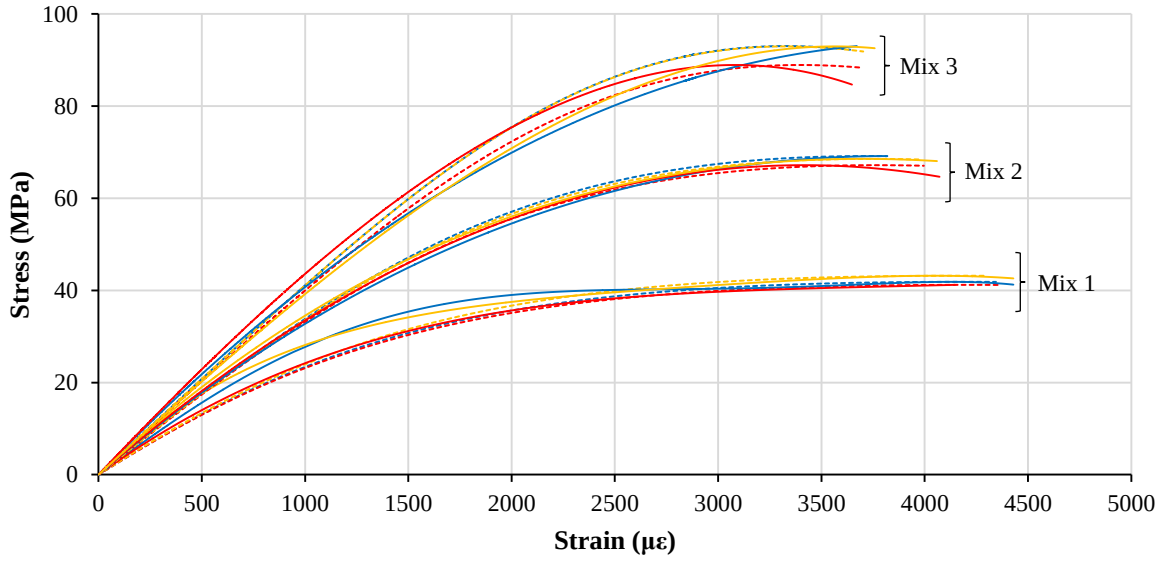

Figure 4.55 Actual and Carreira & Chu (1985) (Dotted Line) Model for 100 mm Specimens

© University of Pretoria

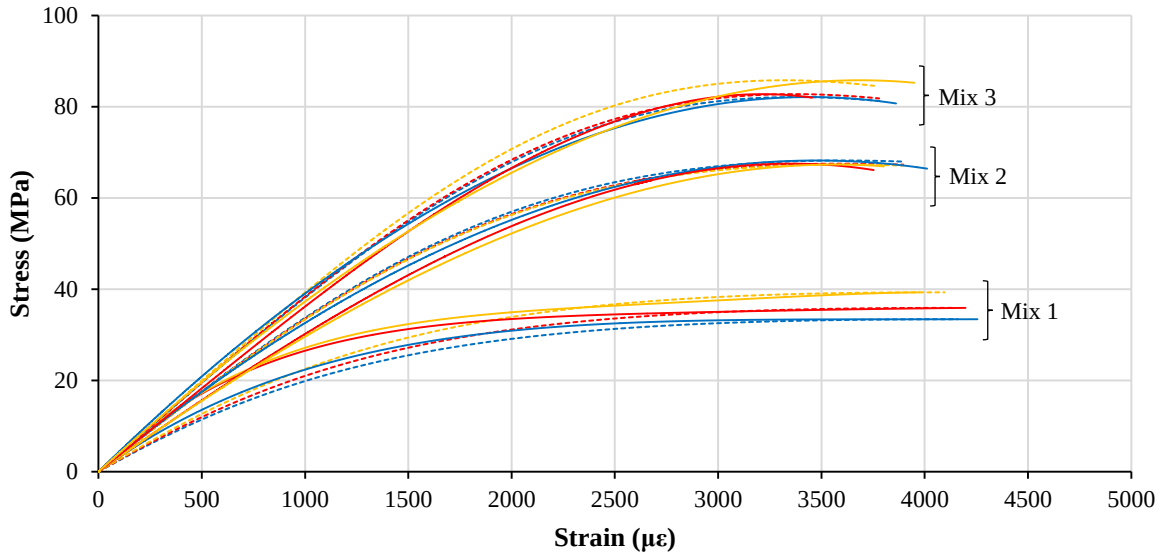

Figure 4.56 Actual and Carreira & Chu (1985) (Dotted Line) Model for 200 mm Specimens

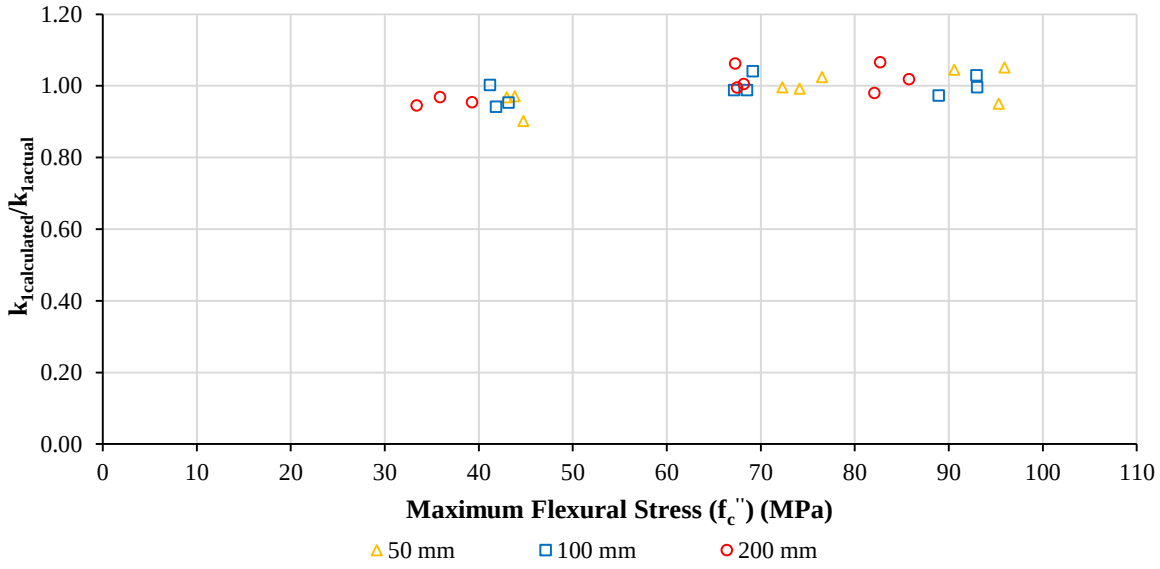

Figure 4.57 Ratio between Calculated and Actual values of k_1

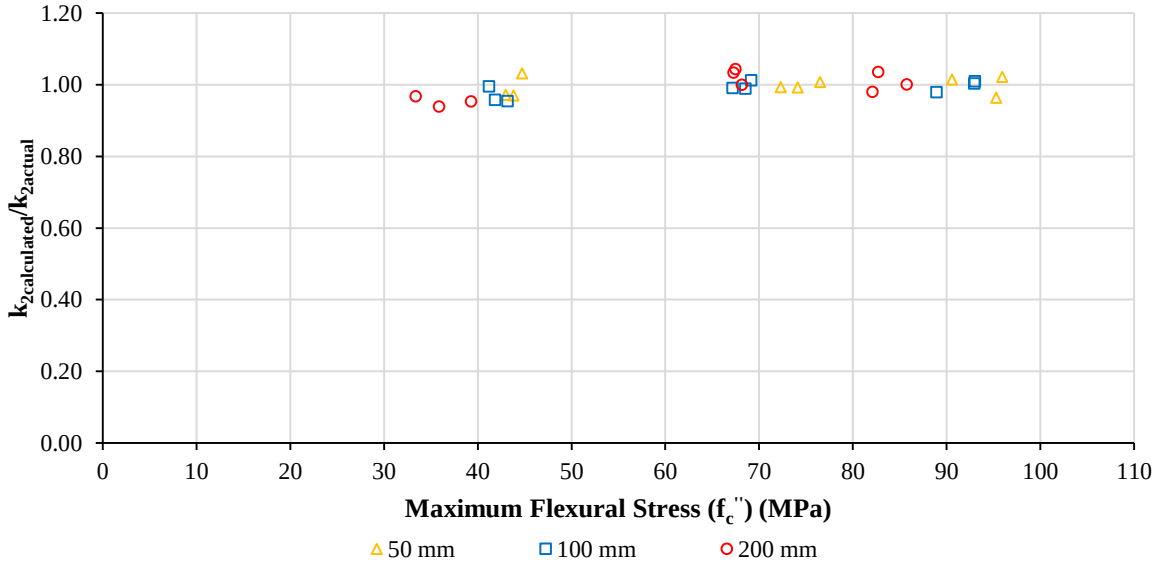

Figure 4.58 Ratio between Calculated and Actual values of k_2

© University of Pretoria

Figure 4.57 and Figure 4.58 show that the ratio between the calculated and actual values of k_1 and k_2 hovers about the value of 1, with the calculated k_1 values varying between 0.94 and 1.04 times the actual k_1 values, and the calculated k_2 values varying between 0.91 and 1.06 times the actual k_2 values. On average the proposed relationship provides an excellent description of k_1 and k_2 and can be used to obtain the stress block parameters.

4.7 CONCLUSIONS AND IMPLICATIONS FOR DESIGN

During the course of the study cubes and cylinders (subjected to uniaxial compression), and flexural compression members were tested. On the basis of 150 mm cylinder strength, k_1, k_2, and β_1 were all found independent of the specimen size, while four different equations were used to define the specimen size effect for k_3, k_1k_3, α_1, and ε_{cu}. Where applicable, i.e. for k_3, k_1k_3, and α_1, the size effect in flexural compression could be eliminated by using the associated cylinder strength for the 50 mm and 100 mm flexural compression specimens. With this in mind, it can be concluded that if the neutral axis depth of a flexural or flexural compression member were to be less than 203 mm, the increased capacity (obtained from α_1) could range between 6% and 24%, with an average of 14% for 50 mm deep neutral axis, and 0% to 21% with an average of 8%, for a 100 mm deep neutral axis. Alternatively, as the size effect in the 50 mm and 100 mm flexural compression specimens can be eliminated by using the associated cylinder strength, the same stress block parameter models, proposed for the conventional sized specimens, can be used for the design of a flexural or flexural compression member. If this is the case, the increased specimen capacity associated with the reduced neutral axis depth can be taken into consideration by using the size effect in cylinders.

With more testing on 50 mm and 100 mm specimens, relationships between the cylinder-strength-calculated stress block parameters (k_3, k_1k_3, and α_1) and the conventional 150 mm cylinder strength can be established, possibly leading to more cost efficient designs. On the other hand, if the 50 mm and 100 mm flexural compression specimens are used in conjunction with the associated cylinder strength, a much easier and more cost effective investigation into the conventional stress block parameters can be made. The reduction in specimen size has the benefit of not only improving the handleability, but also paves a way for further investigations into the flexural compression behaviour of ultra-high strength concrete, a study field previously limited due to compression testing machine capacity limitations.

After comparing the percentage error obtained from the BS 8110-1 (1997), SANS 0100-1 (2000), ACI-318 (2014), and EN 1992-1-1 (2004) codes, it can be concluded that the stress block parameters obtained for concrete containing South African materials (particularly Dolomitic aggregate), lies within the range of values obtained by other researchers and are mostly underestimated. Furthermore, it can be concluded that the BS 8110-1 (1997), SANS 0100-1 (2000), and ACI-318 (2014) codes, are safe for the design of concrete with strengths up to 80 MPa, while the EN 1992-1-1 (2004) code can safely be employed for strengths in excess of 90 MPa.

The fact that the uniaxial strain curve correctly describes the ascending portion of the flexural stress-strain curve, can result in a significant simplification of the procedure used to obtain the stress block parameters. The flexural stress-strain curve can be accurately modelled using the relationships for ε_{c0}, ε_{cu}, and E_i in conjunction with the model proposed by Carreira & Chu (1985), providing an excellent description of both the stress-strain behaviour in flexural compression and the stress block parameters.

© University of Pretoria

CHAPTER 5

CONCLUSIONS AND RECOMMENDATIONS

5.1 INTRODUCTION

This chapter summarises the conclusions reached during the course of this investigation, in which the flexural stress-strain behaviour of concrete containing Dolomitic aggregate was considered. The test setup was based on a modification of the method originally proposed by Hognestad et al. (1955), which simulated the compression zone of a flexural member. The main test variables were water/cement ratio (compressive strength) and specimen size, with nine 50 x 50 x 300 mm, nine 100 x 100 x 500 mm, and nine 200 x 200 x 1000 mm flexural compression specimens being tested. Additionally, the size effect of both cubes and cylinders were investigated, and compared to that observed by previous researchers.

A comparison of the error between the predicted Moment-Axial force (M-N) interaction diagram obtained by using BS 8110-1 (1997), SANS 0100-1 (2000), ACI-318 (2014), and EN 1992-1-1 (2004), and the actual M-N interaction diagram obtained from the experimental points, were made, and conclusions regarding their applicability for the design of concrete containing South African materials drawn. Lastly, the flexural stress-strain behaviour was modelled, and a comparison made between the calculated and actual stress block parameters by using estimates of ε_{c0}, ε_{cu}, and E_i, in conjunction with the stress-strain model proposed by Carreira & Chu (1985).

5.2 CONCLUSIONS

Observations and conclusions were based on both the analysis of the results obtained during the course of this study and results obtained by other researchers.

5.2.1 CUBE AND CYLINDER DATA

The following conclusions regarding the compressive behaviour of cubes and cylinders were drawn:

- The ratio between the cylinder and cube compressive strength for Dolomitic concrete does not conform to the value of 0.8 (assumed in most design codes) but lies in the region of 0.93.
- The coefficients of the MSEL equation for cubes and cylinders are shown in Table 5.1 and Table 5.2, and confirms that the compressive strength of concrete does influence the specimen size effect, with the β value increasing as the compressive strength increases. A comparison between the average and the

© University of Pretoria

results obtained by Yi et al. (2006) (Table 5.3), showed that the specimen size effect cannot be described with a single equation.

Table 5.1 Size Effect Coefficients for Cubes

	Mix 1	Mix 2	Mix 3	Average
β	1.17	1.41	1.41	1.33
$\lambda_0 d_a$	0.95	0.95	0.95	0.95
α	0.72	0.71	0.71	0.72

Table 5.2 Effect Coefficients for Cylinders

	Mix 1	Mix 2	Mix 3	Average
β	0.81	1.21	1.42	1.15
$\lambda_0 d_a$	0.95	0.95	0.95	0.95
α	0.78	0.70	0.62	0.70

Table 5.3 Regression Coefficients of Study Results and Results of Yi et al. (2006)

	Cubes			Cylinders		
	Average	Yi et al. (2006)	Yi et al. (2006) Modified	Average	Yi et al. (2006)	Yi et al. (2006) Modified
β	1.33	1.17	1.28	1.15	0.49	0.55
$\lambda_0 d_a$	0.95	2.6	2.6	0.95	2.6	2.6
α	0.72	0.62	0.58	0.7	0.81	0.79

5.2.2 FLEXURAL COMPRESSION SPECIMEN DATA

The following conclusions regarding the flexural compressive behaviour of concrete were drawn:

- The assumption that plane sections remain plane during bending holds true for concrete containing Dolomitic aggregate, irrespective of the compressive strengths or specimen sizes considered in this study.
- With the addition of the new data, the global estimate of the Poisson ratio changed from 0.191 to 0.197, with the previously assumed value of 0.2 being even more applicable now than it previously was. Additionally the Poisson ratio of 150 mm cylinders tends to remain constant at 0.23, while the Poisson ratio of the flexural compression specimens, increases with an increase in compressive strength from Mix 1 to Mix 2, but remains relatively constant from Mix 2 to Mix 3. No explanation for this behaviour could be provided.
- The ultimate compressive strain tends to reduce with an increase in the compressive strength, tending to 3000 με for the 200 mm and 100 mm specimens, and no clear lower limit for the 50 mm specimens.
- Regardless of the specimen size, the shape of the ascending branch of the stress-strain curve changes with an increase in strength from parabolic-rectangular to a triangular form.
- The stress block parameters of k_1, k_2, and β_1 are independent of specimen size.
- The stress block parameter k_3, showed a clear specimen size effect for all three mixes. The coefficients of the MSEL equation, obtained from a LSM regression analysis of the data, are shown in Table 5.4, with the average relationship (considered to represent the specimen size effect) presented in Equation 5.1.

© University of Pretoria

Table 5.4 MSEL Coefficients for $k_3/k_{3ave(20cm)}$

	Mix 1	Mix 2	Mix 3	Average
β	1.11	0.49	0.65	0.75
$\lambda_0 d_a$	0.95	0.95	0.95	0.95
α	0.79	0.88	0.88	0.85

$$k_3 = \frac{0.75k_{3(20cm)}}{\sqrt{1+\frac{c}{0.95}}} + 0.85k_{3(20cm)} \qquad \textbf{5.1}$$

- The stress block parameter, k_1k_3, showed a clear specimen size effect for all three mixes. The coefficients of the MSEL equation, obtained from a LSM regression analysis of the data, are shown in Table 5.5, with the average relationship (considered to represent the specimen size effect) presented in Equation 5.2.

Table 5.5 MSEL Coefficients for $k_1k_3/k_1k_{3ave(20cm)}$

	Mix 1	Mix 2	Mix 3	Average
β	0.94	0.81	0.66	0.80
$\lambda_0 d_a$	0.95	0.95	0.95	0.95
α	0.82	0.83	0.87	0.84

$$k_1k_3 = \frac{0.8k_1k_{3(20cm)}}{\sqrt{1+\frac{c}{0.95}}} + 0.84k_1k_{3(20cm)} \qquad \textbf{5.2}$$

- The stress block parameter, α_1, showed a clear specimen size effect for all three mixes. The coefficients of the MSEL equation, obtained from a LSM regression analysis of the data, are shown in Table 5.6, with the average relationship (considered to represent the specimen size effect) presented in Equation 5.3.

Table 5.6 MSEL Coefficients for $\alpha_1/\alpha_{1ave(20cm)}$

	Mix 1	Mix 2	Mix 3	Average
β	1.07	0.63	0.61	0.77
$\lambda_0 d_a$	0.95	0.95	0.95	0.95
α	0.79	0.86	0.88	0.84

$$\alpha_1 = \frac{0.77\alpha_{1(20cm)}}{\sqrt{1+\frac{c}{0.95}}} + 0.84\alpha_{1(20cm)} \qquad \textbf{5.3}$$

- The Ultimate Compressive Strain showed a clear specimen size effect for all three mixes. The coefficients of the MSEL equation, obtained from a LSM regression analysis of the data, are shown in Table 5.7, with the average relationship (considered to represent the specimen size effect) presented in Equation 5.4.

Table 5.7 MSEL Coefficients for $\varepsilon_{cu}/\varepsilon_{cuave(20cm)}$

	Mix 1	Mix 2	Mix 3	Average
β	0.30	0.31	0.41	0.34
$\lambda_0 d_a$	0.95	0.95	0.95	0.95
α	0.94	0.94	0.89	0.92

$$\varepsilon_{cu} = \frac{0.34\varepsilon_{cu(20cm)}}{\sqrt{1+\frac{c}{0.95}}} + 0.92\varepsilon_{cu(20cm)} \qquad \textbf{5.4}$$

© University of Pretoria

- The size effect of non-standard (50 mm or 100 mm) flexural compression members may be taken into account by using the associated cylinder strength. By testing cylinders with a diameter similar to the dimensions of the flexural compression member (structural member), the size effect observed for k_3, k_1k_3, and α_1 can be eliminated. In conclusion, this means that the stress block parameters obtained by testing 200 mm specimens may be used for all specimen sizes, and the increased or decreased strength of the specimen taken into consideration by using the size effect for cylinders in uniaxial compression. The size effect for the ultimate compressive strain cannot be eliminated and needs to be taken into consideration in the calculation of the moment capacity and reinforcing requirements.
- The error between the experimental M-N interaction diagram and the M-N interaction diagram generated by using the BS 8110-1 (1997) and SANS 0100-1 (2000) code recommendations is not constant, underestimating for concrete strengths less than 80 MPa, and overestimating for concrete strengths in excess of 80 MPa.
- The error between the experimental M-N interaction diagram and the M-N interaction diagram generated by using the ACI-318 (2014) code recommendations is not constant, underestimating for concrete strengths less than 80 MPa, and overestimating for concrete strengths in excess of 80 MPa.
- The error between the experimental M-N interaction diagram and the M-N interaction diagram generated by using the EN 1992-1-1 (2004) code recommendations does appear to be constant, underestimating for all concrete strengths. For strengths in excess of 90 MPa, the EN 1992-1-1 (2004) code produces an ever increasing underestimation of strength.
- As all four design codes are calibrated to provide a suitable factor of safety against collapse, and the study results were mostly underestimated, it can be concluded that the BS 8110-1 (1997), SANS 0100-1 (2000), and ACI-318 (2014) codes can be used for the design of flexural members and flexural compression members up to 80 MPa, while EN 1992-1-1 (2004) code is suitable for the design of members with strengths up to 90 MPa. Furthermore, the EN 1992-1-1 (2004) code can be used for the safe design of flexural members with strengths in excess of 90 MPa, however, this would require a significant amount of steel in the compression zone of the flexural member, likely resulting in an uneconomical design
- The uniaxial stress-strain model of concrete can be used to accurately model the ascending branch of the flexural stress-strain curve.
- The flexural stress-strain behaviour of concrete can be modelled by combining the stress-strain model proposed by Carreira & Chu (1985) (Equation 5.5 and Equation 5.6), the estimate of E_i (Equation 5.7), and the linear relationships for ε_{c0} and ε_{cu} shown in Table 5.8.

$$f_c = f_c'' \times \left[\frac{\beta_2(\varepsilon_c/\varepsilon_{c0})}{\beta_2\text{-}1 + (\varepsilon_c/\varepsilon_{c0})^{\beta_2}}\right] \quad \textbf{5.5}$$

With:

$$\beta_2 = 1/(1\text{-}\, f_c''/(\varepsilon_{c0}E_i)) \quad \textbf{5.6}$$

$$E_i = 4.31\sqrt{f_c''} \quad \textbf{5.7}$$

© University of Pretoria

Table 5.8 Linear Trend Line Coefficients (y=ax+b) for ε_{c0} and ε_{cu}

	50 mm		100 mm		200 mm	
	a	**b**	**a**	**b**	**a**	**b**
ε_{c0} (με)	-5.67	4216	-16.77	4888	-15.86	4680
ε_{cu}(με)	-6.41	4633	-13.44	4905	-7.68	4416.4

5.3 RECOMMENDATIONS

- The results presented in this study were based on a single aggregate type. As the aggregate constitutes such a significant volumetric portion of the mix, further investigation is required into the influence of specimen size on the stress block parameters of concrete containing other sources of South African aggregate.
- As the size effect is applicable for geometrically similar members, the use of 50 x 50 x 300 mm, 100 x 100 x 500 mm, and 200 x 200 x 1000 mm *prisms* to eliminate the specimen size effect needs to be investigated.
- Based on the results obtained in this project, if a scaled down version of the conventional 200 x 200 x 1000 mm specimen is to be used, the 100 x 100 x 500 mm specimen would provide the best possible results, owing to the reduced variability of the 100 mm cylinder compressive strength.
- The EN 1992-1-1 (2004) code may be adopted in South Africa for the safe design of reinforced concrete flexural and flexural compression members.

© University of Pretoria

CHAPTER 6

REFERENCES

AASHTO LRFD Bridge Design Specifications 2012. Washington DC: American Association of State Highway and Transportation Officials.

ACI Committee 363 1992. *State-of-the-Art Report on High-Strength Concrete*. Farmington Hills, MI: American Concrete Institute.

ACI-318 2014. *Building Code Requirements for Structural Concrete (ACI 318-95) and Commentary (ACI 318R-95)*. Michigan: American Concrete Institute.

AfriSam Technical Reference Guide 2013. *AfriSam Technical Reference Guide*. 4th ed. Weltevreden Park: AfriSam.

Ahmad, S.H. & Shah, S.P. 1985. Structural Properties of High Strength Concrete and its Implications for Precast Prestressed Concrete. *PCI Journal* 30(6): 92-119.

AS 3600 1994. *SAA. Astralian Concrete Structures Code*. New South Wales: Standards Australia International.

ASTM C150/C150M 2015. *Standard Specification for Portland Cement*. West Conshohocken, PA: ASTM International.

ASTM C39/C39M 2015. *Standard Test Method for Compressive Strength of Cylindrical Concrete Specimens*. West Conshohocken, PA: ASTM International.

ASTM C469/C469M 2014. *Standard Test Method for Static Modulus of Elasticity and Poisson's Ratio of Concrete in Compression*. West Conshohocken, PA: ASTM International.

ASTM C470/C470M 2015. *Standard Specification for Molds for Forming Concrete Test Cylinders Vertically*. West Conshohocken, PA: ASTM International.

Attard, M.M. & Setunge, S. 1996. Stress-Strain Relationship of Confined and Unconfined Concrete. *ACI Materials Journal* 93(5): 432-442.

Attard, M.M. & Stewart, M.G. 1998. A Two Parameter Stress Block for High Strength Concrete. *ACI Structural Journal* 93(5): 432-442.

Azizinamini, A., Kuska, S.S.B., Brungardt, P. & Hatfield, E. 1994. Seismic Behavior of Square High-Strength Concrete Columns. *ACI Structural Journal* 91(3): 336-345.

Bae, S. & Bayrak, O. 2003. Stress Block Parameters for High-Strength Concrete Members. *ACI Structural Journal* 100(5): 626-636.

Bazant, Z.P. 1984. Size Effect in Blunt Fracture: Concrete, Rock, Metal. *Journal of Engineering Mechanics* 110(4): 518-535.

© University of Pretoria

Bazant, Z.P. 1999. Size effect on structural strength: a review. *Applied Mechanics* 69: 703-725.

BS 8110-1 1997. *Structural use of Concrete-Part 1: Code of practice for design and Construction*. 2nd ed. British Standards Institute.

BS EN12390-4 2000. *Testing hardened concrete. Compressive strength. Specification for testing machines*. Brussels: European Committee for Standardization.

Carrasquillo, R.L., Nilson, A.H. & Slate, F.O. 1981. Properties of High-Strength Concrete Subject to Short-Term Loads. *ACI Structural Journal* 78(3): 171-178.

Carreira, D.J. & Chu, K.H. 1985. Stress-Strain Relationship for Plain Concrete in Compression. *ACI Structural Journal* 82(6): 797-804.

CEB-FIB Model Code 1993. *CEB-FIB Model Code 1990: Design Code*. London: Thomas Telford Services Ltd.

Cordon, W.A. & Gillispie, H.A. 1963. Variables in Concrete Aggregates and Portland Cement Paste which Influence the Strength of Concrete. *Journal of the American Concrete Institute* 60(8): 1029-1052.

CSA S6 2001. *Canadian Highway Bridge Design Code*. Rexdale, Ontario: Canadian Standards Association.

CSA Standard A23.3 2004. *Design of concrete structures*. Mississauga, Ontario, Canada: Canadian Standards Association.

Desayi, P. & Krishnan, S. 1964. Equation for the Stress Strain Curve of Concrete. *Journal of the American Concrete Institute* 61(3): 345-350.

Domone, P. & Illston, J. (eds.) 2010. Construction Materials, Their nature and behaviour. Spon Press.

EN 1992-1-1 2004. *Eurocode 2: Design of concrete structures - Part 1-1 : General rules and rules for buildings*. Brussels: European Committee for Standardization.

Hognestad, E. 1951. *A Study of Combined Bending and Axial Load in Reinforced Concrete Members*. Bullitin Series No. 399. Illinois: University of Illinois Engineering Experimental Station University of Illinois.

Hognestad, E., Hanson, N.W. & McHenry, D. 1955. Concrete Stress Distribution in Ultimate Strength Design. *Journal of the American Institute* 52: 455-479.

Ho, J.C.M., Kwan, A.K.H. & Pam, H.J. 2002. Ultimate concrete strain and equivalent rectangular stress block for design of high strength concrete beams. *The Structural Engineer* 80(23/24): 26-32.

Hsu, L.S. & Hsu, C.-T.T. 1994. Complete stress-strain behaviour of high strength concrete under compression. *Magazine of Concrete Research* 46(169): 301-312.

Ibrahim, H.H.H. 1994. *Flexural Behavior of High-Strength Concrete Columns*. Ph.D. Thesis. Alberta, Edmonton, Alberta, Canada: Department of Civil and Environmental Engineering University of Alberta.

Ibrahim, H.H.H. & MacGregor, J.G. 1997. Modification of the ACI Rectangular Stress Block for High Strength Concrete. *ACI Structural Journal* 94(1): 40-48.

IS 456 2000. *Indian standard code of practice for plain and reinforced concrete*. 4th ed. New Delhi, India: Bureau of Indian Standards.

Iravani, S. 1996. Mechanical Properties of High-Strength Concrete. *ACI Materials Journal* 93(5): 416-426.

Jensen, V.P. 1943. The Plasticity Ratio of Concrete and Its Effect on the Ultimate Strength of Beams. *Journal of the American Concrete Institute* 14(6): 565-582.

Jerath, S. & Yamane, L.C. 1987. Mechanical Properties and Workability of Superplasticized Concrete. *Cement Concrete and Aggregates* 9(1): 12-19.

© University of Pretoria

Kaar, P.H., Fiorato, A.E., Carpenter, J.E. & Corley, W.G. 1978b. *Limiting Strains of Concrete Confined by Rectangular Hoops*. Research and Development. 5420 Old Orchard Road Skokie, IL 60077 USA: Portland Cement Association Research and Development / Construction Technologies Laboratories.

Kaar, P.H., Hanson, N.W. & Campell, H.T. 1978a. Stress-Strain Characteristics of High Strength Concrete. *Special Publication 55-7, American Concrete Institute* 55: 161-186.

Kent, D.C. & Park, R. 1971. Flexural members with confined concrete. *Journal of the Structural Division, Proc. of the American Society of Civil Engineers* (97): 1969-1990.

Khadiranaikar, R.B. & Awati, M.M. 2012. Concrete Stress Distribution Factors for High-Performance Concrete. *Journal of Structural Engineering* 138(3): 402-415.

Kim, J.K. & Eo, S.H. 1990. Size Effect in Concrete Specimens with Dissimilar Initial Cracks. *Magazine of Concrete Research* 42(153): 233-238.

Kim, J.-K., Yi, S.-T., Park, C.-K. & Eo, S.-H. 1999. Size Effect on Compressive Strength of Plain and Spirally Reinforced Concrete Cylinders. *American Concrete Institute Structural Journal* 96(1): 88-94.

Kim, J.-K., Yi, S.-T. & Yang, E.-I. 2000. Size Effect on Flexural Compressive Strength of Concrete Specimens. *ACI Structural Journal* 97(2): 291-296.

Komendant, J., Nicolayeff, V., Polivka, M. & Pirtz, D. 1978. Effect of Temperature, Stress Level, and Age at Loading on Creep of Sealed Concrete. *American Concrete Institute Special Publication 55* 55-82.

Li, B. 1993. *Strength and Ductility of Reinforced Concrete Members and Frames Constructed Using High Strength Concrete*. Ph. D. Thesis. Christchurch, New Zealand: Department of Civil Engineering University of Canterbury.

Logan, A.T. 2005. *Short-Term Material Properties of High-Strength Concrete*. M.S. Thesis. Raleigh, NC: Department of Civil, Construction and Environmental Engineering North Carolina State University.

Mahachi, J. 2013. *Design of Structural Steelwork to SANS 10162*. 3rd ed. Randburg: Xsi-tec.

Mattock, A.H., Kriz, L.B. & Hognestad, E. 1961. Rectangular Concrete Stress Distribution in Ultimate Strength Design. *Journal of the American Concrete Institute* 57(2): 875-928.

Mehta, P.K. 1986. *Concrete: Structure, Properties and Materials*. Prentice Hall.

Mertol, H.M., Rizkalla, S., Zia, P. & Mirmiran, A. 2008. Characteristics of Compressive Stress Distribution in High-Strength Concrete. *American Concrete Institute Structural Journal* 105(2): 626-633.

Nedderman, H. 1973. *Flexural Stress Distribution in Very-High Strength Concrete*. M.Sc. Thesis. Arlington, Texas: Department of Civil Engineering University of Texas at Arlington.

Newman, J. & Choo, B.S. (eds.) 2003. *Advanced Concrete Technology, Concrete Properties*. Lodon: Elsevier.

NZS 3101 :Part 1 2006. *Concrete structures standard Part 1 - The Design of Concrete Structures*. Wellington: Standards New Zealand.

Ownes, G. (ed.) 2009. *Fulton's concrete technology*. 9th ed. Cement & Concrete Institute.

Ozbakkaloglu, T. & Saatcioglu, M. 2004. Rectangular Stress Block for High-Strength Concrete. *ACI Structural Journal* 101(4): 475-483.

Oztekin, E., Pul, S. & Husem, M. 2003. Determination of Rectangular Stress Block Parameters for High Strength Concrete. *Engineering Structures* 25(3): 371-376.

Park, R. & Paulay, T. 1975. *Reinforced Concrete Structures*. New Zealand: JOHN WILEY & SONS.

© University of Pretoria

Pastor, J.A. 1986. *High Strength Concrete Beams*. Ph.D. Thesis. Ithaca, New York: Department of Civil Engineering Cornell University.

Pendyala, R. & Mendis, P.A. 1998. A Rectangular Stress Block for High Strength Concrete. *Structural Engineering Journal* CE39(4): 135-144.

Perenchio, W.F. & Klieger, P. 1978. Some Physical Properties of High-Strength Concrete. *Research and Development Bulletin RD056.01T, Portland Cement Association* 6.

Popovics, S. 1973. A numerical approach to the complete stress-strain curves of concrete. *Cement and Concrete Research* 3(5): 583-599.

Radain, T.A., Samman, T.A. & Wafa, F.F. 1993. Mechanical Properties of High Strength Concrete. In *Utilization of High-Strength Concrete Symposium*. Lillehammer, Norway, 1993: 1209-1216.

Rangan, B.V. 1999. Studies on High-Performance High Strength Concrete (HPHSC) Columns. *ACI Special Publication-186* 745-764.

Robberts, J.M. & Marshall, V. 2010. *Analysis and Design of Concrete Structures*. cement & concrete institute.

Rusch, H. 1960. Researches Toward a General Flexural Theory for Structural Concrete. *Journal of the American Concrete Institute* 57(1): 1-28.

SANS 0100-1 2000. *Code of practice for the structural use of concrete Part 1: Design. Part 2: Materials*. Pretoria: South African Bureau of Standards.

SANS 10162-1 2011. *South African National Standard: The structural use of steel, Part 1: Limit-states design of hot-rolled steelwork*. 21st ed. Pretoria: South African Bureau of Standards.

SANS 1083 2014. *Aggregates from natural sources-Aggregates for concrete*. Pretoria: South African Bereau of Standards.

SANS 50197-1 2000. *Cement-Part 1: Composition, specifications and conformity criteria for common cements*. 11th ed. Pretoria: South African Bureau of Standards.

SANS 5860 2006. *Concretre tests- Dimentions, tolerances and use of cast test specimens*. 11th ed. Pretoria: South African Bureau of Standards.

SANS 5861:1 2006. *Concrete Tests, Part 1: Mixing of fresh concrete in the laboratory*. 21st ed. Pretoria: South African Bureau of Standards.

SANS 5861:3 2006. *Concrete tests, Part 3: Making and curing of test specimens*. 21st ed. Pretoria: South African Bureau of Standards.

SANS 5863 2006. *Concrete tests — Compressive strength of hardened concrete*. 21st ed. Pretoria: South African Bureau of Standards.

SANS 920 2011. *Steel bars for concrete reinforcement*. Pretoria: South African Bureau of standards.

Sargin, M. 1971. *Stress-Strain Relationship for Concrete and the Analysis of Structural Concrete Sections*. Study No. 4. Ontario: Solid Mechanics Division University of Waterloo.

Sargin, M., Ghosh, S.K. & Handa, V.K. 1971. Effects of Lateral Reinforcement upon the Strength and Deformation Properties of Concrete. *Magazine of Concrete Research* 23(75-76): 99-110.

Sargin, M. & Handa, V.K. 1969. *A General Formulation for the Stress-Strain Properties of Concrete*. Report No. 3. Waterloo, Ontario, Canada: Solid Mechanics Division University of Waterloo.

Schade, J.E. 1992. *Flexural Concrete Stress in High Strength Concrete Columns*. M.S. Thesis. Calgary, Alberta, Canada: Department of Civil Engineering University of Calgary.

© University of Pretoria

Soliman, M.T.M. & Yu, C.W. 1967. The Flexural Stress-Strain Relationship of Concrete. *Magazine of Concrete Research* 19(61): 223-238.

Sun, C., Girgis, A., Tadros, M.K. & Badie, S. 2003. Structural Behavior of Flexural Member with High-Strength Concrete. In *ISHPC.*, 2003

Swartz, S.E. et al. 1985. Structural Bending Properties of Higher Strength Concrete. *ACI Special Publication-87 High-Strength Concrete* 87: 145-178.

Tan, T.H. & Nguyen, N.B. 2005. Flexural Behavior of Confined High-Strength Concrete Columns. *American Concrete Institute (ACI) Structural Journal* 102(2): 198-205.

Tsai, W.T. 1988. Uniaxial compression stress-strain relation of concrete. *Journal of Structural Engineering* 114(9): 2133-2136.

Van Gysel, A. & Taerwe, L. 1996. Analytical Formulation of the Complete Stress-Strain Curve for High Strength Concrete. *Materials and Structures* 29: 529-533.

Wang, P.T., Shah, S.P. & Naaman, A.E. 1978a. Stress-Strain Curves of Normal and Lightweight Concrete in Compression. *American Concrete Institute Structural Journal* 75(11): 603-611.

Wang, P.T., Shah, S.P. & Naaman, A.E. 1978b. High-Strength Concrete in Ultimate Strength Design. *ASCE Journal of Structural Division* 104(11): 1761-1773.

Wee, T.H., Chin, M.S. & Mansur, M.A. 1996. Stress-Strain Relationship of High-Strength Concrete in Compression. *ASCE Journal of Materials in Civil Engineering* 8(2): 70-76.

Whitney, C.S. 1937. Design of Reinforced Concrete Members under Flexure of Combined and Direct Compression. *Journal of American Concrete Institute* 33: 483-498.

Yi, S.-T., Yang, E.-I. & Choi, J.-C. 2006. Effect of specimen sizes, specimen shapes, and placement directions on compressive strength of concrete. *Nuclear Engineering and Design* 236(2): 115-127.

Zia, P. 1983. Review of ACI Code for Design with High-Strength Concrete. *Concrete International* 5(8): 16-20.

© University of Pretoria

APPENDIX A

PREVIOUS RESEARCH RESULTS

A.1 ECCENTRIC SPECIMEN TEST DATA

Table A.1 Hognestad et al. (1955)

Specimen ID	f_c' (MPa)	k_1	k_2	k_3	k_1k_3	α_1	β_1	ε_{cu} (με)
1	5.3	-	0.49	-	1.05	1.08	0.97	-
2	9.6	-	0.48	-	0.91	0.94	0.97	-
3	11.7	-	0.48	-	0.95	0.99	0.97	-
4	11.7	-	0.47	-	0.9	0.95	0.95	-
5	15.2	-	0.48	-	0.88	0.91	0.96	-
6	20.0	-	0.44	-	0.82	0.93	0.88	-
7	20.7	-	0.46	-	0.81	0.89	0.91	-
8	21.4	-	0.46	-	0.9	0.99	0.91	-
9	25.5	-	0.48	-	0.74	0.78	0.95	-
10	26.9	-	0.48	-	0.8	0.83	0.97	-
11	31.7	-	0.43	-	0.76	0.88	0.86	-
12	35.8	-	0.45	-	0.73	0.81	0.9	-
13	37.2	-	0.44	-	0.63	0.71	0.88	-
14	37.9	-	0.47	-	0.72	0.76	0.94	-
15	39.3	-	0.41	-	0.67	0.81	0.83	-
16	42.0	-	0.42	-	0.64	0.77	0.83	-
17	44.8	-	0.39	-	0.65	0.82	0.79	-
18	44.8	-	0.42	-	0.65	0.78	0.84	-
19	46.9	-	0.41	-	0.65	0.79	0.81	-
20	52.4	-	0.37	-	0.63	0.84	0.75	-
21	52.4	-	0.41	-	0.65	0.8	0.81	-
22	71.0	-	0.39	-	0.57	0.72	0.79	-
23	71.7	-	0.38	-	0.56	0.73	0.76	-

Table A.2 Sargin et al. (1971)

Specimen ID	f_c' (MPa)	k_1	k_2	k_3	k_1k_3	α_1	β_1	ε_{cu} (με)
PE-1	30.0	-	-	0.93	-	-	-	3500
PE-2	32.2	-	-	1.02	-	-	-	2800
PE-3	28.8	-	-	0.97	-	-	-	3900

Table A.3 Nedderman (1973)

Specimen ID	f_c' (MPa)	k_1	k_2	k_3	k_1k_3	α_1	β_1	ε_{cu} (με)
2	95.4	-	0.37	-	0.59	0.8	0.74	3200
4	95.4	-	0.39	-	0.55	0.71	0.78	2900
5	96.5	-	0.37	-	0.61	0.82	0.74	3400
6	97.6	-	0.38	-	0.59	0.78	0.76	3200

© University of Pretoria

7	79.2	-	0.34	-	0.57	0.84	0.68	3000
9	89.4	-	0.36	-	0.58	0.81	0.72	3300
10	85.6	-	0.36	-	0.58	0.81	0.72	3200
11	83.0	-	0.38	-	0.56	0.74	0.76	2800
12	84.1	-	0.38	-	0.55	0.72	0.76	3000

Table A.4 Kaar et al. (1978a)

Specimen ID	f_c' (MPa)	k_1	k_2	k_3	k_1k_3	α_1	β_1	ε_{cu} (με)
A6	44.8	0.75	0.45	1.01	0.76	0.84	0.9	4500
A6P	47.5	0.73	0.45	0.98	0.72	0.8	0.9	3800
A8	58.4	0.7	0.39	0.93	0.65	0.83	0.78	3400
A10	71.7	0.68	0.37	0.92	0.63	0.85	0.74	3600
A10P	64.6	0.64	0.36	1	0.64	0.89	0.72	3000
A12	78.1	0.62	0.36	1.12	0.69	0.96	0.72	3100
A14	96.5	0.56	0.34	1.03	0.58	0.85	0.68	3300
A14P	91.5	0.65	0.37	1.09	0.71	0.96	0.74	3800
D6	45.3	0.75	0.42	0.98	0.74	0.86	0.84	2800
D6P	48.9	0.74	0.42	0.89	0.66	0.79	0.84	3300
D8	58.0	0.64	0.4	0.95	0.61	0.76	0.8	2400
D10	67.6	0.66	0.38	0.94	0.62	0.82	0.76	3100
D10P	69.6	0.63	0.41	0.98	0.62	0.76	0.82	3200
D12	77.0	0.59	0.36	1.2	0.71	0.99	0.72	3200
D14	88.7	0.55	0.38	1.08	0.59	0.78	0.76	2800
D14P	102.3	0.6	0.36	1.03	0.62	0.86	0.72	3500
F10	77.8	0.65	0.37	0.99	0.64	0.86	0.74	3200
F12	87.4	0.57	0.36	1.12	0.64	0.89	0.72	2900
F14	94.4	0.65	0.38	0.91	0.59	0.78	0.76	3500
E4*	29.2	0.66	0.35	1.16	0.77	1.09	0.7	2400
E6*	44.4	0.61	0.47	0.92	0.56	0.7	0.94	5200
E8*	56.6	0.67	0.36	0.99	0.66	0.92	0.72	3800
E8P*	58.2	0.68	0.46	0.84	0.57	0.62	0.92	3700
E10*	78.1	0.58	0.33	1.06	0.61	0.92	0.66	3700
E12*	86.1	0.63	0.37	0.75	0.47	0.64	0.74	3100
E12P*	82.3	0.6	0.34	0.97	0.58	0.85	0.68	3600
C4*	25.0	0.75	0.43	1.03	0.77	0.9	0.86	3600
C4P*	24.5	0.77	0.44	0.95	0.73	0.84	0.88	5100
C6*	41.4	0.64	0.42	0.96	0.61	0.73	0.84	3500
C8*	56.6	0.61	0.34	0.94	0.57	0.84	0.68	3000
C8P*	56.2	0.58	0.38	0.96	0.56	0.74	0.76	3000
C10*	65.9	0.57	0.34	1.06	0.60	0.9	0.68	3200
C12*	66.7	0.53	0.39	1.2	0.64	0.82	0.78	2900
C12P*	68.8	0.45	0.43	1.19	0.54	0.62	0.86	2900
***Lightweight Aggregate Concrete**								

Table A.5 Kaar et al. (1978b)

Specimen ID	f_c' (MPa)	k_1	k_2	k_3	k_1k_3	α_1	β_1	ε_{cu} (με)
1	22.9	0.74	0.44	1.07	0.79	0.9	0.88	3000
17	46.5	0.74	0.45	0.95	0.70	0.78	0.9	4000
20	22.0	0.75	0.44	1.23	0.92	1.05	0.88	3000

Table A.6 Swartz et al. (1985)

Specimen ID	f_c' (MPa)	k_1	k_2	k_3	k_1k_3	α_1	β_1	ε_{cu} (με)
1	57.9	0.77	0.41	1.11	0.85	1.04	0.82	2000
2	64.8	0.73	0.37	0.9	0.66	0.89	0.74	3100
3B	66.8	0.73	0.41	0.96	0.70	0.85	0.82	2700
3C	66.8	0.73	0.41	0.94	0.69	0.84	0.82	2600
4A	77.0	0.81	0.43	0.92	0.75	0.87	0.86	3300

© University of Pretoria

4B	77.0	0.72	0.37	0.97	0.70	0.94	0.74	3100
4C	77.0	0.68	0.37	1.06	0.72	0.97	0.74	2800
4D	77.0	0.63	0.34	0.97	0.61	0.9	0.68	2400

Table A.7 Pastor (1986)

Specimen ID	f_c' (MPa)	k_1	k_2	k_3	k_1k_3	α_1	β_1	ε_{cu} (με)
SP-1	17.9	0.88	0.48	0.96	0.84	0.88	0.96	4300
SP-2	18.6	0.86	0.48	0.93	0.80	0.83	0.96	3600
SP-3	36.9	0.81	0.44	0.9	0.73	0.83	0.88	3600
SP-4	42.5	0.79	0.41	0.91	0.72	0.88	0.82	3800
SP-8	59.6	0.64	0.38	1.06	0.68	0.89	0.76	3200
SP-9	63.3	0.67	0.37	0.97	0.65	0.88	0.74	3400
SP-10	63.4	0.69	0.41	0.99	0.68	0.83	0.82	3500
SP-11	64.6	0.7	0.39	0.98	0.69	0.88	0.78	3100
SP-12	75.8	0.65	0.33	0.93	0.60	0.92	0.66	3100
SP-13	79.7	0.63	0.36	0.96	0.60	0.84	0.72	3200

Table A.8 Schade (1992)

Specimen ID	f_c' (MPa)	k_1	k_2	k_3	k_1k_3	α_1	β_1	ε_{cu} (με)
Column 1	105.8	0.56	0.36	1	0.56	0.78	0.71	3000
Column 2	105.8	0.62	0.36	0.97	0.60	0.85	0.71	3400
Column 3	105.8	0.6	0.36	0.96	0.58	0.81	0.71	3300
Column 4	105.8	0.65	0.37	0.94	0.61	0.83	0.73	3600
Column 5	105.8	0.65	0.36	0.92	0.60	0.83	0.72	3500
Column 6	105.8	0.67	0.37	0.89	0.60	0.83	0.73	3900

Table A.9 Ibrahim (1994)

Specimen ID	f_c' (MPa)	k_1	k_2	k_3	k_1k_3	α_1	β_1	ε_{cu} (με)
V4	72.8	0.71	0.39	0.9	0.64	0.81	0.79	3480
V5	124.7	0.59	0.34	0.92	0.54	0.78	0.69	3960
V6	98.7	0.63	0.37	0.89	0.56	0.75	0.75	3780

Table A.10 Tan & Nguyen (2005)

Specimen ID	f_c' (MPa)	k_1	k_2	k_3	k_1k_3	α_1	β_1	ε_{cu} (με)
S40-A-N2	46.4	-	0.4	-	0.69	0.86	0.8	2900
S40-A-N3	48.3	-	0.38	-	0.65	0.86	0.76	2900
S70-A-N	71.4	-	0.38	-	0.54	0.71	0.76	3000

Table A.11 Mertol et al. (2008)

Specimen ID	f_c' (MPa)	k_1	k_2	k_3	k_1k_3	α_1	β_1	ε_{cu} (με)
10EB2	75.8	0.65	0.38	1.03	0.67	0.9	0.75	3738
10EB3	78.5	0.62	0.36	1.12	0.69	0.95	0.72	3138
10EB4	80.6	0.65	0.36	1.14	0.74	1.02	0.73	3407
10EB5	71.7	0.64	0.36	1.2	0.77	1.06	0.73	3102
10EB6	75.1	0.62	0.36	1.16	0.72	1.01	0.72	3023
14EB1	100.6	0.63	0.37	1	0.63	0.85	0.74	3316
14EB2	98.5	0.6	0.36	1.08	0.65	0.85	0.72	3162
14EB3	101.3	0.61	0.36	1.09	0.66	0.93	0.71	3177
14EB4	103.4	0.58	0.35	1.1	0.64	0.92	0.7	3032
14EB5	106.1	0.57	0.34	1.1	0.63	0.92	0.68	2868
14EB6	104.7	0.6	0.35	1.06	0.64	0.91	0.69	2954
18EB1	108.9	0.69	0.38	0.82	0.57	0.74	0.77	3684
18EB2	110.2	0.67	0.37	0.85	0.57	0.77	0.74	3364
18EB3	107.5	0.63	0.37	0.81	0.51	0.69	0.73	2914
18EB4	108.9	0.65	0.36	0.88	0.57	0.78	0.73	3306
18EB5	110.2	0.65	0.36	0.85	0.55	0.76	0.72	3144

© University of Pretoria

18EB6	106.8	0.66	0.37	0.88	0.58	0.78	0.74	3404
18EB7	103.4	0.64	0.37	1.05	0.67	0.9	0.75	3585
18EB8	99.9	0.65	0.37	1.03	0.67	0.91	0.74	3507
18EB9	102.7	0.62	0.36	1.06	0.66	0.91	0.72	3494
18EB10	100.6	0.64	0.38	0.97	0.62	0.82	0.77	3532

Table A.12 Khadiranaikar & Awati (2012)

Specimen ID	f_c' (MPa)	k_1	k_2	k_3	k_1k_3	α_1	β_1	ε_{cu} (με)
SBII2	74.5	0.58	0.37	1.06	0.62	0.84	0.73	3000
SBII3	67.0	0.62	0.37	1.12	0.69	0.93	0.75	3100
SBII4	69.9	0.65	0.37	1.07	0.69	0.94	0.74	2915
SBII5	67.0	0.61	0.37	1.07	0.65	0.89	0.73	2990
SBIII1	85.1	0.57	0.37	1.13	0.64	0.87	0.74	3250
SBIII2	85.0	0.57	0.36	1.08	0.61	0.84	0.72	2915
SBIII3	86.0	0.70	0.38	0.95	0.68	0.90	0.75	3500
SBIII4	81.5	0.62	0.37	1.07	0.66	0.89	0.74	3200
SBIV1	105.0	0.55	0.35	0.99	0.54	0.78	0.69	3400
SBIV2	104.5	0.59	0.36	1.01	0.59	0.84	0.71	3350
SBIV3	102.0	0.64	0.36	1.03	0.66	0.91	0.73	3450
SBIV4	105.5	0.59	0.36	0.97	0.58	0.81	0.71	3490
SBIV5	102.0	0.60	0.36	0.97	0.58	0.82	0.71	3390
SBV1	115.6	0.55	0.34	0.98	0.54	0.78	0.69	3562
SBV2	115.6	0.56	0.34	1.07	0.60	0.88	0.68	3780
SBV3	115.6	0.60	0.36	1.01	0.61	0.84	0.72	3336

A.2 POISSON RATIO TEST DATA

Table A.13 Komendant et al. (1978), Perenchio & Klieger (1978), and Carrasquillo et al. (1981)

Komendant et al. (1978)		Perenchio & Klieger (1978)		Carrasquillo et al. (1981)	
f_c' (MPa)	υ	f_c' (MPa)	υ	f_c' (MPa)	υ
43.3	0.22	76.9	0.24	33.8	0.19
46.7	0.22	79.8	0.22	32.4	0.22
45.9	0.23	77.0	0.21	32.2	0.2
52.5	0.22	70.0	0.28	58.7	0.21
65.5	0.22	76.6	0.26	57.1	0.21
45.4	0.19	73.0	0.2	59.0	0.24
49.5	0.22	65.8	0.25	73.5	0.22
61.5	0.22	74.8	0.23	76.1	0.21
45.2	0.2	65.3	0.21	76.5	0.21
51.0	0.21	61.9	0.24	33.8	0.19
66.5	0.22	70.6	0.24	30.3	0.19
-	-	65.0	0.23	31.5	0.19
-	-	55.8	0.22	54.2	0.21
-	-	66.1	0.22	48.9	0.2
-	-	59.0	0.24	49.2	0.21
-	-	49.7	0.23	64.0	0.21
-	-	57.5	0.221	65.6	0.25
-	-	-	-	65.5	0.21

Table A.14 Swartz et al. (1985), Jerath & Yamane (1987), Radain et al. (1993), and Iravani (1996)

Swartz et al. (1985)		Jerath and Yamane (1987)		Radain et al. (1993)		Iravani (1996)	
f_c' (MPa)	υ	f_c' (MPa)	υ	f_c' (MPa)	υ	f_c' (MPa)	υ
66.7	0.16	65.6	0.19	39.8	0.15	65.2	0.16
66.7	0.16	57.6	0.22	42.3	0.15	65.9	0.11
66.7	0.16	57.5	0.18	45.5	0.16	66.1	0.2
66.7	0.16	56.2	0.21	47.8	0.17	66.3	0.15

© University of Pretoria

77.0	0.23	45.7	0.21	50.0	0.17	66.4	0.19
77.0	0.23	52.4	0.18	53.3	0.18	66.4	0.14
77.0	0.23	38.5	0.22	58.5	0.19	67.0	0.16
77.0	0.23	38.0	0.23	62.5	0.18	90.8	0.19
79.2	0.13	36.0	0.2	63.7	0.17	94.1	0.15
79.2	0.13	29.7	0.21	64.8	0.17	95.8	0.18
-	-	29.6	0.18	65.9	0.17	97.4	0.19
-	-	25.7	0.23	67.7	0.19	97.8	0.16
-	-	-	-	68.4	0.19	103.4	0.18
-	-	-	-	73.8	0.21	102.3	0.2
-	-	-	-	78.1	0.22	105.0	0.18
-	-	-	-	79.0	0.22	106.1	0.18
-	-	-	-	79.4	0.21	106.5	0.18
-	-	-	-	83.6	0.22	106.0	0.16
-	-	-	-	85.6	0.22	115.4	0.2
-	-	-	-	89.9	0.23	119.6	0.19
-	-	-	-	-	-	120.5	0.2
-	-	-	-	-	-	121.5	0.2
-	-	-	-	-	-	124.9	0.2

Table A.15 Logan (2005) and Methol et al. (2008)

Logan (2005)						Methol et al. (2008)	
f_c' (MPa)	υ	f_c' (MPa)	υ	f_c' (MPa)	υ	f_c' (MPa)	υ
65.9	0.12	42.5	0.29	41.3	0.22	75.8	0.25
65.9	0.15	42.5	0.29	41.3	0.2	78.5	0.21
34.9	0.11	92.8	0.27	41.3	0.22	80.6	0.19
34.9	0.18	92.8	0.15	90.5	0.11	71.7	0.2
34.9	0.17	92.8	0.16	90.5	0.11	100.6	0.22
34.9	0.14	78.2	0.17	90.5	0.26	98.5	0.2
69.5	0.17	78.2	0.18	90.5	0.18	101.3	0.23
69.5	0.14	96.4	0.22	82.7	0.21	103.4	0.23
57.0	0.13	100.1	0.17	82.7	0.22	106.1	0.24
57.0	0.12	100.1	0.14	82.7	0.19	104.7	0.23
57.0	0.15	100.1	0.14	95.2	0.24	108.9	0.23
57.0	0.11	100.1	0.24	95.2	0.14	110.2	0.22
67.2	0.16	98.1	0.15	95.2	0.17	107.5	0.23
67.2	0.16	98.1	0.15	103.0	0.2	108.9	0.2
67.2	0.14	98.1	0.18	103.0	0.26	110.2	0.24
67.2	0.13	98.1	0.16	103.0	0.1	106.8	0.22
74.6	0.12	107.8	0.23	103.0	0.12	103.4	0.24
74.6	0.13	107.8	0.19	99.2	0.17	99.9	0.22
71.3	0.15	107.8	0.25	99.2	0.22	102.7	0.23
71.3	0.12	97.3	0.19	115.3	0.17	100.6	0.24
71.3	0.11	97.3	0.25	115.3	0.2	-	-
83.4	0.1	97.3	0.23	115.3	0.21	-	-
83.4	0.14	97.3	0.27	115.3	0.21	-	-
80.1	0.2	100.9	0.15	107.8	0.22	-	-
80.1	0.18	100.9	0.18	107.8	0.19	-	-
80.1	0.13	114.4	0.17	107.8	0.26	-	-
80.1	0.17	114.4	0.19	107.8	0.27	-	-
72.5	0.17	114.4	0.12	101.2	0.16	-	-
72.5	0.22	110.6	0.19	101.2	0.25	-	-
88.1	0.1	110.6	0.16	101.2	0.22	-	-
83.6	0.24	110.6	0.17	101.2	0.2	-	-
83.6	0.24	110.6	0.16	115.8	0.15	-	-
87.8	0.17	78.4	0.11	115.8	0.12	-	-
87.8	0.18	113.2	0.24	115.8	0.17	-	-

© University of Pretoria

87.8	0.18	78.4	0.24	115.8	0.2	-	-
87.8	0.15	78.4	0.24	113.2	0.16	-	-
42.5	0.27	78.4	0.19	113.2	0.22	-	-
42.5	0.29	78.4	0.19	113.2	0.21	-	-

A.3 SIZE EFFECT SPECIMEN DATA

Table A.16 Yi et al. (2006)

w/c	Cube Size (mm)						Cylinder Diameter (h/d=2) (mm)				
	50		100	150	200		50		100	150	200
0.67	35.2	36.4	30.9	33.3	31.8	27	28.5	27.4	28.2	26.8	25.3
	32.6	37.5	32	33.9	29.7	-	27.8	27.1	27.6	27.2	24.3
	38.5	37	33.8	33.2	-	-	29.2	29.1	28.1	27.1	-
	-	-	32.1	-	-	-	-	-	26.5	-	-
0.5	61.7	62.1	51	45.7	46.2	42.9	50.4	45.8	48.1	44.2	43.7
	63.1	58.1	49.6	44.3	-	-	52.5	43.1	45.5	40.4	46.5
	61.6	64.9	44.8	43.7	-	-	44.2	47.2	43.9	44.2	-
			52.6	-	-	-	-	-	45.2	-	-
0.35	82.2	82.1	73.5	65.7	66.8	65.9	69.4	74.8	67.5	62.7	64.4
	77	-	74.8	70.4	64.8		71.1	72.9	66.6	66.3	66.5
	79.8	-	71.1	-	-	-	74	74.9	65.5	68.8	-
	-	-	-	-	-	-	-	-	64.4	-	-
0.28	95	95.7	81.2	75.8	57	78.1	97.8	92.4	75.9	80.1	71.3
	100	89.6	80.5	-	-	-	91.5	83.4	79.9	76.1	-
	90.2	94.1	84.2	-	-	-	92.5	-	80.6	-	-
	-	-	-	-	-	-	-	-	84	-	-

© University of Pretoria